FLEXURAL RESISTANCE OF LONGITUDINALLY STIFFENED PLATE GIRDERS

A Dissertation
Presented to
The Academic Faculty

By

Lakshmi Priya Palamadai Subramanian

In Partial Fulfillment
of the Requirements for the Degree
Doctor of Philosophy in the
School of Civil Engineering

Georgia Institute of Technology
December 2015

FLEXURAL RESISTANCE OF LONGITUDINALLY STIFFENED

PLATE GIRDERS

Approved by:

Dr. Donald W.White, Advisor
School of Civil and Environmental
Engineering
Georgia Institute of Technology

Dr. Abdul-Hamid Zureick
School of Civil and Environmental
Engineering
Georgia Institute of Technology

Dr. Arash Yavari
School of Civil and Environmental
Engineering
Georgia Institute of Technology

Dr. Reginald DesRoches
School of Civil and Environmental
Engineering
Georgia Institute of Technology

Dr. Dewey H.Hodges
School of Aerospace Engineering
Georgia Institute of Technology

Date Approved: November 13, 2015

To my family, for their unconditional love and support

ACKNOWLEDGEMENTS

My Ph.D. has been a journey that could not have been undertaken and completed without the support of several people, who deserve my deepest gratitude. I would first of all like to thank my advisor, Dr. Donald White who is undoubtedly the best mentor one could wish for. His prodigious knowledge of structural engineering, his enthusiasm and love for research and his accessibility to his students is exceptional. His immense respect and consideration for his students' ideas and opinions is a mark of his humility and is truly inspiring, coming from a man of his stature.

I would also like to thank the other members of my committee, Dr. Abdul-Hamid Zureick, Dr. Arash Yavari, Dr. Reginald DesRoches and Dr. Dewey Hodges for their valuable suggestions.

I would like to thank AASHTO and AISI for their support and funding of this research.

I am especially thankful to Dr.Engelhardt at The University of Texas at Austin, for stoking my passion for research, and encouraging me to apply to work with Prof. White.

I would also like to thank my peers and friends at graduate school who have made my time at Georgia Tech fulfilling intellectually and emotionally. I would like to thank Dr. Cliff Bishop and Dr. Yoon Duk Kim for their guidance during the initial stages of my research. I would like to thank Thanh, Woo Yong, Ajinkya, Pradeep, Swarnava, Oghuzan and Sujith for making the office a friendly workplace. I would also like to thank my roommate and friend, Sangeetha for helping make our apartment feel like a home away from home. I am extremely grateful to Vacha and Gayatri, who always made me believe in myself.

TABLE OF CONTENTS

LIST OF TABLES

xvi

LIST OF FIGURES

SUMMARY

The American Association of State Highway and Transportation Officials Load and Resistance Factor Design Specifications (AASHTO LRFD) require the use of longitudinal stiffeners in plate girder webs when the web slenderness D/t_w is greater than 150. This practice is intended to limit the lateral flexing of the web plate during construction and at service conditions. AASHTO accounts for an increase in the web bend-buckling resistance due to a longitudinal stiffener in a plate girder. However, when the theoretical bend-buckling capacity of the stiffened web is exceeded under strength load conditions, the Specifications do not consider any contribution from the longitudinal stiffeners to the girder resistance. That is, the AASHTO LRFD web bend-buckling strength reduction factor R_b applied in these cases is based on an idealization of the web neglecting the longitudinal stiffener. This deficiency can have significant impact on girder resistance in regions of negative flexure. This research is aimed at evaluating the improvements that may be achieved by fully considering the contribution of the longitudinal stiffeners to the girder flexural resistance.

Based on refined Finite Element (FE) test simulations, this research establishes that minimum size longitudinal stiffeners, per current AASHTO LRFD requirements, contribute significantly to the postbuckling flexural resistance of plate girders, and can bring about as much as 60% increase in the strength of the compression flange. A simple cross-section R_b model is developed that can be used to calculate the girder flexural resistance at the yield limit state. This model is based on test simulations of straight homogenous girders subjected to uniform bending, and is tested extensively and validated for hybrid girders and other limit states. Hybrid girders use web plates of lower yield

strengths than the compression flange plates, leading to early yielding in the web, and potential impact on girder strength.

In testing the Lateral Torsional Buckling (LTB) limit state, it is found that there is a substantial deviation between the AISC/AASHTO LTB resistance equations and FE test simulations. A comprehensive parametric study is conducted to determine the appropriate parameters to use in FE test simulations. The recommended parameters are identified as the ones that provide the best fit to the mean of experimental data. Based on FE simulations on unstiffened girders using these recommended parameters, a modified LTB resistance equation is proposed. This equation, used in conjunction with the proposed R_b model from the yield limit state also provides an improved handling of combined web buckling and lateral torsional buckling of longitudinally stiffened plate girders.

In the course of evaluating the above limit states, it is observed that the noncompact web slenderness limit in the Specifications, which is an approximation based on nearly rigid edge conditions for the buckling of the web plate in flexure is optimistic for certain cross-sections with narrow flanges. This research shows that the degree of restraint at the edges of the web depend largely on the relative areas of the compression flange and the area of the web in compression. An improved equation for the noncompact web slenderness limit is proposed which leads to a better understanding and representation of the true behavior of these types of members.

It is found that there is negligible interaction between the Flange Local buckling (FLB) limit state and the LTB limit states for noncompact flanges with the flange slenderness restricted as per the AASHTO 2014 Specifications. Also, the R_b calculated from the proposed model, used along with the current Specification FLB equations is shown to

provide a better characterization of the flange local buckling capacity of longitudinally stiffened girders.

Tests subjected to High-Shear High-Moment, and High-Moment High Shear are considered in order to characterize the girder shear resistances and potential moment-shear interaction for both homogenous and hybrid girders in the context of the above improvements.

Preliminary studies on curved homogenous girders indicate that the proposed yield limit state model is valid for yield limit state of these types of members.

CHAPTER 1

INTRODUCTION

1.1 Current AASHTO Provisions

Plate girders used in longer-span bridges typically have slender webs combined with longitudinal stiffening to prevent theoretical web bend-buckling during construction and under service loads. The current American Association of State Highway and Transportation Officials Load and Resistance Factor Design Specifications (AASHTO LRFD) (AASHTO 2014) require the use of longitudinal stiffeners on plate girders when the web slenderness D/t_w is greater than 150. In addition to the above considerations, this requirement is largely to alleviate web distortion induced fatigue concerns. The bend-buckling resistance of a longitudinally stiffened plate girder is higher than that of an unstiffened web. However, for cases where the longitudinally-stiffened web bend-buckling resistance (i.e., the web local buckling resistance under flexural compression) is exceeded by the strength loading combinations, AASHTO LRFD currently neglects the beneficial influence of the longitudinal stiffeners in determining the contribution of the postbuckled web to the girder flexural resistance. This is due to the fact that the research behind the AASHTO provisions has not considered the strength behavior of stiffened web panels in the post-buckled condition. The background research considers only the restraining effects of the longitudinal stiffeners on the theoretical bend-buckling resistance of the web panels.

Once a girder's web bend buckles, the portion of the web in compression becomes less effective in carrying additional load and the corresponding flexural stresses are shed largely to the girder's compression flange. The stress variation through the depth of the web

1

becomes highly nonlinear at postbuckling load levels. The term R_b in AASHTO (2014) is a reduction factor on the flexural resistance of the compressive flange that accounts for this load shedding from the web. The tension flange stresses are not significantly impacted by load shedding from the web (Basler and Thurliman 1961), and as such, the AASHTO provisions do not consider any strength reduction in the flexural checks of the tension flange. Also, the broader AASHTO provisions ensure that the reduction in the compressive flange flexural resistance due to web bend-buckling is negligible in composite sections subjected to positive flexure. The factor R_b is a function of the slenderness of the web in compression as well as the area of the web relative to the area of the compression flange. In cases where web bend-buckling occurs under strength loading combinations, the current AASHTO expressions for R_b do not account for the potentially significant effect of web longitudinal stiffening on the flexural resistance. These expressions are based conservatively on the response of the web neglecting the presence of the longitudinal stiffening.

The Commentary to Article 6.10.1.10.2 of the AASHTO LRFD Specifications permits the use of the compression flange stress at the governing strength condition based on the flexural resistance equations with R_b taken equal to 1.0 to be used in place of F_{yc} in the calculation of R_b in case of LTB or FLB when the compression flange stress is smaller than F_{yc}. This approach recognizes the fact that the post-buckled web is generally more effective when the compression flange stress is smaller in the governing strength condition.

This research is aimed at proposing a new R_b model that accounts for the influence of longitudinal stiffeners on increasing the postbuckling girder resistance. This research

addresses the resistance of longitudinally stiffened girders under various limit states and loading conditions, while making few modifications to the current Specification equations.

1.2 Origin of R_b in the AASHTO Equations

The current equation for R_b in AASHTO (2014) is derived principally from the equations developed by Basler and Thurliman (1961) for webs without longitudinal stiffeners. The current AASHTO LRFD Specification requirements for R_b neglect the contribution of the longitudinal stiffeners toward the development of the girder post web buckling flexural resistance. This can have a significant impact in regions of negative flexure. R_b is given by AASHTO equation 6.10.1.10.2-3,

$$R_b = 1 - \left(\frac{a_{wc}}{1200 + 300a_{wc}} \right) \left(\frac{2D_c}{t_w} - \lambda_{rw} \right) \leq 1.0 \qquad (1.1)$$

which was originally suggested by Basler and Thurliman for non-longitudinally stiffened doubly-symmetric girders, but used in the same form for singly-symmetric girders as well. In the equation, a_{wc} is the ratio of two times the web area in compression to the area of the compression flange, D_c is the web depth in compression, t_w is the thickness of the web, and λ_{rw} is the noncompact web slenderness limit (given by Equation 6.3).

In developing the expression for R_b, Basler and Thurliman made several simplifying assumptions:

1. They assumed that after the bend-buckling of the web, the width of the web effective in carrying compressive stresses is only $30t_w$, located at the top of the web.

This assumption was based on a web with slenderness ratio of 360 with no longitudinal stiffener.

2. Their expressions were developed based on the assumption of doubly-symmetric girders.

3. The yield strength of the girders tested directly by Basler and Thurliman was 33 ksi.

Figure 1-1 shows the model Basler and Thurliman used in calculating R_b.

$30t_w$

Neutral Axis
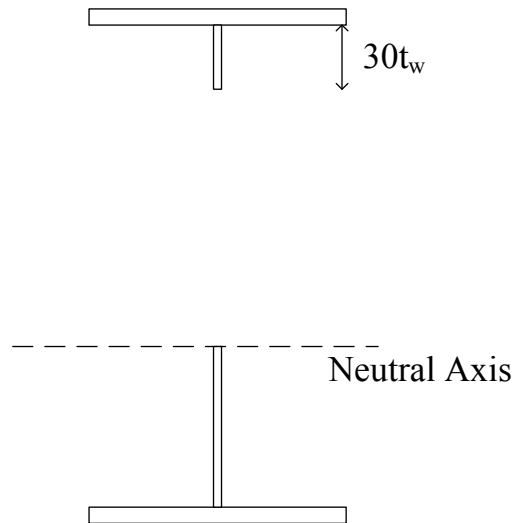
Figure 1-1: Basler and Thurliman's model used in developing the R_b equations

Although AASHTO's R_b equations have always been intended as a simplified conservative characterization of the true behavior, the extent of this conservatism is largely unknown for longitudinally stiffened girders. This is partly because the AASHTO provisions for sizing of the longitudinal stiffeners do not necessarily ensure that these stiffeners can develop a "node line" of negligible lateral deflection for a web that is stressed to its postbuckling capacity. It is expected that the AASHTO R_b equation may be

considerably conservative when longitudinal stiffeners are used along with smaller web slenderness ratios within the slender web range. Hence, there is clearly a need to revisit the current AASHTO provisions.

Prior research on longitudinally stiffened girders, and the current AASHTO and Eurocode provisions is discussed in Chapter 2.

1.3 Research Scope

The research encompasses several types of girder cross-sections, loading conditions and limit states. The following summarize the scope of the current research.

1. This research is focused primarily on straight girders.

2. The studies are first conducted on homogenous girders, and then extended to hybrid girders.

3. Tests are subjected to both uniform bending and combined bending and shear. The flexural limit states that are studied are compression flange yielding, lateral torsional buckling (LTB), flange local buckling (FLB) and tension flange yielding (TFY).

1.4 Research Methodology and Challenges

The following section briefly describes the challenges encountered and addressed in various aspects of this research.

1.4.1 Improved R_b Model

This research is aimed at evaluating the impact of longitudinal stiffeners on the flexural resistance (i.e., the resistance of plate girders subjected to general flexural and shear loadings) as well as the requirements on the longitudinal stiffeners to develop the web

5

postbuckling capacity. As such, a comprehensive study is performed to investigate the influence of various design parameters such as the panel aspect ratio (d_o/D), the size of the compression flange relative to the web (A_{fc}/A_w), the web slenderness ratio ($2D_c/t_w$), the area, slenderness and lateral rigidity of the longitudinal stiffeners (A_l, b_l/t_s and I_l), and the position of the longitudinal stiffeners through the web depth (d_s). This is done by means of finite element test simulations using ABAQUS (Simulia 2013). The studies are limited to I-girders with single web longitudinal stiffeners.

The research first focuses on straight homogenous girders at the yield limit state under uniform bending. The term "yield limit state" is used to describe the response corresponding to the plateau in the lateral torsional buckling and flange local buckling resistance curves, for which AASHTO generally characterizes the resistance of the compression flange as R_bF_{yc}. For the yield limit state, the "true R_b" values (R_{bFEA}) are calculated from the test simulations as M_{max}/M_y, where M_y is the girder yield moment determined including the contribution of the longitudinal stiffener to the section modulus of the girder and M_{max} is the maximum girder moment developed in the test. A cross-section model is proposed that predicts the postbuckling flexural capacity of longitudinally stiffened plate girders at the yield limit state and gives estimates comparable to the capacities predicted by the test simulations. This is the first time such a model has been proposed by looking at various cross-section types, and ultimately validated for all potential design limit states.

1.4.2 Flange Local Buckling

The improved R_b model is evaluated for longitudinally stiffened girders with noncompact flanges, with flange slenderness less than 12.0, as limited by AASHTO LRFD Specifications.

1.4.3 Lateral Torsional Buckling

The characterization of the LTB resistance of girders is challenging because of the disconnect between typical FE test simulations and the current Specifications equations. The reasons for this disconnect are evaluated and resolved as part of this research. In doing so, minor modifications to the current LTB resistance equations are proposed. The current equations are fit to a large volume of experimental data (White 2008). This research also takes a fresh look at the experimental data encompassing more recent test results with the proposed modifications to the LTB equations.

The parameter C_b is a moment modifier used in the inelastic and elastic LTB resistance equations of the Specifications. This factor was developed based on elastic buckling solutions. The LTB resistance of girders subjected to combined bending moment and shear poses interesting questions regarding the rationality of using the moment modifier, C_b derived based on such elastic buckling solutions in the inelastic LTB region of the LTB resistance curve. It is shown that rigorous inelastic buckling solutions that account for stiffness reductions, using computational tools such as SABRE2 (White et al. 2015), provide more realistic estimates of the true behavior of girders in the inelastic LTB region.

Potential interaction between FLB and LTB for noncompact flanges within the limits specified by AASHTO is also assessed in the studies.

Another significant contribution of this research is the recommended improvement to the noncompact web slenderness limit, λ_{rw} in the Specifications. It is found that the current equations result in certain types of narrow flange cross-sections to be erroneously classified as noncompact webs, while their true behavior is more akin to slender web cross-sections. The proposed improvement accounts for the relative areas of the compression flange and the web in determining the web classification.

The focus on LTB for homogenous and hybrid girders, with unstiffened and stiffened webs is a major component of this research, and is dealt with in detail in Chapters 6-8.

1.4.4 Hybrid Girders

The research evaluates the performance of the proposed R_b model for straight hybrid girders. The research is restricted to web plates and longitudinal stiffeners with yield strengths only one grade lower than that of the compression flange.

1.4.5 Horizontally Curved Girders

A preliminary evaluation of the proposed R_b model is presented for horizontally curved homogenous girders subjected to uniform bending, designed to fail at the yield limit state.

CHAPTER 2

LITERATURE REVIEW OF LONGITUDINALLY STIFFENED

GIRDER RESEARCH

There have been experimental tests conducted in Europe, Japan and North America during 1950–1980 on longitudinally stiffened girders. The research findings from these tests establish the beneficial effects of web longitudinal stiffeners on the girder resistance, but do not provide a simple design model that explicitly accounts for the contribution of the stiffeners to the girder flexural resistance. The research is however significant in our understanding of the physical behavior of these types of members, and has been discussed in this chapter.

2.1 Earliest Work on Longitudinally Stiffened Plates

Cooper (1963) reviewed the early work done on longitudinally stiffened plate girders, and a brief summary of his review is presented here. Timoshenko (1921) conducted the earliest work on the stability of longitudinally stiffened plates for pure compression and pure shear loading using energy method. The application of this work is in aircraft and ship design. Early research on longitudinally stiffened plate girders was done by Chwalla (1936a; 1936b), Hampl (1937) and Massonnet (1940), who presented discussions on the stability of simply-supported rectangular plates subjected to uniform bending. It was then that Massonet introduced the concept of optimum stiffener rigidity. Minimum stiffener requirements were defined by Kromm (1944) and Chwalla (1944), both of whom considered longitudinally stiffened plates under uniform bending.

Dubas (1948) established that the optimum position of the longitudinal stiffener on a plate subjected to uniform bending is $D/5$. This has since been validated by several other researchers for I-girders, and is the basis of several Specification requirements in both Europe and North America. He also provided buckling coefficients for various combinations of stiffener rigidity and area for this stiffener position. This work was expanded by Kloppel and Scheer (1956) who provided a series of charts that included various stiffener positions and loading conditions for simply-supported longitudinally stiffened rectangular plates.

Subsequent research examined the effects of longitudinal fixity on rectangular plates, and the torsional rigidity of the stiffeners on plate girder resistance. Experimental tests were limited. Longbottom and Heyman (1956) verified the British Specifications using two model tests and two full size tests. Massonet (1960), and Rockey and Leggett (1962) provided the first most extensive series of tests, the results of which are discussed in detail in this chapter.

Most of the prior work was focused on determining the optimum stiffener locations for bending and shear, and the ideal stiffness of the longitudinal stiffener column required to hold a near zero nodal line of deflection until the ultimate load is reached. (The longitudinal stiffener column refers to the combined cross-section that includes the stiffener and a portion of the adjoining web, which together acts as an equivalent column). In satisfying this criterion by providing very rigid stiffeners, various researchers concluded that the stiffeners prevent redistribution of stresses from the web to the compression flange, and the girders may be designed without concern for web bend-buckling. However, as discussed in Section 1.1, the current AASHTO provisions only require the stiffener to

prevent flexing of the web plate under construction loads and service load conditions. The current research establishes the contribution of these minimally sized stiffeners to the flexural resistance of the girders, despite the fact that the lateral deformations of the web plate are not required to be restricted at the ultimate load.

This chapter discusses some of the significant early research on I-girders, which provides an insight into the provisions in AASHTO and Eurocode.

2.2 Massonnet (1960)

Massonet (1960) conducted experimental tests on doubly-symmetric longitudinally stiffened plate girders with D/t_w ranging between 250 and 400, and panel aspect ratios, d_o/D ranging between 0.65 and 1.50. The following were his key findings.

1. He found that $D/5$ is the optimum location for the longitudinal stiffener from the compression flange in a girder with $d_o/D = 1$ and subjected to uniform bending, and that the stiffener should be placed lower down the panel in the presence of shear. This is based on the assumption that the longitudinal edges of the web plate are simply-supported.

2. He developed charts for the optimum stiffener locations based on the ratio of the bending stress to the shear stress at a given panel aspect ratio.

3. He observed, similar to Dubas (1948) that an effective width of the web of $20t_w$ can be used in calculating the moment of inertia of the stiffener. He also noted, however that it was more accurate to calculate the moment of inertia about the neutral axis of the effective stiffener section, instead of along the web centerline, as was the practice at that time.

4. Massonet published charts to calculate the theoretical rigidity of the stiffener required to maintain a zero line of lateral deflection at the location of the stiffener until the ultimate load of the girder is reached. This is a factor over the optimum rigidity to hold the zero line until the critical buckling stress of the plate is reached. The optimum rigidity is primarily a function of the panel aspect ratio, web slenderness, the area of the stiffener, and the depth of the stiffener through the web. Massonet suggested that a rigidity of 7 times the optimum rigidity is required for a stiffener located at the optimum position to facilitate the girder to reach its ultimate strength without load shedding.

5. He also observed that if the flanges of a girder are too flexible, "then when the web plate is loaded beyond its buckling load, the flanges will deflect under the lateral load imposed by the membrane stresses and the transverse deflections of the web will rapidly become excessive." This indicates that web buckling and postbuckling behavior is also dependent on the rigidity of the adjoining flanges.

6. Importantly, he concluded that an increase of 25% in the safety factor can be obtained in the resistance of the girders by virtue of accounting for the longitudinal stiffeners.

2.3 Rockey and Leggett (1962)

Rockey and Leggett studied the optimum location of the longitudinal stiffener for uniform bending when the longitudinal edges are clamped, i.e., the rotation and deflection at the web-compression flange junctures are restrained. They recommended an optimum location of $0.22D$ as opposed to the $0.2D$ for simply-supported edges. They also demonstrated that the required flexural rigidity of the longitudinal stiffener is significantly

reduced under the clamped edge condition. They found that the theoretical critical buckling load of the stiffened plate under the clamped edge conditions was much higher than the solutions derived by Dubas (1948).

2.4 Cooper (1965; 1967)

Cooper's early work was primarily intended to assess the validity of Basler and Thurliman's equation for R_b discussed in Section 1.2 for girders with slenderness ratios of up to 450. He also studied the effects of longitudinal stiffeners on girder flexural and shear resistance. He conducted five bending and eight shear tests on doubly-symmetric girders with D/t_w in the vicinity of 450.

In the flexure tests conducted by Cooper (1965), the longitudinal stiffener was positioned at the optimum location of $D/5$ from the compression flange. All girder parameters except the panel aspect ratios and the size of the longitudinal stiffeners were held constant. Cooper found that while there was an improvement in the deflection control of the longitudinally stiffened web, there was no noticeable increase in the girder ultimate strength. The strengths attained by the longitudinally stiffened girders were practically the same as the girder with no longitudinal stiffener. He concluded that longitudinal stiffeners did not contribute to the flexural resistance of the girders, while observing that Basler's R_b equation for girders without longitudinal stiffeners may be used for webs with slenderness of 450. It is worthwhile to note that there was a local failure in the longitudinal stiffener in addition to compression flange yield and flange vertical buckling in Cooper' uniform bending tests.

He subsequently restated that longitudinal stiffeners when proportioned and positioned properly, can in fact prevent redistribution of stresses to the compression flange and the

girder can attain its ultimate load. This was demonstrated with the aid of an additional test in Cooper (1967). The guidelines given by Cooper form the basis of several Specification requirements currently in AASHTO for sizing and proportioning the longitudinal stiffeners. He proposed that the following proportioning requirements for longitudinal stiffeners be met in order to prevent stress redistribution from the web to the compression flange. In the event that these requirements are not met, he suggested the use of Basler and Thurliman's Eq.1.1 for transversely stiffened girders.

1. He suggested that the stiffener rigidity proposed by Massonnet (1954) given by

$$\gamma_L^* = 3.87 + 5.1\alpha + \left(8.82 + 77.6\delta_L\right)\alpha^2 \tag{2.1}$$

be adopted, where, α is the panel aspect ratio, δ_L is the ratio of the stiffener area to area of the web, and γ_L^* is the ratio of the longitudinal stiffener moment of inertia to the moment of inertia of the web plate.

2. In order to control web deflections up to the ultimate load, he postulated that it was important to ensure the stability of the longitudinal stiffener column, and prevent its failure before the failure of the compression flange column. Thus, the requirement for the lateral buckling stress of the longitudinal stiffener column at a stiffener depth of $D/5$ is given by

$$\left(\frac{\sigma_{cr}}{\sigma_y}\right)_{ls} \geq 0.6\left(\frac{\sigma_{cr}}{\sigma_y}\right)_1 \tag{2.2}$$

where, the left hand side of the equation gives the lateral buckling stress of the stiffener column, and the right hand side gives the lateral buckling stress of the compression flange column.

Cooper suggested that an effective width of the web equal to $20t_w$ be used along with the stiffener in calculating the moment of inertia of the stiffener column through an axis passing through the web-stiffener interface.

Further, Cooper (1965) studied the contribution of the longitudinal stiffeners to the shear strength of the girder and found that longitudinally stiffened girders developed higher shear strengths than those predicted by shear strength theories for transversely stiffened girders. In his tests, he observed the formation of separate tension fields in each individual subpanel. Based on his observations, he recommended that the shear strength of a longitudinally stiffened girder may be calculated by computing the shear strength of each individual sub-panel and summing them algebraically. However, Cooper used relatively rigid longitudinal stiffeners in the shear tests, and does not comment on the validity of assuming a formation of two separate tension fields in every longitudinally stiffened girder subjected to combined bending and shear. It is shown as part of this research in Chapter 9 that when stiffeners are sized to meet minimum AASHTO requirements for controlling web deflections up to service loads, the formation of two separate tension fields is not observed.

In addition, a comparison of the test simulation data to Cooper's model is presented in Section 10.5.1.

2.5 Owen et al. (1970)

Owen et al. (1970) studied the influence of the rigidity of a single sided longitudinal stiffener on the postbuckled behavior of web plates in bending. They positioned the stiffeners at an optimum depth of $0.2D$ from the compression flange, and only varied the size of the longitudinal stiffeners. They tested girders with web slenderness of 750, and

designed the girders such that FLB and LTB were precluded from being possible modes of failure. The following were some of their key observations.

1. They noted that an increase in the stiffener size clearly resulted in an increase in the ultimate load.

2. They observed very large deflections in the vicinity of the ultimate load, which was in the order of 4.5 times the web thickness. However, the lateral deformation of the web at the location of the longitudinal stiffener was practically prevented (deflection of $0.83t_w$) when a very heavy stiffener was used.

3. They noted that a single stiffener located at $0.2D$ from the compression flange on a girder with D/t_w of 300, and girder yield stress of 33ksi can have a buckling stress equal to the yield stress when the stiffener rigidity is about six times the optimum rigidity.

Chapter 4 discusses finite element test simulations on longitudinally stiffened girders, and observes similar trends where a definite increase in strength is observed with an increase in the stiffener rigidity, and a rapid increase in the lateral deflections of the web occurs at load levels close to the ultimate load.

The final failure mode in all the tests discussed above was generally vertical flange buckling after the compression flange had yielded. It is important to note that these tests were conducted on extremely slender webs. Cooper's tests in 1965 failed by premature stiffener buckling.

2.6 Ostapenko and Chern (1971)

Ostapenko and Chern studied the behavior of longitudinally stiffened webs in unsymmetric plate girders. They provided an analytical model for combined bending and shear loading.

In the development of their model, they assumed that two separate tension fields are always formed in each web sub-panel, based on studies by Cooper (1965). They also assumed that the web plates were fixed, rather than simply-supported at the flanges and the longitudinal stiffener. They suggested that in the event of premature failing of the longitudinal stiffener, the girder strength may either be computed by limiting the girder strength to the stiffener failure load or by calculating the strength of the girder as if it had no longitudinal stiffener. Depending on the proportions of the panel and the relative magnitudes of moment and shear, one or the other limit will yield a higher value.

They demonstrated that a substantial increase in strength can be achieved by introducing a longitudinal stiffener for girders subjected to high shear, and high bending moment. They showed that their model predicted experimental test results with reasonable accuracy. However, the model proposed by them involves lengthy and iterative operations, and requires an understanding of the complex behavior of the stiffened girder, and the interaction between the various plate elements along with several underlying assumptions of the model. Their model, as acknowledged by Ostapenko and Chern, is unsuitable for design and normal use.

2.7 Fukumoto and Kubo (1977)

Fukumoto and Kubo (1977) studied the ultimate strength of longitudinally stiffened plate girders when the compression flange is likely to fail by lateral torsional buckling.

They studied two-sided stiffeners placed at $0.2D$ from the compression flange. They recommended a cross-section model with an effective area in compression that includes the compression flange, the longitudinal stiffener, and the web compression zone between them, with an elastic stress distribution between the edges of the effective compression zone. The moment capacity is to be determined as $P_u.h$, where P_u is the maximum strength of the effective cross-section of the beam in compression, obtained by numerical integration techniques with assumed residual stresses and imperfections, and h is the distance between the resultants of the compressive and tensile forces in the cross-section. They found that the longitudinal stiffeners increase the lateral buckling capacity of plate girders. They demonstrated an increase ranging between 10 to 30% on account of using longitudinal stiffeners in the ultimate moment capacities of the girders.

They also observed that one of their tests, which employed a more rigid stiffener but possessed a much higher measured initial lateral imperfection, attained a lower strength, and failed by inelastic LTB. This clearly showed an impact of the magnitude of initial imperfections on the inelastic LTB strength of longitudinally stiffened girders, similar to the trends observed in unstiffened girders.

However, they did not explicitly note the minimum stiffener rigidity that can provide an increase in the lateral stability of such girders.

2.8 AASHTO (2014) Provisions for Longitudinal Stiffeners

This section describes the provisions in the current AASHTO LRFD Specifications that give directions on sizing and proportioning of longitudinal stiffeners. AASHTO Section 6.10.11.3 deals with the provisions on longitudinal stiffeners. The rationale behind these provisions were first explained in Vincent (1969).

18

1. AASHTO 6.10.11.3.1-1:

$$f_s \leq \phi_f R_h F_{ys}$$
(2.3)

where, f_s is the flexural stress in the longitudinal stiffener, ϕ_f is the resistance factor

for flexure, R_h is the hybrid factor, and F_{ys} is the yield strength of the longitudinal

stiffener.

This provision limits the flexural stress in the longitudinal stiffener due to

factored loads at the strength limit state and at construction loads to the yield stress

of the longitudinal stiffener. Yielding of the stiffeners is not permitted as the

stiffeners are required to have sufficient rigidity in order to transmit the stresses in

the longitudinal stiffener column (Cooper 1967). The lateral bending of

longitudinal stiffeners due to eccentricity of the stiffener with respect to the web

plate, and due to horizontal curvature is neglected.

2. AASHTO 6.10.11.3.2-1:

$$b_l \leq 0.48 t_s \sqrt{\frac{E}{F_{ys}}}$$
(2.4)

where, b_l is the projecting width of the longitudinal stiffener, and t_s is the thickness

of the stiffener plate.

Equation 2.4 limits the maximum width to thickness of the longitudinal stiffener

in order to avoid local buckling of the stiffener prior to reaching their yield strength

in uniform axial compression. This provision can be traced back to Ostapenko

(1964).

3. AASHTO 6.10.11.3.3-1:

$$I_l \geq D t_w^3 \left[2.4 \left(\frac{d_o}{D} \right)^2 - 0.13 \right] \beta \tag{2.5}$$

where, I_l is the moment of inertia of the longitudinal stiffener along with an effective width of the adjoining web equal to $18t_w$, calculated along the neutral axis of the combined cross-section. For webs with lower yield strengths than the longitudinal stiffener, the effective width of the web plate adjoining the stiffener is to be reduced by F_{yw}/F_{ys}. The horizontal curvature correction factor, β is taken as 1.0 for straight girders. The effective web width adjoining the stiffener is recommended conservatively as $18t_w$, as opposed to the recommendation of $20t_w$ by Cooper (1967) and Massonet (1960).

Equation 2.5 gives the minimum stiffness required to maintain a near zero line of lateral deflection at the web bend-buckling load level. It is a reasonable fit to the results given by Dubas (1948) for a single sided stiffener placed at an optimum depth of $D/5$ from the compression flange, and a limiting ratio of the stiffener area to the web area, $A_s/A_w = 0.1$. The web bend-buckling resistance of a longitudinally stiffened girder in AASHTO (2014) is given by Frank and Helwig (1995). Since the results from Dubas are based on linear buckling analysis, Equation 2.5 is recommended only for the development of the web bend-buckling resistance. As discussed in the previous sections of this chapter, longitudinal stiffeners of rigidity 6 to 7 times the above limit is required for controlling web deformations up to the ultimate load.

Equation 2.5 neglects the influence of the position of the stiffener through the web depth, and the web depth in compression on the required stiffener rigidity. It has also been conservatively recommended in AASHTO (2014) that the moment of inertia of the longitudinal stiffener be neglected in calculating the girder moment of inertia or section modulus.

4. AASHTO 6.10.11.3.3-2:

$$r \geq \frac{0.16 d_o \sqrt{\dfrac{F_{ys}}{E}}}{\sqrt{1 - 0.6 \dfrac{F_{yc}}{R_h F_{ys}}}} \tag{2.6}$$

where, r is the radius of gyration of the cross-section including the longitudinal stiffener and an effective width of web equal to $18 t_w$, taken about the neutral axis of the combined cross-section. Equation 2.6 is derived by enforcing that the longitudinal stiffener column does not fail by flexural buckling prior to the compression flange developing its yield stress. It is assumed that this equivalent stiffener column fails by inelastic buckling and the traditional CRC column buckling curve is used to obtain the above equation. It is also assumed that the stiffener is positioned at the optimum depth of $D/5$ from the compression flange, and that the stress distribution in the web is linear.

2.9 Eurocode (CEN 2006a) Approach to Calculate Girder Resistance

Eurocode imposes minimum requirements on longitudinal stiffeners that are concerned with preventing torsional buckling. Section 9.2.2 in CEN (2006a) lists the requirements on longitudinal stiffeners. Equation 2.7 (Equation 9.3 in CEN (2006a)) is a criterion for stiffeners with open cross-sections.

$$\frac{I_t}{I_p} \geq 5.3 \frac{f_y}{E} \tag{2.7}$$

where, I_t is the St. Venant torsional constant for the stiffener alone, and I_p is the polar second moment of area of the stiffener alone around the edge fixed to the plate. For an open flat stiffener, the above equation can be simplified as

$$b_l \leq t_s \sqrt{\frac{E}{5.3 F_{ys}}} \tag{2.8}$$

which is more stringent than the requirement in AASHTO, given by Equation 2.4 (Beg et al. 2010).

Eurocode disallows the consideration of discontinuous longitudinal stiffeners (stiffeners that are not connected to either side of transverse stiffeners) in global analysis or in the calculation of stresses. It does, however, allow the longitudinal stiffeners to be considered in the computation of effective sub-panel widths and in the calculation of elastic critical stresses.

The Eurocode design provisions (CEN 2006a) do not use the term R_b to quantify the increased stresses in the compression flange due to web postbuckling per se. They use an explicit effective width approach to account for the behavior of the slender elements of the cross-section.

As illustrated by Figure 2-1, the Eurocode approach involves calculating effective widths of the various sub-panels in a slender web cross-section. The stress distribution in this cross-section is assumed to be elastic and to vary linearly through the effective web depth. The compression flange stress is taken at the yield stress when quantifying the influence of the web post-buckling behavior. The fact that the reduction in the effective area of the web is not as large when the compression flange stress is actually smaller than

22

F_{yc} (e.g., due to lateral torsional buckling or flange local buckling at a stress level less than F_{yc}) is not accounted for in the Eurocode procedures.

In the Eurocode model, the reduced effective plate widths of each web sub-panel are based on the calculated stress distribution in the full panel. The girder effective area includes the area of the longitudinal stiffener. The girder elastic section modulus is calculated based on this reduced effective cross-section and used for subsequent calculations of the member resistance.
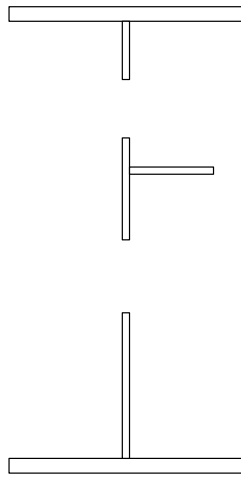
Figure 2-1: Effective cross-section of plate girder as per Eurocode

The principal shortcoming of the effective width approach in Eurocode has been summarized by Johansson and Veljkovic (2009) as " One objection to the effective width method maybe that a plate in compression may show a sharp drop in resistance after the maximum load has been passed. This may be correct for an isolated plate, but if the plate is connected to other plates that have not reached their yield strength, the strains will be controlled by these other plates. This means that the strains will be elastic and small, and the drop in the resistance of the plate that has buckled will be small until the other plates reach their yield strength". This objection is shown to be valid in Chapter 4, where it is

demonstrated that in most girders, where the stiffeners satisfy the minimum rigidity criteria in AASHTO, the girders continue to take load until the stiffeners begin to yield.

In the research reported herein, the effective "R_b" from the Eurocode procedures is calculated as $R_{bEC} = S_{xc.eff}/S_{xc}$, where $S_{xc.eff}$ is the section modulus to the compression flange for the effective elastic cross-section and S_{xc} is the corresponding section modulus for the fully-effective (i.e., the gross) cross-section.

CHAPTER 3

FINITE ELEMENT MODELING OF PLATE GIRDERS

All the tests presented in this dissertation are full nonlinear finite element (FE) simulations using the commercial software ABAQUS (Simulia 2013). This chapter describes the various FE modeling parameters used in this research. A basic verification of the FE simulation results is presented in Appendix E.

3.1 Elements and Mesh Discretization

The plate girder flanges, the web and the longitudinal stiffener are each modeled using four-node shell elements degenerated from a 3D solid element (the S4R shell element in ABAQUS). The S4R element is a general purpose shell element with reduced integration, at a single centroidal integration point, and a large strain formulation. These elements may be used for both thick and thin shells, and are not subject to hourglass effects or transverse shear locking.

The transverse stiffeners are modeled using the B31 beam element in ABAQUS, which is a two-node shear deformable beam element compatible with the S4R shell element. The transverse stiffener plate sizes used in this research are such that beam kinematics are satisfied, and no local distortion effects within the stiffener are observed or studied.

Targeted benchmark studies conducted in this research have found that five integration points through the thickness of the shell elements, using Simpson's rule, provide effectively a fully-converged solution with respect to the order of the integration through the shell thickness. The finite element mesh used is very dense with 60 elements through the web depth, 12 elements across the width of each flange and 10 elements across the

width of the longitudinal stiffener. The finite element meshing of the web and longitudinal stiffener is relatively dense in order to capture the postbuckling behavior with high accuracy, including the consideration of residual stress effects. In the studies focused on LTB response of members with no longitudinal stiffeners, 20 elements through the web depth is deemed sufficient. The number of elements used along the length of the members is selected such that the shell element aspect ratio in the web panels is approximately equal to 1.0 within the test specimens. A mesh discretization study is performed and the selected mesh is found to perform well in terms of the convergence of the finite element solution.

3.2 Boundary Conditions

The girder test specimens plus any test fixtures are simply-supported units in all of the studies conducted in this research, unless noted otherwise. To model a hinge support at the left end of a test specimen, all the displacement degrees of freedom are restrained at the bottom web flange juncture. To model a roller at the right support, the vertical and out-of-plane displacement degrees of freedom are restrained at the bottom web flange juncture, while releasing the axial displacement degree of freedom. Both ends of the girder are restrained against twist by restraining the lateral (out-of-plane) displacements throughout the web height. Warping of the flanges is unrestrained at the simply-supported ends of the tests.

3.3 Material Properties

In this research, the yield stress of the steel, F_y, is taken as 50 ksi for homogenous girders. The longitudinal and transverse stiffeners also are modeled with a yield stress of 50 ksi. In case of hybrid girders, the flanges are modeled with yield strengths of 70 ksi,

while the web is modeled with a yield stress of 50 ksi. The modulus of elasticity, E is taken as 29000 ksi. The material is modeled with a small tangent stiffness within the yield plateau region of $E/1000$ up to a strain-hardening strain of $\varepsilon_{sh} = 10\varepsilon_y$, where ε_y is the yield strain of the material. Beyond this strain, a constant strain-hardening modulus of $E_{sh} = E/50$ is used. The maximum stress reached in the test simulations is significantly less than the ultimate stress of the steel F_u, therefore justifying this common simplified representation of the stress-strain response.

3.4 Nonlinear Analysis using Riks Algorithm

It is essential for the current research, that the girder response past the peak load be captured accurately, in order to fully understand the postbuckling behavior of the girders. The Modified Riks method can be used for unstable postbuckling and geometrically nonlinear responses (Simulia 2013). The Riks method is also useful for problems with material nonlinearity and for obtaining solutions to limit load problems.

The Modified Riks method uses proportional loading, and relies on smooth response of the system (i.e. no bifurcation behavior). While the basic algorithm to solve the equilibrium equations is the Newton method, it incorporates the arc length procedure in tracing the single equilibrium path. It is essential to limit the increment size in order to obtain the correct equilibrium path. The initial increment size is provided by the user, but is automatically adjusted by the algorithm implemented in ABAQUS for subsequent increments depending on the convergence rate and the minimum increment size specified by the user.

3.5 Nominal Residual Stress for Longitudinally Stiffened Girders

The self-equilibrating residual stress pattern shown in Figure 3-1 is based on residual stresses measured by Prawel et al. (1974) in three-plate girder construction without longitudinal stiffeners. This pattern, which has been employed previously by Kim (2010), is taken in this work as a representative nominal residual stress distribution for the flange and web plates of general welded longitudinally stiffened I-girders. This pattern will henceforth be referred to as the Best-Fit Prawel pattern.
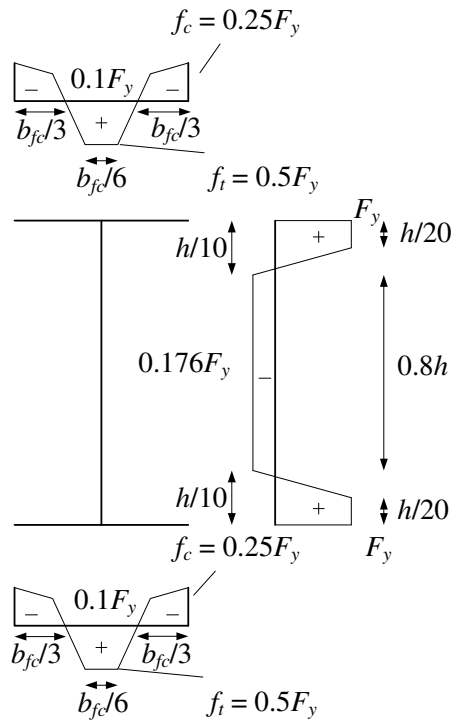
Figure 3-1: Best-Fit Prawel residual stress distribution (Kim, 2010)

The web compressive residual stress shown in the above pattern is 0.176 F_{yw}. However, in these studies and in the studies by Kim (2010), this stress is limited to the web buckling stress under uniform longitudinal compression, calculated assuming idealized simply-supported edge conditions. As such, the web residual stress is typically a small fraction of 0.176 F_{yw}. The web residual stresses are limited in this way because the physical web

cannot be manufactured to develop residual stresses that significantly exceed the web longitudinal buckling stress. The web residual stresses in the heat affected zone of the web, equal to F_{yw} in Figure 3-1, are scaled by the ratio of the above approximation of the web buckling stress under uniform longitudinal compression to 0.176 F_{yw}. This maintains the self-equilibrating nature of the web residual stress pattern.

A self-equilibrating residual stress pattern in the longitudinal stiffener is developed based on the assumption of an initial heat affected zone of $b_l/5$. Figure 3-2 shows the residual stress distribution in the longitudinal stiffener. This pattern is obtained by starting with a representative residual stress pattern where the heat-affected zone has a tensile residual stress equal to F_y and the remainder of the plate has a self-equilibrating residual compression. This base stress pattern makes the total sum of longitudinal forces equal to zero. The elastic flexural stresses necessary to put the plate in moment equilibrium are then added to the above base stresses to create a statically admissible residual stress distribution in the longitudinal stiffener.
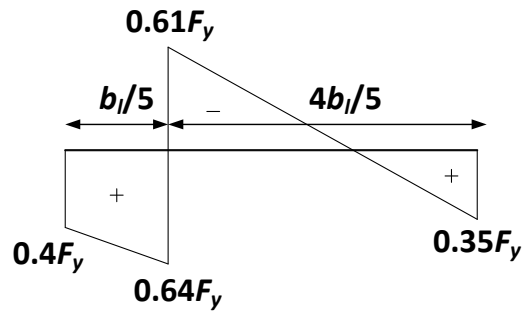
Figure 3-2: Residual stress distribution in longitudinal stiffener

3.6 Geometric Imperfections for Longitudinally Stiffened Girders

To determine the most critical geometric imperfection that may be experienced by the test girders, six base imperfection patterns are studied in ABAQUS for the condition of

uniform bending. Figure 3-3 shows the six base imperfection patterns used in the imperfection sensitivity analyses. The girder dimensions for this study mirror those of the test girder LB3 from Cooper's (1965) experimental tests. The web is 55 inches x 0.125 inches, and the flanges are 12 inches by 0.75 inches in all cases. The yield stress of the flanges is $F_{yc} = F_{yt} = 37$ ksi and the yield stress of the web is $F_{yw} = 34$ ksi. The transverse stiffeners are 3 inches x 0.25 inches and are spaced at $d_o = D$, and the longitudinal stiffener is placed at $d_s = 0.2D$ from the top of the web. Table 3-1 shows four specific variations on the longitudinal stiffeners considered in this study.

Table 3-1: Longitudinal stiffeners used in imperfection sensitivity studies on Cooper's (1965) test LB3

Girder Name	Longitudinal Stiffener Size (in)	Description
1	NA	Girder with no longitudinal stiffener
2	1.75 x 0.125	Cooper's test specimen with the size of longitudinal stiffener set at the maximum b_l/t_s ratio permitted by AASHTO
3	2.5 x 0.125	Cooper's test specimen (LB3)
4	3.5 x 0.25	Same b_l/t_s as Girder 2, but with the longitudinal stiffener cross-section area increased four times.

3.6.1 Imperfection Sensitivity Studies

The imperfection patterns shown in Figure 3-3 are used as the base patterns for the imperfection sensitivity studies. The test simulations are first run using these base imperfection patterns, and the limit load and failure mode is determined from these analyses. The web lateral deflection at the limit load, which is taken as the failure mode pattern, is then scaled as described below to form the actual imperfection for the final test simulation analysis. In other words, the test simulation is run twice; once with the base imperfection patterns shown in Figure 3-3 as the initial geometric imperfection, and then a

second time by using the failure mode from the first analysis, scaled to satisfy the AWS (2010) tolerances on the maximum web out-of-flatness, as the initial imperfection. In the imperfection sensitivity analyses, this process is repeated a third time, by using the failure mode from the second analysis, and again scaling it as an imperfection for a third analysis. It is observed that the failure mode and the limit load do not change significantly by running the analysis a third time. Therefore, the models are only analyzed through the above steps one and two for the subsequent parametric studies discussed in this dissertation. This relatively elaborate procedure is similar to an approach recommended by Hendy and Murphy (2007), and is believed to provide a reasonable estimate of the worst-case geometric imperfections for calculation of the "true R_b" of the test girders.
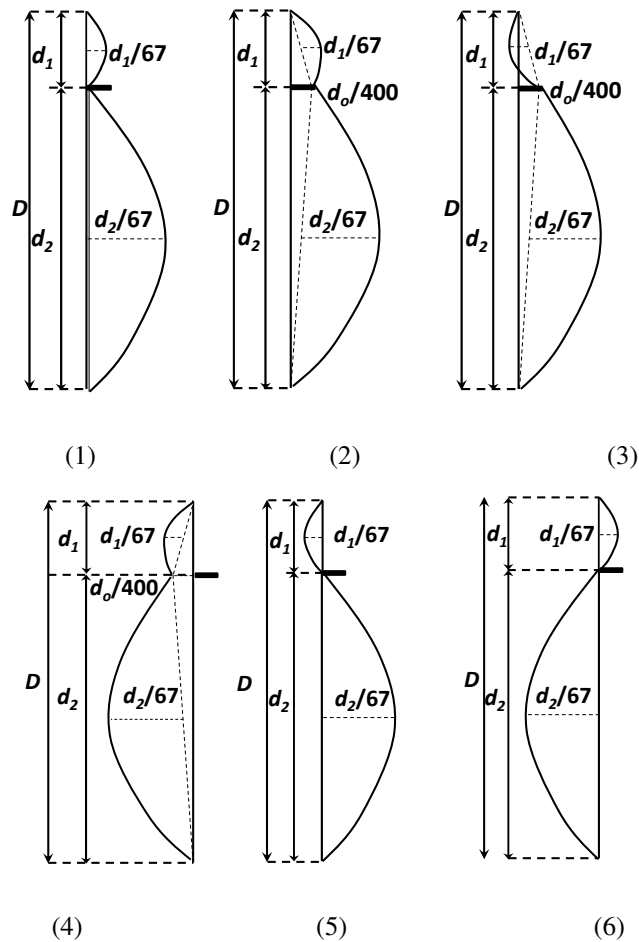
Figure 3-3: Base imperfection patterns on web for first analyses

31

3.6.2 Characteristics Assessed for Imperfection Sensitivity

The following characteristics are assessed as part of the imperfection sensitivity studies:

1. Sensitivity of limit load to the base imperfection pattern.

2. Sensitivity of limit load to the magnitude of the imperfection.

3. Sensitivity of limit load to the web slenderness ratio, D/t_w.

   a. Cooper's test girder LB3 ($D/t_w = 440$) is studied as part of the sensitivity analyses.

   b. A similar girder with a stockier web ($D/t_w = 300$) is also studied, since this is the maximum limit on web slenderness imposed by the AASHTO Specifications.

4. Sensitivity of limit load to the size of the longitudinal stiffener.

   a. As part of assessing the effect of longitudinal stiffener size, girders without longitudinal stiffeners are also studied to understand their behavior relative to the stiffened girders.

   b. Girders with three different sizes of longitudinal stiffeners are studied. The different stiffener sizes are shown in Table 3-1.

The maximum web imperfection allowed by AWS (2010) is 1/67 times the least panel dimension. The imperfection patterns shown in Figure 3-3 are also analyzed using a maximum amplitude of 1/120 of the least panel dimension to assess the sensitivity of the girder resistances to the magnitude of the imperfection.

The longitudinal stiffener is taken to have a maximum sweep of $d_o/400$ in several of the base imperfection patterns shown in Figure 3-3. This sweep is based on

recommendations by Hendy and Murphy (2007) pertaining to the application of the Eurocode 3 EN 1993-2 provisions (CEN 2006b). AWS (2010) does not specify any direct limit on the out-of-straightness of web longitudinal stiffeners.

The failure modes from the analyses are scaled such that the maximum out-of-plane imperfection on the web panel is never greater than $D/67$ (or $D/120$), while also simultaneously ensuring that the maximum deviation from a straight edge measured in each of the web sub-panels is less than $1/67$ (or $1/120$) times its least panel dimension. The scaled failure mode is then seeded as an initial imperfection for the subsequent analysis. Flange initial imperfections (i.e., flange sweep and flange tilt) are not considered in these imperfection sensitivity studies. Only the web geometric imperfections, taken as web displacements relative to a vertical plane through the juncture of the web with the flanges, are considered. Flange sweep and flange tilt imperfections are addressed subsequently in the studies in Section 8.1 and Section 5.2 respectively. The longitudinal stiffeners are taken to follow the profile of the web imperfection without any tilt (the web geometric imperfections generally induce some significant torsional rotation of the longitudinal stiffener however).

Figure 3-4 shows the failure mode profile at the middle of the test panel after the first analysis using imperfection pattern 2 from Figure 3-3. This is scaled as described above and then used as the web imperfection for the final analysis. One should note that there is a measurable lateral deflection at the level of the longitudinal stiffener because of the initial imperfection at the stiffener location, but the longitudinal stiffener restrains the web plate from larger lateral deflections.

Tables 3-2 and 3-3 show the R_b values obtained for Girders 1 through 4, which have an overall web slenderness ratio of D/t_w = 440, with maximum imperfection magnitudes of *D/67* and *D/120*. Since Girder 1 does not have a longitudinal stiffener, it was analyzed with only a single web out-of-flatness corresponding to an overall bowing of the web panel in one direction. This is labeled as imperfection pattern 0 in the table. Table 3-4 shows the R_b values obtained for Girders 1 to 4 using an overall web slenderness ratio of D/t_w = 300 and a maximum imperfection magnitude of *D/67*. Figure 3-5 shows the longitudinal normal stresses at the mid-thickness of the web at the test limit load for Girder 4 with a web slenderness ratio of D/t_w 440 and a maximum imperfection magnitude of *D/67*. This distribution is representative of those obtained for all the girders with different slenderness ratios and maximum imperfection magnitudes.
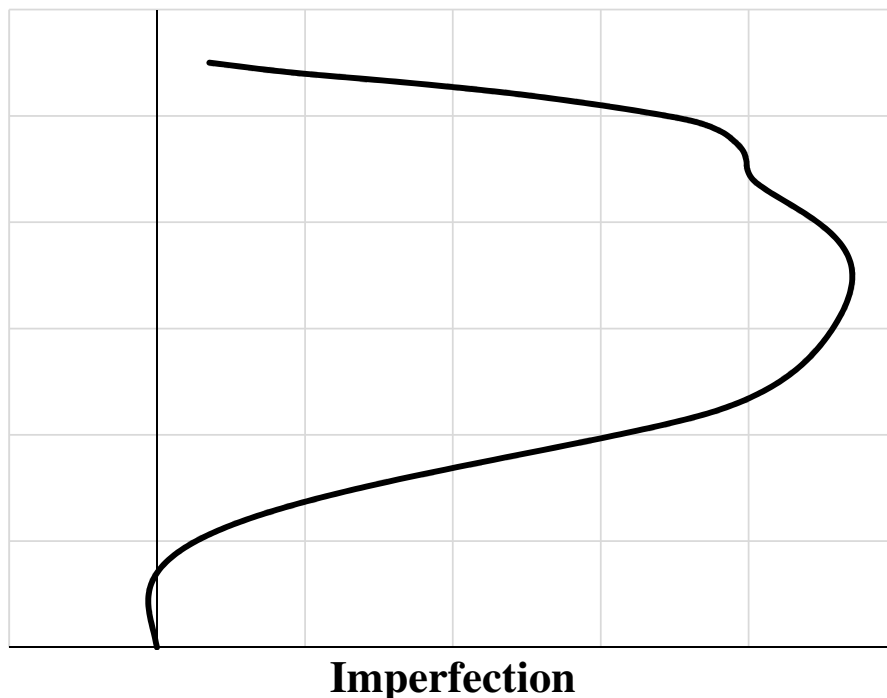
Imperfection

Figure 3-4: Imperfection pattern on web for second analysis (failure mode from first analysis with imperfection 2- Not to Scale)

Table 3-2: R_b for girders in Table 1 with D/t_w =440 with maximum imperfection magnitude $D/67$

Girder	Imperfection							% Difference between Max and Min R_b
	0[*]	1	2	3	4	5	6	
1	0.92	NA	NA	NA	NA	NA	NA	NA
2	NA	0.94	0.94	0.94	0.95	0.94	0.95	1.27
3	NA	0.95	0.94	0.95	0.96	0.97	0.95	2.24
4	NA	1.00	1.01	1.01	1.00	1.01	1.01	0.75

[*] Imperfection 0 is a simple overall bowing of the web panel in one direction, and applies only to Girder 1, which does not have a longitudinal stiffener.

Table 3-3: R_b for Girders 1 to 4 with D/t_w =440 and with maximum imperfection magnitude $D/120$

Girder	Imperfection							% Difference between Max and Min R_b
	0	1	2	3	4	5	6	
1	0.93	NA	NA	NA	NA	NA	NA	NA
2	NA	0.94	0.94	0.94	0.94	0.95	0.94	0.84
3	NA	0.95	0.95	0.98	0.96	0.97	0.95	3.17
4	NA	0.98	0.98	0.99	0.98	0.99	0.99	0.95

Table 3-4: R_b for Girders 1 to 4 with D/t_w =300 and with maximum imperfection magnitude $D/67$

Girder	Imperfection							% Difference between Max and Min R_b
	0	1	2	3	4	5	6	
1	0.91	NA	NA	NA	NA	NA	NA	NA
2	NA	0.94	0.93	0.93	0.93	0.94	0.94	0.58
3	NA	0.95	0.94	0.94	0.96	0.94	0.96	2.23
4	NA	1.00	1.00	1.00	0.99	1.00	1.00	1.19

3.6.3 Choosing the Critical Imperfection Pattern

From the above tables, it can be surmised that the limit load is not sensitive to the base imperfection patterns or the magnitude of the web out-of-flatness, when the flexural limit state is governed by compression flange yielding. This observation is consistent with the findings presented by Jakab et al. (2006) for girders that fail by via a flange yield limit state combined with web bend-buckling. It is also observed that the normal stresses at the mid-thickness of the web are not sensitive to the base imperfection pattern. Figure 3-5 shows

the normal stresses in the web at its mid-thickness in Girder 4 for the different imperfection patterns defined in Figure 3-3. Imperfection 2 is one of several imperfection patterns that typically produce higher web lateral deflections at the location of the longitudinal stiffener, thus tending to place larger demands on the longitudinal stiffener. Imperfection pattern 2 also is similar to the imperfection patterns measured by Vigh and Dunai (2010) for girders with multiple web longitudinal stiffeners. Therefore, this pattern is chosen as the initial base imperfection seed to be used in all the parametric studies for longitudinally stiffened plate girders discussed in this dissertation.
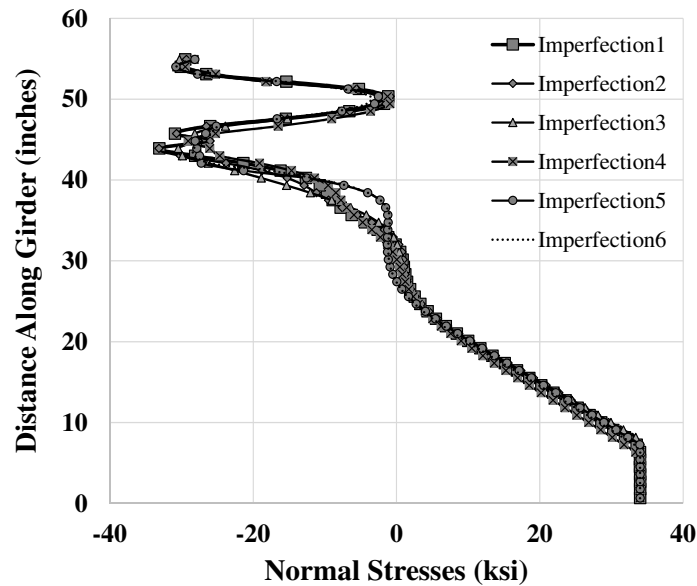
Figure 3-5: Normal stresses in web – Girder 4 with an amplitude of the initial web out-of-flatness of _D_/67

3.7 Residual Stress Patterns and Geometric Imperfections in LTB Studies

Details of sensitivity studies using various residual stress patterns and different magnitudes of imperfections for rolled beams and welded girders with unstiffened webs is given in Chapter 6. The residual stress patterns and imperfections recommended for FE modeling in Chapter 6 is specific to the studies on LTB failure mode.

CHAPTER 4

FLEXURAL RESISTANCE OF STRAIGHT GIRDERS AT THE

YIELD LIMIT STATE

In this chapter, parametric studies are conducted on straight homogenous girders with single longitudinal stiffeners. Various design parameters are evaluated for their impact on the post web buckling flexural capacity of girders at the yield limit state. That is, in these tests, the compression flanges are sized and braced adequately such that Lateral Torsional Buckling (LTB) and Flange Local Buckling (FLB) are not possible modes of failure. As such, the compression flange may be expected to reach the yield stress in the physical tests (the web bend-buckling strength reduction factor R_b reduces the nominal capacity of the compression flange to account for load shedding from the post-buckled web). The studies presented herein are performed under uniform bending load conditions.

4.1   Constant Test Parameters

The following parameters are held constant in all the tests presented in this chapter:

1. The yield stress of all plated elements, F_y, is 50 ksi.

2. The depth of the web panel, D, is taken as 150 inches.

3. A single-size transverse stiffener is designed to meet the AASHTO (2014) minimum requirements for all the tests.

4.2 Variable Test Parameters

To understand the influence of longitudinal stiffeners on the flexural capacity of plate girders in a comprehensive manner, the following parameters are varied to create a suite of tests:

1. D/t_w = 300, 240, 200

2. d_o/D = 0.75,1.0, 1.5, 2.0

3. b_{fc} = $D/6$, $D/5$, $D/4$

4. t_{fc} = 1.5, 1.75, 2.25 corresponding to the three different values of b_{fc}

5. D_c/D = 0.5, 0.625, 0.75

6. A_l/A_{wc}, varied as discussed below

7. I_l, varied as discussed below

8. d_s/D_c = 0.266, 0.40, 0.533

9. b_l/t_s = 0.6 x (AASHTO limit), 1.0 x (AASHTO limit), 1.2 x (AASHTO limit)

where:

D_c = depth of web in compression, calculated based on the gross cross-sectional area neglecting the longitudinal stiffener.

t_w = thickness of web

d_o = distance between transverse stiffeners (panel width)

d_s = location of the longitudinal stiffener relative to the top of the girder web.

b_{fc} = width of compression flange

t_{fc} = thickness of compression flange

A_l = area of cross-section of longitudinal stiffener

A_{wc} = area of web in compression

38

b_l = projecting width of the longitudinal stiffener

t_s = thickness of the longitudinal stiffener

I_l = moment of inertia of the longitudinal stiffener including an effective width of web

(18t_w) taken about the neutral axis of the combined section

In varying the different girder dimensions, the ratios of t_f/t_w is also varied between 2 and 4.5. The parameters A_l/A_{wc} and I_l are varied by designing the longitudinal stiffener to meet the minimum requirements per AASHTO. In all cases, unless noted otherwise, the stiffeners are sized at the maximum b_l/t_s limit. Given this selection, the stiffener size is governed by the AASHTO I_l requirement (AASHTO Eq. 6.10.11.3.3-1). The parameters A_l/A_{wc} and I_l are a function of d_o/D and D/t_w. This process minimizes the area of the longitudinal stiffener while satisfying all the AASHTO LRFD longitudinal stiffener requirements listed in Section 2.8. The range of A_l/A_w studied in this research varies between 0.05 and 0.30.

4.3 Test Setup

The straight girders in this study are subjected to four-point bending with the test specimen subjected to uniform bending and flanked by an end fixture on each side. The end fixtures are designed to develop the flexural strength limit in the test specimens for all of the cases studied. The web and flange plates in the end fixtures are significantly thicker (2 to 3 times) than the plates used in the test specimens. The test setup is similar to that used in Cooper's experiments (Cooper 1965) and is shown in Figure 4-1. The compression flange is compact and is braced adequately such that flange local buckling (FLB) and lateral torsional buckling (LTB) do not have any significant influence on the load capacity in these tests.
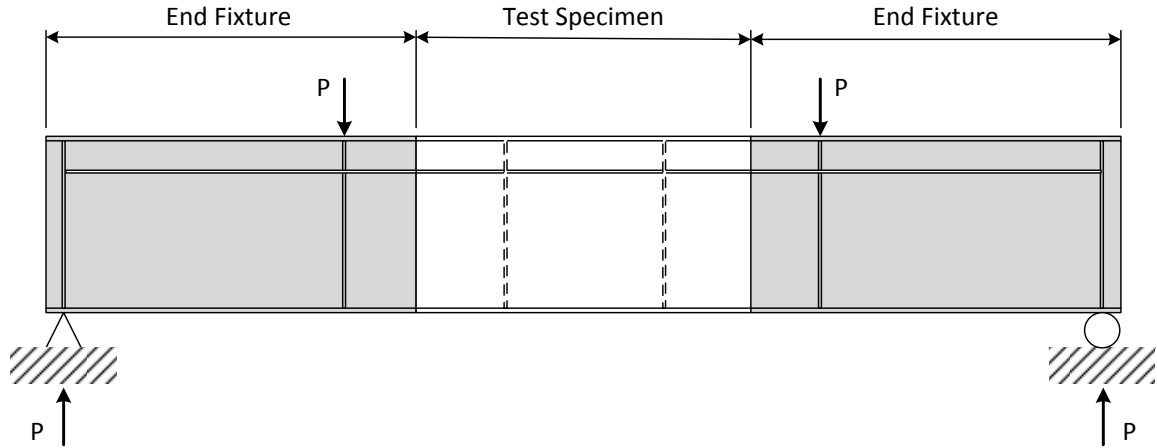
Figure 4-1: Test setup for uniform bending

4.4 Simulation Parameters

The residual stresses and imperfections used in the studies are as described in Sections 3.5 and 3.6.

4.5 Case Studies

The twelve cases defined in Table 4-1 are assessed as part of the parametric studies. Each case corresponds to a specific web panel aspect ratio (d_o/D), a specific approach to sizing of the longitudinal stiffener, and a specific ratio of the depth of the longitudinal stiffener relative to the depth of the web in compression (d_s/D_c). The parameters D_c/D, D/t_w, and b_{fc} and t_{fc} are varied as follows for each of the cases:

- $D_c/D = 0.5$, 0.625 and 0.75,

- $D/t_w = 200$, 240 and 300, and

- $b_{fc} = D/6$, $D/5$ and $D/4$.

- $t_{fc} = 1.5$, 1.75, 2.25 in corresponding to the three values of compression flange width, b_{fc}.

40

For instance, Case 1 is a set of parametric studies with $d_o/D = 1$, the longitudinal stiffener designed to a minimum size based on the AASHTO requirements, and placed at the theoretical optimum position for flexure, $0.4d_s/D_c$ (Dubas 1948; Massonnet 1960). Cases 2, 3, and 4 are comparable studies with $d_o/D = 1.5$, 2, and 0.75 respectively. In addition, the test specimens in Cases 1 through 4 are analyzed without longitudinal stiffeners to assess the relative performance of the girders without longitudinal stiffening.

Table 4-1: Case studies for straight girders at yield limit state

Case	d_o/D	Longitudinal Stiffener	d_s/D_c
1	1	AASHTO min	0.4
2	1.5	AASHTO min	0.4
3	2	AASHTO min	0.4
4	0.75	AASHTO min	0.4
5	1	I_l same as Case 2 $I_l \sim 2.2$ x that for Case 1	0.4
6	1	I_l 3 x that for Case 1	0.4
7	1	AASHTO min	0.533
8	1	AASHTO min	0.266
9	1.5	b_l/t_s 0.6 x that for Case2 I_l same as Case 2	0.4
10	1.5	b_l/t_s 0.6 x that for Case2 I_l 0.7x that for Case 2	0.4
11	1.5	b_l/t_s 1.2 x that for Case2 I_l same as Case 2	0.4
12	1.5	Same as Case 2, Stiffener not continuous	0.4

The longitudinal stiffener sizes for the girders in each case are designed such that they are just sufficient to satisfy the corresponding AASHTO design criteria for I_l, with the exception of Cases 5, 6 and 10. The longitudinal stiffener width-to-thickness ratio, b_l/t_s in Cases 1-8 is set at the maximum limit allowed by the AASHTO provisions, $0.48\sqrt{E/F_{ys}}$.

This decision is combined with setting the stiffener moment of inertia to the limit given by AASHTO Equation (6.10.11.3.3-1), thus resulting in a minimum area of the longitudinal stiffeners unless noted otherwise (i.e., Cases 5, 6 and 10). (For a given moment of inertia, longitudinal stiffeners with larger b_l/t_s have a smaller area.) As alluded to in Section 2.8, Equation 6.10.11.3.3-1 in AASHTO is a theoretical minimum required moment of inertia for the longitudinal stiffeners to be able to hold a "node line" of near zero lateral deflection at incipient bend-buckling of the girder web. Conceptually, this equation does not give a stiffener moment of inertia large enough to restrain the lateral movement of the web in its postbuckled condition. This is the reason for the conservative AASHTO approximation of completely neglecting any contribution of the longitudinal stiffener to the ultimate strength of the girder in situations where the bend-buckling stress of the longitudinally stiffened web is exceeded. It is found that the AASHTO Equation (6.10.11.3.3-2) for the minimum radius of gyration never governs in homogenous girders when the stiffener is sized at the maximum permitted b_l/t_s. The yield strength of the longitudinal stiffeners is taken as $F_{ys} = 50$ ksi in all cases in this research.

It should be noted that the rigidity requirement for the longitudinal stiffener in AASHTO is a function of d_o/D and thus the minimum rigidity requirement for the longitudinal stiffener is greater for larger values of d_o/D. Thus, Cases 2 and 3 employ longitudinal stiffeners with larger area and rigidity than Case 1.

To assess the importance of d_o/D as a parameter, Case 5 is designed with $d_o/D = 1$, but using the same (larger) stiffener size as used in Case 2 (for $d_o/D = 1.5$), thereby making every parameter for every girder in Cases 2 and 5 the same except for d_o/D. The stiffener rigidity in Case 5 is approximately 2.2 times that of the stiffener rigidity in Case 1 for the

same panel aspect ratio. This allows for some investigation of the influence of increasing the longitudinal stiffener size on the girder flexural resistance.

Similarly, Case 6 is designed such that every parameter for every test in Cases 1 and 6 is the same except for the size of the longitudinal stiffener. The longitudinal stiffeners in Case 6 have a rigidity that is three times that of Case 1, while also having a width-to-thickness ratio b_l/t_s equal to the maximum allowed by AASHTO.

The results from Cases 1 through 6 indicate that d_o/D does not impact the flexural resistance of the girders directly. However, d_o/D influences the minimum required size of the longitudinal stiffener, which in turn influences the flexural resistance of the girders. For a larger panel aspect ratio, the minimum required lateral rigidity of the stiffener is larger, and thus the girder flexural capacity is also increased. In accordance with this observation, Cases 7 and 8 are designed with panel aspect ratios of one, and are aimed at evaluating the influence of the longitudinal stiffener position through the web depth. The longitudinal stiffeners are placed below the optimum depth of $0.4D_c$, at $0.533D_c$, in Case 7, while they are placed above the optimum depth, at $0.266D_c$, in Case 8.

Cases 9, 10 and 11 are designed to examine the influence of the slenderness of the longitudinal stiffener (b_l/t_s) on the girder flexural resistance. The panel aspect ratio for these cases is set to 1.5. The stiffener slenderness b_l/t_s in Case 9 is only 0.6 times that of the AASHTO limit used in Case 2. The longitudinal stiffener rigidity in Case 9 and 2 are the same. This allows a direct investigation of the impact of the parameter, b_l/t_s on the girder resistance. Case 10 employs the same ratio of b_l/t_s, while also reducing the stiffener rigidity to a value that is only 0.7 times that of the AASHTO limit used in Cases 2 and 9. This serves the dual purpose of assessing the relative importance of b_l/t_s and I_l on the flexural

resistance of the stiffened girders, while at the same time evaluating the sufficiency of the AASHTO requirement for the stiffener rigidity I_l. Case 11 is designed to gage the consequences of exceeding the b_l/t_s limit in the current AASHTO specifications. The stiffener in Case 11 has a slenderness of 1.2 times that of the maximum allowable limit, while the rigidity is at the minimum value stipulated in the Specifications.

In addition to these 11 cases, an additional case (Case 12) is discussed in Section 4.6.8 that evaluates the integrity of the stiffener in the postbuckling response of the girder, when it is not continuous over the transverse stiffeners.

A 9.5 x ¾ inch transverse stiffener is used for all of the test simulations in these studies. This size satisfies the minimum size requirements from AASHTO for all the girders in all cases. For the constant moment flexure tests addressed in this chapter, where the shear force is zero within the test specimen, the AASHTO transverse stiffener moment of inertia requirements reduce to the value I_{t1} given by AASHTO Equation 6.10.11.1.3-3, supplemented by Equation 6.10.11.1.3-9, which is an additional requirement for transverse stiffeners in longitudinally stiffened webs. The parameter I_{t1} is a theoretical minimum transverse stiffener moment of inertia required to hold a node line of negligible lateral deflection along the length of the transverse stiffeners at incipient shear buckling of the web panels (if the web panels are subjected to shear force). AASHTO Equation 6.10.11.1.3-9 essentially requires that the effective elastic section modulus of the transverse stiffeners must be greater than or equal to $0.333/(d_o/D)$ of the effective elastic section modulus of the longitudinal stiffeners. This requirement stems from the restraining action of the longitudinal stiffeners on the web that cause concentrated reactions at the transverse stiffeners.

In the subsequent studies that focus on the girder resistance under combined moment and shear (Chapter 9), the transverse stiffeners are sized based on the limit I_{t2} from AASHTO Equation 6.10.11.1.3-4. This equation ensures that the transverse stiffeners are able to hold a node line of near zero lateral deflection for all potential shear postbuckling conditions of the web panels. In all cases, the transverse stiffener yield strength is $F_{ys} = 50$ ksi.

The compression flange of the test specimens is braced such that LTB, according to the AASHTO LRFD provisions, does not govern any of the resistances in the studies presented in this chapter. That is, the effective unbraced length of the compression flange, KL_b, is always set such that it is less than L_p in the uniform bending tests presented in this chapter. Furthermore, all the girder flanges are compact. The largest D/b_{fc} considered in this research is 6, which is the limit specified by AASHTO 6.11.2.2-2. Therefore, the girder nominal resistance is the "plateau" resistance on the AASHTO LTB strength curve.

A total of 324 different girder tests are discussed in this chapter.

4.6 Results

The "true R_b" values are calculated from the test simulations as M_{max}/M_y, where M_y is the girder yield moment determined including the contribution of the longitudinal stiffener to the section modulus of the girder and M_{max} is the maximum moment developed in the test. All the girders studied in this chapter have a nominal resistance of M_y per the AASHTO Specifications when $R_b = 1$. The inclusion of the longitudinal stiffener in the girder moment of inertia (I_x) and elastic section modulus (S_{xc}) calculations increases the girder yield moment. The eccentricity of the longitudinal stiffener with respect to the web centerline is neglected in these calculations. That is, it is assumed that the principal axes of

the girder are still parallel to and perpendicular to the web in all cases. It is found that the maximum R_b values from the test simulations, designated henceforth as R_{bFEA} are closer to 1.0 when the longitudinal stiffener is included in the calculation of the girder section modulus as described above, and that they are larger than 1.0 in a number of cases if the contribution of the longitudinal stiffener to S_{xc} is neglected.

Upon a detailed investigation of the girder responses from the tests, the typical failure mode of a longitudinally stiffened homogenous girder designed as per the AASHTO criteria for the yield limit state is as shown in Figure 4-2. At the limit load, the longitudinal stiffener and a portion of the adjacent web are yielded or close to nominal yielding. It is this condition that actually determines the ultimate strength for straight girders designed to fail at the yield limit state. The light shaded contours are locations where the mid-thickness of the plates has yielded.
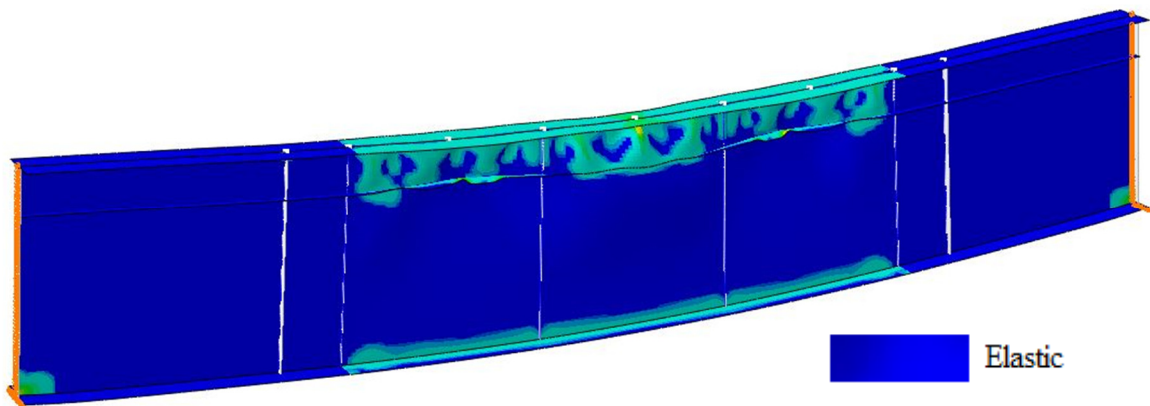
Figure 4-2: Typical snapshot of the failure mode at the limit load of uniform bending tests

4.6.1 Influence of Web and Longitudinal Stiffener Residual Stresses

Case 1 is analyzed twice, once with the residual stress distribution discussed in Section 3.5 and a second time omitting the residual stresses only in the web. Table 4-2 compares the values obtained from these two sets of analyses. The difference in the R_{bFEA} values

obtained is small (less than 0.5% for most cases). This suggests that the web residual stresses have a minor influence on the response. Therefore, the residual stresses in the web (which are small, to begin with) are neglected in the remaining studies.

Case 2 is also analyzed twice, once with the flange and stiffener residual stresses, and another time with only the flange residual stresses, and no residual stresses in the longitudinal stiffener, and with no web residual stresses in either set of analyses. Table 4-3 shows that the case with the residual stresses included often have negligibly higher strengths than the case without the stiffener residual stresses. This is because the welding of the stiffener to the web causes a tensile yield zone at the web-stiffener junction. Since the stiffener is located in the portion of the web that is in compression, this has a mildly beneficial effect on the girder strength. However, such a residual stress distribution as shown in Figure 3-2 is a reasonable assumption, and hence the flange and the longitudinal stiffener residual stresses are included in all of the test simulations.

Table 4-2: R_{bFEA} values for Case 1, comparing the results with full residual stresses and with web residual stresses neglected

(a): $D/t_w = 300$

b_{fc}	D_c/D	W/RS	W/O RS	% DIFF	W/RS	W/O RS	% DIFF
		WITH LONG. STIFFENER			NO LONG. STIFFENER		
D/6	0.50	0.96	0.96	0.62	0.85	0.86	-1.72
	0.625	0.88	0.88	0.58	0.80	0.79	0.67
	0.75	0.83	0.82	1.40	0.76	0.74	1.61
D/5	0.50	0.96	0.96	-0.04	0.87	0.87	0.62
	0.625	0.91	0.90	0.42	0.86	0.84	2.79
	0.75	0.86	0.85	1.02	0.81	0.80	1.17
D/4	0.50	0.98	0.98	0.35	0.92	0.92	0.42
	0.625	0.94	0.94	0.21	0.92	0.90	1.31
	0.75	0.91	0.90	0.47	0.87	0.88	-0.21

(b): $D/t_w = 240$

b_{fc}	D_c/D	W/RS	W/O RS	% DIFF	W/RS	W/O RS	% DIFF
		WITH LONG. STIFFENER			NO LONG. STIFFENER		
D/6	0.50	1.01	1.01	0.10	0.85	0.84	0.32
	0.625	0.93	0.93	-0.04	0.79	0.78	0.85
	0.75	0.86	0.85	1.15	0.75	0.74	1.57
D/5	0.50	1.01	1.01	0.25	0.89	0.88	0.25
	0.625	0.93	0.94	-1.02	0.84	0.83	0.68
	0.75	0.89	0.88	0.55	0.80	0.79	1.21
D/4	0.50	1.01	1.01	0.19	0.93	0.92	1.27
	0.625	0.95	0.95	0.04	0.89	0.89	0.36
	0.75	0.92	0.91	0.15	0.86	0.86	0.66

(c): $D/t_w = 200$

b_{fc}	D_c/D	W/RS	W/O RS	% DIFF	W/RS	W/O RS	% DIFF
		WITH LONG. STIFFENER			NO LONG. STIFFENER		
D/6	0.50	1.03	1.04	-0.62	0.86	0.85	1.39
	0.625	0.99	1.00	0.16	0.79	0.79	0.19
	0.75	0.93	0.93	-0.29	0.75	0.73	1.48
D/5	0.50	1.06	1.03	2.67	0.89	0.88	1.38
	0.625	0.99	1.00	-1.05	0.84	0.83	0.18
	0.75	0.93	0.94	-0.46	0.79	0.80	-0.35
D/4	0.50	1.01	1.04	-3.01	0.93	0.93	0.61
	0.625	1.00	1.00	-0.34	0.90	0.89	0.32
	0.75	0.95	0.955	-0.41	0.86	0.86	0.05

Table 4-3: R_{bFEA} values for Case 2, comparing the results with and without residual stresses in the longitudinal stiffener

(a): $D/t_w = 300$

b_{fc}	D_c/D	W/RS	W/O RS	% DIFF
	0.50	0.99	0.99	0.38
D/6	0.625	0.92	0.94	-1.42
	0.75	0.87	0.86	0.87
	0.50	0.99	0.99	-0.17
D/5	0.625	0.96	0.96	0.25
	0.75	0.90	0.89	0.71
	0.50	1.00	1.00	0.26
D/4	0.625	0.95	0.95	0.29
	0.75	0.93	0.92	0.39

(b): $D/t_w = 240$

b_{fc}	D_c/D	W/RS	W/O RS	% DIFF
	0.50	1.03	1.01	1.94
D/6	0.625	0.97	0.98	-0.74
	0.75	0.92	0.91	0.65
	0.50	1.01	1.01	-0.45
D/5	0.625	0.99	1.00	-1.07
	0.75	0.95	0.94	1.09
	0.50	1.01	1.00	0.88
D/4	0.625	1.00	1.00	-0.13
	0.75	0.95	0.94	1.05

(c): $D/t_w = 200$

b_{fc}	D_c/D	W/RS	W/O RS	% DIFF
	0.50	1.08	1.02	5.76
D/6	0.625	1.02	1.03	-0.70
	0.75	0.96	0.96	-0.13
	0.50	1.01	1.01	0.16
D/5	0.625	1.03	1.03	-0.03
	0.75	0.98	0.97	0.29
	0.50	1.01	1.00	1.19
D/4	0.625	1.03	1.03	-0.07
	0.75	0.99	0.99	-0.05

4.6.2 Comparison of Girders With and Without a Longitudinal Web Stiffener

Figures 4-3 and 4-4 show the normalized lateral displacement of the web relative to the initial imperfect geometry (U/t_w) versus the applied moment as a fraction of the girder yield moment M_y. The displacement U is measured at the mid-length of the test panel and at the section depth corresponding to the longitudinal stiffener. In addition, M_y is calculated neglecting the contribution of longitudinal stiffener to the girder section modulus in these figures. This is done so that the ordinate in both figures is normalized by the same reference moment, allowing comparison of the web lateral deformations of stiffened and unstiffened webs at identical loads. These figures indicate that, at the limit load of the girders with webs that do not have a longitudinal stiffener, the same girder with a longitudinal stiffener tends to have a smaller web lateral deflection (up to 78% smaller) at the location of the stiffener. It is observed that the longitudinal stiffener tends to reduce the lateral deflection more for the stockier webs ($D/t_w = 200$) than for the more slender webs ($D/t_w = 300$). In some cases, at lower load levels, the webs with $D/t_w = 300$ have a larger displacement when the web is stiffened.

The longitudinal stiffeners sized per the minimum AASHTO requirements perform better in terms of restraining the web lateral displacement for the stockier webs than they do for the more slender webs.

The deflections observed at the ultimate load for girders with longitudinal stiffeners are less than $1.0t_w$ for girders with $D/t_w = 200$ and in the order of $1.5t_w$ for girders with $D/t_w = 300$ at the ultimate load, and much smaller than $1.0t_w$ for smaller load levels (service and construction). Previous researchers (Rockey and Leggett 1962) considered deflections of the magnitude $0.8t_w$ to be negligible. In view of this, it is concluded that AASHTO

provisions for minimum stiffener rigidity is sufficient in containing web deflections at service and construction loads, and up to the ultimate load for smaller web slenderness ratios.
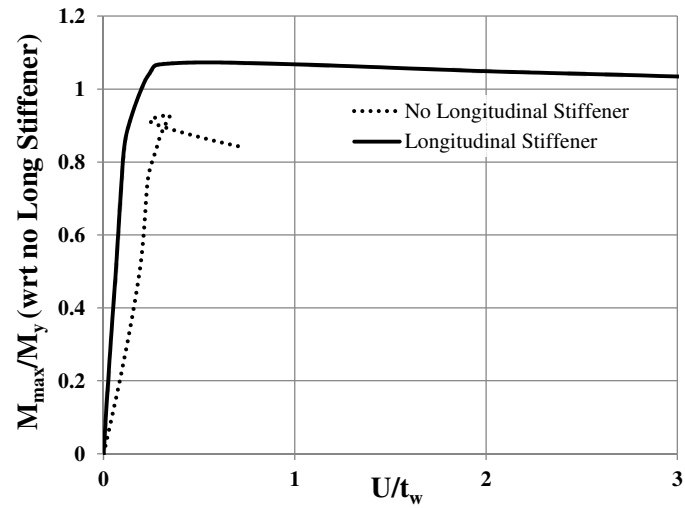
(a) $D_c/D = 0.5$, $D/b_{fc} = 4$
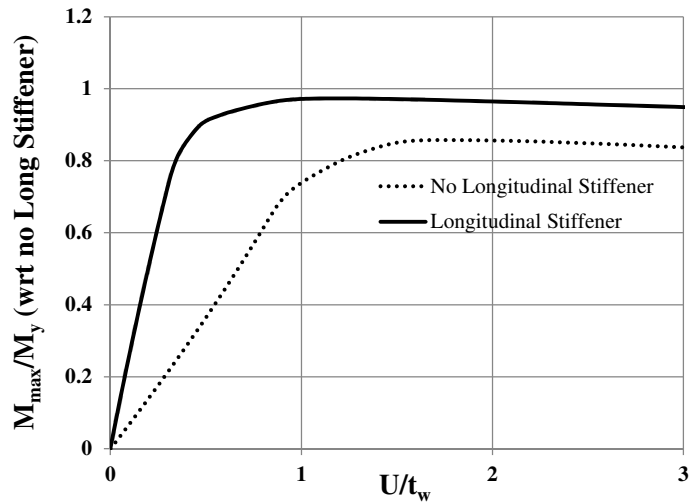
(b) $D_c/D = 0.75$, $D/b_{fc} = 4$

Figure 4-3: Normalized lateral displacement at location of longitudinal stiffener (U/t_w) for $D/t_w = 200$ versus M/M_y, with M_y calculated neglecting the contribution of the longitudinal stiffener (Case1)

51
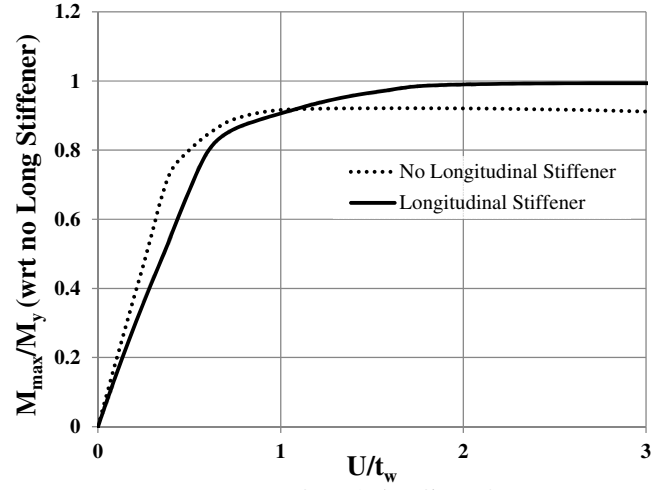
(a) $D_c/D = 0.5$, $D/b_{fc} = 4$
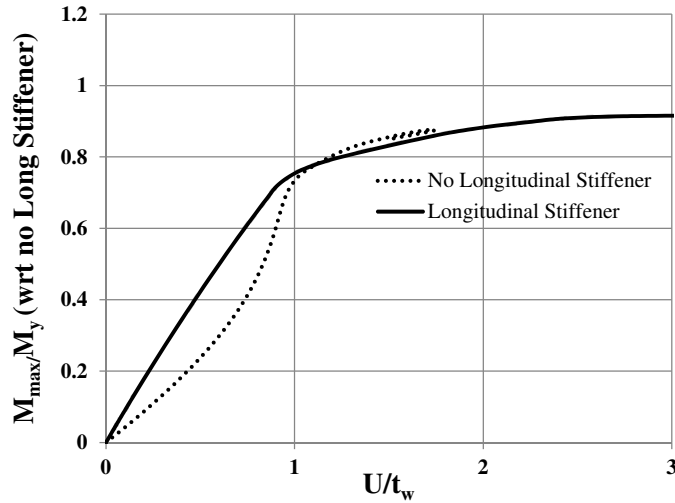
(b) $D_c/D = 0.75$, $D/b_{fc} = 4$

Figure 4-4: Normalized lateral displacement at location of longitudinal stiffener (U/t_w) for $D/t_w = 300$ versus M/M_y, with M_y calculated neglecting the contribution of the longitudinal stiffener (Case1)

4.6.3 Comparison of AASHTO, Eurocode and FE Test Simulations

Tables 4-4 through 4-7 provide R_{bFEA} for Cases 1 ($d_o/D = 1$) and 3 ($d_o/D = 2$) and compare these values with the corresponding resistance ratios estimated from the current AASHTO (2014) and Eurocode EN 1993-1-5 (CEN 2006a) provisions. These tables show results obtained from the FE test simulations for the girders with and without longitudinal stiffeners. The following can be gleaned from these tables.

1. Tables 4-4 and 4-6 show the results for girders with web longitudinal stiffeners.

The results indicate that both AASHTO and Eurocode predict lower strengths than those obtained by the FE test simulations. Although the Eurocode equations also predict lower strengths, they give higher strengths than the AASHTO equations for higher web slenderness ratios.

$R_{bFEA} > R_{bEC} > R_{bAASHTO}$

The Eurocode calculations are conceptually more rigorous, and more elaborate, and take into account the stress states in the web and the stiffener in calculating the plate buckling resistance using cross-section effective plate widths, as detailed in Section 2.9.

For the cases presented in this thesis, the Eurocode provisions predict a smaller R_b for smaller D/t_w values in girders with no longitudinal stiffening. This can be explained physically by the fact that the girders with smaller D/t_w in the current study have the same overall web panel depth, but thicker web plates. Hence, they have larger moments of inertia (I_x), and larger contributions to the moment of inertia from the web, than the girders with larger D/t_w. This increases the value of M_y, but results in a reduction in the values of R_b due to the loss of effectiveness of the web from bend-buckling, based on the Eurocode effective cross-section model. This behavior is confirmed by the FE test simulation results.

2. It is clear that including a longitudinal stiffener always provides an improvement in the flexural resistance of the girders, compared to the corresponding girders without longitudinal stiffeners, although theoretically the minimum size longitudinal stiffeners from AASHTO LRFD are not sufficient to develop more than the initial bend-buckling capacity of the girders.

3. Increasing the ratio of D_c/D or increasing the ratio A_{wc}/A_{fc} results in a reduction in the AASHTO LRFD R_b values. This is also the case with the FE test simulations. The behavior is more pronounced for more slender webs. However, AASHTO significantly under-predicts the true R_b (i.e., R_{bFEA}, as determined by the simulations), particularly for higher D_c/D, both with and without longitudinal stiffeners. The under-predictions range from 9 to 50%. Tables 4-5 and 4-7 show that for high D_c/D ratios of 0.75, $R_{bAASHTO}$ can be significantly conservative even for cases that do not have a longitudinal stiffener. This is due to the fact that the original derivation of R_b by Basler and Thurliman is based largely on the idealized extreme girder geometry discussed previously in Section 1.2 (I-girders with $D/t_w = 360$), and the fact that the equations are more conservative for larger A_{wc}/A_{fc}. The prediction by AASHTO improves for larger b_{fc}/D ratios (i.e., for girders with larger flanges compared to the web).

4. It is observed that the effect of b_{fc}/D on R_b is less substantial than the effect of D_c/D. Both of these variables influence the ratio A_{wc}/A_{fc}, which then has a strong influence on R_b. However, the influence of b_{fc}/D and D_c/D on the physical girder response is more complex than just the influence of these variables on A_{wc}/A_{fc}.

5. It is also observed that the AASHTO predictions are lower for higher ratios of d_o/D (Case 1 vs. Case 3). This can be attributed to the fact that the rigidity of the longitudinal stiffener is higher for the larger d_o/D (Case 3) and that results in the AASHTO equations (which excludes the moment of inertia of the stiffener in the calculation of the girder section modulus) being more conservative.

Table 4-4: R_{bFEA} **values for Case 1 from FE, AASHTO and Eurocode for girders with a web longitudinal stiffener**

(a) $D_c/D = 0.5$

b_{fc}	D/t_w	$R_{bAASHTO}$	R_{bEC}	R_{bFEA}	$R_{bFEA}/R_{bAASHTO}$	R_{bFEA}/R_{bEC}
	300	0.82	0.86	0.96	1.17	1.11
D/6	240	1.00	0.87	1.01	1.01	1.16
	200	1.00	0.90	1.04	1.04	1.16
	300	0.86	0.89	0.96	1.12	1.08
D/5	240	1.00	0.90	1.01	1.01	1.13
	200	1.00	0.92	1.03	1.03	1.13
	300	0.90	0.92	0.98	1.08	1.06
D/4	240	1.00	0.93	1.01	1.01	1.09
	200	1.00	0.94	1.04	1.04	1.11

(b) $D_c/D = 0.625$

b_{fc}	D/t_w	$R_{bAASHTO}$	R_{bEC}	R_{bFEA}	$R_{bFEA}/R_{bAASHTO}$	R_{bFEA}/R_{bEC}
	300	0.70	0.81	0.88	1.26	1.09
D/6	240	0.76	0.81	0.93	1.23	1.15
	200	1.00	0.84	1.00	1.00	1.19
	300	0.76	0.84	0.90	1.20	1.07
D/5	240	0.81	0.85	0.94	1.17	1.11
	200	1.00	0.87	1.00	1.00	1.15
	300	0.83	0.89	0.94	1.13	1.05
D/4	240	0.86	0.89	0.95	1.11	1.07
	200	1.00	0.90	1.00	1.00	1.11

(c) $D_c/D = 0.75$

b_{fc}	D/t_w	$R_{bAASHTO}$	R_{bEC}	R_{bFEA}	$R_{bFEA}/R_{bAASHTO}$	R_{bFEA}/R_{bEC}
	300	0.55	0.76	0.82	1.48	1.07
D/6	240	0.64	0.76	0.85	1.33	1.11
	200	0.71	0.78	0.93	1.31	1.19
	300	0.64	0.81	0.85	1.34	1.06
D/5	240	0.70	0.81	0.88	1.25	1.09
	200	0.76	0.82	0.94	1.24	1.15
	300	0.74	0.91	0.90	1.22	0.99
D/4	240	0.78	0.91	0.91	1.17	1.01
	200	0.82	0.91	0.95	1.16	1.04

Table 4-5: R_{bFEA} **values for Case 1 from FE, AASHTO and Eurocode for girders without a web longitudinal stiffener**

(a) $D_c/D = 0.5$

b_{fc}	D/t_w	$R_{bAASHTO}$	R_{bEC}	R_{bFEA}	$R_{bFEA}/R_{bAASHTO}$	R_{bFEA}/R_{bEC}
	300	0.82	0.78	0.85	1.04	1.09
D/6	240	0.87	0.75	0.84	0.97	1.12
	200	0.91	0.74	0.85	0.93	1.15
	300	0.86	0.83	0.87	1.01	1.05
D/5	240	0.89	0.81	0.88	0.99	1.09
	200	0.93	0.79	0.89	0.96	1.12
	300	0.90	0.88	0.92	1.03	1.05
D/4	240	0.93	0.87	0.92	1.00	1.06
	200	0.95	0.86	0.93	0.98	1.09

(b) $D_c/D = 0.625$

b_{fc}	D/t_w	$R_{bAASHTO}$	R_{bEC}	R_{bFEA}	$R_{bFEA}/R_{bAASHTO}$	R_{bFEA}/R_{bEC}
	300	0.70	0.72	0.79	1.14	1.10
D/6	240	0.76	0.69	0.79	1.03	1.14
	200	0.82	0.67	0.79	0.97	1.18
	300	0.76	0.78	0.84	1.11	1.07
D/5	240	0.81	0.75	0.83	1.04	1.11
	200	0.85	0.72	0.79	0.94	1.10
	300	0.83	0.69	0.79	0.95	1.14
D/4	240	0.86	0.67	0.79	0.92	1.18
	200	0.89	0.78	0.84	0.94	1.07

(c) $D_c/D = 0.75$

b_{fc}	D/t_w	$R_{bAASHTO}$	R_{bEC}	R_{bFEA}	$R_{bFEA}/R_{bAASHTO}$	R_{bFEA}/R_{bEC}
	300	0.55	0.68	0.75	1.36	1.11
D/6	240	0.64	0.65	0.75	1.17	1.16
	200	0.71	0.62	0.75	1.05	1.20
	300	0.64	0.75	0.81	1.27	1.08
D/5	240	0.70	0.72	0.80	1.14	1.12
	200	0.76	0.69	0.80	1.05	1.15
	300	0.74	0.82	0.87	1.18	1.06
D/4	240	0.78	0.80	0.86	1.10	1.08
	200	0.82	0.78	0.86	1.05	1.11

Table 4-6: R_{bFEA} values for Case 3 from FE, AASHTO and Eurocode for girders with a web longitudinal stiffener

(a) $D_c/D = 0.5$

b_{fc}	D/t_w	$R_{bAASHTO}$	R_{bEC}	R_{bFEA}	$R_{bFEA}/R_{bAASHTO}$	R_{bFEA}/R_{bEC}
	300	0.82	0.86	1.00	1.22	1.17
D/6	240	1.00	0.88	1.05	1.05	1.19
	200	1.00	0.90	0.99	0.99	1.09
	300	0.86	0.89	1.00	1.17	1.13
D/5	240	1.00	0.90	1.00	1.00	1.11
	200	1.00	0.92	1.03	1.03	1.12
	300	0.90	0.92	1.00	1.11	1.09
D/4	240	1.00	0.93	0.99	0.99	1.06
	200	1.00	0.94	1.04	1.04	1.11

(b) $D_c/D = 0.625$

b_{fc}	D/t_w	$R_{bAASHTO}$	R_{bEC}	R_{bFEA}	$R_{bFEA}/R_{bAASHTO}$	R_{bFEA}/R_{bEC}
	300	0.70	0.80	0.94	1.35	1.17
D/6	240	0.76	0.82	1.00	1.31	1.22
	200	1.00	0.84	1.04	1.04	1.23
	300	0.76	0.84	0.98	1.29	1.16
D/5	240	0.81	0.85	1.01	1.26	1.19
	200	1.00	0.87	1.04	1.04	1.20
	300	0.83	0.89	0.99	1.19	1.11
D/4	240	0.86	0.89	1.01	1.17	1.13
	200	1.00	0.90	1.04	1.04	1.15

(c) $D_c/D = 0.75$

b_{fc}	D/t_w	$R_{bAASHTO}$	R_{bEC}	R_{bFEA}	$R_{bFEA}/R_{bAASHTO}$	R_{bFEA}/R_{bEC}
	300	0.55	0.76	0.89	1.61	1.17
D/6	240	0.64	0.77	0.95	1.48	1.23
	200	0.71	0.79	1.00	1.40	1.27
	300	0.64	0.81	0.91	1.43	1.13
D/5	240	0.70	0.81	0.96	1.37	1.19
	200	0.76	0.82	1.00	1.31	1.21
	300	0.74	0.86	0.93	1.26	1.08
D/4	240	0.78	0.86	0.98	1.25	1.14
	200	0.82	0.87	1.01	1.23	1.16

Table 4-7: R_{bFEA} values for Case 3 from FE, AASHTO and Eurocode for girders without web a longitudinal stiffener

(a) $D_c/D = 0.5$

b_{fc}	D/t_w	$R_{bAASHTO}$	R_{bEC}	R_{bFEA}	$R_{bFEA}/R_{bAASHTO}$	R_{bFEA}/R_{bEC}
	300	0.82	0.78	0.82	1.01	1.06
D/6	240	0.87	0.75	0.83	0.96	1.10
	200	0.91	0.74	0.82	0.90	1.11
	300	0.86	0.83	0.87	1.01	1.05
D/5	240	0.89	0.81	0.88	0.99	1.09
	200	0.93	0.79	0.86	0.93	1.09
	300	0.90	0.88	0.93	1.03	1.05
D/4	240	0.93	0.87	0.92	1.00	1.06
	200	0.95	0.86	0.93	0.98	1.09

(b) $D_c/D = 0.625$

b_{fc}	D/t_w	$R_{bAASHTO}$	R_{bEC}	R_{bFEA}	$R_{bFEA}/R_{bAASHTO}$	R_{bFEA}/R_{bEC}
	300	0.70	0.72	0.78	1.12	1.08
D/6	240	0.76	0.69	0.76	0.99	1.09
	200	0.82	0.67	0.75	0.92	1.12
	300	0.76	0.78	0.84	1.12	1.08
D/5	240	0.81	0.75	0.81	1.01	1.08
	200	0.85	0.73	0.81	0.95	1.10
	300	0.83	0.85	0.90	1.08	1.06
D/4	240	0.86	0.83	0.88	1.02	1.06
	200	0.89	0.81	0.87	0.98	1.08

(c) $D_c/D = 0.75$

b_{fc}	D/t_w	$R_{bAASHTO}$	R_{bEC}	R_{bFEA}	$R_{bFEA}/R_{bAASHTO}$	R_{bFEA}/R_{bEC}
	300	0.55	0.68	0.74	1.35	1.09
D/6	240	0.64	0.65	0.73	1.13	1.12
	200	0.71	0.62	0.71	1.00	1.14
	300	0.64	0.75	0.80	1.26	1.07
D/5	240	0.70	0.72	0.80	1.14	1.12
	200	0.76	0.69	0.77	1.02	1.12
	300	0.74	0.82	0.87	1.17	1.05
D/4	240	0.78	0.80	0.86	1.11	1.08
	200	0.82	0.78	0.84	1.03	1.09

Table 4-8 shows values of R_{bFEA} obtained for girders with longitudinal stiffeners (the primary focus of this research), with the cases arranged in the order of increasing longitudinal stiffener size (to emphasize the importance of this parameter). The b_l/t_s for all these cases are approximately 11.5. The values in each subsequent row of the table indicate an increase in R_b for larger stiffener sizes. The longitudinal stiffeners are located at the optimum position for flexure ($d_s/D_c = 0.4$) in the 162 tests shown in this table.

4.6.4 Impact of Panel Aspect Ratio

In Table 4-8, the difference in values of R_{bFEA} between Cases 2 and 5 is small (1 to 2%). Figure 4-5 shows the web lateral deflection at the depth of the longitudinal stiffener versus the load level for these cases with $D_c/D = 0.75$ and $D/b_{fc} = 4$, for $D/t_w = 200$ and 300. The only difference between Cases 2 and 5 is the value of d_o/D. These two cases use the same girder and stiffener dimensions. While the stiffener size used in these cases is the minimum as required for Case 2 ($d_o/D = 1.5$), it is much larger than the minimum requirements per AASHTO for Case 5 ($d_o/D = 1$). These results indicate, as would be expected, that d_o/D plays a negligible role in influencing the R_b value.
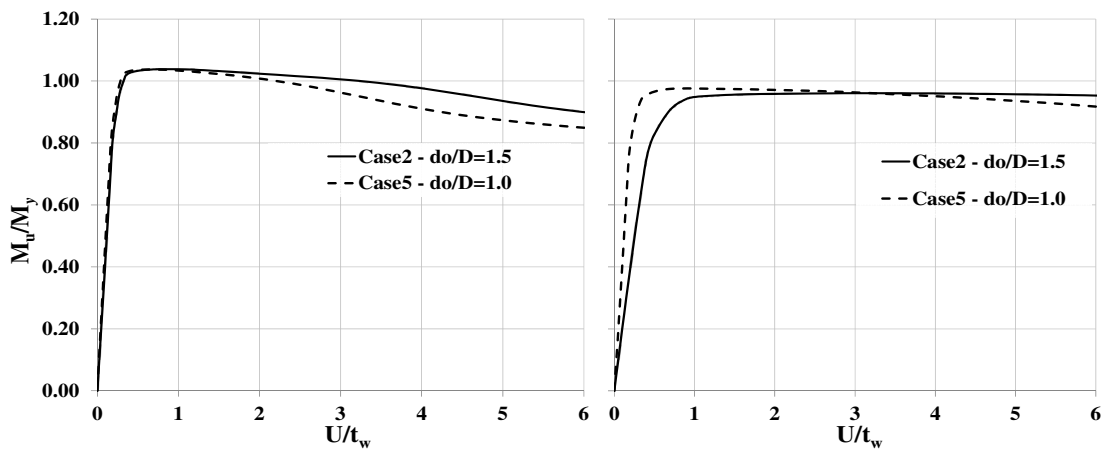
Figure 4-5: **Normalized load vs lateral deflection at location of longitudinal stiffener (U/t_w) for $D/t_w = 200$ (left) and $D/t_w = 300$ (right), Cases 2 and 5 with $D_c/D = 0.75$ and $D/b_{fc} = 4$**

59

Table 4-8: R_{bFEA} values for Cases 1 through 6, arranged in increasing order of longitudinal stiffener size

(a) $D/t_w = 300$

Case	A_l	I_l	D_c/D =0.5, b_{fc}= D/6	D_c/D= 0.625, b_{fc}= D/6	D_c/D= 0.75, b_{fc}= D/6	D_c/D =0.5, b_{fc}= D/5	D_c/D= 0.625, b_{fc}= D/5	D_c/D= 0.75, b_{fc}= D/5	D_c/D= 0.5, b_{fc}= D/4	D_c/D= 0.625, b_{fc}= D/4	D_c/D= 0.75, b_{fc}= D/4
4	2.77	23.78	0.93	0.86	0.81	0.95	0.89	0.85	0.97	0.93	0.90
1	4.38	49.15	0.96	0.88	0.82	0.96	0.90	0.85	0.98	0.94	0.90
2	6.85	105.33	0.99	0.92	0.87	0.99	0.96	0.90	1.00	0.95	0.93
5	6.85	105.33	1.00	0.94	0.88	1.00	0.98	0.90	1.00	0.99	0.92
6	7.72	127.70	1.00	0.95	0.90	1.01	0.96	0.91	1.01	0.97	0.94
3	9.56	180.87	1.01	0.97	0.91	1.01	0.97	0.93	1.01	0.98	0.95

(b) $D/t_w = 240$

Case	A_l	I_l	D_c/D =0.5, b_{fc}= D/6	D_c/D= 0.625, b_{fc}= D/6	D_c/D= 0.75, b_{fc}= D/6	D_c/D =0.5, b_{fc}= D/5	D_c/D= 0.625, b_{fc}= D/5	D_c/D= 0.75, b_{fc}= D/5	D_c/D= 0.5, b_{fc}= D/4	D_c/D= 0.625, b_{fc}= D/4	D_c/D= 0.75, b_{fc}= D/4
4	3.75	45.50	0.98	0.90	0.84	0.99	0.92	0.87	0.99	0.95	0.91
1	5.60	88.07	1.01	0.93	0.85	1.01	0.94	0.88	1.01	0.95	0.91
2	9.08	195.01	1.03	0.97	0.92	1.01	0.99	0.95	1.01	1.01	0.95
5	12.99	351.64	1.05	1.00	0.94	1.00	1.01	0.95	0.99	1.01	0.97
6	9.08	195.01	1.03	1.00	0.93	1.04	1.00	0.95	1.03	1.01	0.97
3	10.51	249.46	1.02	1.01	0.95	1.01	1.01	0.96	1.03	1.02	0.97

(c) $D/t_w = 200$

Case	A_l	I_l	D_c/D =0.5, b_{fc}= D/6	D_c/D= 0.625, b_{fc}= D/6	D_c/D= 0.75, b_{fc}= D/6	D_c/D =0.5, b_{fc}= D/5	D_c/D= 0.625, b_{fc}= D/5	D_c/D= 0.75, b_{fc}= D/5	D_c/D= 0.5, b_{fc}= D/4	D_c/D= 0.625, b_{fc}= D/4	D_c/D= 0.75, b_{fc}= D/4
4	4.88	79.32	1.03	0.96	0.89	1.02	0.97	0.91	1.02	0.98	0.94
1	7.20	149.08	1.04	1.00	0.93	1.03	1.00	0.94	1.04	1.00	0.95
2	11.68	335.93	1.08	1.02	0.96	1.01	1.03	0.98	1.01	1.03	0.99
5	16.64	603.70	0.99	1.04	0.98	1.03	1.04	0.99	1.04	1.04	1.01
6	11.68	335.93	1.02	1.04	0.98	1.06	1.04	0.99	1.05	1.04	1.00
3	13.53	430.72	1.01	1.05	0.99	1.07	1.06	1.00	1.05	1.05	1.00

4.6.5 Impact of Stiffener Rigidity

From Table 4-8 , it is observed that as the size of the longitudinal stiffener is increased, a larger value of R_{bFEA} is obtained. When the size of the longitudinal stiffener is increased to three times the minimum required lateral rigidity per AASHTO (Case 6), the value of R_{bFEA} is increased only 5 to 7%.

Figure 4-6 compares the applied moment versus the normalized web lateral deflection for two different Case 6 and Case 5 girders versus the corresponding Case 1 girders. The R_{bFEA} obtained for stiffeners with three times the minimum lateral rigidity (Case 6) is not significantly larger than for stiffeners having approximately two times the minimum lateral rigidity (Case 5). This is an indication that, while it may be beneficial to increase the stiffener rigidity to some extent from the current AASHTO minimum requirements, there are diminishing returns as the stiffener size is made larger and larger.

It is also observed from Figure 4-6 that for stiffeners with approximately twice the minimum AASHTO requirement (Case 5), the lateral web deflection at the location of the stiffener is practically restrained (approximately $0.5t_w$) at the limit load.

It is noteworthy that significant improvements over the current AASHTO provisions, which neglect the contribution of the longitudinal stiffener to the flexural resistance of the girder in the postbuckling range of the response, are obtained by determining the "true R_b" even using the current AASHTO minimum size longitudinal stiffener. However, as stated above, beyond a certain size of the longitudinal stiffener, no significant increase in R_{bFEA} is obtained. That is, the "law of diminishing returns" applies.

A brief study on the effect of using a stiffener with lower rigidity that the AASHTO minimum is discussed in Section 4.6.7.
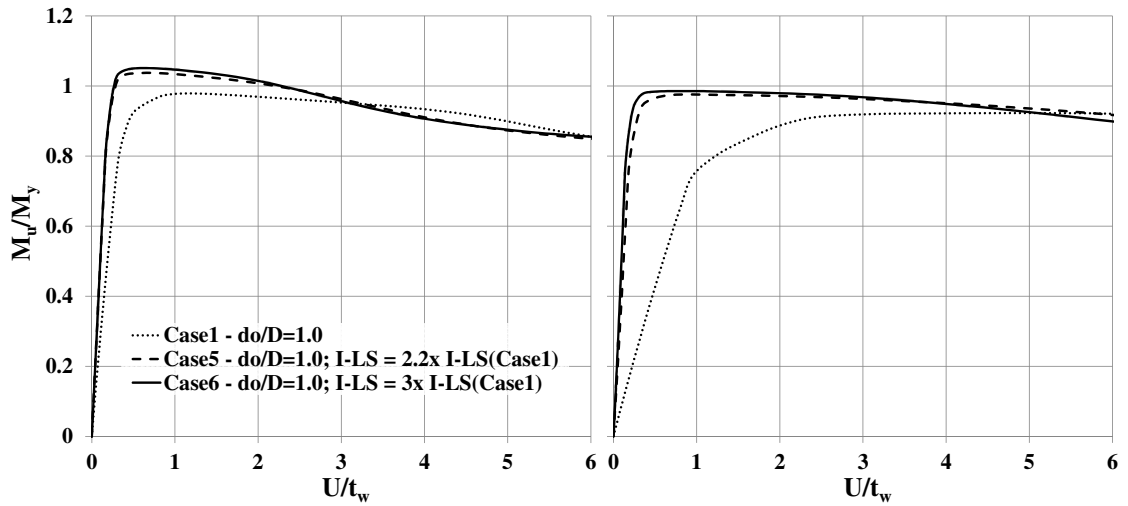
Figure 4-6: Normalized load vs lateral deflection at location of longitudinal stiffener for $D/t_w = 200$ (left) and $D/t_w = 300$ (right), Cases 1, 5 and 6 with $D_c/D = 0.75$ and $D/b_{fc} = 4$

4.6.6 Impact of Stiffener Position along Web Depth

Table 4-9 compares the results for another 54 longitudinally stiffened girder tests from Cases 7 and 8, with $d_s/D_c = 0.533$ and 0.266, to the corresponding results from Case 1. All of the tests considered in Table 4-9 have $d_o/D = 1$.

It is observed that the position of the stiffener slightly influences the overall flexural capacity of the girders. It is observed that when the longitudinal stiffener is positioned lower through the web depth, the girder flexural capacity marginally increases. This can be explained from the observation in Figure 4-2 that the lowered position of the longitudinal stiffener delays the progression of yielding within stiffener and the adjacent portion of the web panel. However, Table 4-9 shows that this effect is relatively small.

62

Table 4-9: R_{bFEA} values for girders with d_o/D=1 and different positions of a minimum size longitudinal stiffener per AASHTO LRFD

D/t_w = 300	d_s/D_c	D_c/D =0.5, b_{fc}= D/6	D_c/D= 0.625, b_{fc}= D/6	Dc/D= 0.75, bfc= D/6	D_c/D =0.5, b_{fc}= D/5	D_c/D= 0.625, b_{fc}= D/5	D_c/D= 0.75, b_{fc}= D/5	D_c/D =0.5, b_{fc}= D/4	D_c/D= 0.625, b_{fc}= D/4	D_c/D= 0.75, b_{fc}= D/4
Case1	0.40	0.96	0.88	0.82	0.96	0.90	0.85	0.98	0.94	0.90
Case7	0.53	0.96	0.90	0.85	0.98	0.95	0.89	0.99	0.95	0.92
Case8	0.26	0.93	0.87	0.82	0.95	0.90	0.86	0.97	0.94	0.91

D/t_w = 240	d_s/D_c	D_c/D =0.5, b_{fc}= D/6	D_c/D= 0.625, b_{fc}= D/6	Dc/D= 0.75, bfc= D/6	D_c/D =0.5, b_{fc}= D/5	D_c/D= 0.625, b_{fc}= D/5	D_c/D= 0.75, b_{fc}= D/5	D_c/D =0.5, b_{fc}= D/4	D_c/D= 0.625, b_{fc}= D/4	D_c/D= 0.75, b_{fc}= D/4
Case1	0.40	1.01	0.93	0.85	1.01	0.94	0.88	1.01	0.95	0.91
Case7	0.53	0.99	0.97	0.89	1.01	0.99	0.91	1.02	0.98	0.94
Case8	0.26	0.95	0.89	0.84	0.97	0.92	0.87	0.98	0.95	0.91

D/t_w = 200	d_s/D_c	D_c/D =0.5, b_{fc}= D/6	D_c/D= 0.625, b_{fc}= D/6	Dc/D= 0.75, bfc= D/6	D_c/D =0.5, b_{fc}= D/5	D_c/D= 0.625, b_{fc}= D/5	D_c/D= 0.75, b_{fc}= D/5	D_c/D =0.5, b_{fc}= D/4	D_c/D= 0.625, b_{fc}= D/4	D_c/D= 0.75, b_{fc}= D/4
Case1	0.40	1.04	1.00	0.93	1.03	1.00	0.94	1.04	1.00	0.95
Case7	0.53	1.02	1.00	0.93	1.04	1.00	0.94	1.03	1.01	0.97
Case8	0.26	0.98	0.92	0.87	0.99	0.94	0.90	1.00	0.96	0.93

4.6.7 Impact of Longitudinal Stiffener Width-to-Thickness Ratio

Cases 9, 10 and 11 as described in Section 4.4 are designed to study the influence of the width-to-thickness ratio of the longitudinal stiffener plate on the girder flexural strength. The results from Case 2 are reproduced here, as a benchmark case for comparing the results in this section. Case 2 has a d_o/D of 1.5, same as in Cases 9, 10, and 11, and with the longitudinal stiffener designed to meet the limits of the AASHTO requirements. The longitudinal stiffener sizes used in Cases 9, 10 and 11 are duplicated in Table 4-10.

Table 4-10: Summary of stiffener parameters used in Cases 9, 10, and 11

Long. Stiffener	Case 9	Case 10	Case 11
b_l/t_s	0.6 x (Case 2)	0.6 x (Case 2)	1.2 x (Case 2)
I_l	1.0 x (Case 2)	0.7 x (Case 2)	1.0 x (Case 2)

Table 4-11 compares the test results for these three cases along with the results from Case 2. The following can be gleaned from the table.

1. There is negligible difference in girder strengths between Cases 2, and 9, i.e. for a given moment of inertia that satisfies the AASHTO rigidity criteria, the width-to-thickness ratio of the longitudinal stiffener has little influence on the overall flexural capacity of the girder. Figure 4-7 shows the load-deflection responses for two girders with stiffeners designed as per Cases 2 and 9. It is interesting to note that, while the ultimate load carrying response of the girders are essentially the same, the response of the girders in Case 9 is less stiff than the girders in Case 2. This can be attributed to the fact that the longitudinal stiffener column in Case 9 is more slender than the one in Case 2 (the girders in Case 9 have the same rigidity as in Case 2, but have a smaller b_l/t_s and hence have a larger area, and thereby a smaller radius of gyration). Thus, the stiffener column in Case 9 is less stiff in the lateral direction.

2. The results for Case 10 help examine the consequence of using a stiffener that does not satisfy the minimum rigidity requirement in AASHTO (2014). It is observed from Table 4-11 that strengths obtained in Case 10 is lower than the strengths obtained in Case 9. This observation corroborates the discussion in Section 4.6.5 where it was established that the girder strength is sensitive to the lateral stiffness

of the longitudinal stiffener column. Figure 4-8 shows the difference in the load-deflection response between Cases 9 and 10. It is clear that using a stiffener with a rigidity of only 70% of the minimum stipulated requirement in AASHTO does not hold a near zero line of web lateral deflection at the location of the longitudinal stiffener. This also implies that, when the stiffener rigidity requirement is not met, R_b cannot be taken as 1.0 at service or construction load conditions.

$D/t_w = 300$, $D_c/D = 0.50$ and $D/b_{fc} = 6$ (left) and $D/t_w = 300$, $D_c/D = 0.75$ and $D/b_{fc} = 6$ (right)
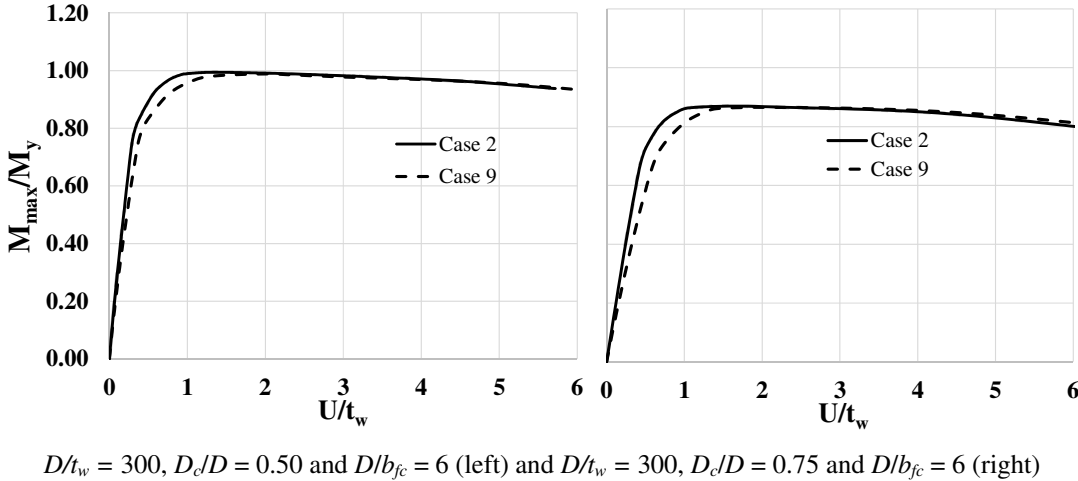
Figure 4-7: Normalized load vs lateral deflection at location of longitudinal stiffener Cases 2 and 9

$D/t_w = 300$, $D_c/D = 0.50$ and $D/b_{fc} = 6$ (left) and $D/t_w = 300$, $D_c/D = 0.75$ and $D/b_{fc} = 6$ (right)
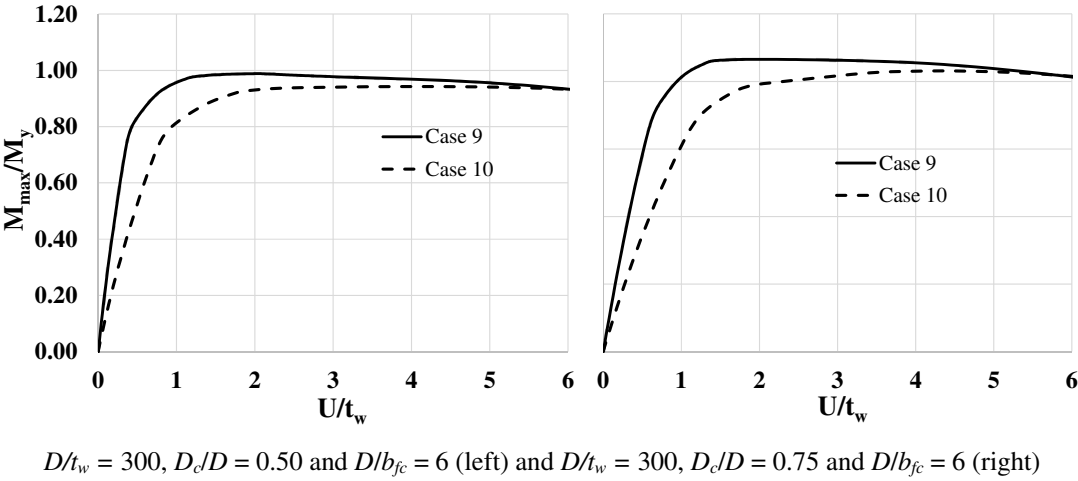
Figure 4-8: Normalized load vs lateral deflection at location of longitudinal stiffener Cases 9 and 10

3. It is also evident from Table 4-11 that the strengths obtained from Cases 2, 9 and 11 are essentially the same. This shows that when b_l/t_s is 1.2 times the maximum limit in AASHTO, the girder strength is not greatly affected, and suggests that the maximum stipulated limit in AASHTO is conservative as noted in Vincent (1969). However, small local buckles are observed in the failure mode for the girders in Case 11, and it may be prudent to use the currently specified limit on b_l/t_s.

Table 4-11: Comparison of R_{bFEA} values for Cases 9, 10 and 11 with Case 2

(a): $D/t_w = 300$

b_{fc}	D_c/D	Case 2	Case 9	Case 10	Case 11
	0.50	0.99	0.99	0.94	0.98
D/6	0.625	0.92	0.93	0.88	0.93
	0.75	0.87	0.87	0.83	0.85
	0.50	0.99	0.99	0.96	0.98
D/5	0.625	0.96	0.93	0.91	0.94
	0.75	0.90	0.89	0.87	0.88
	0.50	1.00	1.00	0.98	0.99
D/4	0.625	0.95	0.95	0.94	0.95
	0.75	0.93	0.93	0.91	0.92

(b): $D/t_w = 240$

b_{fc}	D_c/D	Case 2	Case 9	Case 10	Case 11
	0.50	1.03	1.04	1.02	1.02
D/6	0.625	0.97	0.98	0.94	0.97
	0.75	0.92	0.93	0.87	0.92
D/5	0.625	0.99	1.00	0.95	0.98
	0.75	0.95	0.95	0.90	0.93
	0.50	1.01	0.99	1.02	1.01
D/4	0.625	1.00	1.01	0.96	0.99
	0.75	0.95	0.97	0.93	0.94

Table 4-11 (Continued): Comparison of R_{bFEA} values for Cases 9, 10 and 11 with Case 2

(c): $D/t_w = 200$

b_{fc}	D_c/D	Case 2	Case 9	Case 10	Case 11
	0.50	1.08	1.08	1.01	1.02
D/6	0.625	1.02	1.03	1.01	1.02
	0.75	0.96	0.97	0.94	0.95
D/5	0.625	1.03	1.04	1.02	1.02
	0.75	0.98	0.99	0.96	0.97
	0.50	1.01	0.99	1.04	1.05
D/4	0.625	1.03	1.04	1.02	1.03
	0.75	0.99	1.00	0.97	0.98

4.6.8 Impact of Longitudinal Stiffener Continuity

All the tests discussed until now in this chapter (Cases 1-11) are based on the test setup shown in Figure 4-1, wherein the longitudinal stiffener is modeled continuous over the transverse stiffeners into the end fixtures. In order to assess the effects of the stiffener continuity on girder strength, Case 2 is re-modeled with the longitudinal stiffener continuous over the transverse stiffener in the central test panel, but stopped 1′ away from the end fixture in the end panel of the test specimen.

Table 4-12 compares the results for Cases 2 and 12, where Case 12 examines the integrity of the post-buckling response of the girder when the longitudinal stiffener is not continuous over the transverse stiffeners. It is clear that the girder strength is substantially decreased under the condition of discontinuous longitudinal stiffeners.

Figure 4-9 shows the typical failure mode of such girders. It is observed that the portion of the flange in the unstiffened panel undergoes vertical flange buckling (VFB), i.e. the combined effects of the compression flange yielding and the buckled state of the web with

no restraint from the longitudinal stiffener has increased the susceptibility of the girder to fail by VFB.

There is no recommendation for the termination requirements for longitudinal stiffeners in CEN (2006a). But, a recommendation of $a \leq 3t$ is given by Johansson et al. (2007) to prevent local failure of the plate elements, where a is the distance between the transverse stiffener and the discontinuous edge of the longitudinal stiffener, and t is the thickness of the web plate.

Further studies are required to evaluate the maximum termination distance of the longitudinal stiffener from the transverse stiffener in order to be able to count on the full postbuckling capacity of the girder. Based on the current research, it is recommended that the contribution of the longitudinal stiffener to the postbuckling flexural resistance of the girder be neglected when the panel has discontinuous longitudinal stiffeners.
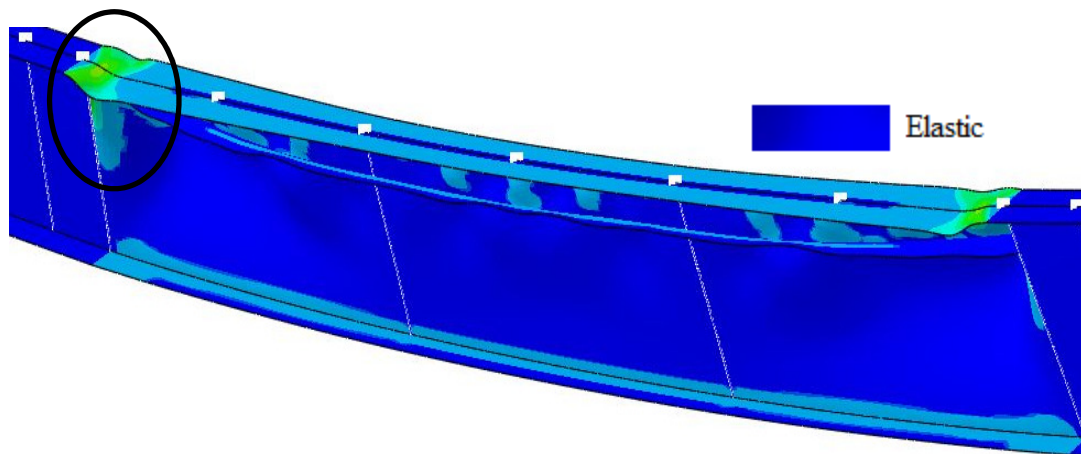
Figure 4-9: Typical snapshot of the failure mode for tests with discontinuous longitudinal stiffeners

Table 4-12: Comparison of R_{bFEA} values for Cases 2 and 12

(a): $D/t_w = 300$

b_{fc}	D_c/D	Case 2	Case 12
	0.50	0.99	0.85
D/6	0.625	0.92	0.81
	0.75	0.87	0.78
	0.50	0.99	0.90
D/5	0.625	0.96	0.85
	0.75	0.90	0.82
	0.50	1.00	0.94
D/4	0.625	0.95	0.92
	0.75	0.93	0.89

(b): $D/t_w = 240$

b_{fc}	D_c/D	Case 2	Case 12
	0.50	0.99	0.87
D/6	0.625	0.92	0.82
	0.75	0.87	0.78
	0.50	0.99	0.89
D/5	0.625	0.96	0.85
	0.75	0.90	0.82
	0.50	1.00	0.95
D/4	0.625	0.95	0.91
	0.75	0.93	0.88

(c): $D/t_w = 200$

b_{fc}	D_c/D	Case 2	Case 12
	0.50	0.99	0.88
D/6	0.625	0.92	0.88
	0.75	0.87	0.83
	0.50	0.99	0.92
D/5	0.625	0.96	0.86
	0.75	0.90	0.82
	0.50	1.00	0.95
D/4	0.625	0.95	0.91
	0.75	0.93	0.88

4.7 Proposed Model for Evaluating Flexural Resistance of Straight Girders

The cross-section model shown in Figure 4-10 is proposed to predict the overall flexural capacity of a plate girder at the yield limit state (i.e., the resistance corresponding to the plateau of the AASHTO LTB capacity for a slender-web I-girder). This figure indicates the portion of the web in the two sub-panels that is effective at the yield limit state. D_c^* is the depth of the neutral axis of the cross-section, and is calculated via an iterative process such that equilibrium and strain compatibility are satisfied based on the stress distribution shown in the compressed portion of the girder. The portion of the web adjacent to the compression flange is assumed to be at the yield stress, and the stress is assumed to vary linearly and elastically below that portion. Figure 4-11 shows the variation of normal stresses through the depth of the web for different depths of the web in compression for girders with $D/t_w = 240$ studied as part of Case 1. The stress distribution shown is computed as the average stress through the mid-thickness of the web plate. This is representative of the general trend in all the cases studied and also for other web slenderness ratios. In addition, the stress distribution through the web depth in Figure 4-11 is clearly different for different D_c/D and exhibits similar behavior for girders with different D/b_{fc} but equal D_c/D values.
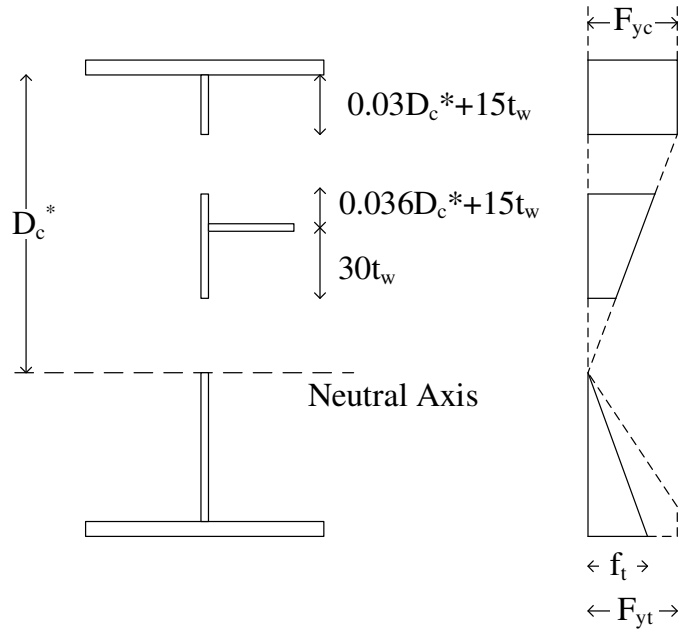
Figure 4-10: Proposed cross-section model and stress distribution
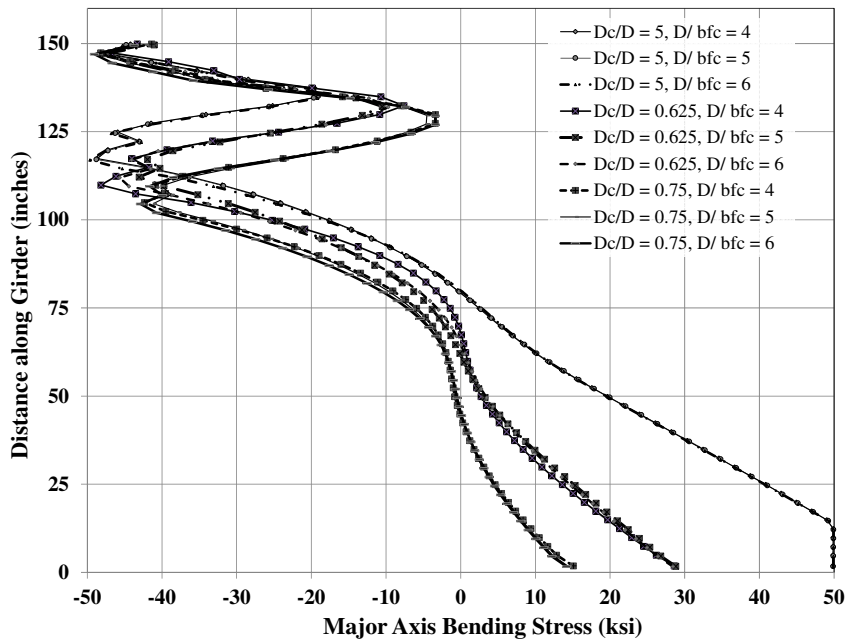
Figure 4-11: Major axis bending stresses in the web, girders with $D/t_w = 240$

Figure 4-10 provides a reasonable approximation of the stress distributions obtained in

Figure 4-11, and can be used to determine the yield limit state flexural resistance of the

girder using basic strength of materials concepts. The compressive stresses to be used in

71

the flexural capacity calculations are calculated from the stress distribution and the effective panel widths shown in Figure 4-10. The neutral axis, $D_c{}^*$ is calculated via an iterative process that satisfies equilibrium and strain compatibility. The moment of the area of the longitudinal stiffener about the calculated neutral axis, $D_c{}^*$ should be included in the calculation of the cross-sectional flexural resistance. The tension stresses are also computed to satisfy overall longitudinal equilibrium (i.e., total sum of forces equal to zero in the longitudinal direction). In this regard, the tension side of the girder near the bottom flange may or may not be yielded. One can write separate equations for the internal moment produced by the assumed stress distribution based on the following assumptions:

1. The entire section is elastic on the tension side of the neutral axis. In this case, the elastic stress distribution below the neutral axis is scaled such that the total longitudinal force in the cross-section is equal to zero.

2. Nominal yielding is reached where the elastic stress reaches F_y at some depth on the tension side of the neutral axis. In this case, the section is assumed to have a constant tensile stress equal to F_y below this depth, and a linearly varying elastic stress distribution above this depth up to the neutral axis.

The tension force and compression force vary with each iteration of the neutral axis until, in the final step both longitudinal equilibrium and strain compatibility is satisfied.

For composite sections in negative bending, the calculations are the same as those shown above, but the area of the tension reinforcing is included. If the longitudinal stress in the reinforcing steel at a given depth exceeds its nominal yield strength, the reinforcing bars are assumed to be at their yield strength. Otherwise, the longitudinal stress in the rebar

is calculated elastically, based on an assumed linear strain variation from the assumed

neutral axial location at the depth D_c*.

The symbol R_{bPr} denotes the value of R_b predicted using the above proposed model.

This quantity is calculated as M_{nPr}/M_y, where M_{nPr} is the moment resistance of the cross-

section model shown in Figure 4-10 using the stress distribution shown. A comparison of

the statistics for R_{bPr} versus R_{bFEA} for the 297 tests considered in Cases 1-11 in this chapter

is shown in Table 4-13. One can observe that the proposed model provides an accurate

prediction of the flexural resistance of longitudinally stiffened plate girders at the yield

limit state.

Table 4-13: Statistics for R_{bFEA}/R_{bPr} for straight girders at yield limit state

Statistical Parameter	R_{bFEA}/R_{bPr}
Mean	1.01
Coefficient of Variation	0.04
Maximum	1.10
Minimum	0.89
Median	1.02

It should be noted that the smallest ratio of d_s/D_c considered in these studies is 0.266.

If this is combined with the largest ratio of D_c/D of 0.75 and with the smallest applicable

D/t_w of 150 (for longitudinally stiffened webs), the sum of the effective widths within the

portion of the web between the longitudinal stiffener and the compression flange is

0.2495D, which is larger than 0.266D_c = 0.200D (for D_c/D = 0.75). In any extreme cases

where the sum of these effective widths exceeds d_s, the web is to be taken as fully effective

between the longitudinal stiffener and the compression flange. Furthermore, the width of

the effective web plate between the longitudinal stiffener and the neutral axis is 30t_w =

30(D/150) = 0.2D for the smallest applicable D/t_w of 150. The smallest value of $D_c - d_s$ considered in these studies is $(D_c - 0.533D_c) = 0.467D_c = 0.233D$ (for $D_c/D = 0.5$). Therefore, even for the smallest web slenderness for which AASHTO LRFD requires a longitudinal stiffener ($D/t_w = 150$), and for the smallest D_c/D considered in this research, the web plate between the longitudinal stiffener and the girder neutral axis is not fully effective in the proposed model. Similar to the above, in any extreme cases where the effective width 30t_w exceeds $D_c - d_s$, the web is to be taken as fully effective between the longitudinal stiffener and the neutral axis.

Figure 4-12 illustrates how R_b from the proposed model compares with the R_b from current AASHTO equations for four of the 11 cases. All other cases show similar trends in behavior. It is evident that R_{bPr} is a much better model to predict the true strengths of the girders and gives excellent correlation with test simulation results. The values for R_{bFEA}/R_{bPr} are consistently around 1.0, while $R_{bAASHTO}$ is extremely conservative for very slender webs. It is also observed from (c) and (d) of Figure 4-12 that the predictions are slightly conservative for the stiffener located below the optimum depth, and are slightly optimistic when the stiffener is located above the optimum stiffener location of 0.4D_c. The predictions from the proposed model are the best when $d_s/D_c = 0.4$. However, as shown in Table 4-13, the coefficient of variation is reasonably low, and the model can be used for any location of the stiffener within the compression area of the web.

If the stiffener is located at the neutral axis, or on the tension side of the web, the stiffener shall not be considered to contribute to the girder resistance, and should not be used in the calculation of the girder section modulus.
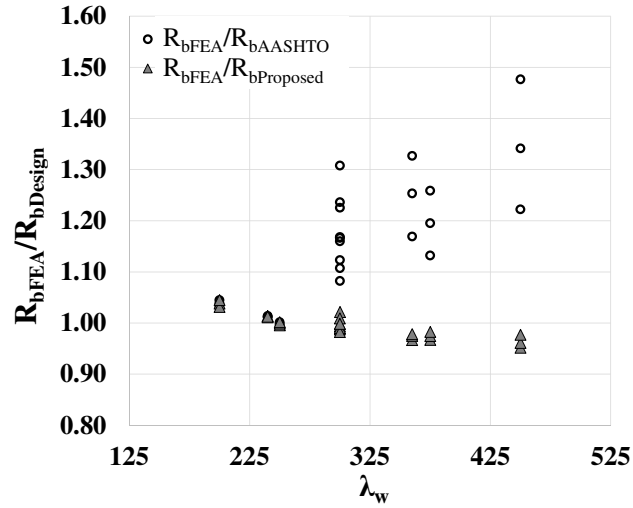
(a) Case 1, $d_o/D = 1$, $d_s/D_c = 0.40$
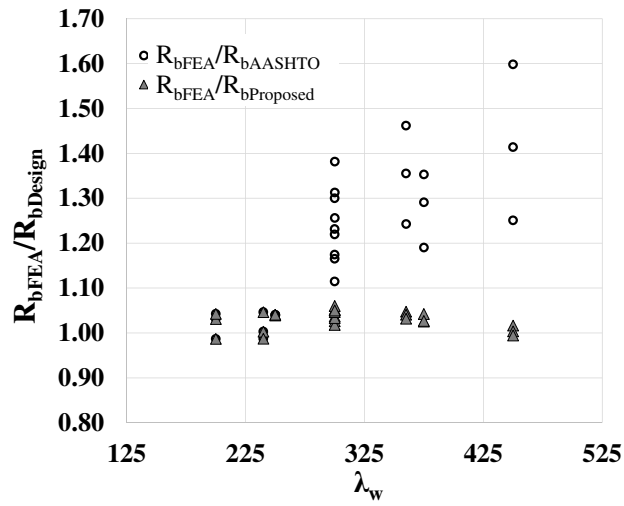
(b) Case 3, $d_o/D = 2$, $d_s/D_c = 0.40$
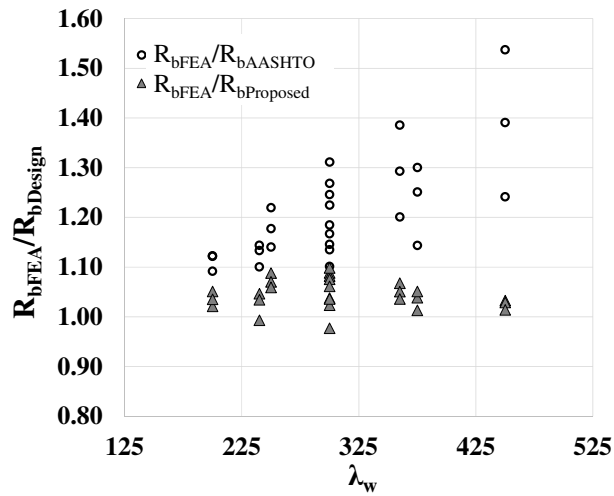
(c) Case 7, $d_o/D = 1$, $d_s/D_c = 0.53$

Figure 4-12: Comparison of $R_{bProposed}$ with $R_{bAASHTO}$

75
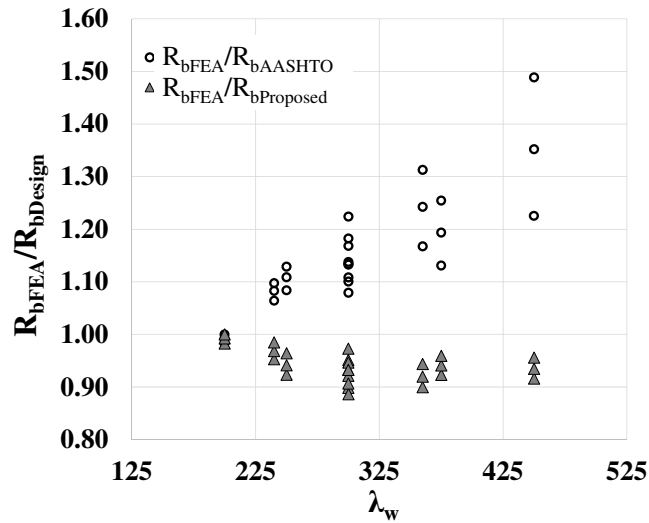
(d) Case 8, $d_o/D = 1$, $d_s/D_c = 0.27$

Figure 4-12 (Continued): Comparison of $R_{bProposed}$ with $R_{bAASHTO}$

It is observed that the stresses in the longitudinal stiffener and the web adjoining the stiffener often reach levels very close to the yield strengths of the web and stiffener plates. An alternative simplified model shown in Figure 4-13 can be used for a quick manual calculation. All the compressive stresses are assumed to be at the yield stress, F_y in the alternative model. It is found to provide approximately 1 to 3% higher strengths than the proposed model in Figure 4-10. The neutral axis D_c^* in the alternative model can simply be taken as the elastic neutral axis of the gross cross-sectional area including the area of the longitudinal stiffener. It is recommended that the alternative model only be used when the ratio of the stiffener area to the area of the web, A_l/A_w is less than 0.15. Longitudinal stiffeners with larger areas may over-compensate for the area of the compression web that is considered ineffective, and the neutral axis of the effective cross-section in such a case will shift upwards from the elastic section neutral axis in order to develop the tension stresses in the cross-section for equilibrium. The proposed "exact" model in Figure 4-10 accounts for any shift in the neutral axis, upwards or downwards from the elastic section

76

neutral axis, while the alternative model fixes the position of the neutral axis at the elastic

neautral axis of the gross cross-sectional area.
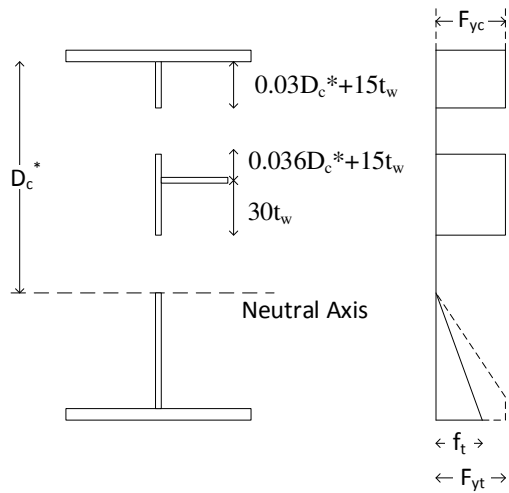
Figure 4-13: Alternative simplified cross-section model for calculating flexural resistance

CHAPTER 5

FLANGE LOCAL BUCKLING OF LONGITUDINALLY STIFFENED

PLATE GIRDERS

Selected tests are conducted to assess the performance of the proposed R_b model in Chapter 4 while evaluating the strengths of longitudinally stiffened plate girders that are controlled by the Flange Local Buckling (FLB) limit state. AASHTO (2014) restricts the flange slenderness ($b_{fc}/2t_{fc}$) to 12 in Section 6.11.2.2. This prevents the use of slender flanges for flanges with yield strengths of up to 70ksi. This chapter examines the applicability of the flange local buckling resistance in the current AASHTO provisions for longitudinally stiffened homogenous girders. Only uniform bending studies are studied in this chapter.

5.1 AASHTO Procedure for calculating FLB Resistance

The FLB resistance equations are given in Section 6.10.8.2.2 of the AASHTO Specifications. When the compression flange is compact, the local buckling resistance of the flange is taken as $R_b F_{yc}$. In case of a noncompact flange, AASHTO Equation 6.10.8.2.2-2,

$$F_{nc} = \left[1 - \left(1 - \frac{F_{yr}}{R_h F_{yc}} \right) \left(\frac{\lambda_f - \lambda_{pf}}{\lambda_{rf} - \lambda_{pf}} \right) \right] R_b R_h F_{yc} \tag{5.1}$$

is used to compute the local buckling resistance of the flange. The FLB resistance for slender web girders is computed by scaling down the FLB equations for a compact or noncompact web plate girder by the load shedding factor R_b. The applicability of these

equations in conjunction with the proposed R_b model is discussed in this chapter. The same test setup used in Chapter 4 is used in the FLB studies.

5.2 Simulation Parameters

The Best-Fit Prawel residual stresses is used in the FLB test studies, as described in Section 3.5. The initial geometric imperfections used in these tests are also modeled via the same procedure described in Section 3.6. In addition to the web imperfection, a flange tilt as shown in Figure 5-1 is modeled for the FLB sensitive studies in this chapter, also satisfying the AWS (2010) criteria.

AWS requires a flange tilt, which is the smaller of b_{fc}/100 and 0.25 inches. The failure mode from the first analysis is scaled such that this limit on the compression flange tilt, in addition to the limit on maximum web out-of-flatness discussed in Section 3.6 is also satisfied.

Min (b_{fc}/200 , 0.125)

← Min (b_{fc}/200 , 0.125)

Min (b_{fc}/200 , 0.125)
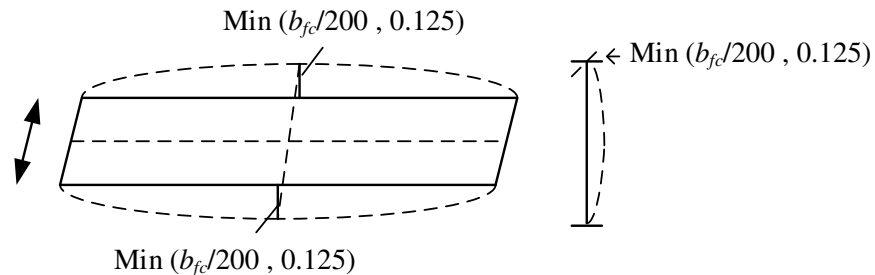
Figure 5-1: Flange tilt imperfection used for studies on FLB limit state

5.3 Case Studies

Only two cases are studied for validating the FLB equations. The cases correspond to Cases 1 and 3 in Section 4.5, with d_o/D = 1, and 2. They are designated as Cases 1-a, and 3-a in Table 5-1. The compression flange slenderness, $b_{fc}/2t_{fc}$ is set to 12.0 for all the girders studied here. The following parameters are varied here, same as in Section 4.5.

79

- D_c/D = 0.5, 0.625 and 0.75,

- D/t_w = 200, 240 and 300, and

- b_{fc} = D/6, D/5 and D/4.

- t_{fc} = 1.04, 1.25 and 1.57 corresponding to the three different values of b_{fc}.

The clear web depth between the flanges is 150 in, and the yield stress of all the plate elements is 50 ksi. The transverse stiffeners sizes are the same as those used in Chapter 4. A total of 54 girders are studied in this chapter.

Table 5-1: Case studies for straight girders at FLB limit state

Case	d_o/D	Longitudinal Stiffener	d_s/D_c
1a	1	AASHTO min	0.4
3a	2	AASHTO min	0.4

5.4 Results

The results are tabulated in Tables 5-2 and 5-3 for Cases 1-a and 3-a. The results are presented as a comparison between M_{max}/M_{nPr} and $M_{max}/M_{nAASHTO}$, where M_{max} is the maximum moment obtained in the FE test simulation, M_{nPr} is the flange local buckling capacity calculated using R_{bPr} and $M_{nAASHTO}$ is calculated using $R_{bAASHTO}$.

Table 5-2: Comparison of FLB capacities using R_{bPr} and $R_{bAASHTO}$ for Case 1-a

(a): $D/t_w = 300$

b_{fc}	D_c/D	M_{max}/M_{nPr}	$M_{max}/M_{nAASHTO}$
	0.50	1.11	1.28
D/6	0.625	1.12	1.26
	0.75	1.13	1.22
	0.50	1.12	1.42
D/5	0.625	1.11	1.33
	0.75	1.11	1.25
	0.50	1.11	1.64
D/4	0.625	1.11	1.49
	0.75	1.11	1.34

(b): $D/t_w = 240$

b_{fc}	D_c/D	M_{max}/M_{nPr}	$M_{max}/M_{nAASHTO}$
	0.50	1.11	1.11
D/6	0.625	1.14	1.14
	0.75	1.14	1.14
	0.50	1.14	1.38
D/5	0.625	1.16	1.34
	0.75	1.14	1.26
	0.50	1.13	1.50
D/4	0.625	1.14	1.42
	0.75	1.06	1.23

(c): $D/t_w = 200$

b_{fc}	D_c/D	M_{max}/M_{nPr}	$M_{max}/M_{nAASHTO}$
	0.50	1.17	1.17
D/6	0.625	1.16	1.16
	0.75	1.17	1.17
	0.50	1.11	1.11
D/5	0.625	1.13	1.13
	0.75	1.14	1.14
	0.50	1.14	1.42
D/4	0.625	1.15	1.38
	0.75	1.16	1.32

Table 5-3: Comparison of FLB capacities using R_{bPr} and $R_{bAASHTO}$ for Case 3-a

(a): $D/t_w = 300$

b_{fc}	D_c/D	M_{max}/M_{nPr}	$M_{max}/M_{nAASHTO}$
D/6	0.50	1.15	1.33
	0.625	1.14	1.28
	0.75	1.11	1.20
D/5	0.50	1.14	1.46
	0.625	1.15	1.39
	0.75	1.13	1.28
D/4	0.50	1.13	1.71
	0.625	1.14	1.56
	0.75	1.12	1.37

(b): $D/t_w = 240$

b_{fc}	D_c/D	M_{max}/M_{nPr}	$M_{max}/M_{nAASHTO}$
D/6	0.50	1.12	1.12
	0.625	1.11	1.11
	0.75	1.14	1.14
D/5	0.50	1.15	1.41
	0.625	1.16	1.36
	0.75	1.15	1.29
D/4	0.50	1.13	1.54
	0.625	1.15	1.47
	0.75	1.16	1.37

(c): $D/t_w = 200$

b_{fc}	D_c/D	M_{max}/M_{nPr}	$M_{max}/M_{nAASHTO}$
D/6	0.50	1.13	1.13
	0.625	1.11	1.11
	0.75	1.10	1.10
D/5	0.50	1.14	1.14
	0.625	1.16	1.16
	0.75	1.17	1.17
D/4	0.50	1.14	1.46
	0.625	1.16	1.42
	0.75	1.17	1.35

It is evident from the above tables and from Figure 5-2 that the proposed model provides satisfactory prediction of the girder resistances for noncompact flange longitudinally stiffened girders. This is mainly due to the inherent conservative nature of the FLB resistance equations in the Specifications. The FLB resistance has a postbuckling reserve that has not been fully utilized by the Specification equations. This is observed in a series of tests studied in Chapter 6, the results of which are presented in Appendix A. It is also clear that the AASHTO equations tend to under-predict the true capacities by virtue of the fact that R_b is highly conservative for singly-symmetric slender web girders, as demonstrated in Chapter 4.
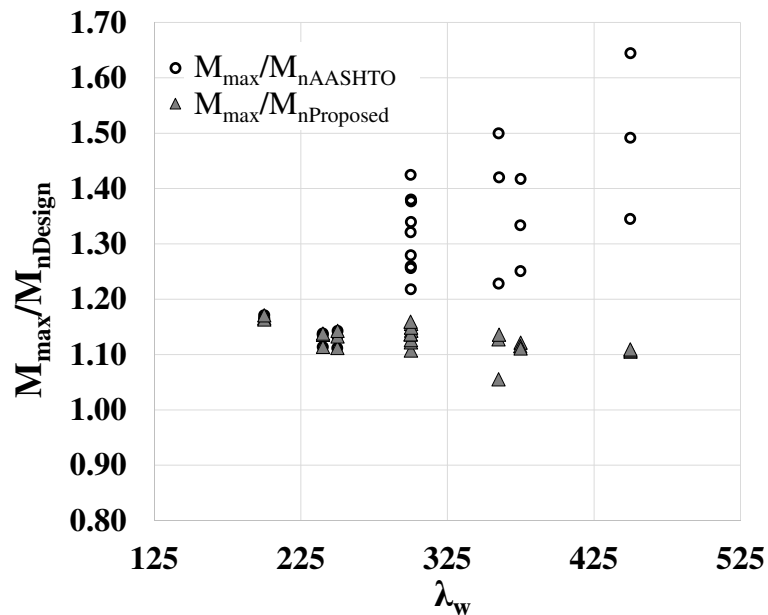
(a) Case 1-a, d_o/D =1, d_s/D_c = 0.4

Figure 5-2: Comparison of $M_{nProposed}$ with $M_{nAASHTO}$ for FLB of longitudinally stiffened girders
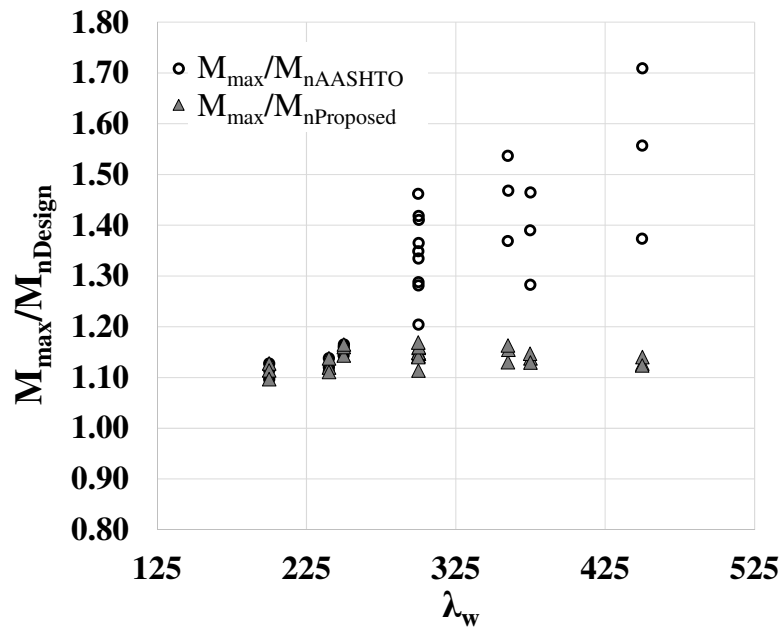
(b) Case 3-a, $d_o/D = 2$, $d_s/D_c = 0.4$

Figure 5-2 (Continued): Comparison of $M_{nProposed}$ with $M_{nAASHTO}$ for FLB of longitudinally stiffened girders

It is recommended in this research, based on the tests discussed in this chapter, that the same form of the equations as in the current Specifications be used for FLB resistance calculations. However, R_b may now be computed using the proposed model in Section 4.7.

Table 5-4 shows the overall statistics of the proposed R_b model for longitudinally stiffened girders governed by the yield limit state.

Table 5-4: Statistics for M_{max}/M_{nPr} for straight girders at FLB limit state

Statistical Parameter	M_{max}/M_{nPr}
Mean	1.13
Coefficient of Variation	0.02
Maximum	1.17
Minimum	1.06
Median	1.14

CHAPTER 6

LATERAL TORSIONAL BUCKLING OF STRAIGHT

UNSTIFFFENED GIRDERS SUBJECTED TO UNIFORM MOMENT

The AASHTO and AISC (2010a) strength curves are based on calibration to a wide range of experimental results as discussed by White (2008). But, it is observed in this research, and by others (e.g., Kim (2010)) that in many cases, predictions of flexural resistance by FE test simulations, using typical nominal residual stresses and geometric imperfections, tend to be somewhat low compared to the experimental test results, particularly for the case of uniform bending. It is observed that in many cases, the nominal LTB resistance curve recommended by AASHTO (2014) and by AISC (2010a) tends to predict higher LTB resistances than those obtained from FE test simulations. Although the AISC/AASHTO curves represent a vast collection of experimental data, there are indications that there are some shortcomings in capturing the resistances in some areas of the design space. The curves have been found to over-predict the capacities from certain experimental tests, particularly in the inelastic LTB region (e.g., Righman (2005)). It is also true, however, that FE simulations tend to be conservative in many cases due to the use of idealized boundary conditions, as well as assumed nominal residual stresses and geometric imperfections. This chapter primarily addresses the disconnect between FE test simulations and the AISC/AASHTO LTB resistance equations for I-girders with webs without longitudinal stiffeners.

The LTB curve for I-section members in AISC and AASHTO consists of three distinct regions: the plateau region, the inelastic LTB region and the elastic LTB region.

The plateau resistance is the plastic moment capacity for compact sections, while for other compact and noncompact web sections; it is the yield moment multiplied by the web plastification factor, R_{pc}. The plateau capacity for slender web sections is the yield moment reduced by the web bend buckling factor, R_b. Members with unbraced lengths that are greater than L_r are expected to fail in uniform bending by elastic LTB and are designed for the theoretical elastic LTB strength, where L_r is the limiting unbraced length at which yielding effects start to influence the nominal resistance. Members with unbraced lengths between L_p and L_r are designed for the inelastic LTB buckling resistance, obtained by linearly interpolating between plateau and the elastic LTB anchor points.

This chapter presents extensive sensitivity analyses with different magnitudes of imperfections and different residual stress patterns using selected experimental tests of compact and noncompact web members subjected to uniform bending and having general boundary conditions. In addition, sensitivity analyses are conducted using members with fork boundary conditions (simply-supported with twist restrained, and lateral bending and warping free at ends of the member). Based on these studies, nominal residual stresses and geometric imperfections to be used when conducting FE simulations are recommended, such that the simulations are more representative of the mean experimental strengths captured by the AISC/AASHTO resistance equations.

While recognizing that FE test simulations with idealized characteristics often tend to be conservative, some incontrovertible inconsistencies in the design resistance curves are pointed out. One of the significant shortcomings of the AISC/AASHTO curves is that several types of members cannot attain their plateau moment capacities at the limiting plateau length, L_p regardless of the residual stress or magnitude of geometric imperfection

considered in FE simulations. In addition, it is shown that the AISC/AASHTO curves indicate larger strengths than FE simulation data throughout the inelastic LTB region in all cases where predominant flange compressive residual stresses are considered in the simulations.

In addition to the recommendation of FE modeling parameters, this research also proposes an improved form of the LTB equations that provides a better fit to FE simulation data, and experimental data that encompasses more recent research. Both rolled sections and welded plate girders are considered in these studies.

6.1 Simulation Parameters

Full nonlinear analyses are performed in ABAQUS with the S4R shell elements for the flanges and the web, while the B31 beam elements are used for transverse stiffeners. These elements are described in detail in Section 3.1. Twelve elements are used across both flanges, and twenty elements are used through the web depth. The material modeling is the same as that described in Section 3.3.

6.2 Imperfection and Residual Stress Sensitivity Studies

This section discusses a comprehensive set of sensitivity studies conducted on experimental tests, as well as parametric simulation studies with various imperfection magnitudes and residual stresses.

6.2.1 Imperfections

Figure 6-1 shows the web initial out-of-flatness, flange tilt and flange sweep assumed in this work. Only the flange sweep is considered for rolled beams with compact webs while all three types of imperfection are included for members with noncompact and

slender webs. The flange sweep is sufficient to capture the dominant attributes of the response for compact-section beams; however, noncompact web members can be sensitive to the other imperfections as well.

AWS (2010) allows a maximum web out-of-flatness of D/150 for girders with no intermediate stiffeners and a flange tilt equal to the smaller of b_{fc}/100 and 0.25 inches. The imperfection magnitudes shown in Figure 6-1 for the web out-of-flatness and flange tilt are taken as one-half of the corresponding AWS maximum tolerance (half of that used in Chapter 5, Figure 5-1). In addition, AWS allows a maximum flange out-of-straightness of L_b/960, where L_b is the unbraced length of the member. The maximum out-of-straightness permitted in the AISC COSP (2010b) is effectively L_b/1000. Sensitivity studies are performed with four different magnitudes of flange sweep, L_b/1000, L_b/2000, L_b/4000 and L_b/8000. L_b/8000 is effectively a case with near zero imperfection in the flange sweep. It is shown that the use of the full tolerance values in FE simulations may be overly conservative. The three types of imperfections are superimposed in the directions shown in Figure 6-1.

(a) Web out-of-flatness

(b) Flange tilt

(c) Flange sweep
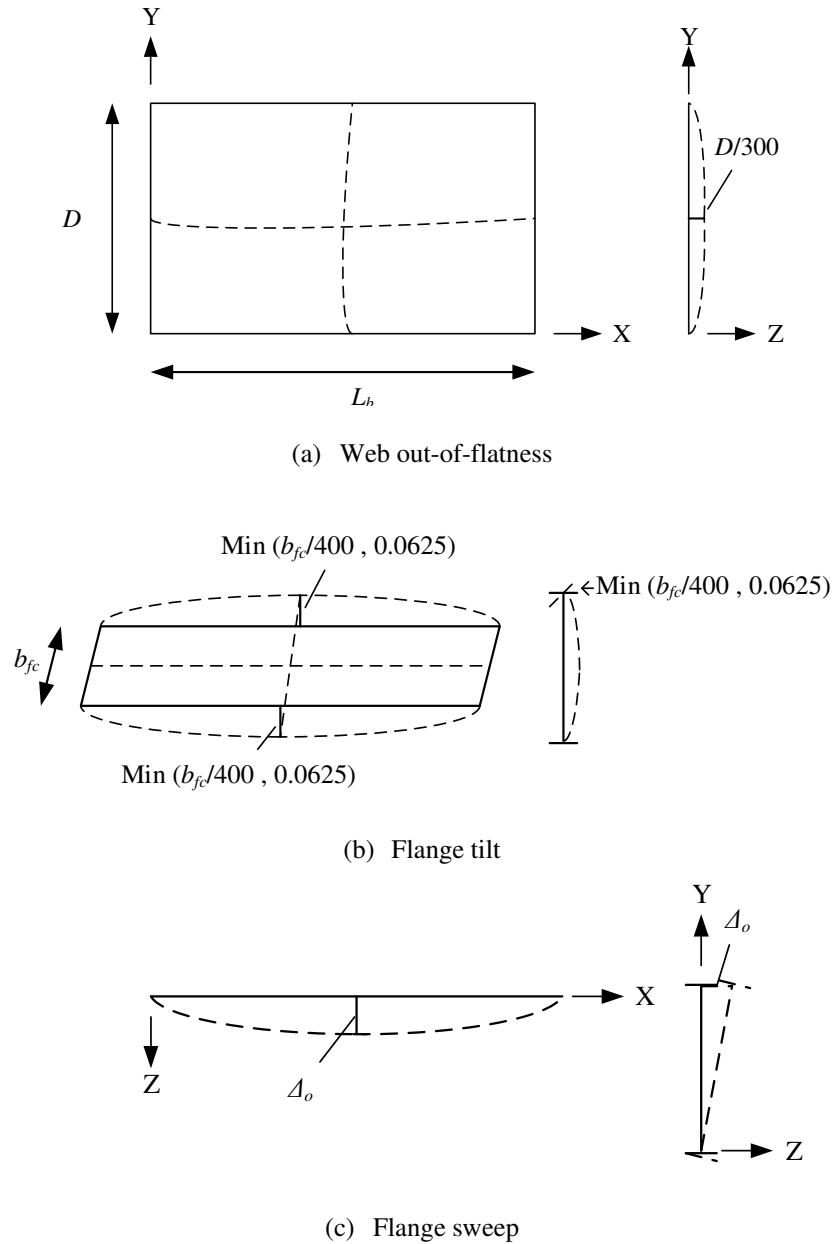
Figure 6-1: Initial geometric imperfections used in LTB studies

6.2.2 Residual Stress Patterns

Figure 6-2 shows various residual stress patterns used in the sensitivity studies presented in this research. The Dux and Kitipornchai (1983) residual stresses shown in Figure 6-2 (e), with tensile residual stresses in the flanges are representations of measured values in rolled sections. It should be noted that other test programs (e.g. Dibley (1969))

also have measured residual stresses similar to those measured by Dux & Kitipornchai for rolled beams. The residual stresses shown in Figure 6-2 (e) do not precisely satisfy equilibrium on the cross-section under zero load. In using this residual stress pattern for the studies presented in this research, the authors allowed the members to equilibrate under these stresses at zero applied loads in the FE program. This means that the initial imperfections and residual stresses are slightly different from the nominal values assumed.

The other residual stress patterns shown in Figure 6-2 are in equilibrium on the perfect member geometry. It should also be noted that ECCS recommends using a peak compressive residual stress of $0.5F_y$ for column type of cross-sections, which will result in lower resistances than the peak compressive residual stress of $0.3F_y$. However, the objective of including this pattern in the studies is to study the sensitivity of resistances to the pattern itself, and not the magnitude of the peak compressive residual stress. Hence, the ECCS pattern is considered in this research as shown Figure 6-2 (b) for all types of cross-sections.

The sensitivity of the LTB resistance to the magnitude of the residual stresses is evaluated by studying one half and one quarter of the Lehigh and Best-Fit Prawel residual stresses. The Best-Fit Prawel residual stress pattern shown in Figure 6-2 (d) is replicated here from Figure 3-1.
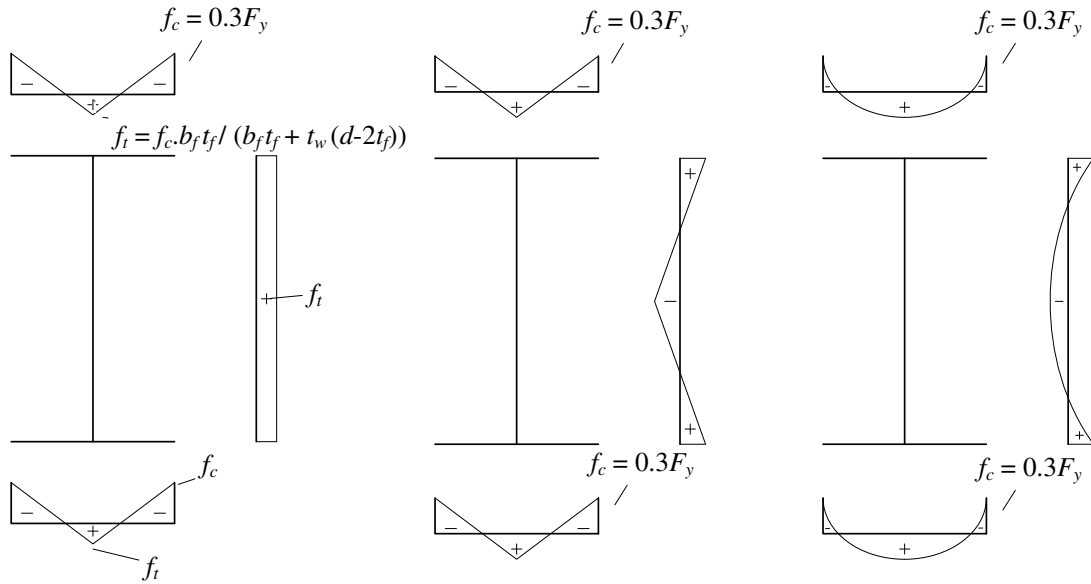
(a) Lehigh (Galambos and Ketter 1959)

(b) ECCS (Boissonnade et al. 2002)

(c) Polynomial (Szalai and Papp 2005)
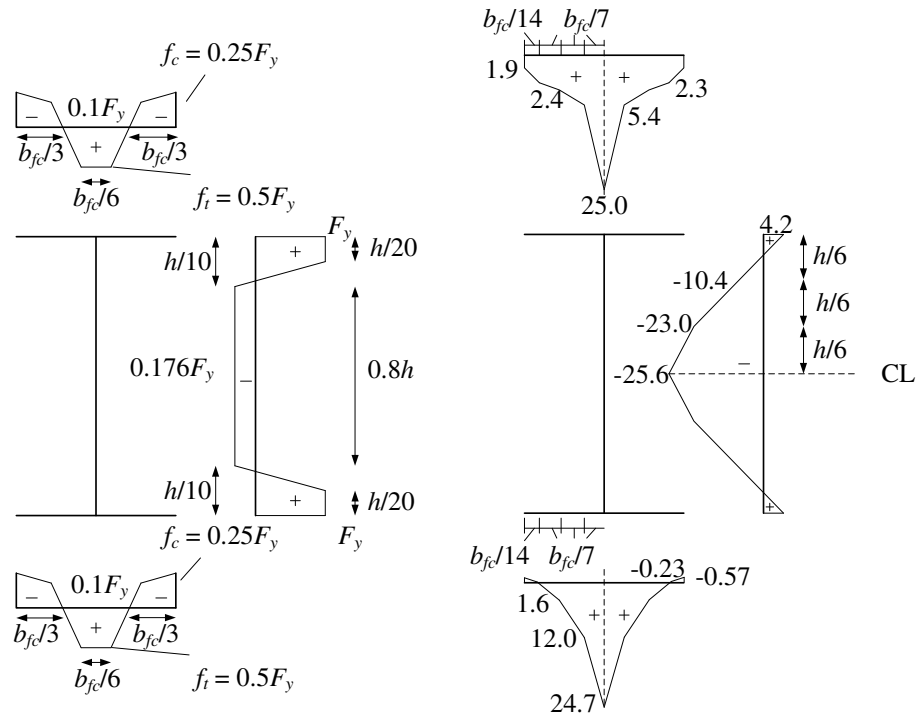
(d): Best Fit Prawel (Kim 2010)

(e): Dux & Kit (Dux and Kitipornchai 1983)

Figure 6-2: Residual Stress Patterns for LTB Sensitivity Studies

91

6.2.3 Sensitivity Studies on Experimental Test Specimens

A total of six uniform bending experimental tests with compact and noncompact webs are considered in this section. Residual stresses and imperfections were seldom measured in experimental tests. In the events where such data is available, the experimental results and FE test simulation predictions are nearly equal (see Kim (2010)). Various imperfection magnitudes and residual stresses are hence evaluated to determine the conditions in which the simulation results predict the reported experiment values with greatest accuracy. This is done to identify the simulation parameters that do not lead to overly unconservative predictions relative to the experimental results. The complete details of the test configurations are catalogued in White and Jung (2004). The six selected tests are expected to fail by inelastic LTB, which is the region with greatest sensitivity to imperfections and residual stresses. Table 6-1 lists the tests modeled in the simulation studies.

Table 6-1: Experimental tests modeled by FE simulations for LTB sensitivity studies

Reference	Section Type	Test No	Flange	Web	Designation in Thesis
Dux and Kitipornchai (1983)	Rolled	6	Compact	Compact	DK 6
Wongchung and Kitipornchai (1987)	Rolled	1	Compact	Compact	WK 1
	Rolled	5	Compact	Compact	WK 5
	Rolled	9	Compact	Compact	WK 9
Richter (1998)	Welded	5	Compact	Noncompact	R5
	Welded	9	Compact	Noncompact	R9

Tables 6-2 through 6-4 list the results for the sensitivity studies conducted on the above tests. These tables list the ratios of the moment capacities obtained via FE test simulations to the reported experimental moment capacities (M_{max}/M_{Exp}).

Table 6-2: M_{max}/M_{Exp} **using Best-Fit Prawel and half Best-Fit Prawel residual stresses**

Residual Stress	Best -fit Prawel				Half Best-Fit Prawel			
Imperfection	L_b/1000	L_b/2000	L_b/4000	L_b/8000	L_b/1000	L_b/2000	L_b/4000	L_b/8000
DK 6	0.97	0.99	0.99	1.02	1.01	1.03	1.04	1.05
WK 1	0.84	0.89	0.93	0.94	0.91	0.95	0.96	0.96
WK 5	0.85	0.88	0.90	0.91	0.92	0.97	0.99	1.04
WK 9	0.94	0.95	0.96	0.97	0.97	1.00	1.01	1.03
R5	0.92	0.93	0.93	0.93	0.96	0.97	0.97	0.98
R9	0.77	0.84	0.87	0.92	0.85	0.97	0.93	1.01
Mean	0.88	0.91	0.93	0.95	0.94	0.98	0.98	1.02

Table 6-3: M_{max}/M_{Exp} **using Lehigh and half Lehigh residual stresses**

Residual Stress	Lehigh				Half Lehigh			
Imperfection	L_b/1000	L_b/2000	L_b/4000	L_b/8000	L_b/1000	L_b/2000	L_b/4000	L_b/8000
DK 6	0.95	0.97	0.98	0.99	0.99	1.02	1.03	1.05
WK 1	0.84	0.89	0.92	0.93	0.90	0.95	0.96	0.96
WK 5	0.85	0.89	0.91	0.92	0.92	0.96	0.98	1.01
WK 9	0.92	0.94	0.95	0.96	0.97	0.99	0.98	1.01
R5	0.93	0.94	0.95	0.96	0.96	0.97	0.97	0.98
R9	0.77	0.79	0.84	0.89	0.83	0.92	0.97	1.00
Mean	0.88	0.90	0.93	0.94	0.93	0.97	0.98	1.00

Table 6-4: M_{max}/M_{Exp} **using ECCS residual stresses**

Residual Stress	ECCS			
Imperfection	L_b/1000	L_b/2000	L_b/4000	L_b/8000
DK 6	0.99	1.01	1.02	1.03
WK 1	0.87	0.91	0.93	0.96
WK 5	0.89	0.93	0.95	0.96
WK 9	0.96	0.98	0.99	1.00
R5	0.95	0.96	0.96	0.97
R9	0.81	0.87	0.90	0.92
Mean	0.91	0.94	0.96	0.97

It can be observed that using the half Best-Fit Prawel residual stresses or half Lehigh residual stresses along with a flange sweep of $L_b/2000$ gives the best correlation with the reported experimental test results. These residual stresses and geometric imperfections would appear to be good choices for parametric studies to investigate other aspects of the LTB resistance. Although imperfection magnitude of $L_b/4000$ gives comparable results, it is shown in Section 6.2.4 that this magnitude of imperfection results in a very flat inelastic LTB curve, and is not representative of true girder behavior.

6.2.4 Sensitivity Studies using FE Simulations on Torsionally Simply-Supported Members

In this section, LTB curves are generated using FE test simulations for two rolled and two welded sections using the various residual stress patterns shown in Figure 6-2 and the imperfections shown in Figure 6-1. Four different magnitudes of flange sweep are studied: $L_b/1000$, $L_b/2000$, $L_b/4000$ and $L_b/8000$. $L_b/8000$ may be considered as a negligible imperfection. These studies aim to examine the sensitivities of the LTB resistance curve to various imperfections and residual stresses on several types of cross-sections.

The members are modeled as flexurally and torsionally simply-supported units with twist and lateral deflection restrained at their ends (fork boundary conditions). Equal and opposite moments are applied at member ends and Vlasov kinematics are enforced at the member ends by the use of multi-point constraints. The LTB effective length factor, K, for these members is 1.0. Figure 6-3 shows a representative sketch of the member test setup used in all the FE test simulations discussed henceforth in this chapter.
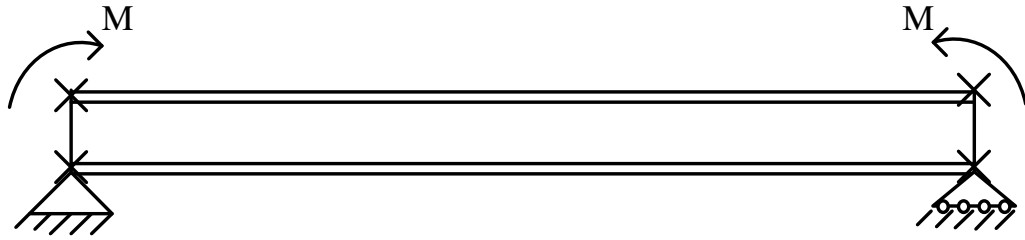
Figure 6-3: Flexurally and torsionally simply-supported member with end moments

6.2.4.1 <u>Sensitivity studies on rolled beams</u>

Sensitivity studies are performed using two rolled sections, a W21x44 (d/b_{fc} = 3) and a W14x68 (d/b_{fc} = 1.3). The sensitivity of the rolled beam test simulation results to seven different residual stress patterns is studied. The Lehigh pattern (Figure 6-2 (a)) is considered with its full magnitude, half of its specified magnitude, and one quarter of its specified magnitude. In addition, the ECCS pattern (Figure 6-2 (b)), the polynomial pattern (Figure 6-2 (c)), the pattern measured by Dux and Kitipornchai (1983) (Figure 6-2 (e)), and a case with zero residual stresses are considered.

Figure 6-4 shows the results for a W21x44 with a flange sweep of $L_b/2000$ for various residual stress patterns. Figures 6-5 and 6-6 show the results for a W21x44 for various imperfection magnitudes at half the Lehigh residual stress and at zero residual stress.

It is observed that the sensitivity of the member capacities to the residual stress pattern and imperfection magnitude is most significant in the inelastic LTB region. The Lehigh residual stress pattern gives the smallest resistance for all imperfection magnitudes, while the residual stresses measured by Dux and Kitipornchai (1983) give the highest resistance. The relative effects of various residual stresses are essentially the same at imperfection magnitudes of $L_b/4000$ and $L_b/8000$. However, the capacities in these cases are closer to the AISC resistance curves.
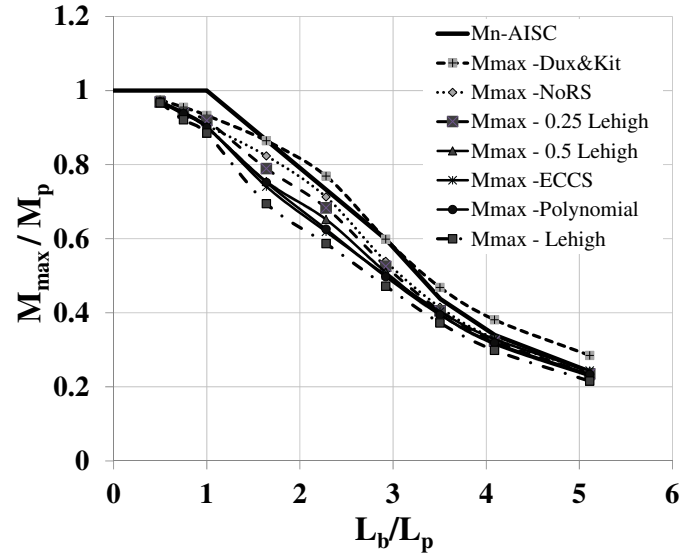
Figure 6-4: LTB curves for W21x44 with L_b/2000 flange sweep
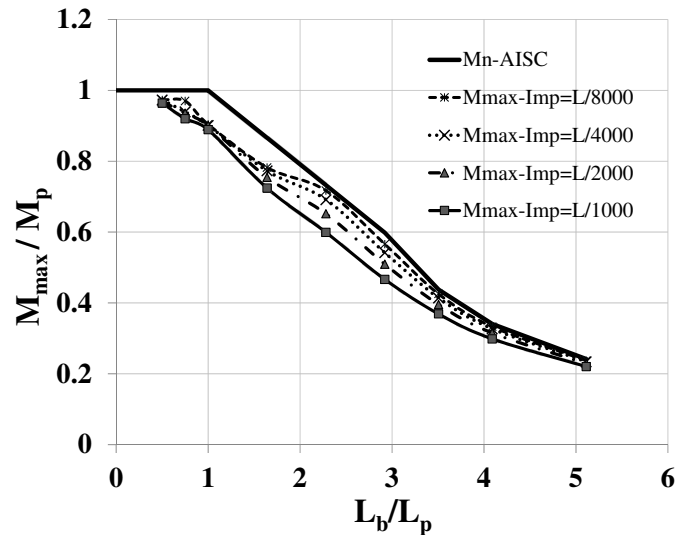
Figure 6-5: LTB curves for W21x44 with Half-Lehigh residual stress
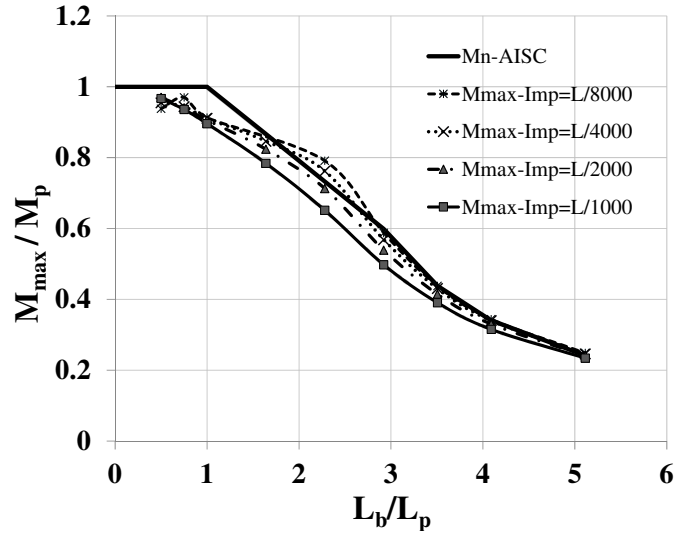
Figure 6-6: LTB curves for W21x44 with zero residual stress

Plots for the W14x68 (not shown), which has a smaller d/b_{fc}, show trends similar to the W21x44 curves. The "Dux & Kit" residual stresses often give resistances higher than the AISC resistance curve in the inelastic and elastic LTB ranges. This is due to the net tensile residual stresses in the flanges in these tests. Figures 6-5 and 6-6 show how the resistances increase with decreasing imperfection magnitude for a given residual stress pattern, and that they are especially sensitive to the imperfection magnitude in the inelastic LTB region. This behavior is typical of all the residual stresses studied in this research. Clearly, it is imperative to choose an appropriate residual stress pattern and imperfection magnitude if test simulations are to be used to evaluate design LTB resistances.

It is observed that using the Lehigh pattern, which is a common residual stress pattern employed in North America for simulation studies on rolled I-section members, along with a flange sweep of $L_b/1000$, gives capacities up to 28% smaller than the AISC resistance equation in the inelastic region for the W21x44, and 19% smaller for the W14x68. Also, the AISC prediction with these parameters is 15% larger compared to the test simulation

results in the elastic LTB region at an unbraced length of $1.75L_r$ for the W21x44, while it is only 3% unconservative at an unbraced length of $1.75L_r$ for the W14x68. The plateau strength as per AISC for both these beams is less than 4% conservative at $0.5L_p$. However, as shown in Figures 6-4 to 6-6, the plastic moment is never reached in the FE simulations at L_p, even in near-ideal cases with zero residual stress and imperfections of $L_b/8000$, i.e., a smaller unbraced length than L_p is needed to achieve M_p.

Tables 6-5 to 6-8 list the results obtained from the FE test simulations at four unbraced lengths of the above two members as a function of the various residual stresses and imperfection magnitudes. The mean of the simulation strengths for the selected residual stress patterns is calculated neglecting the two case studies with flange tensile residual stresses and zero residual stresses. These two cases are neglected in order to focus on the influence of compressive flange residual stresses. The unbraced lengths L_p and L_r presented in the table represent the limiting unbraced lengths of the plateau region and the inelastic LTB region while $1.75L_r$ represents a point significantly into the elastic LTB region. In addition, the results are shown for an intermediate unbraced length in the inelastic LTB region. Table 6-6 shows the results for an intermediate unbraced length in the inelastic LTB region, and Table 6-7 shows the results at L_r. Both of these tables show similar trends, with AISC tending to give larger resistances in the inelastic LTB region, as is also evident from Figures 6-4 to 6-6.

Table 6-5: $M_{max}/ M_{n\,AISC}$ **for W21x44 and W14x68 for different residual stresses and imperfection magnitudes at the unbraced length** L_p

Section	W21x44				W14 x68			
Imperfection	L_b/1000	L_b/2000	L_b/4000	L_b/8000	L_b/1000	L_b/2000	L_b/4000	L_b/8000
Lehigh	0.88	0.89	0.89	0.90	0.89	0.90	0.91	0.91
0.5 Lehigh	0.89	0.90	0.90	0.90	0.91	0.91	0.93	0.93
0.25 Lehigh	0.89	0.92	0.92	0.92	0.92	0.93	0.94	0.94
ECCS	0.89	0.90	0.91	0.91	0.91	0.92	0.93	0.93
Polynomial	0.89	0.90	0.90	0.91	0.92	0.93	0.94	0.95
Dux & Kit	0.93	0.93	0.94	0.94	0.94	0.95	0.96	0.96
Zero RS	0.90	0.91	0.91	0.91	0.93	0.94	0.95	0.95
Mean neglecting the Dux & Kit and Zero RS Cases	0.89	0.90	0.90	0.91	0.91	0.92	0.93	0.93

Table 6-6: $M_{max}/ M_{n\,AISC}$ **for W21x44 and W14x68 for different residual stresses and imperfection magnitudes at the unbraced length** $L_p + 2/3\ (L_r\text{-}L_p)$

Section	W21x44				W14 x68			
Imperfection	L_b/1000	L_b/2000	L_b/4000	L_b/8000	L_b/1000	L_b/2000	L_b/4000	L_b/8000
Lehigh	0.74	0.80	0.84	0.87	0.81	0.86	0.90	0.93
0.5 Lehigh	0.82	0.89	0.94	0.98	0.88	0.94	1.00	1.04
0.25 Lehigh	0.85	0.93	1.00	1.04	0.91	0.98	1.04	1.06
ECCS	0.79	0.85	0.88	0.90	0.84	0.89	0.93	0.95
Polynomial	0.80	0.85	0.89	0.92	0.87	0.92	0.96	0.98
Dux & Kit	0.98	1.05	1.10	1.14	0.97	1.05	1.11	1.12
Zero RS	0.89	0.97	1.04	1.08	0.94	1.02	1.06	1.12
Mean neglecting the Dux & Kit and Zero RS Cases	0.80	0.86	0.91	0.94	0.86	0.92	0.96	0.99

Table 6-7: $M_{max}/M_{n\,AISC}$ for W21x44 and W14x68 for different residual stresses and imperfection magnitudes at the unbraced length L_r

Section	W21x44				W14 x68			
Imperfection	L_b/1000	L_b/2000	L_b/4000	L_b/8000	L_b/1000	L_b/2000	L_b/4000	L_b/8000
Lehigh	0.72	0.79	0.84	0.89	0.81	0.86	0.91	0.95
0.5 Lehigh	0.78	0.85	0.91	0.95	0.86	0.92	0.97	1.00
0.25 Lehigh	0.81	0.88	0.93	0.96	0.88	0.95	0.99	1.02
ECCS	0.77	0.84	0.89	0.93	0.83	0.89	0.93	0.97
Polynomial	0.77	0.83	0.88	0.93	0.85	0.91	0.95	0.99
Dux & Kit	0.94	1.00	1.05	1.07	0.95	1.01	1.05	1.07
Zero RS	0.83	0.90	0.95	0.98	0.91	0.97	1.01	1.03
Mean neglecting the Dux & Kit and Zero RS Cases	0.77	0.84	0.89	0.93	0.85	0.90	0.95	0.99

Table 6-8 : $M_{max}/M_{n\,AISC}$ for W21x44 and W14x68 for different residual stresses and imperfection magnitudes at the unbraced length $1.75L_r$

Section	W21x44				W14 x68			
Imperfection	L_b/1000	L_b/2000	L_b/4000	L_b/8000	L_b/1000	L_b/2000	L_b/4000	L_b/8000
Lehigh	0.85	0.89	0.92	0.94	0.97	1.04	1.05	1.06
0.5 Lehigh	0.91	0.95	0.97	0.98	1.00	1.09	1.10	1.10
0.25 Lehigh	0.94	0.97	0.99	1.00	1.09	1.11	1.12	1.12
ECCS	0.97	1.01	1.04	1.05	1.06	1.08	1.08	1.08
Polynomial	0.93	1.00	1.00	1.01	1.08	1.09	1.10	1.11
Dux & Kit	1.15	1.20	1.20	1.21	1.15	1.17	1.18	1.19
Zero RS	0.97	1.02	1.02	1.03	1.01	1.13	1.14	1.14
Mean neglecting the Dux & Kit and Zero RS Cases	0.92	0.97	0.98	0.99	1.04	1.08	1.09	1.09

6.2.4.2 Sensitivity studies on welded plate girders

Sensitivity studies are performed on a noncompact web, compact flange and a slender web, compact flange welded plate girders (G1 and G5). Girders G1 and G5 are two girders that are part of a series of studies discussed subsequently in Section 6.4. The girder G1 is

doubly-symmetric with $D = 150$ in, $D/t_w = 130$, $D/b_{fc} = 6$, and $b_{fc}/2t_{fc} = 9$. R_{pc} (the web plastification or cross-section effective shape factor, which accounts for the typical increase in the LTB plateau strength above M_{yc} for noncompact and compact web sections) for this girder is 1.03. Hence, its theoretical plateau capacity is close to M_y. The girder G5 is also doubly-symmetric with $D = 150$ in, $D/t_w = 180$, $D/b_{fc} = 6$, and $b_{fc}/2t_{fc} = 9$. R_b for this member is 0.93. R_{pc} for a slender homogenous girder is 1.0, while R_b for a noncompact web memberr is 1.0. The LTB plateau strength is $R_bR_{pc}M_y$. The sensitivity of the test strengths to three different nominal residual stress patterns is studied: the Best-Fit Prawel in Figure 6-2(d) with its full magnitude, half of its magnitude, and with zero residual stresses. The four imperfection magnitudes of $L_b/1000$, $L_b/2000$, $L_b/4000$ and $L_b/8000$ on the flange sweep considered for the rolled beams are studied here as well. In addition, the initial geometric imperfections include the flange tilt and web out-of-flatness with the magnitudes shown in Figure 6-1.

Figure 6-7 shows the results for G1 with a flange sweep of $L_b/2000$ for various residual stress magnitudes. Figures 6-8 and 6-9 show the results for G1 with various imperfection magnitudes at half Best-Fit Prawel residual stress and zero residual stress. Tables 6-9 to 6-12 list the results obtained from FE test simulations at four unbraced lengths for G1 and G5 as a function of the different residual stresses and imperfection magnitudes.
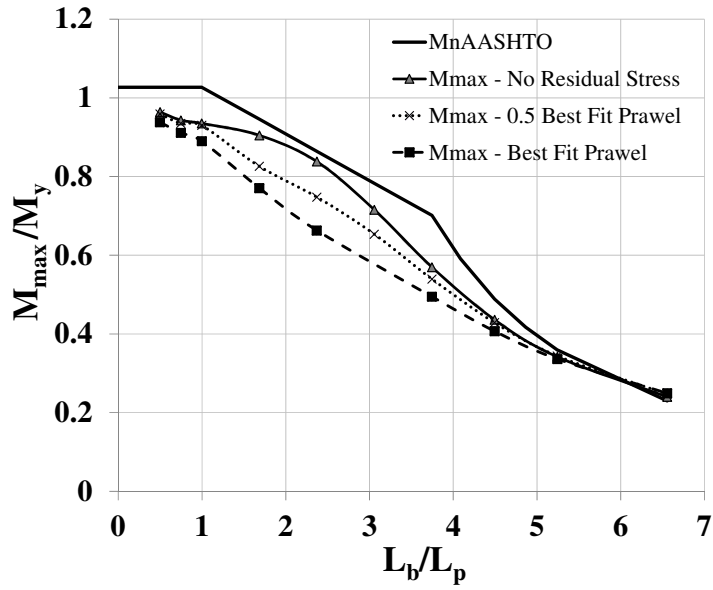
Figure 6-7: LTB curves for G1 with L_b/2000 flange sweep
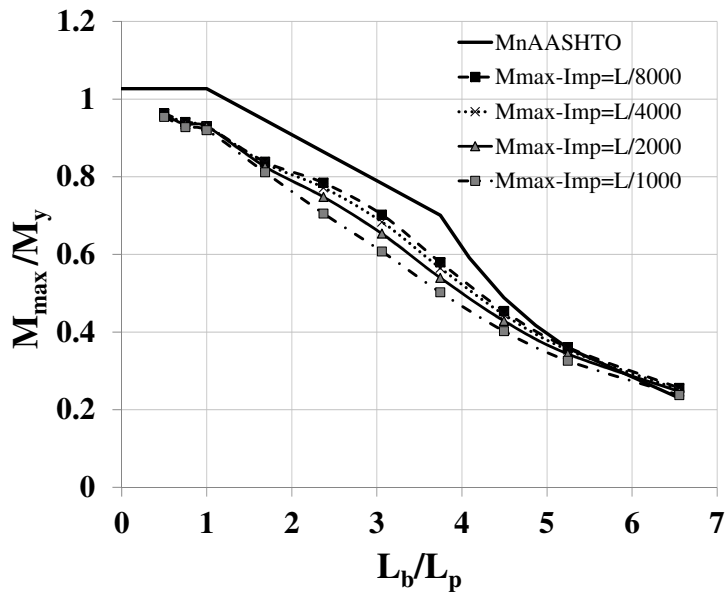
Figure 6-8: LTB curves for G1 with Half Best-Fit Prawel residual stress
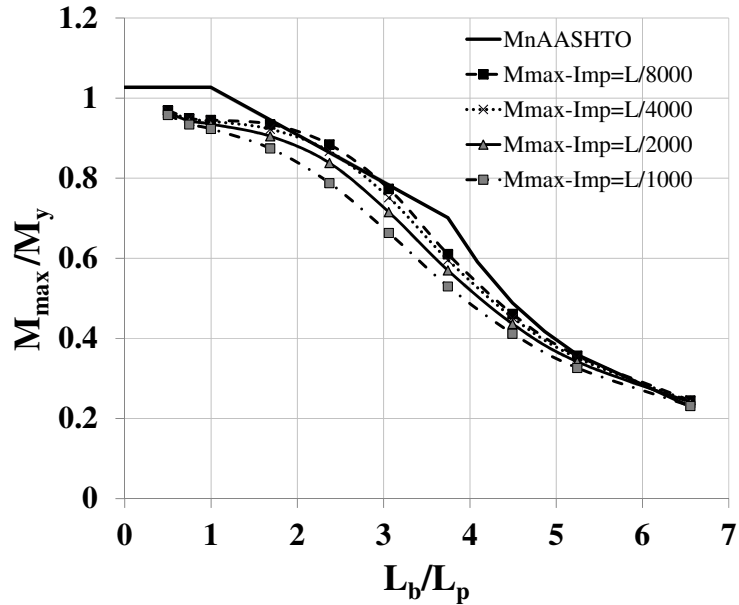
Figure 6-9: LTB curves for G1 with zero residual stress

As observed previously, the sensitivity of the capacities to the residual stress pattern or imperfection magnitude is significant in the inelastic LTB region. The Best-Fit Prawel residual stress pattern gives the lowest resistance for any imperfection magnitude. The relative effects of various residual stresses are essentially the same for imperfection magnitudes of $L_b/4000$ and $L_b/8000$. However, the capacities in these cases are larger in the inelastic LTB region than for the cases with smaller imperfection magnitudes.

Table 6-9 : $M_{max}/M_{nAASHTO}$ for G1 and G5 for different residual stresses and imperfection magnitudes at unbraced length L_p

Section	G1				G5			
Imperfection	$L_b/1000$	$L_b/2000$	$L_b/4000$	$L_b/8000$	$L_b/1000$	$L_b/2000$	$L_b/4000$	$L_b/8000$
Best-Fit Prawel	0.87	0.87	0.88	0.88	0.91	0.92	0.92	0.92
0.5 Best-Fit Prawel	0.90	0.91	0.91	0.91	0.93	0.94	0.95	0.95
Zero RS	0.90	0.91	0.92	0.92	0.95	0.96	0.96	0.96
Mean neglecting the case with Zero RS	0.88	0.89	0.89	0.89	0.92	0.93	0.93	0.94

103

Table 6-10: $M_{max}/M_{nAASHTO}$ **for G1 and G5 for different residual stresses and imperfection magnitudes at unbraced length** $L_p + 1/2\ (L_r - L_p)$

Section	G1				G5			
Imperfection	$L_b/1000$	$L_b/2000$	$L_b/4000$	$L_b/8000$	$L_b/1000$	$L_b/2000$	$L_b/4000$	$L_b/8000$
Best-Fit Prawel	0.73	0.76	0.78	0.79	0.80	0.84	0.86	0.87
0.5 Best-Fit Prawel	0.81	0.86	0.89	0.90	0.89	0.93	0.96	0.97
Zero RS	0.91	0.97	1.00	1.02	0.97	1.03	1.06	1.08
Mean neglecting the case with Zero RS	0.77	0.81	0.84	0.85	0.85	0.88	0.91	0.92

Table 6-11: $M_{max}/\ M_{nAASHTO}$ **for G1 and G5 for different residual stresses and imperfection magnitudes at unbraced length** L_r

Section	G1				G5			
Imperfection	$L_b/1000$	$L_b/2000$	$L_b/4000$	$L_b/8000$	$L_b/1000$	$L_b/2000$	$L_b/4000$	$L_b/8000$
Best-Fit Prawel	0.65	0.70	0.73	0.75	0.73	0.79	0.84	0.86
0.5 Best-Fit Prawel	0.71	0.76	0.80	0.82	0.77	0.84	0.89	0.92
Zero RS	0.75	0.81	0.84	0.86	0.81	0.88	0.92	0.94
Mean neglecting the case with Zero RS	0.68	0.73	0.76	0.78	0.75	0.82	0.86	0.89

Table 6-12: $M_{max}/\ M_{nAASHTO}$ **for G1 and G5 for different residual stresses and imperfection magnitudes at unbraced length** $1.5L_r$

Section	G1				G5			
Imperfection	$L_b/1000$	$L_b/2000$	$L_b/4000$	$L_b/8000$	$L_b/1000$	$L_b/2000$	$L_b/4000$	$L_b/8000$
Best-Fit Prawel	0.97	1.01	1.03	1.04	1.05	1.10	1.12	1.14
0.5 Best-Fit Prawel	0.96	1.00	1.01	1.03	1.06	1.10	1.13	1.14
Zero RS	0.93	0.97	0.98	0.99	1.06	1.10	1.12	1.13
Mean neglecting the case with Zero RS	0.96	1.00	1.02	1.04	1.06	1.10	1.13	1.14

From Table 6-12, it appears that the AASHTO flexural capacity is conservative for the slender web section, G5 in the elastic LTB region. This is due to the fact that AASHTO recommends neglecting the St.Venant torsional constant, *J* in the calculation of the elastic LTB strengths of slender web sections. It is clear that there are certain trends in the rolled

sections and welded plate girder type sections that share similarities. The following observations can be made from the sensitivity studies in Sections 6.2.4.1 and 6.2.4.2.

1. For both rolled beams and plate girders, the plateau strength, taken as the strength achieved for the smallest unbraced length considered, is insensitive to the imperfection magnitude and the residual stress pattern.

2. The plateau moment capacity is never reached with either of the rolled beam sections or the noncompact web and slender web plate girders at L_p, even for zero residual stress and near zero imperfections.

3. At the unbraced length L_p, the AISC/AASHTO resistance is unconservative by an average of 10% compared to FE simulations for rolled beams and noncompact web and slender web plate girders (note that this strength is insensitive to the imperfection magnitude and the residual stress pattern, as explained above). This suggests that the actual plateau strength for beams having an effective length factor, $K = 1$ is shorter than that specified by the design curves. This assertion is validated further in Section 6.3. Since the Specification curves are calibrated to experimental data, the specified plateau length would appear to be a result of incidental and unquantified additional end restraints arising from continuity with adjacent unbraced lengths and attachment to test apparatus. Although calibrating the design curves to experimental data has its merits, it is worthwhile to assess the appropriate K factor to assume for incidental restraints, and to question whether $K < 1$ should be built implicitly into the design equations or left to the judgment of the engineer.

4. The elastic LTB strengths specified by the design codes provide a reasonably accurate prediction for rolled sections and doubly-symmetric noncompact and slender web plate girders.

5. The LTB strengths predicted by the Specifications tend to be higher than the simulation data throughout the inelastic LTB region.

Based on the sensitivity studies on experimental tests and simulations of members with ideal fork boundary conditions, the following recommendations are made for the geometric imperfections and residual stresses to be used in FE test simulations to achieve a reasonable correlation with the Specification equations. The imperfection magnitude of $L_b/2000$ combined with one-half of the Lehigh residual stresses provides the best correlation with the AISC and AASHTO LTB resistance equations for rolled sections. Also, a flange sweep of $L_b/2000$, and one-half of the AWS tolerances on flange tilt and web out-of-flatness along with the half Best-Fit Prawel residual stresses appear to be reasonable FE modeling parameters to use for LTB simulation studies on welded plate girders. Combinations more severe than these give simulated strengths that are inconsistent with available experimental data in a large number of cases. In addition, these values are shown to be logical for calculation of the mean results from experimental tests, which often have imperfections and residual stresses that are less severe than the fabrication tolerances and the nominal residual stress patterns. Imperfection or residual stress magnitudes smaller than these are too low, and do not seem appropriate to correlate with the AISC/ AASHTO design curves.

As discussed above, even with using the recommended FE test modeling parameters, there is a lingering disconnect between the Specifications and the test simulation data in

the inelastic LTB region. This is studied further in this chapter, and modifications to the LTB resistance equations are proposed such that this disconnect is minimized.

In all the subsequent studies on LTB, the above recommended geometric imperfections and residual stresses are modeled in FE test simulations.

6.3 Substantiation of Implicit $K_{inelastic}$ in the Specification LTB Equations

Adams et al. (1964) conducted several experimental tests that are valuable to consider. Two of their tests, HT29 and HT36, are rolled beams with compact webs and compact flanges, and have $L_b \cong L_p$, where L_p is defined as $1.1r_t\sqrt{E/F_y}$. The test configuration is four-point bending as shown in Figure 6-10. The crosses denote lateral brace locations. This configuration gives uniform moment in the middle unbraced length while the adjacent segments are less severely loaded and are subjected to moment gradient. The theoretical elastic effective factor for the critical segment in this case, obtained from a rigorous elastic buckling analysis, is $K_{elastic} = 0.83$.
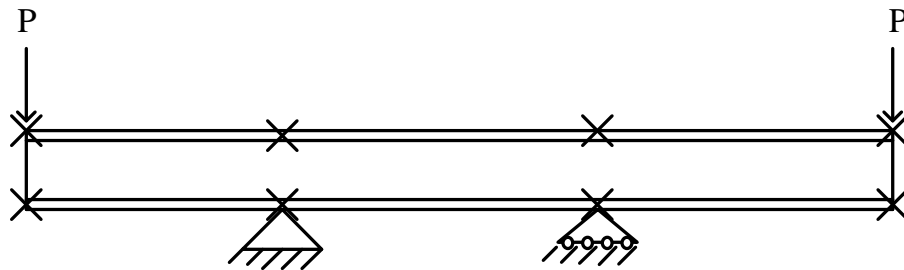
Figure 6-10: Four-point bending test setup by Adams et al. (1964)

It is observed that FE modeling of the girders using the reported configuration gives the plastic moment capacity as reported by Adams, et al. However, modeling of an isolated beam with the same cross-section, fork end conditions and an unbraced length of $0.83L_p$ gives only $0.95M_p$. Modeling with fork end conditions is useful in understanding the

behavior within an unbraced segment with no restraint effects from adjoining segments. When fork end conditions are employed, the unbraced length needs to be reduced to almost $0.50L_p$ to achieve the full plastic moment capacity. The state of the beam at failure in the original experimental test indicated that, while the critical unbraced length was heavily yielded, the adjacent restraining segments were still predominantly elastic. This suggests that the calibration of L_p to experimental data, using $K_{elastic}$ as discussed by White (2008), is insufficient to represent the true behavior. The use of the inelastic effective length factor, $K_{inelastic}$, is more appropriate for the calibration to experimental data. It is evident from the above manipulation of Adams' tests that there is an implicit $K_{inelastic} < K_{elastic}$ that is necessary to properly calibrate the equations.

The use of a calculated $K_{elastic}$ for the calibration unconservatively shifts the LTB curve to the left, leading to an over-prediction of the true capacity in cases that have a true effective length factor close to 1.0. It should be noted that AISC uses an alternate equation, $L_p = 1.76 r_y \sqrt{E/F_y}$, for I-section members with compact flanges and compact webs, which further increases the design plateau length for the girders in Adams' tests by 1.4 times the equation $1.1 r_t \sqrt{E/F_y}$.

6.4 Proposed Model for LTB Resistance

The studies discussed in Section 6.2 and by Kim (2010) have shown that the Specification equations tend to give larger member capacities compared to simulation results at L_p, and in the inelastic LTB region for compact, noncompact and slender web cross-sections. Furthermore, the discussion in Section 6.3 validates the presence of an implicit $K_{inelastic}$ in the current LTB resistance equations. The magnitude of the disconnect

between test simulation strength predictions and the Specification strength estimates in the inelastic LTB region is particularly worrisome. An improvement to the inelastic LTB portion of the strength curve is presented here to rectify the problem. In the proposed approach, a reduced value of $L_p = 0.63 r_t \sqrt{E/F_y}$ originally recommended by Kim (2010), and a smaller maximum stress level for elastic LTB limit of F_L or $F_{yr} = 0.5F_y$ is recommended. The calculations from this model are presented for various doubly-symmetric and singly-symmetric cross-sections along with FE test simulation strengths and current Specification predictions.

Table 6-13 lists the compact-web rolled sections selected for the uniform bending studies and the moment gradient tests discussed subsequently in Chapter 7. All of these sections have compact flanges barring the W14x90 which has a noncompact flange.

Table 6-13: Rolled beams for uniform moment and moment gradient FE simulation tests

Girder	D/t_w	D/b_{fc}	$b_{fc}/2t_{fc}$	Web	Flange
W 21 x 44	57	3	7	Compact	Compact
W 14 x 68	30	1.3	7	Compact	Compact
W 10 x 30	32	1.6	6	Compact	Compact
W 16 x31	55	2.7	6	Compact	Compact
W 14 x 90	29	0.9	10	Compact	Noncompact

Table 6-14 summarizes the non-dimensional parameters for 61 welded plate girder cross-sections studied in this work. The clear depth of the web panel is 150 inches in all girders. These include noncompact and slender web cross-sections with compact and noncompact flanges. Selected girders indicated in the table are also subjected to moment gradient loadings in Chapter 7. AASHTO disallows slender flanges in bridge girders. Cross-sections with slender flanges are expected to fail predominantly by flange local

buckling (FLB) rather than LTB, and are not considered in this research. The noncompact web slenderness limit, λ_{rw}, is equal to 137 for $F_y = 50$ ksi. The cross-sections with web slenderness ($2D_c/t_w$) smaller than this limit are classified as noncompact web sections, while the ones with slenderness greater than this limit are classified as slender web sections. The limiting slenderness for a compact flange, λ_{pf}, is equal to 9.15 for $F_y = 50$ ksi. Cross-sections with flange slenderness ratios greater than this limit are classified as noncompact flange sections.

Table 6-14: Welded plate girders for uniform moment and moment gradient FE simulation tests

Girder	D/t_w	D_c/D	$2D_c/t_w$	D/b_{fc}	$b_{fc}/2t_{fc}$
G1[a, c]	130	0.50	130.0	6	9
G2	130	0.50	130.0	5	11
G3 [a, c]	130	0.50	130.0	3	9
G4	130	0.50	130.0	3	11
G5 [a, c]	180	0.50	180.0	6	9
G6	180	0.50	180.0	6	11
G7 [c]	180	0.50	180.0	3	9
G8	180	0.50	180.0	3	11
G9 [a, c]	130	0.63	162.4	6	9
G10	130	0.63	162.5	5	11
G11 [c]	130	0.63	162.4	3	9
G12	130	0.63	162.6	3	11
G13 [a, c]	180	0.63	224.9	6	9
G14	180	0.63	225.1	6	11
G15 [c]	180	0.63	224.8	3	9

a. Selected for moment gradient tests in Chapter 7.
b. Omitted for moment gradient studies with reverse curvature, as flanges exceed AASHTO limits
c. Selected for studies on noncompact web slenderness limit in Section 6.6

Table 6-14 (Continued): Welded plate girders for uniform moment and moment gradient FE simulation tests

Girder	D/t_w	D_c/D	$2D_c/t_w$	D/b_{fc}	$b_{fc}/2t_{fc}$
G16	180	0.63	224.9	3	11
G17 [c]	130	0.75	194.8	6	9
G18	130	0.75	194.7	5	11
G19 [c]	130	0.75	193.8	3	9
G20	130	0.75	196.0	3	11
G21 [c]	180	0.75	271.6	6	9
G22	180	0.75	271.2	6	11
G23 [c]	180	0.75	268.6	3	9
G24	180	0.75	270.5	3	11
G25 [c]	130	0.50	130.0	5	9
G26	130	0.50	130.0	5	11
G27 [c]	130	0.50	130.0	4	9
G28	130	0.50	130.0	4	11
G29 [c]	130	0.63	162.5	5	9
G30	130	0.63	162.5	5	11
G31 [c]	130	0.63	162.4	4	9
G32	130	0.63	162.5	4	11
G33 [c]	130	0.75	194.9	5	9
G34	130	0.75	194.8	5	11
G35 [c]	130	0.75	194.9	4	9
G36	130	0.75	194.9	4	11
G37 [a, b]	130	0.44	114.2	6	9
G38	130	0.44	115.5	5	11
G39	130	0.44	114.3	5	9
G40	130	0.44	115.2	5	11
G41	130	0.44	115.2	4	9
G42	130	0.44	115.3	4	11
G43	130	0.44	115.5	3	9
G44 [a, b]	130	0.44	115.6	3	11

a. Selected for moment gradient tests in Chapter 7.
b. Omitted for moment gradient studies with reverse curvature, as flanges exceed AASHTO limits
c. Selected for studies on noncompact web slenderness limit in Section 6.6

Table 6-14 (Continued): Welded plate girders for uniform moment and moment gradient FE simulation tests

Girder	D/t_w	D_c/D	$2D_c/t_w$	D/b_{fc}	$b_{fc}/2t_{fc}$
G45 [a, b]	100	0.44	88.0	6	7
G46 [a]	100	0.44	88.4	3	7
G47 [a, c]	100	0.50	100.0	6	7
G48 [c]	100	0.50	100.0	3	7
G49 [a, c]	100	0.63	125.0	6	7
G50 [c]	100	0.63	124.9	3	7
G51 [c]	110	0.50	110.3	7	7
G52 [c]	88	0.63	110.3	7	6
G53 [c]	88	0.63	110.7	6	7
G54 [c]	88	0.63	110.4	3	9
G55 [c]	117	0.50	116.6	7	8
G56 [c]	93	0.63	116.6	7	6
G57 [c]	93	0.63	116.5	3	9
G58 [c]	85	0.63	106.7	7	6
G59 [c]	85	0.63	106.9	3	9
G60 [c]	104	0.63	130.6	7	7
G61 [c]	110	0.63	137.3	7	7

a. Selected for moment gradient tests in Chapter 7.
b. Omitted for moment gradient studies with reverse curvature, as flanges exceed AASHTO limits
c. Selected for studies on noncompact web slenderness limit in Section 6.6

6.5 Verification of Proposed Model

This section discusses the statistics for members at select unbraced lengths tested in this research using the cross-sections summarized in Tables 6-13 and 6-14. Predictions from the proposed model and from the AISC and AASHTO equations are compared in this section. The simulations studies are conducted with fork end conditions as shown in Figure 6-3. The complete set of results for all the 66 girders in Tables 6-13 and 6-14 is presented in Appendix A.

6.5.1 Assessment of Proposed Model for Rolled Beams

Table 6-15 summarizes the statistics for the proposed model and the current AISC equations for rolled beams at specific unbraced lengths.

Table 6-15: Comparison of simulation test predictions with proposed model and current AISC equations at different unbraced lengths for rolled beams in Table 6-13

Statistics	$L_p{}^a$		$L_p + 2/3\ (L_r - L_p)$		$L_r{}^a$		$1.75L_r$	
	$M_{max}/$ M_{nPr}	$M_{max}/$ M_{nAISC}	$M_{max}/$ M_{nPr}	$M_{max}/$ M_{nAISC}	$M_{max}/$ M_{nPr}	$M_{max}/$ M_{nAISC}	$M_{max}/$ M_{nPr}	$M_{max}/$ M_{nAISC}
Mean	1.00	0.91	1.02	0.94	0.98	0.92	1.07	1.07
COV	0.02	0.03	0.03	0.04	0.06	0.07	0.12	0.12
Min	0.97	0.87	0.98	0.89	0.93	0.85	0.95	0.95
Max	1.03	0.94	1.07	0.98	1.08	1.02	1.26	1.26

a. L_p and L_r are calculated as per AISC (2010a)

The following points can be gleaned from the tests on compact web rolled beams.

1. It can be observed from the above table that the simulation results fall below the Specification strength predictions by an average of ten percent at the limiting plateau length, L_p. The proposed model predicts the simulation strengths with a mean of 1.0 at L_p. The minimum value is improved from 0.87 using the current Specification equations to 0.97 using the proposed model.

2. In the intermediate inelastic LTB region, and at L_r, the proposed model once again performs much better than the Specification equations, with regard to both the mean of the simulation data as well as the COV and minimum and maximum values.

3. The proposed model and the Specification equations coincide at long unbraced lengths in the elastic LTB region. It is observed that the theoretical elastic LTB strength is a good prediction for compact web rolled beams at long unbraced

lengths, but not necessarily at shorter unbraced lengths in the current theoretical elastic LTB region.

Figures 6-11 through 6-15 show the simulation data along with the proposed model and the current AISC and Eurocode (CEN 2005) strength predictions. It can be observed that the proposed model correlates best with simulation data. Although the Eurocode equations provide a longer plateau length than the proposed L_p, it has been noted by Greiner and Kaim (2001) that this cannot be justified from FE simulations. The Eurocode also predicts lower strengths in the inelastic LTB region. This is largely due to the use of more severe residual stresses and geometric imperfections than recommended in Section 6.2.
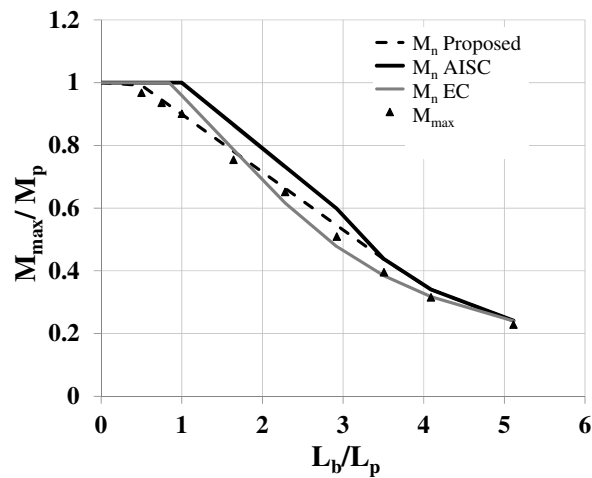
Figure 6-11: LTB curves for W21x44
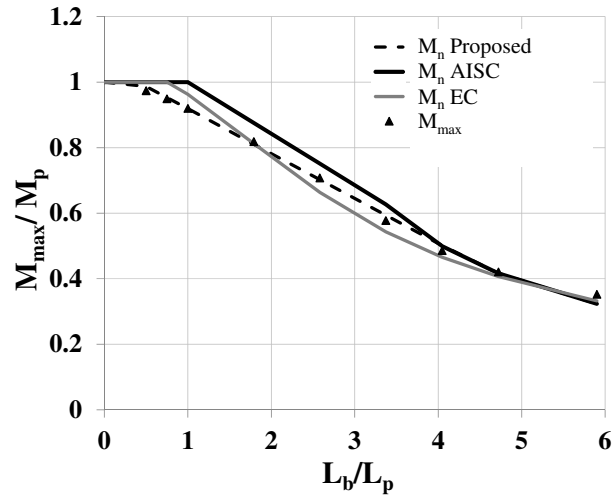
Figure 6-12: LTB curves for W14x68
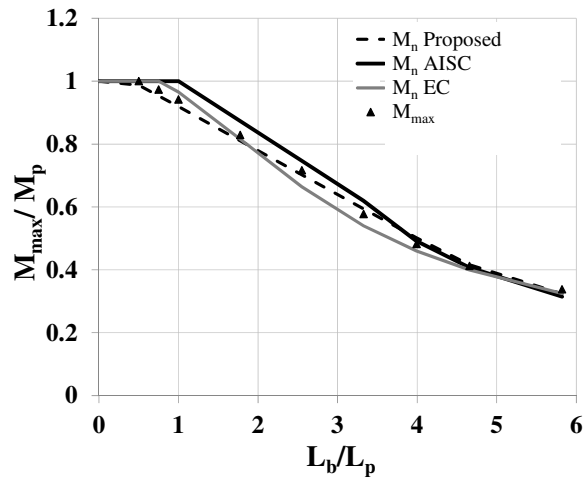
Figure 6-13: LTB curves for W10x30
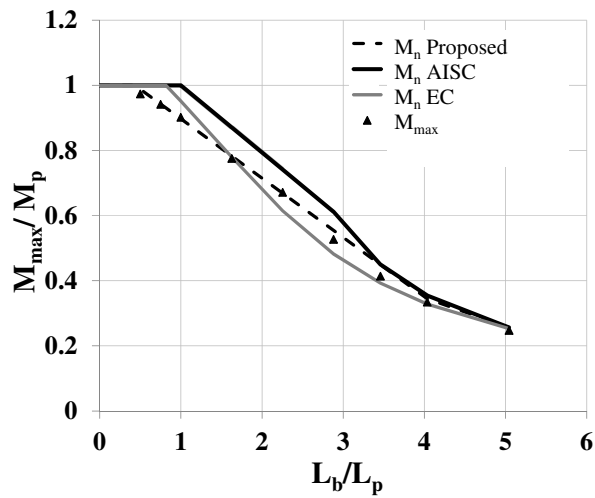
Figure 6-14: LTB curves for W16x31
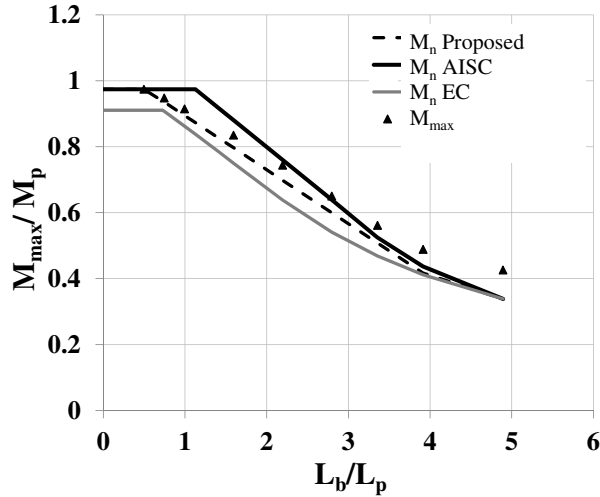
Figure 6-15: LTB curves for W14x90

6.5.2 Assessment of Proposed Model for Noncompact Web Members

Table 6-16 summarizes the statistics for the proposed model and the current AASHTO equations for noncompact webs at specific unbraced lengths. The unbraced lengths at which the results are shown in Tables 6-16 and 6-17 are an approximation to indicate the general region of the LTB curve at which the trends are discussed. The true unbraced lengths used in all the FE test simulations are reported in Appendix A. The values reported are normalized by $M_{nAASHTO}$ because the plateau length L_p is calculated as $1.0r_t\sqrt{E/F_y}$, per

AASHTO instead of $1.1r_t\sqrt{E/F_y}$ per AISC. All other calculations for LTB in the two Specifications remain the same.

The results in Tables 6-16 and 6-17 are grouped by unbraced length using L_r^*, which is calculated from AASHTO Eq. 6.10.8.2.3-5, which neglects the St.Venant torsion constant, J. However, the strengths in Table 6-16 are calculated by including J in the calculations as per the AISC noncompact web member provisions (Eq. F4-8) as well as AASHTO Eq. A6.3.3-5.

Table 6-16: Comparison of simulation test predictions with proposed and current AASHTO equations at different unbraced lengths for noncompact web girders in Table 6-14 (33 girders)

D_c/D	Statistics	$\sim L_p{}^a$		$\sim L_p + 1/2\,(L_r{}^* - L_p)$		$\sim L_r{}^{*\,b}$		$\sim 1.75 L_r{}^*$	
		M_{max}/M_{nPr}	$M_{max}/M_{nAASHTO}$	M_{max}/M_{nPr}	$M_{max}/M_{nAASHTO}$	M_{max}/M_{nPr}	$M_{max}/M_{nAASHTO}$	M_{max}/M_{nPr}	$M_{max}/M_{nAASHTO}$
0.5 (12 No)	Mean	0.99	0.93	0.97	0.89	0.92	0.79	0.99	0.99
	COV	0.06	0.08	0.09	0.09	0.07	0.07	0.03	0.03
	Min	0.90	0.83	0.84	0.76	0.82	0.70	0.93	0.93
	Max	1.08	1.08	1.08	0.99	1.01	0.88	1.01	1.01
0.44 (10 No)	Mean	1.06	1.05	1.03	0.94	0.97	0.84	1.00	1.00
	COV	0.05	0.05	0.04	0.04	0.04	0.04	0.01	0.01
	Min	0.98	0.97	0.95	0.87	0.91	0.80	0.99	0.99
	Max	1.12	1.12	1.08	0.99	1.03	0.89	1.01	1.01
0.63 (11 No)	Mean	0.92	0.88	0.88	0.83	0.86	0.79	0.84	0.84
	COV	0.08	0.08	0.11	0.11	0.09	0.09	0.05	0.07
	Min	0.86	0.82	0.78	0.73	0.76	0.71	0.79	0.73
	Max	1.02	0.98	1.01	0.95	0.95	0.87	0.91	0.91

a. L_p is calculated per Eq. 6.10.8.2.3-4 in AASHTO (2014)
b. $L_r{}^*$ is calculated per Eq. 6.10.8.2.3-5 in AASHTO (2014)

The following can be gleaned from the tests on noncompact web section.

1. As previously observed in Table 6-15 for compact web rolled beams, it may also be noted from Table 6-16 that the simulation results predict lower strengths than the Specification strength equations at the limiting plateau length, L_p, in the cases of doubly and singly-symmetric cross-sections with the larger flanges in tension ($D_c/D = 0.63$). However, both the proposed model, as well as the Specification equations predict lower strengths than the simulation data for the singly-symmetric sections with the smaller flange in tension ($D_c/D = 0.44$). These members are governed by tension flange yielding. It is observed from the FE simulations that R_{pt}, the web plastification factor (or cross-section effective shape factor)

corresponding to the tension flange, which limits the maximum member resistance to a value between M_y and M_p, is typically conservative for these cross-sections.

2. It appears that the proposed model tends to predict higher strengths than FE simulations for some sections in the plateau region. It is observed that some of these noncompact sections, which are expected to reach strengths of $R_{pc}M_{yc} > M_{yc}$ tend to fail before the nominal yield of the cross-section due to load shedding from the web with the advent of web bend-buckling. This behavior is addressed in detail in Section 6.6 and a modified equation to calculate the noncompact web slenderness limit, λ_{rw} is proposed.

3. It should be noted that the AISC/AASHTO equations (with longer L_p and larger F_{yr} than the proposed model) tend to predict the simulation test strengths of some noncompact web sections with $D/b_{fc} \leq 3$ and compact flanges better than they do for narrow flange sections. However, in examining the overall performance of the proposed model, it is a reasonable simplification to use the same limits for wide flange sections as wells as narrow flange sections.

4. In the intermediate inelastic LTB region ($L_p + 1/2\ (L_r^* — L_p)$) and at L_r^*, the proposed model provides a vast improvement (in the order of 13%) over the current AISC and AASHTO equations. It can be observed from Table 6-16, that the mean, minimum and maximum values of M_{max}/M_{nPr} are larger than $M_{max}/M_{nAASHTO}$, while also exhibiting a lower coefficient of variation.

5. The proposed LTB model coincides with the AISC/AASHTO equations at longer unbraced lengths in the elastic LTB region, and the current Specification equations tend to over-predict the simulation test strengths for cross-sections with $D_c/D =$

0.63. The elastic LTB strength equations are conservative by 30 to 40% if J is neglected in the computation of the theoretical LTB strength for these types of members. However, the inclusion of J for these cross-section will tend to be slightly unconservative, by up to approximately 10%.

Figures 6-16 through 6-18 show how the simulation data compare with the proposed and current AASHTO and Eurocode equations for select noncompact web sections with the current λ_{rw} equation. Appendix A shows similar plots for the other girders tested with the proposed equation incorporating the λ_{rw} proposed in Section 6.6.

Figure 6-16 shows the curves for a wide flange noncompact web, compact flange section, while Figures 6-17 and 6-18 compare the data for noncompact web, noncompact flange sections. It is observed that the proposed model is a better fit to the simulation data, especially in the inelastic LTB region.

Furthermore, it is observed that the cross-sections with plateau strengths controlled by flange local buckling (FLB) typically obtain the theoretical capacity specified in the Specification equation for FLB, or obtain higher strengths than the FLB limit states for wider (smaller D/b_{fc}, Figure 6-17) noncompact flanges. Hence, the interaction between FLB and LTB is not a potential problem for cross-sections sized as per AASHTO guidelines. The Eurocode strength predictions are lower than the FE simulation data due to the Eurocode philosophy of providing a lower-bound fit to the data, as well as the assumption of more severe residual stresses for welded plate girder type cross-sections in the development of the Eurocode equations (Greiner and Kaim 2001; Roberts and Narayanan 1988).
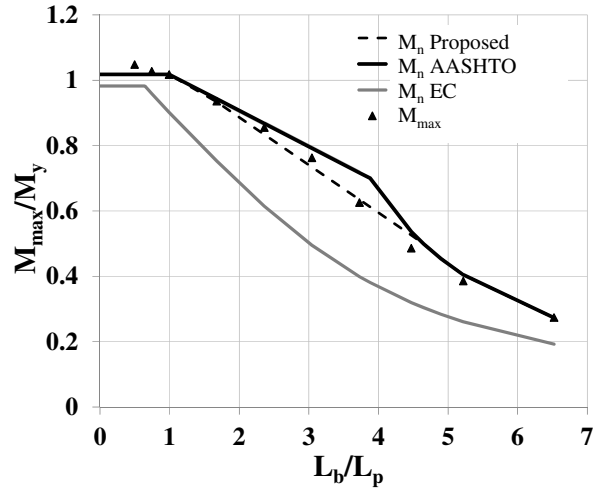
Figure 6-16: LTB curves for welded plate girder with $D/t_w = 130$, $D/b_{fc} = 3$, $D_c/D = 0.5$, $b_{fc}/2t_{fc} = 9$
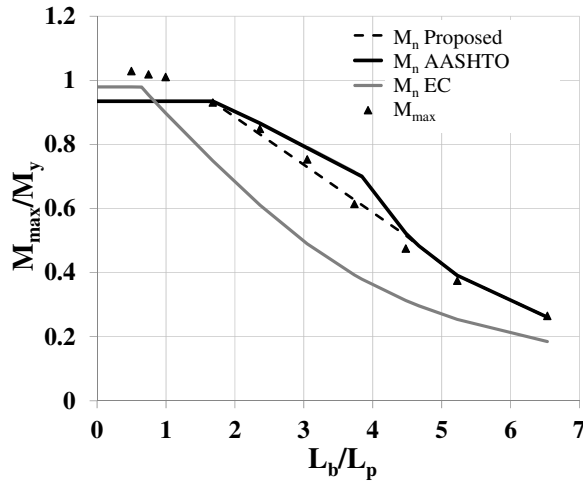
Figure 6-17: LTB curves for welded plate girder with $D/t_w = 130$, $D/b_{fc} = 3$, $D_c/D = 0.5$, $b_{fc}/2t_{fc} = 11$
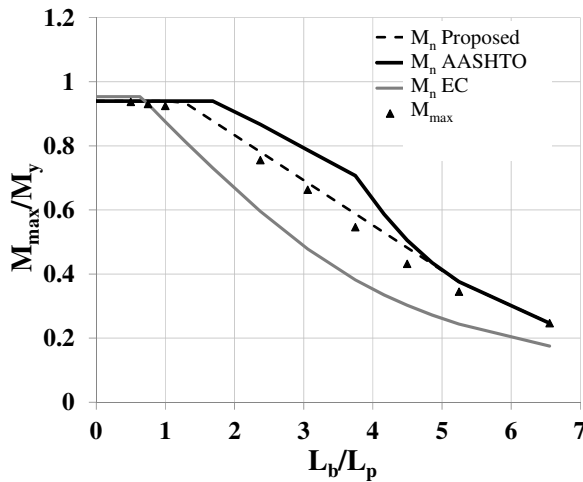
Figure 6-18: LTB curves for welded plate girder with $D/t_w = 130$, $D/b_{fc} = 6$, $D_c/D = 0.5$, $b_{fc}/2t_{fc} = 11$

6.5.3 Assessment of Proposed Model for Slender Web Members

Table 6-17 shows the results from this research for slender web doubly- and singly-symmetric cross-sections. Per the AISC and AASHTO procedures, the St.Venant torsional constant, J, is neglected in the calculations for slender web cross-sections, unlike in the cases of compact and noncompact web cross-section. The following are the key conclusions made from the tests on slender web section.

1. The results from this table at L_p indicate that R_bM_y is a good prediction of the plateau capacity for slender web cross-sections. The R_b in the current AASHTO equations provides a very reasonable estimate of the influence of web bend-buckling on the flexural capacities of slender web cross-sections that are not stiffened longitudinally.

2. The proposed LTB model provides mean M_{max}/M_{nPr} values that are larger than the $M_{max}/M_{nAASHTO}$ values and are closer to 1.0. The proposed LTB model also has a lower coefficient of variation and improves the minimum values of M_{max}/M_n at L_r substantially as compared to the Specification predictions, e.g., the minimum value of M_{max}/M_n for the doubly-symmetric slender-web cross-sections is increased from 0.83 to 0.99 at L_r.

3. The simulation elastic LTB strengths for singly-symmetric cross-sections are larger than the strengths from the resistance equations due to the neglect of J in the calculations. However, including J in the calculations would make the equations up to 50% larger than the simulation strengths. This may be attributed to distortional effects in the web which needs to be studied and quantified in further detail. It is

recommended that neglecting *J* for these cross-sections is the better, albeit conservative approach in computing the elastic LTB strengths of these extreme singly-symmetric cross-sections.

Table 6-17: Comparison of simulation test predictions with proposed model and current AASHTO equations at different unbraced lengths for slender web girders in Table 6-14 (28 girders)

D_c/D	Statistics	$\sim L_p{}^a$		$\sim L_p + 1/2\ (L_r{}^{*2}-L_p)$		$\sim L_r{}^{*b}$		$\geq 1.75L_r{}^*$	
		$M_{max}/$ M_{nPr}	$M_{max}/$ $M_{nAASHTO}$	$M_{max}/$ M_{nPr}	$M_{max}/$ $M_{nAASHTO}$	$M_{max}/$ M_{nPr}	$M_{max}/$ $M_{nAASHTO}$	$M_{max}/$ M_{nPr}	$M_{max}/$ $M_{nAASHTO}$
0.5 (4 No)	Mean	1.03	1.01	1.06	0.97	1.03	0.87	1.12	1.12
	COV	0.04	0.06	0.06	0.06	0.04	0.05	0.03	0.03
	Min	0.99	0.94	1.00	0.91	0.99	0.83	1.10	1.10
	Max	1.08	1.08	1.12	1.02	1.08	0.91	1.17	1.17
0.63 (12 No)	Mean	1.00	0.99	1.05	0.95	1.06	0.90	1.34	1.34
	COV	0.05	0.06	0.06	0.06	0.05	0.05	0.11	0.11
	Min	0.90	0.88	0.95	0.86	0.95	0.82	0.94	0.94
	Max	1.09	1.09	1.13	1.02	1.12	0.95	1.52	1.52
0.75 (12 No)	Mean	1.01	0.99	1.08	0.97	1.10	0.95	1.67	1.67
	COV	0.06	0.07	0.07	0.07	0.07	0.06	0.08	0.08
	Min	0.90	0.86	0.97	0.87	0.98	0.86	1.49	1.49
	Max	1.11	1.11	1.17	1.06	1.19	1.01	1.86	1.86

a. *L_p is calculated per Eq. 6.10.8.2.3-4 in AASHTO (2014)*
b. *L_r * is calculated per Eq. 6.10.8.2.3-5 in AASHTO (2014)*

Figure 6-19 shows the LTB strength curves for a doubly-symmetric slender-web cross-section that has a wide flange (D/b_{fc} = 3). This is consistent with the observations for noncompact web sections that the AISC/AASHTO strength predictions are typically a good match of the simulation predictions for cross-sections having wider flanges relative to the web depth.

To summarize, minor modifications to the LTB resistance equation are proposed, which provides a better fit to simulation data (obtained using reduced imperfections and

residual stresses). The following section discusses a modification to λ_{rw} that completes the resolution of disconnect between simulation data and Specification strengths.
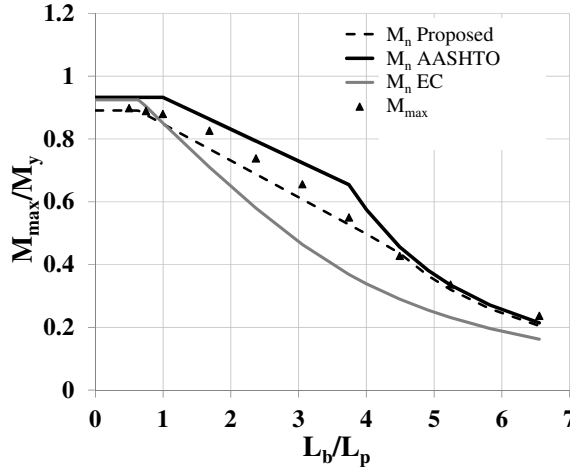
Figure 6-19: LTB curves for welded plate girder with $D/t_w = 180$, $D/b_{fc} = 3$, $D_c/D = 0.5$, $b_{fc}/2t_{fc} = 9$

6.6 Proposed Modification to Noncompact Web Slenderness Limit

The noncompact web slenderness limit, λ_{rw} in AISC and AASHTO is based on an assumed value of the plate buckling coefficient for a web subjected to flexure that is between the values for fixed and simply-supported edge conditions. While the limit provided in the current Specifications is a good representation for cross-sections with larger flanges, the limit overestimates the magnitude of the restraint provided by the flanges for narrow flange sections. This research evaluates this issue and proposes a modified equation to rectify the problem.

6.6.1 Basis of λ_{rw} in Specification Equations and Potential Shortcomings

The web elastic plate buckling equation for an I-section member web may be written in general as,

123

$$\sigma_{cr} = \frac{k.\pi^2 E}{12(1-v^2)}(\frac{t}{b})^2 \tag{6.1}$$

where, $k = 23.9$ for simply-supported edge conditions and $k = 39.6$ for fixed edge conditions

for a doubly-symmetric I-section. By equating σ_{cr} to F_{yc} and performing some algebraic

manipulations, Equation 6.1 may be expressed in the form

$$\frac{b}{t} = c\sqrt{\frac{E}{\sigma_{cr}}} = c\sqrt{\frac{E}{F_{yc}}} \tag{6.2}$$

The coefficient c in Equation 6.2 is 4.6 or 6.0 corresponding to values of k of 23.9 and

39.6. The coefficient c in the current AISC and AASHTO Specifications is 5.7. In these

Specifications, Equation 6.2 is written as the noncompact web slenderness limit

$$\lambda_{rw} = 5.7\sqrt{\frac{E}{F_{yc}}} \tag{6.3}$$

which is compared generally against an effective web slenderness $2D_c/t_w$, where D_c is the

depth of web in compression, and t_w is the thickness of the web. Equation 6.3 clearly

assumes that all I-girder cross-section geometries can provide close to full rotational

restraint from both flanges. Narrow flange sections can have web slenderness values that

satisfy the noncompact web slenderness limit, while their physical behavior involves web

bend-buckling, thus reducing the member plateau strengths to values less than the yield

moment, M_{yc}. In other words, the narrow flanges do not provide sufficient rotational

restraint to the web, resulting in a lower web buckling strength. Hence, the current limit of

λ_{rw} in AISC (2010a) and AASHTO (2014) results in classifying some sections with smaller

flanges as noncompact web sections, whereas these sections should be classified as slender-

web sections. At small unbraced lengths, noncompact web sections are expected to attain strengths $R_{pc}M_{yc} > M_{yc}$. Slender web sections are expected to fail before attaining M_{yc} at strengths equal to $R_bM_{yc} < M_{yc}$. Hence, it is unconservative to design sections that behave as slender-web sections as noncompact web sections.

It is observed that the cross-sections with λ_w in the range of 0.8 to 1.0 times the current λ_{rw} value exhibit the greatest non-conformity to the current code specified classification of web slenderness. This research evaluates various cross-sections, with particular emphasis on sections with λ_w in the above range and proposes a coefficient c in Equation 6.2 that is a function of the ratio of the area of compression flange to area of web in compression, A_{fc}/A_{wc}. The girders tested have compact flanges, and unbraced lengths such that the LTB plateau strength is the controlling limit state.

6.6.2 Test Setup

Table 6-14 lists 33 cross-sections which have web slenderness in the range described above, and are used for the studies on the noncompact web slenderness limit in this section. These cross-sections are marked on a subset of the girders listed in Table 6-14. The simulation testes are conducted on members with fork boundary conditions subjected to uniform moment.

The tests include doubly-symmetric and singly-symmetric cross-sections. However, cross-section geometries that have tension flange yielding as the governing limit state are precluded from these studies because of the observed conservative nature of R_{pt} for several cross-sections, where R_{pt} is the web plastification factor for the tension flange which increases the flexural capacity of the section beyond the moment at first yield of the tension

125

flange. (The behavior for these types of tests is discussed in Section 6.5). The objective of this study is to analyze the variation in the coefficient c for different cross-section geometries, and thereby recommend a value of c in Equation 6.2 that accounts for the edge restraint on the web from the flanges. The ideal value of c (within the limits of 4.6 and 5.7) is computed, which when applied in Equation 6.2, will provide an exact match of the FE simulation strength (M_{max}) to the theoretical plateau strength ($M_{nAASHTO}$). The plateau strength is $R_{pc}M_y$ or R_bM_y, depending on whether a section is noncompact or slender as per the computed value of c for that cross-section.

6.6.3 Results

The database of "c" obtained for the studied cross-sections is analyzed for sensitivity to various cross-section parameters. The coefficient c is restricted to a maximum value of 5.70, which is the coefficient used in the current specifications, since it is observed that this is sufficient for most cross-sections with larger flanges to theoretically achieve the simulation strengths. The coefficient is also restricted to a minimum value of 4.6. It is recognized that the ratio of the area of compression flange to area of web in compression, A_{fc}/A_{wc} is the most dominant parameter in influencing c. The variation of c with this ratio is shown in Figure 6-20.

Figure 6-20: Variation of the coefficient 'c' in Equation 6.2

It can be seen from Figure 6-20 that 4.6 is a lower bound of c for cross-sections with low values of A_{fc}/A_{wc}. The value c may be approximated as a linear variation between 4.6 and 5.7 for values of A_{fc}/A_{wc} between the limits of 0.75 and 1.04. The coefficient c attains a plateau of 5.7 for values of A_{fc}/A_{wc} greater than 1.04. Based on these findings, the modified form is proposed as

$$\lambda_{rw} = (3.1 + 2.5\frac{A_{fc}}{A_{wc}})\sqrt{\frac{E}{F_{yc}}}$$

$$\geq 4.6\sqrt{\frac{E}{F_{yc}}} \qquad (6.4)$$

$$\leq 5.7\sqrt{\frac{E}{F_{yc}}}$$

The variation of the proposed λ_{rw} with A_{fc}/A_{wc} is shown in Figure 6-21.

127

Figure 6-21: Variation of the proposed λ_w with A_{fc}/A_{wc}

The improvement in the prediction of simulation strengths by the use of Equation 6.4 is evaluated by comparing to the current AISC/AASHTO strength predictions. Figures 6-22 and 6-23 show the ratios of $M_{max}/M_{nProposed}$ and $M_{max}/M_{nAASHTO}$ for various web slenderness values, where $M_{nProposed}$ is the flexural capacity using the proposed λ_{rw}. It can be observed that all the data points are shifted higher in Figure 6-23 compared to Figure 6-22. Most of the simulation data points in Figure 6-22 are below 1.0, and are up to 9% smaller than the Specification strength predictions. The proposed model shifts the data points closer to 1.0 or higher, and limits the smallest values of $M_{max}/M_{nProposed}$ to 0.97.
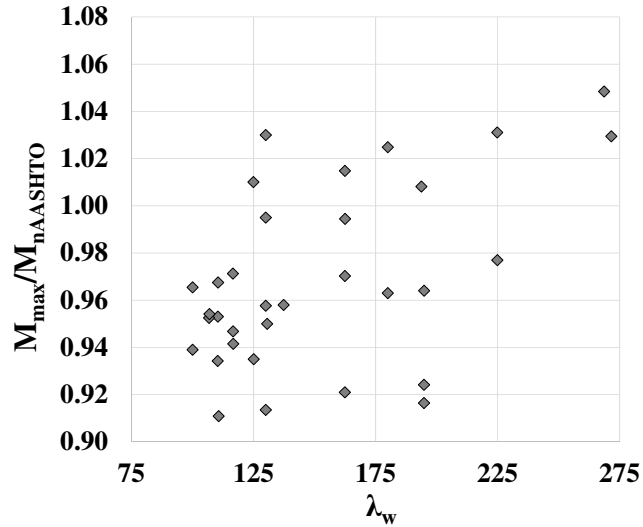
Figure 6-22: Variation of $M_{max}/M_{nAASHTO}$ with web slenderness ratio λ_w
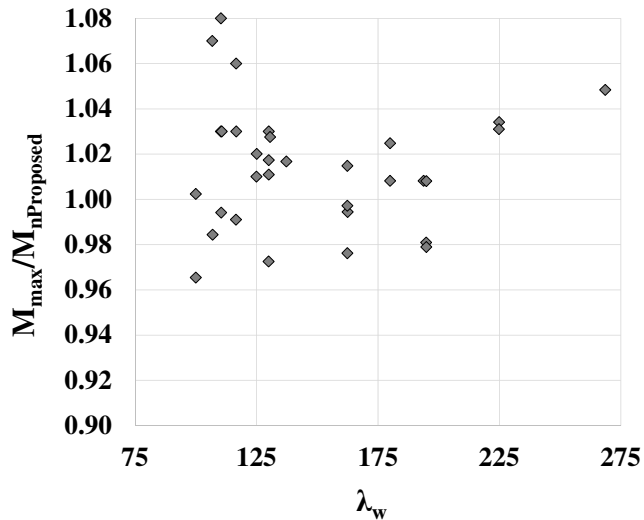
Figure 6-23: Variation of $M_{max}/M_{nProposed}$ with web slenderness ratio λ_w

Tables 6-18 and 6-19 list the overall statistics for the noncompact and slender web girders, with compact flanges considered in this study. R_{pc} and R_b are calculated using the current Specification equations. It should be noted that the predictions not only improve for sections previously classified as noncompact web sections, and now classified as slender web sections, but are also improved for sections classified currently as slender web sections. This is because the proposed equation lowers the value of λ_{rw} for smaller flange sections. The plateau capacity, calculated as R_bM_y, is smaller due to the higher relative

129

slenderness of the web ($2D_c/t_w - \lambda_{rw}$). This effect is most significant for cross-sections with λ_w in the range of 1.0 to 1.2 λ_{rw}.

Table 6-18: Statistics for plateau strengths of noncompact web, compact flange sections comparing $\lambda_{wCurrent}$ and $\lambda_w P_{roposed}$

Statistics	M_{max}/M_{nAISC}	$M_{max}/M_{nProposed}$
Mean	0.96	1.02
COV	0.03	0.03
Max	1.03	1.08
Min	0.91	0.97

Table 6-19: Statistics for plateau strengths of slender web, compact flange sections comparing $\lambda_{wCurrent}$ and $\lambda_w P_{roposed}$

Statistics	M_{max}/M_{nAISC}	$M_{max}/M_{nProposed}$
Mean	0.98	1.02
COV	0.04	0.03
Max	1.05	1.11
Min	0.92	0.98

It can be observed from Tables 6-18 and 6-19 that the proposed values match the simulation strength predictions better than the current Specifications. The minimum values, in particular are improved by 6%. This difference is essential to address because, the proposed model not only helps to address the difference in the plateau capacities, but also the resolves the over-estimation of capacities throughout the inelastic LTB region for these types of members. Thus, the proposed Equation 6.4 is an essential part of capturing the true LTB curve of a cross-section.

6.6.4 Re-examining the Proposed LTB Model Using the Proposed λ_{rw}

Figures 6-24 to 6-26 compare the LTB curves of the current Specifications equations and using the proposed LTB model in Section 6.4, both with the current λ_{rw} and the

proposed λ_{rw} given by Equation 6.4, for a few select sections with web slenderness in the range of 0.8 to 1.2 times of λ_{rw}. Figures 6-24 and 6-25 compare the plots for two noncompact web sections, while Figure 6-26 analyzes the plots for a slender web section.
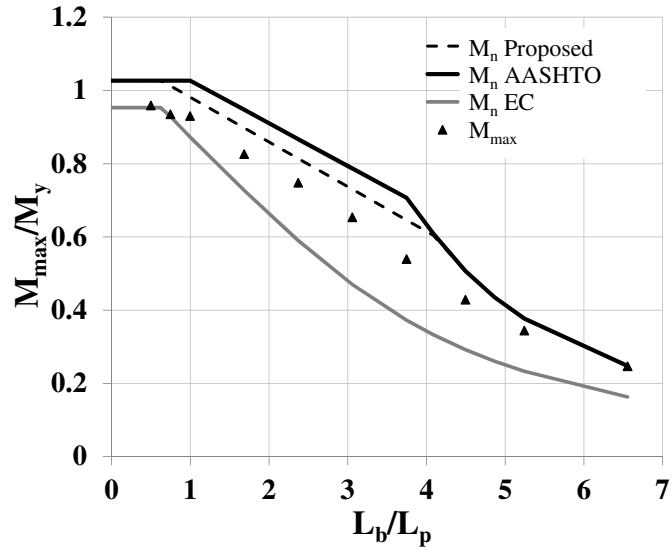
(a) Current λ_{rw}
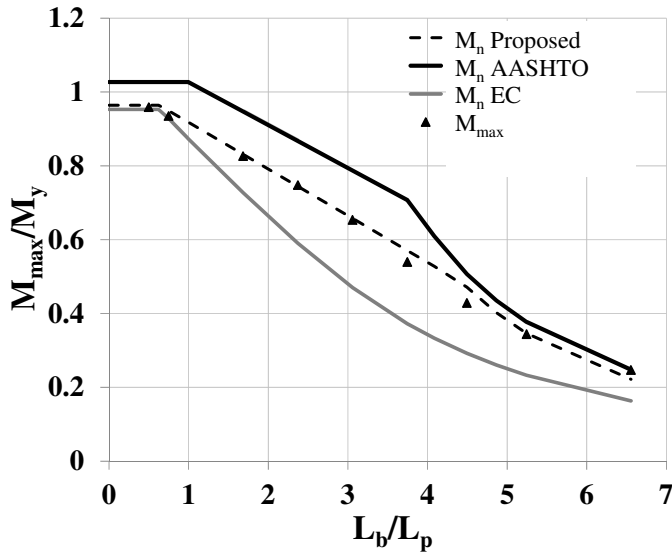
(b) Proposed λ_{rw}

Figure 6-24: LTB curves for welded noncompact web girder with D/t_w =130, $D/b_{fc} = 6$, $D_c/D = 0.5$, $b_{fc}/2t_{fc} = 9$
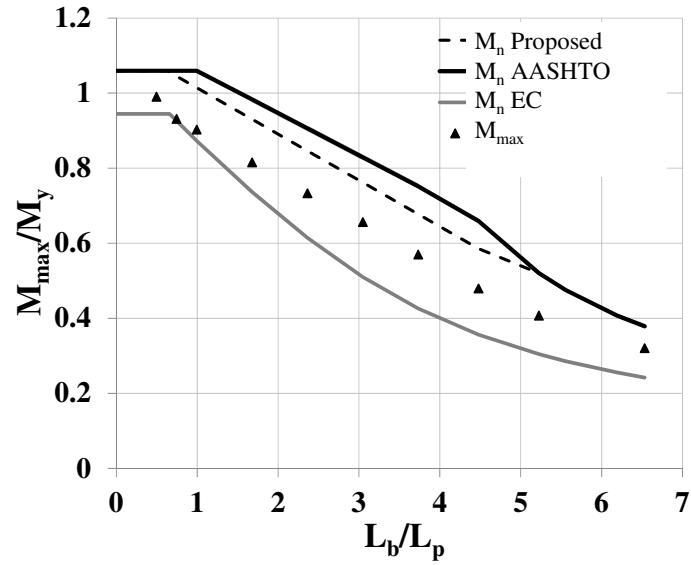
(a) Current λ_{rw}
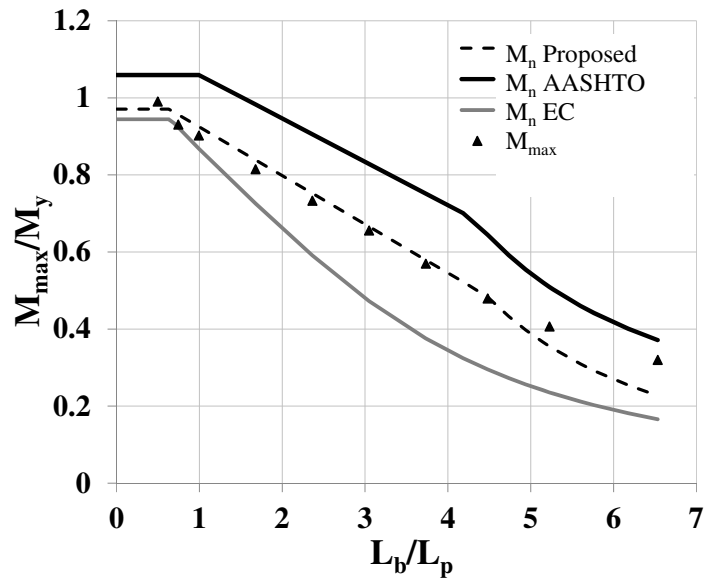
(b) Proposed λ_{rw}

Figure 6-25: LTB curves for welded noncompact web girder with $D/t_w = 100$, $D/b_{fc} = 6$, $D_c/D = 0.63$, $b_{fc}/2t_{fc} = 7$

The elastic LTB strengths obtained by the current Specification equations is higher than the proposed model for the noncompact web sections because the classification of these webs change from noncompact to slender, and the constant J is neglected in the computations.

Henceforth, in this dissertation, the "Proposed LTB model" shall refer to the improved

recommendations suggested in Section 6.4, used along with the proposed λ_{rw}.
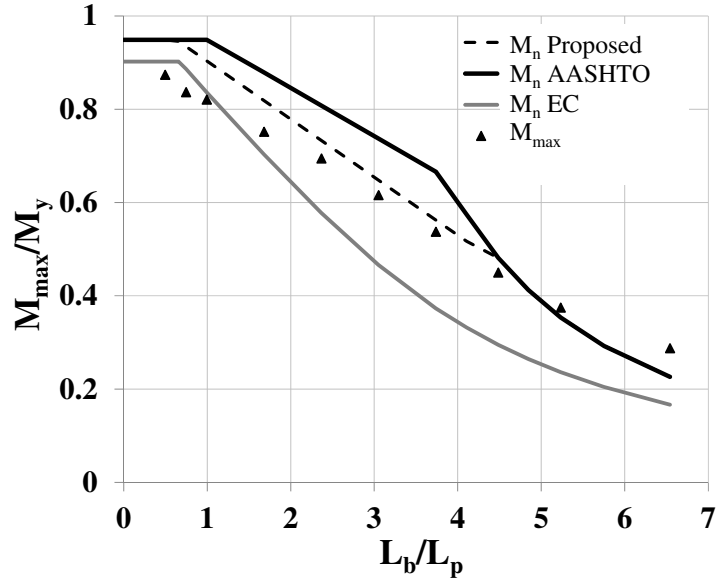
(a) Current λ_{rw}
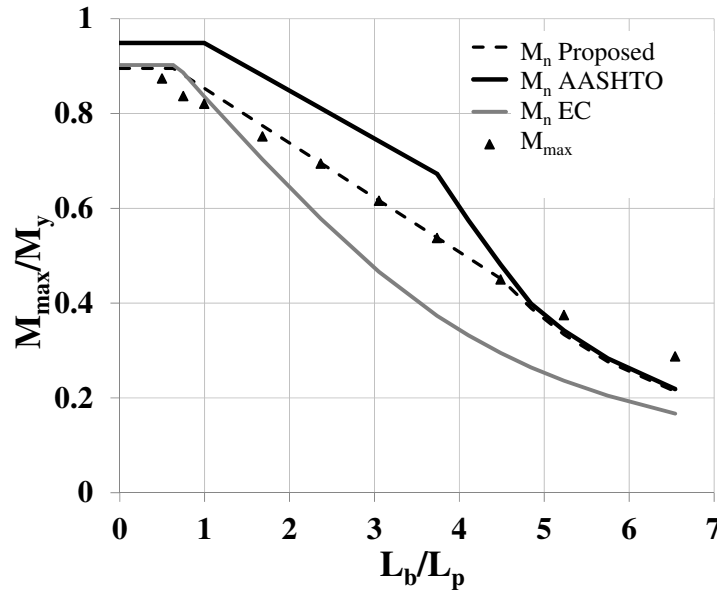
(b) Proposed λ_{rw}

Figure 6-26: LTB curves for welded slender web girder with $D/t_w =130$, $D/b_{fc} = 6$, $D_c/D = 0.63$, $b_{fc}/2t_{fc}$ = 9

6.7 Verification of Proposed Model for Hybrid Girders

Bridge girders are often designed with a higher strength bottom flange (compression flange in negative flexure regions) than the web plate. To account for the early yielding of the web, and hence the reduced contribution of the web to the flexural resistance of the girder at the flange yield limit state, AASHTO introduces a hybrid factor, R_h (given by AASHTO Equation 6.10.1.10.1-1). R_h is taken as 1.0 for homogenous girders and for built-up sections with higher strength steel in the webs. The equation is a non-iterative conservative adaptation of the research conducted originally on doubly-symmetric cross-sections to singly-symmetric cross-sections, with importance given to the side of the neutral axis that yields first. AASHTO also allows a calculation of R_h based on an iterative strain compatibility analysis in lieu of the approximate equation. However, early web yielding is found to have little effect on compression flange yielding (ASCE 1968), and the effect is noticeable only at stress levels close to the compression flange yield stress. The computed values of R_h are typically close to 1.0 and hence the conservative nature of R_h as per AASHTO is not expected to be a severe penalty. The R_h expression in AASHTO is used in the solutions discussed in this section. The LTB plateau strength is calculated as $R_b R_h F_{yc}$ for slender web sections, and $R_{pc} F_{yc}$ for noncompact and compact web sections. Detailed guidelines for calculating the flexural resistance of girders as per the AASHTO provisions is given in White (2008).

The Eurocode strengths are computed by the calculation of the web effective cross-section using the compression flange yield stress rather than the yield stress of the web plate. This also allows for some ductility and partial plastification in the web (Beg et al. 2010). Eurocode also restricts F_{yc} to be not greater than $2F_{yw}$.

The proposed LTB model is based on tests conducted on homogenous girders. Table 6-20 lists 9 girders that are tested to validate the recommendations from this research for hybrid girders. The girders have been numbered from 62 to 70 following the 61 homogenous girders previously studied in Table 6-14. These tests are modeled with fork boundary conditions and subjected to uniform moment. The same residual stresses and geometric imperfections used for homogenous girders are used here as well. It has been noted by Nethercot (1976) that the residual stress distributions in hybrid girders are similar to geometrically similar homogenous girders.

As explained in Section 3.3, the hybrid girders are modeled with both flanges with yield strengths of 70 ksi and webs of 50 ksi. The noncompact web slenderness limit, λ_{rw} as per the current AISC/AASHTO equations is 116. Therefore, only G65 and G66 have noncompact webs, while the rest have slender webs. Per the proposed λ_{rw} limit, only G66 is a noncompact web section, while G65 is a slender web member. The compact limit for the compression flange is 7.73. Only compact flanges are studied in this section, as it has been demonstrated sufficiently that under the limits imposed by AASHTO on the flange slenderness, there is no coupling of the FLB and the LTB limit states, and that they can be considered separately. Girders which are controlled by the TFY limit state are also not considered for this selective study.

Table 6-20: Welded hybrid plate girders subjected to uniform moment

Girder	D/t_w	D_c/D	$2D_c/t_w$	D/b_{fc}	$b_{fc}/2t_{fc}$
G62		0.5	130.0	6	7.14
G63	130	0.5	130.0	3	7.69
G64		0.63	162.6	6	7.14
G65		0.5	100.0	6	7.14
G66	100	0.5	100.0	3	7.69
G67		0.63	125.0	6	7.14
G68		0.5	180.0	6	7.14
G69	180	0.5	180.0	3	7.69
670		0.63	224.5	6	7.14

Figures 6-27 to 6-29 show the results for three of the girders in the above table. The complete set of plots for the 9 girders is presented in Appendix A.
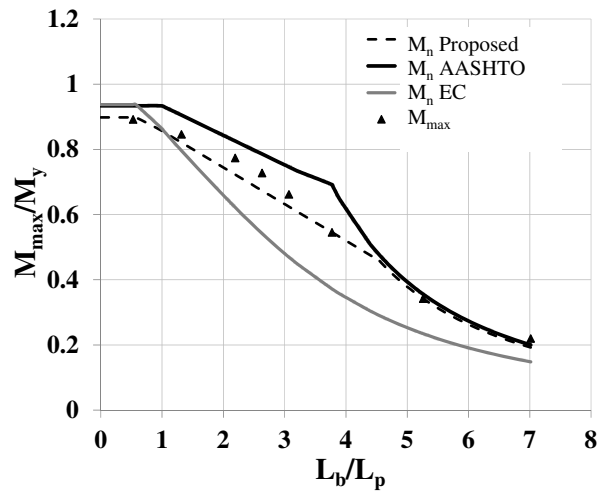
Figure 6-27: LTB curves for hybrid girder G62

136
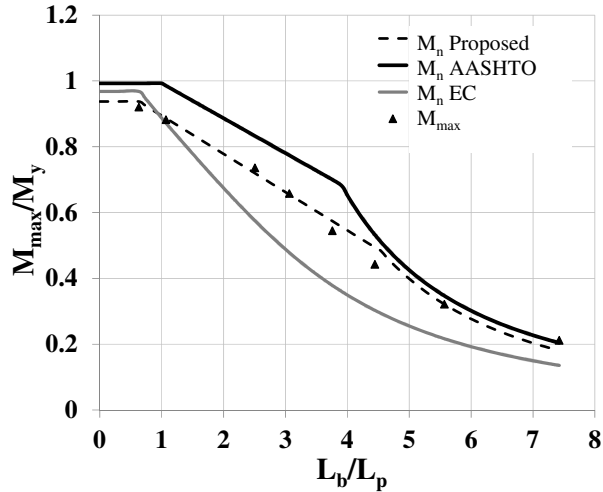
Figure 6-28: LTB curves for hybrid girder G65
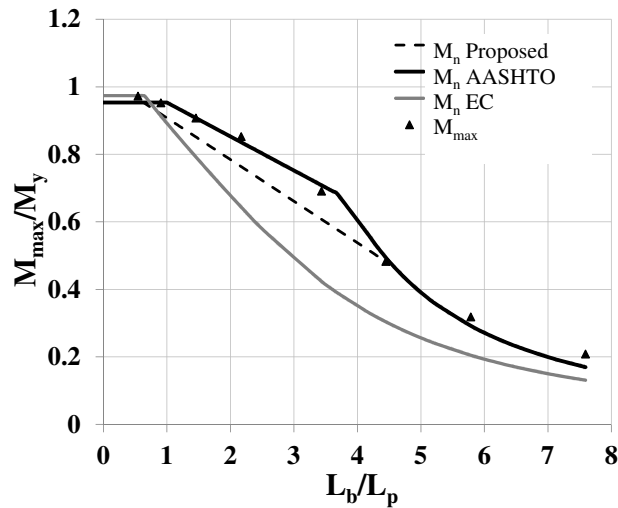
Figure 6-29: LTB curves for hybrid girder G69

It is evident from the above figures that the proposed LTB model fits the test simulation data with higher accuracy than the current Specification equations for hybrid girders as well. However, the proposed equation is conservative by less than 10% in the inelastic LTB regions for some wider flange sections, as shown in Figure 6-29. These observations are consistent with those made by Nethercot (1976), where he noted that early web yielding in hybrid girders has virtually no influence on the lateral stability of the girder, and it is the onset of compression flange yielding that causes large reductions in lateral stiffness and

rapid reductions in stability. He also noted that in general, hybrid girders demonstrated superior strengths as compared to equivalent homogenous girders. Overall, the proposed equations work satisfactorily for girders subjected to uniform moment.

By allowing the use of a single F_{yr} or F_L of $0.5F_{yc}$ in the LTB equations (which currently requires F_{yr} to be the smaller of $0.7F_{yc}$ or F_{yw}, but not less than $0.5F_{yc}$), the design equations have been simplified, and recognizes that early web yielding does not greatly influence the lateral stability of the compression flange. However, this research is focused on girders with the web steel plate only one grade lower than the flange yield plate.

6.8 Summary

The following are the key findings presented in this chapter.

1. Nominal imperfections, which are half of the AWS or AISC COSP tolerances, along with Half-Lehigh (for rolled beams) or Half-Best-Fit Prawel (for welded cross-sections) residual stresses are recommended to be used in FE test simulations.

2. Modifications to the current LTB resistance equations in the Specifications is proposed, by recommending a smaller L_p, and a smaller F_{yr} or F_L.

3. Modifications to the noncompact web slenderness limit, λ_{rw} is proposed and shown to improve the correlation of test data when used in conjunction with the proposed LTB model.

4. The suggested recommendations are shown to perform well for hybrid girders as well, which allows the simplification of the current Specification equations with regard to hybrid girders. F_{yr} is recommended as $0.5\ F_{yc}$ for both homogenous and hybrid girders.

Tests with moment gradients are discussed in Chapter 7.

CHAPTER 7

LATERAL TORSIONAL BUCKLING OF STRAIGHT

UNSTIFFENED GIRDERS SUBJECTED TO MOMENT GRADIENT

Modifications to the LTB resistance equations are proposed in the previous chapter based on uniform bending tests. This chapter evaluates the proposed model for various moment gradient loadings for rolled beams and welded homogenous plate girder cross-sections without longitudinal stiffeners.

AISC accounts for moment gradient by applying an LTB moment modification factor C_b on the resistance equations for uniform moment. The modifier, C_b is taken equal to 1.0 for uniform moment, and is calculated per AISC equation C-F1-1

$$C_b = 1.75 + 1.05 \left(\frac{M_1}{M_2} \right) + 0.3 \left(\frac{M_1}{M_2} \right)^2 \leq 2.3 \tag{7.1}$$

for the linear moment diagrams considered in this research. M_1 and M_2 are the smaller and larger moments at the ends of the unbraced lengths respectively. C_b is calculated as per AISC Eq. C-F1-2

$$C_b = \frac{12.5 M_{max}}{2.5 M_{max} + 3 M_A + 4 M_B + 3 M_C} \tag{7.2}$$

when there is transverse loading within the unbraced segment. M_A, M_B and M_C are the absolute values of the moments at the three quarter points along the unbraced length, and M_{max} is the absolute value of the maximum moment within the unbraced segment of the beam. The Specification equations scale the flexural resistance of the cross-sections by C_b,

while limiting the maximum moment to the plateau capacity (M_p for a compact section rolled beam, and $R_bR_{pc}M_y$ for noncompact and slender sections) of the beam.

7.1 Evaluation of Proposed Model for Rolled Beams Subjected to Moment Gradient

Rolled beams are studied for both linear and nonlinear moment diagrams within the unbraced segment in the following sections.

7.1.1 Rolled Beams Subjected to Linear Moment Gradient

The five rolled beams listed in Table 6-13 are studied for cases of fork boundary conditions and linear moment diagrams, as shown in Figure 7-1. This chapter evaluates moment gradients with β = 0.5, 0 and -1, which yield values of C_b equal to 1.3, 1.75 and 2.3 from Equation 7.1 respectively.
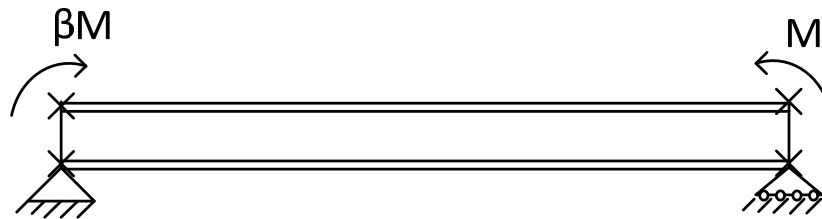
Figure 7-1: Test setup for linear moment gradient studies

Figures 7-2 through 7-6 show the results for the moment gradient studies for the five rolled sections with the three linear moment gradient cases. Eurocode (CEN 2005) does not give explicit directions for the calculation of the moment gradient modifier, C_b. This research uses the same values of C_b as given by the AISC equations for computing the theoretical elastic LTB resistance per the Eurocode equation, which is then used to calculate the slenderness parameter of the member.

The figures also present the moment capacities obtained from SABRE2 (White et al. 2015). SABRE2 is a computational tool that performs rigorous inelastic buckling solutions using stiffness reduction factors based on the AISC & AASHTO LTB resistance equations. This tool implicitly captures the moment gradient effects based on the applied loading as well as the end restraint effects based on the specified boundary conditions. SABRE2 provides an option to compute the stiffness reduction factor in the inelastic buckling solution based on the proposed LTB equation in Chapter 6. Figures 7-2 through 7-6 show SABRE2 results when applied to the proposed LTB equation.
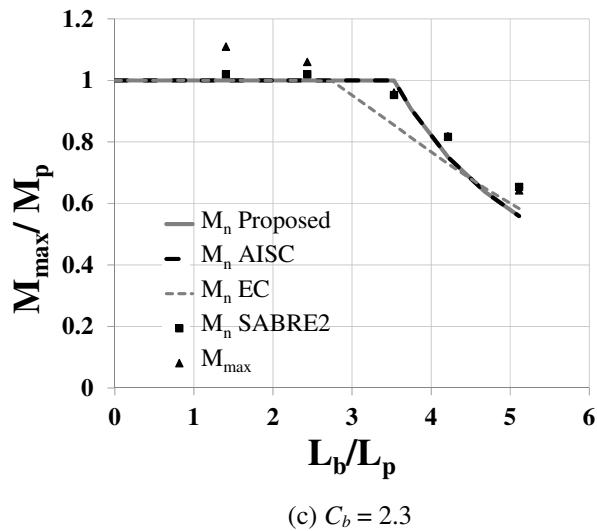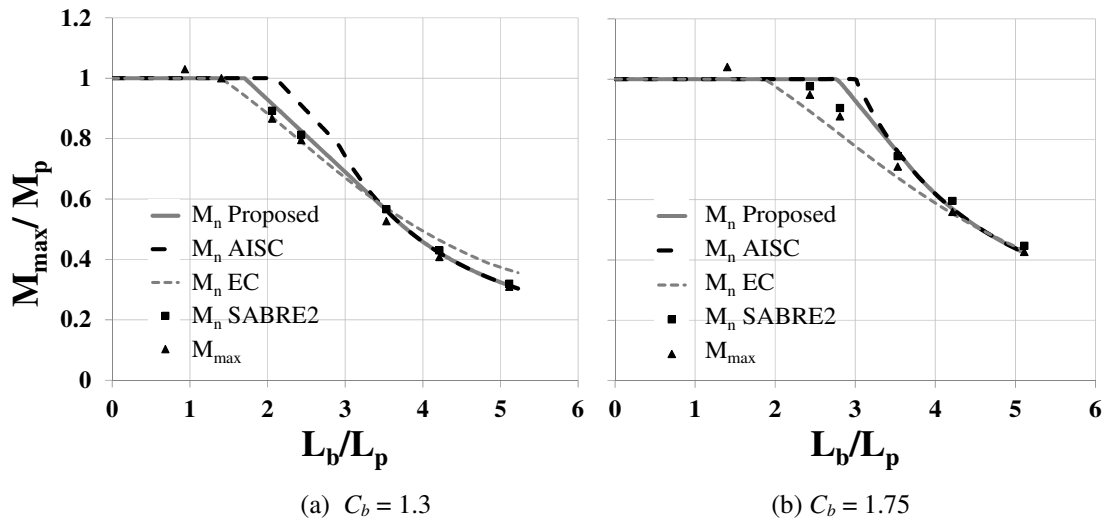
(a) $C_b = 1.3$

(b) $C_b = 1.75$

(c) $C_b = 2.3$

Figure 7-2 : Moment gradient LTB curves for W21x44
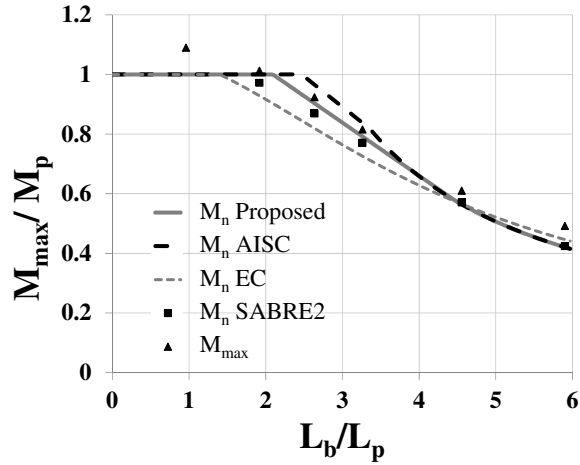
(a) $C_b = 1.3$
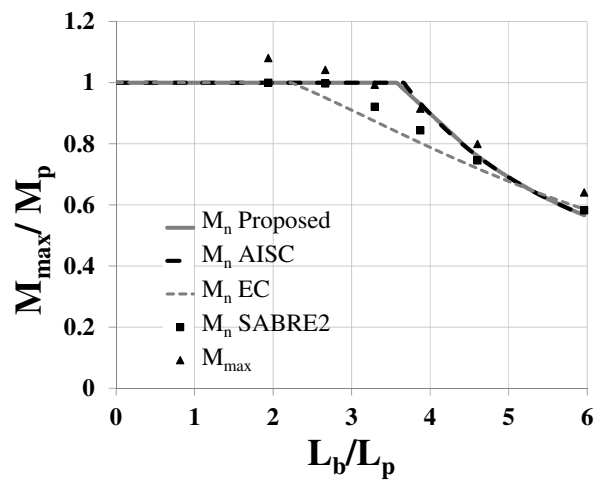
(b) $C_b = 1.75$
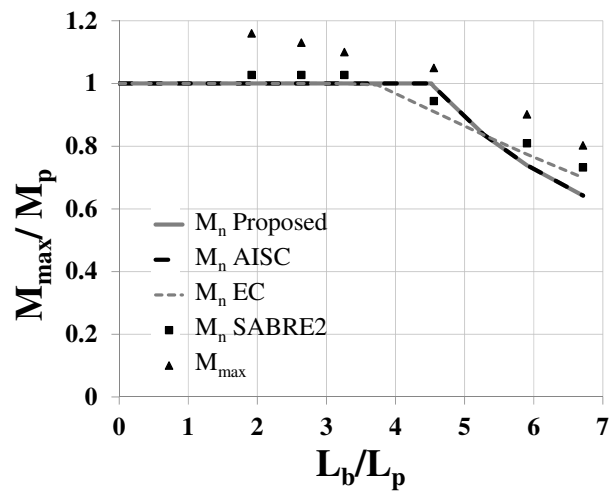
(c) $C_b = 2.3$

Figure 7-3: Moment gradient LTB curves for W14x68
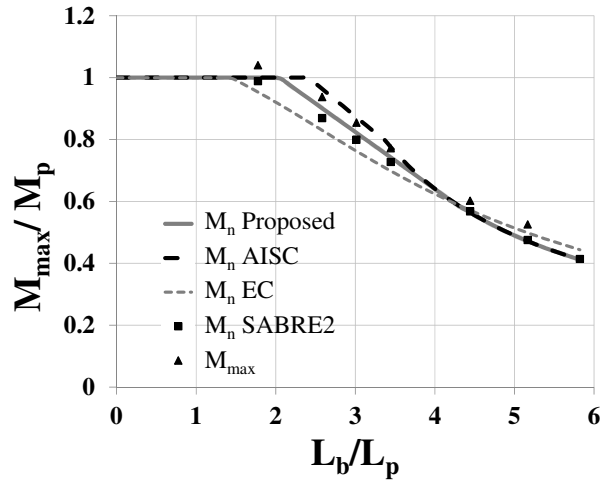
(a) C_b = 1.3
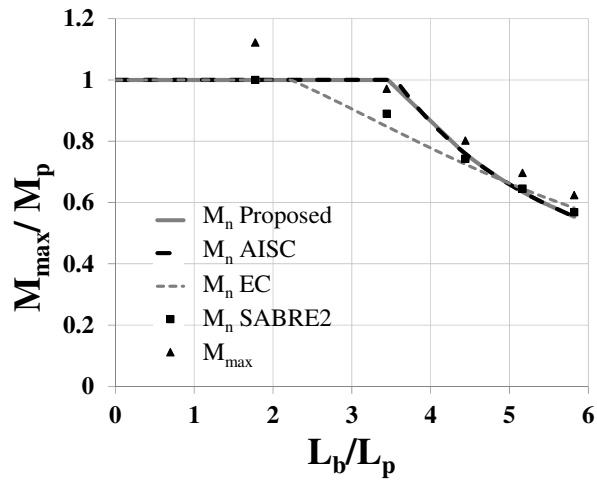
(b) C_b = 1.75
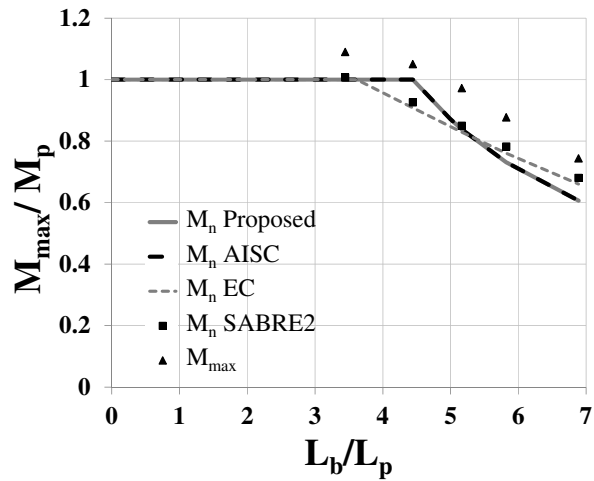
(c) C_b = 2.3

Figure 7-4: Moment gradient LTB curves for W10x30

143
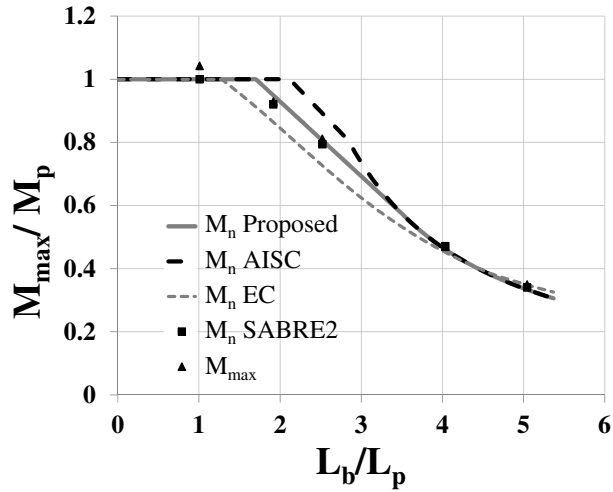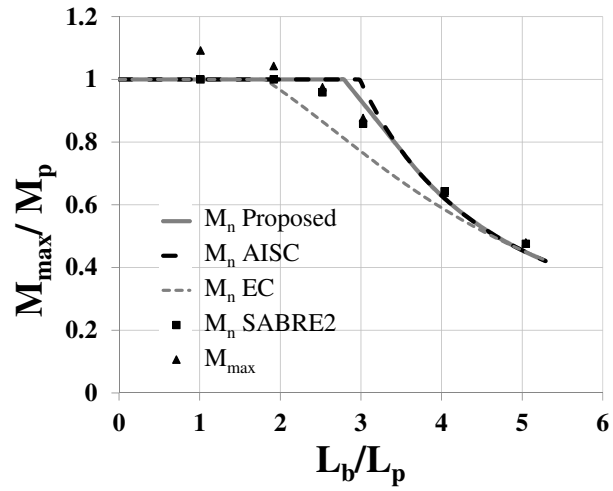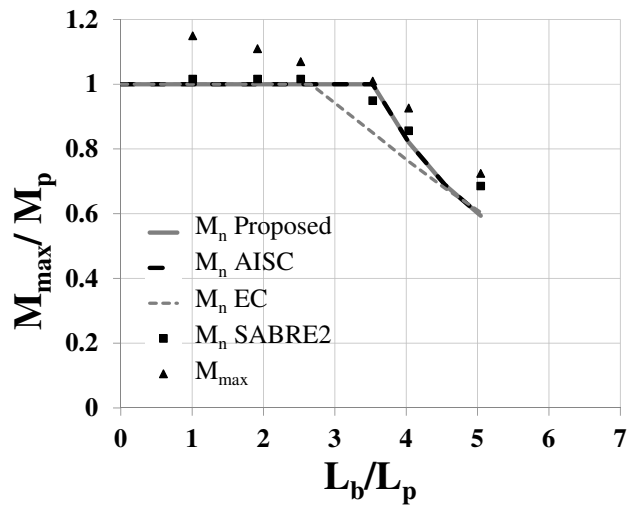
(a) $C_b = 1.3$

(b) $C_b = 1.75$

(c) $C_b = 2.3$

Figure 7-5: Moment gradient LTB curves for W16x31

144
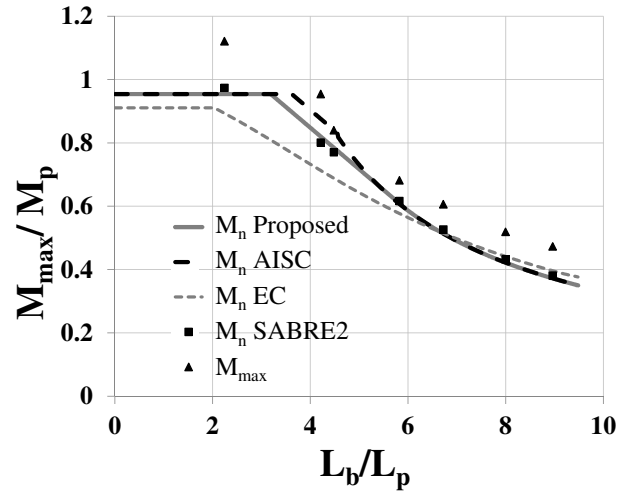
(a) $C_b = 1.3$
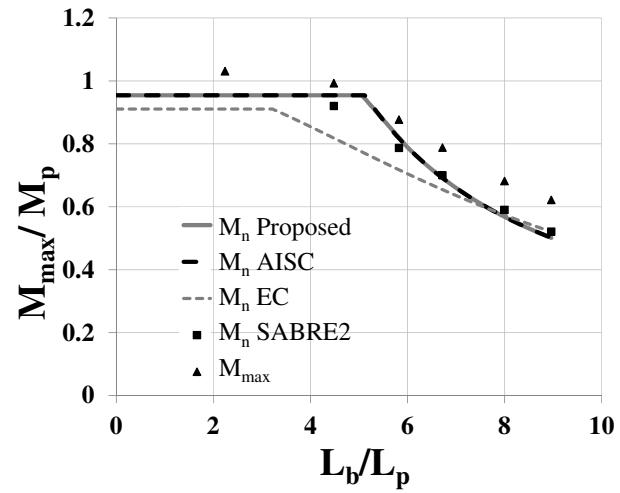
(b) $C_b = 1.75$
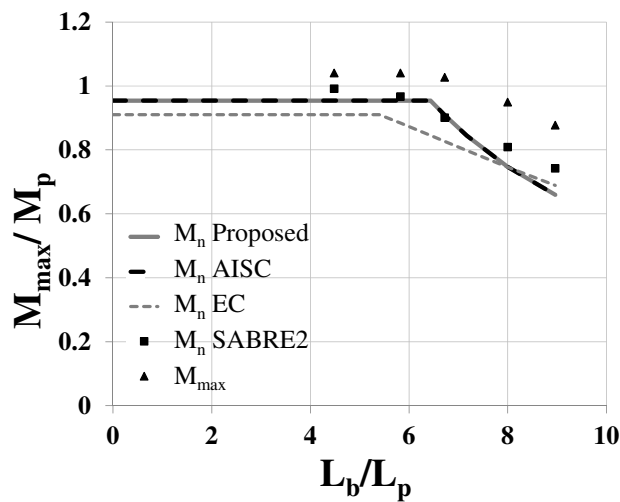
(c) $C_b = 2.3$

Figure 7-6: Moment gradient LTB curves for W14x90

145

The following can be gleaned from the above figures.

1. The proposed model gives the best curve-fit to the simulation data for cases with $C_b = 1.3$. The exception for this is the W14 x 90, for which the current Specification equations provide the best estimate of the capacities. This can be attributed to the fact that the plateau strength is governed by flange local buckling and this mode of failure in general exhibits some postbuckling reserve, making the Specification equations conservative. Also, this cross-section has a very small web depth to compression flange width ratio ($D/b_{fc} < 1.0$). Such wide flange sections in general exhibit larger flexural capacities than narrow flange sections as witnessed in the uniform moment tests presented in Section 6.5.

2. The proposed model and the current Specification equations essentially coincide for the cases with $C_b = 1.75$ and $C_b = 2.3$. It is also observed that the simulation strengths are typically higher than the Specification strength predictions for these cases. The AISC curves match the simulation strengths, or are slightly higher in the inelastic LTB region for the W21x44. The W21x44 is a beam type section with a high ratio of D/b_{fc}. It has been observed that such narrow flange sections tend to exhibit lower flexural strengths than sections with wide flanges. However, it is noteworthy that the simulation strengths in this research with an initial flange sweep of $L_b/2000$ and one-half Lehigh residual stresses predict capacities that are comparable with the Specification equations. Previous work (Kim 2010; Lokhande and White 2014) using more severe geometric imperfections and residual stresses, that are twice the values used in this research predict much lower capacities than the Specification equations. Given that the Specification equations represent the

146

mean of experimental data, the observed results indicate that the FE modeling parameters are adequate and not overly conservative.

3. The LTB moment modifier, C_b, that is currently recommended in the Specifications for the linear moment diagrams represents a lower bound to the true value of C_b for compact web rolled beams. This is clear from the above figures where the simulation data come in consistently higher than the resistance equations in the elastic buckling range. This is especially true for the fully reversed curvature bending case with $C_b = 2.3$.

4. The Eurocode predicts lower capacities in the inelastic LTB range. This is because, while C_b yields a higher elastic buckling strength, the inelastic LTB strength in Eurocode is not modified by C_b. It is observed that the Eurocode predictions for the moment gradient studies on the W21x44 gives excellent correlation with simulation data. This suggests that the differentiation in Eurocode for cross-sections with different D/b_{fc} values is appropriate for narrow flange sections, and may be conservative for wide flange sections. Eurocode also uses more severe geometric imperfections and residual stresses, and the curve is a lower-bound to the data obtained (Greiner and Kaim 2001; Roberts and Narayanan 1988).

5. It is interesting to note that SABRE2 correlates well with the FE simulation data. This is especially true for the narrower flanges sections. Considering that SABRE2 is a rigorous inelastic buckling solution using the proposed LTB equations for uniform moment, the correlation with test data gives confidence in the validity of the proposed model. The proposed model for moment gradient loading tends to predict higher strengths than the simulation data, especially in the region around

147

the knee of the LTB curve. This is due to the fact that the moment modification factor, C_b used in the Specification equations is derived based on elastic buckling solutions, and represents the ratio of the elastic buckling moment under the moment gradient to the elastic buckling moment under uniform moment. While this is a good representation for the elastic LTB region of the curve, it is higher than the true increase in the moment capacity in the beam after the advent of yielding. This "inelastic C_b" effect is captured by SABRE2, and represents the better solution. Hence, the regions where the proposed model appears to over-predict the data, is due to the "inelastic C_b" effect, more than the shortcomings in the model itself.

The moment gradient studies in this section are all flexure-controlled, i.e the design of these members is governed by the moment resistance equations rather than the shear resistance equations in the Specifications. The maximum shear attained in these cases is less than 50% of the shear capacity for the case with $C_b = 2.3$, with the exception of the W21x44 which attained 65% of its shear capacity for the smallest unbraced length studied. These shear loads are low enough where moment-shear (M-V) interaction is not considered to be a factor.

7.1.2 Rolled Beams Subjected to Transverse Loading

Two rolled beams, W21x44 and W14x68 are subjected to transverse loading conditions as shown in Figure 7-7. The designation "SS" indicates flexurally and torsionally simply-supported end conditions, wherein lateral braces are provided such that both lateral movement and twist is restrained at that end, while the flanges are free to warp. Fully-fixed end condition is indicated by "FF", where in the beam is both flexurally and torsionally fixed (warping and twist fixed) at the end. Cases (a), (b) and (c) in Figure 7-7 are beams

with uniformly distributed loads applied at the centroidal axis. Case (d), which has a single concentrated load at the mid-span of the beam, is studied for loading at the top flange, bottom flange and centroidal axis (shear center for a doubly-symmetric beam). The primary objective of this series of studies is to determine the LTB behavior of beams subjected to transverse loading, including cases where the maximum moment is away from the brace point. The cases with transverse loading also have high shear, so they serve as cases for study of potential moment-shear interaction effects.
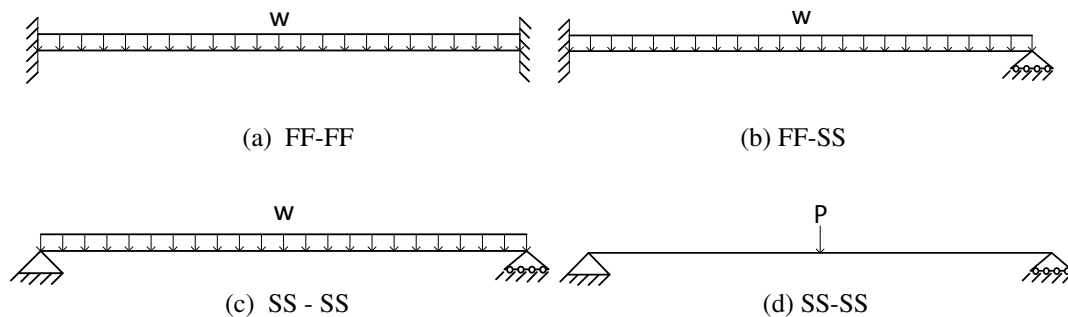
Figure 7-7: Test setup for nonlinear moment gradient studies for rolled beams

It should also be noted that the expressions for C_b in the current Specifications have been derived based on buckling solutions of beams that are torsionally simply-supported, i.e. with warping free at the ends (Helwig et al. 1997). Johnston (1976) and Galambos (1988) offer guidance for calculating moment modifiers for limited number of end restraint and loading conditions. The value of C_b as per Johnston (1976) for Case (a) is 1.72. Galambos (1988) provides equations for loading through the shear center, top flange or bottom flange. The equations are provided for two separate loading conditions: a concentrated load acting at the mid-span of the beam, and a uniformly distributed load acting along the length of the beam. These equations are functions of the cross-section properties and the member span length. For instance, C_b computed for Case (a) for the W21x44 for a span length of 800 inches ($KL_b/L_p = 7.5$) is 2.18. As previously noted, the

149

expressions are only applicable for limited loading and end restraint conditions. Neither of the two resources offer means of calculating C_b for Case (b), which has different end conditions at the two ends of the beam. Both of these alternate values of C_b for Case (a) (1.72 and 2.18) are lower than 2.381, calculated using Equation 7.2. Cases (a) and (b) are designed to examine the adequacy of the equations for C_b in the Specifications.

The transverse loading test cases are tabulated in Table 7-1. The values of C_b listed in Table 7-1 are calculated using Equation 7.2 for transverse loading. The values for Cases d-2 and d-3 with top and bottom flange loadings are calculated using

$$C_b^* = 1.4^{\frac{2y}{h}} C_b \tag{7.3}$$

given by Helwig et al. (1997), where, C_b^* is the modified value of C_b (calculated from Equation 7.2) when the loading axis is located at a distance y from the cross-section mid-height. In case of a bottom or top flange loading, y is taken as $\pm h/2$, where h is the distance between flange centroids. The expression given by Helwig et al. (1997) is chosen rather than the more complex equation given by Galambos (1988) for the purpose of this discussion.

Table 7-1: Transverse loading test cases studied for rolled beams

Case	Left Support	Right Support	Loading	Loading Axis	C_b
Case a	FF	FF	UDL	Centroid	2.381
Case b	FF	SS	UDL	Centroid	2.083
Case c	SS	SS	UDL	Centroid	1.136
Case d-1	SS	SS	Concentrated @ mid-span	Centroid	1.316
Case d-2	SS	SS	Concentrated @ mid-span	Top flange	0.930
Case d-3	SS	SS	Concentrated @ mid-span	Bottom flange	1.800

7.1.2.1 <u>Cases a and b – fixed-fixed and propped cantilever beams with distributed load at centroidal axis</u>

Cases a and b have warping and twist restrained at the fixed ends. This allows the use of an effective length factor, K of less than one for the unbraced length. The effective length factor for LTB is taken as $K = K_y = K_z = 0.5$ for the fixed – fixed beam in Case a and $K = K_y = K_z = 0.7$ for the propped cantilever in Case b. Figures 7-8 and 7-9 show the plots for the two cases. The plots also show the maximum shear attained in the tests (V_{max}) normalized by the shear capacity (per AISC) of the beam. Appendix B provides the numerical values for all the data points shown in the plots. All the data points in Cases a and b are flexure controlled.
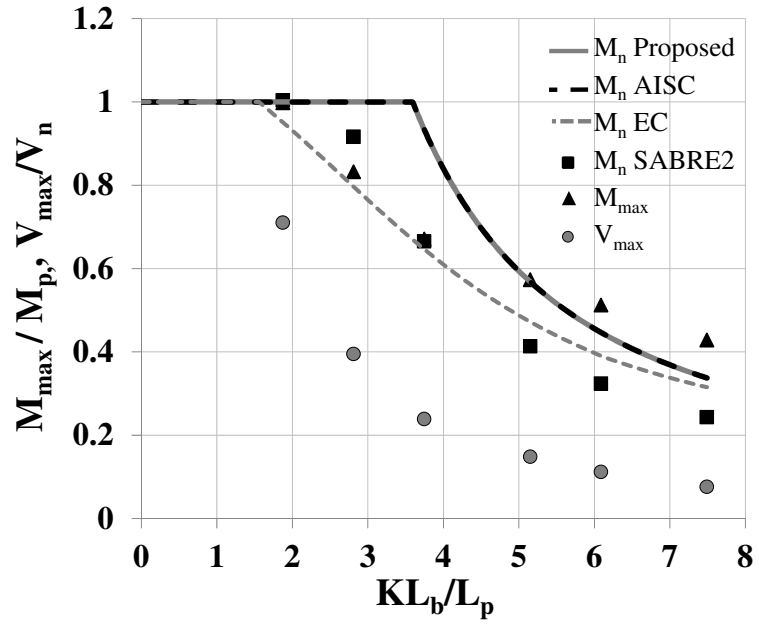
(a) W21x44
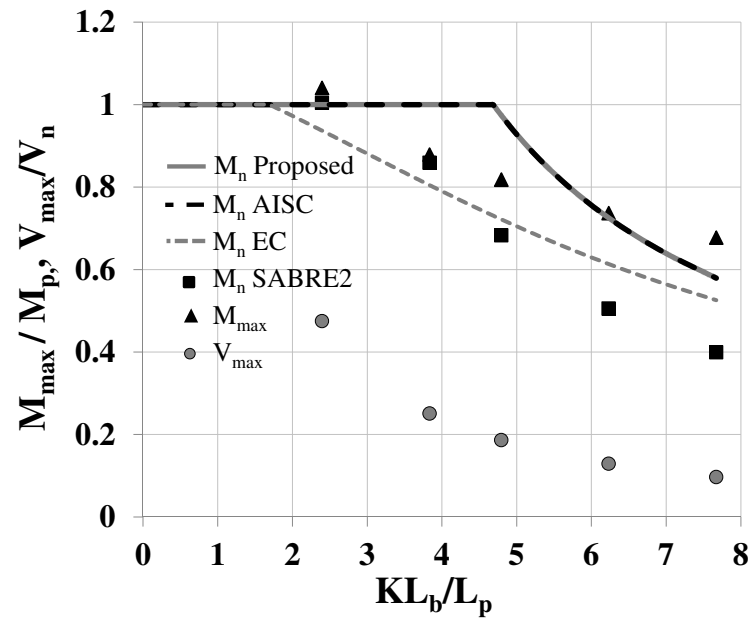
(b) W14x68

Figure 7-8: LTB curves for uniformly distributed load acting at centroid, FF-FF edge conditions
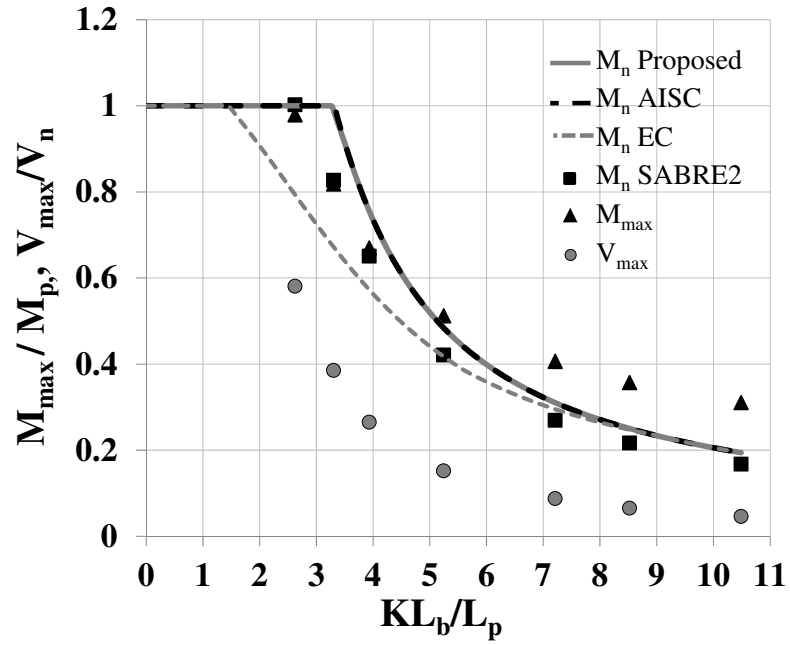
(a) W21x44
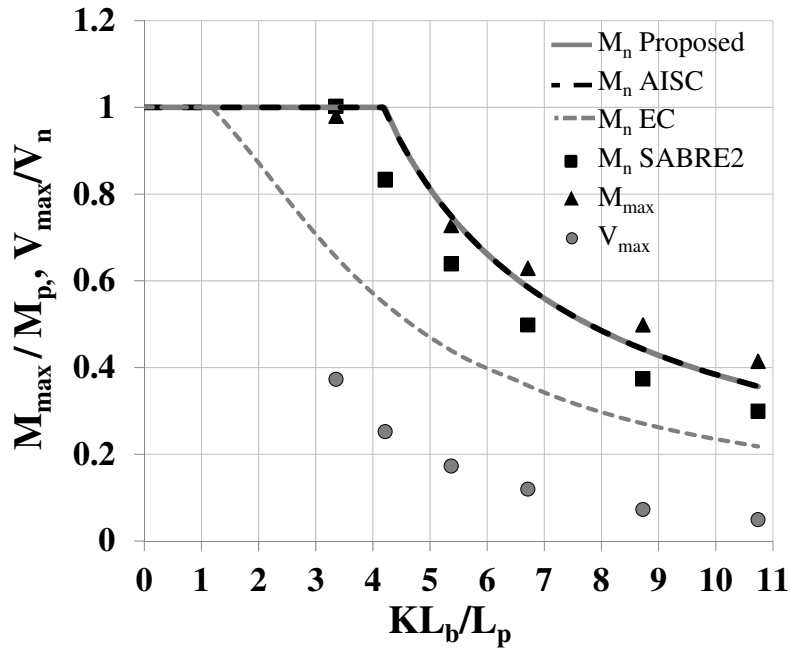
(b) W14x68

Figure 7-9: LTB curves for uniformly distributed load acting at centroid, FF-SS edge conditions

The following can be observed from the above figures.

1. Test simulation data are in the order of 10 to 20% higher than the moment capacities predicted by SABRE2 at long unbraced lengths ($L_b/d = 38$ for W 21x44 @ KL_b/L_p = 7.5 in Figure 7-8 (a)). SABRE2 accurately captures the elastic critical moment of the beam. For these particular cases in question, the unbraced lengths are very long, and the critical moments are less than 50% of the minor axis yield moments. It is observed that these beams tend to exhibit a stable postbuckling response. In such cases, the load-deflection response in ABAQUS captures the limit load at the onset of yielding in the compression flange. Figure 7-10 shows the failure mode of the W21x44 for Case a (warping fixed at both ends) for the left half of the beam. The lighter colored portions on the figure indicates spread of yield. It is evident that this beam has substantial postbuckling reserve beyond the elastic buckling limit, and continues to take load until the onset of compression flange yielding.
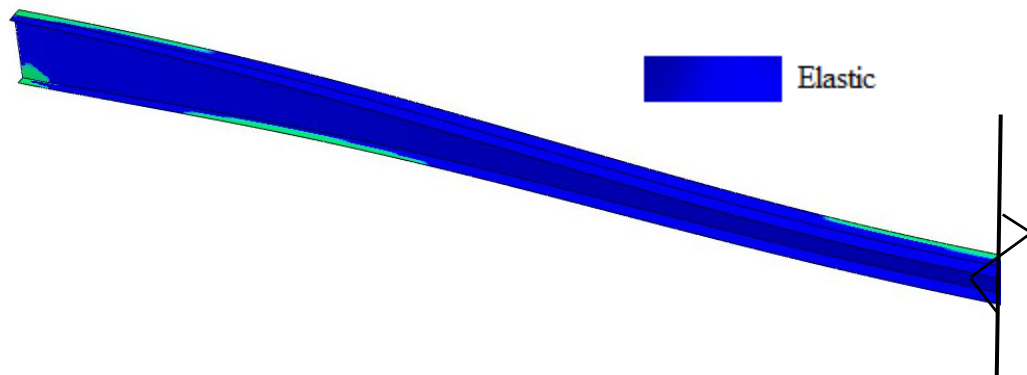
Figure 7-10: Failure mode of W21x44 for a fixed-fixed beam at $L_b/d = 38$ (left half of span)

2. The test simulation points are as low as 20% below the design equations at the knee of the LTB curves. The proposed and current specification equations coincide for these high values of C_b (2.38 and 2.08 respectively). It is also observed that FE data

154

from ABAQUS and SABRE2 match closely. The combination of $K < 1$ and the C_b based on no warping restraint, together with an "inelastic C_b" effect yield poor predictions of the true girder strengths. This also indicates that the warping restraints at the ends of the beam has an influence on C_b, as noted by Johnston (1976) and Galambos (1988). Clearly, the over-prediction of the Specification equations in Case a, with a higher level of warping restraint, is more than the over-prediction in Case b.

The LTB resistance predictions are poor for conditions of moment gradient and warping fixity. There is clearly a need to research the appropriate moment modification factors to use for various levels of torsional fixity. The current expressions for C_b are unsafe to use in design under such scenarios. Computational tools such as SABRE2 account for the inelasticity in beams along with the influence of end restraints for any given loading condition, and offer more accurate estimates of the member strengths.

7.1.2.2 Case c – simply-supported beam with distributed load at centroidal axis

Figure 7-11 shows the plots for the W21x44 and W14x68 beams. SABRE2 results, with stiffness reduction factors based on the proposed LTB model are also shown for the flexure controlled points.

From Figure 7-11, it is evident that the simulation data fall below the proposed and current LTB curves in the inelastic LTB region. This behavior is captured by SABRE2, which shows that there is an "inelastic C_b" effect here as well. The Eurocode equation gives the best fit to the data in this case.

The first two data points for the smaller unbraced lengths in the W21x44 and the first data point for the W14x68 sections are shear controlled. It is evident that the shear capacity

attained by the test simulations is substantially larger than the AISC shear equations, despite the presence of large values of bending moment. Hence, M-V interaction need not be a concern for design when using the current shear equations and the proposed LTB model.
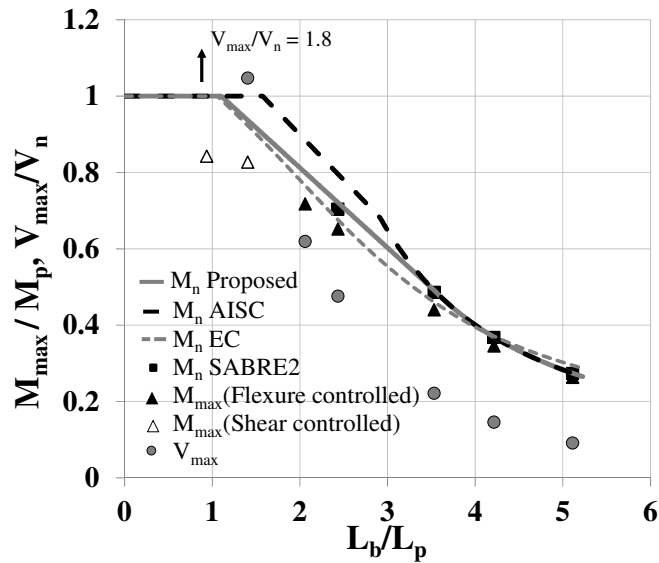
(a) W21x44
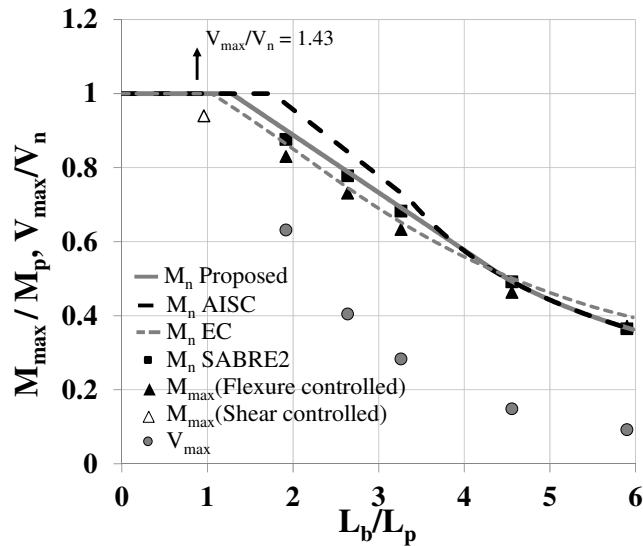
(b) W14x68

Figure 7-11: LTB curves for uniformly distributed load acting at centroid, SS edge conditions

7.1.2.3 <u>Case d – three point bending tests with centroidal, top flange and bottom flange</u>
<u>loading positions</u>

Two rolled beams, W21x44 and W14x68, are subjected to a concentrated load acting
at the center of the beam. The three point bending test setup is analyzed for load at the
centroidal axis, and at the top and bottom flanges to assess the influence of load height
effects. Figures 7-12 through 7-14 show the plots for the two rolled beams at the different
load-height positions. All the data points, barring the shortest unbraced lengths for the top
flange loading case are flexure controlled. The shears are low enough such that M-V
interaction is not a concern in these cases.

The following observations can be made from Figure 7-12 for the case with the
concentrated load acting at the centroidal axis.

1. The FE strength predictions are about 20% lower than the AISC curve, and 15%
   lower than the proposed model at the knee of the LTB curves.

2. SABRE2 gives results that are higher than the test simulation data, and slightly
   lower than the proposed model.
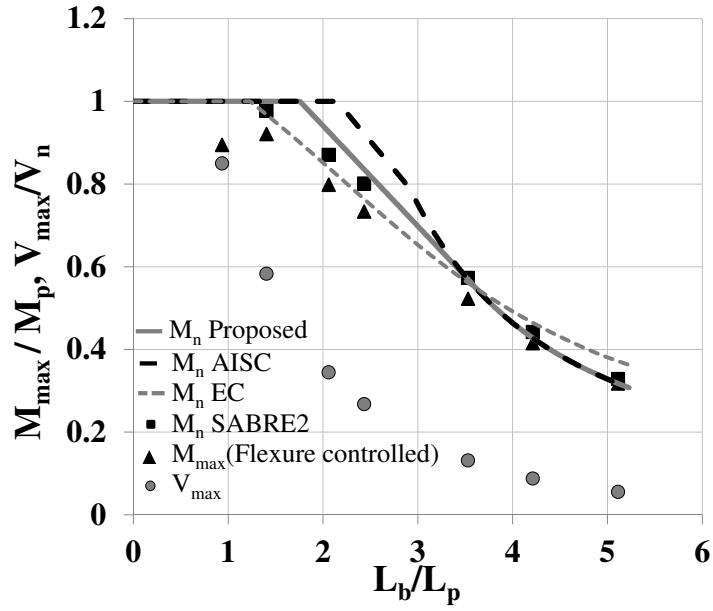
(a) W21x44
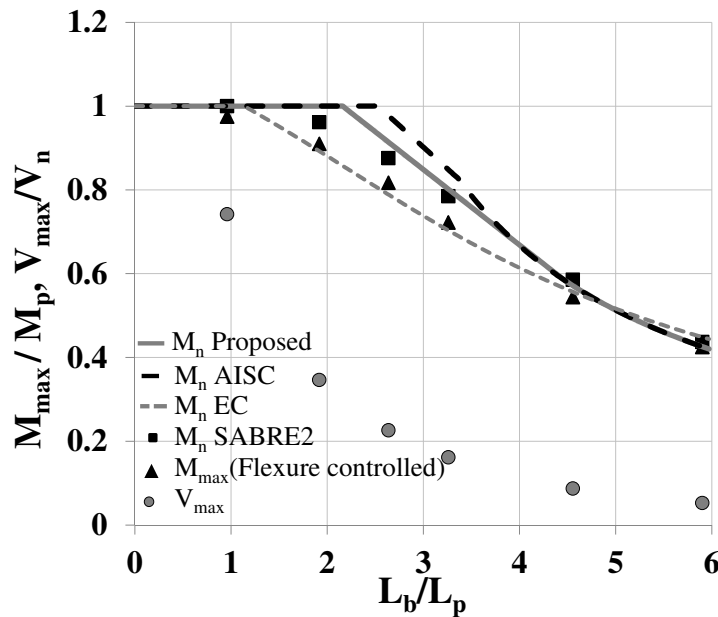
(b) W14x68

Figure 7-12: LTB curves for concentrated load at mid-span, acting at centroid, SS edge conditions

Figure 7-13 compares the data for loading at the top flange. The step in the proposed and current LTB design curves at the plateau length are due to the fact the C_b is calculated from the recommendations given by Helwig et al. (1997) incorporating load height effects. Loading above the centroidal axis has a detrimental effect on lateral stability, and hence C_b

158

is less than 1.0. However, the plateau strength is taken as the full plastic moment capacity in Figure 7-13. Alternate methods of plotting the design curve would be to conservatively restrict the plateau strength to C_bM_p or to allow the inelastic LTB strength line to intersect with the plateau at a length smaller than L_p. AISC (2010a) implicitly assumes that C_b is always greater than or equal to 1.0.
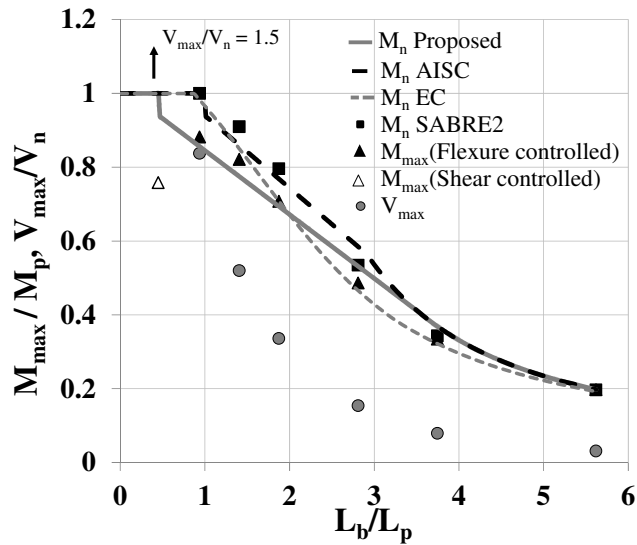
(a) W21x44
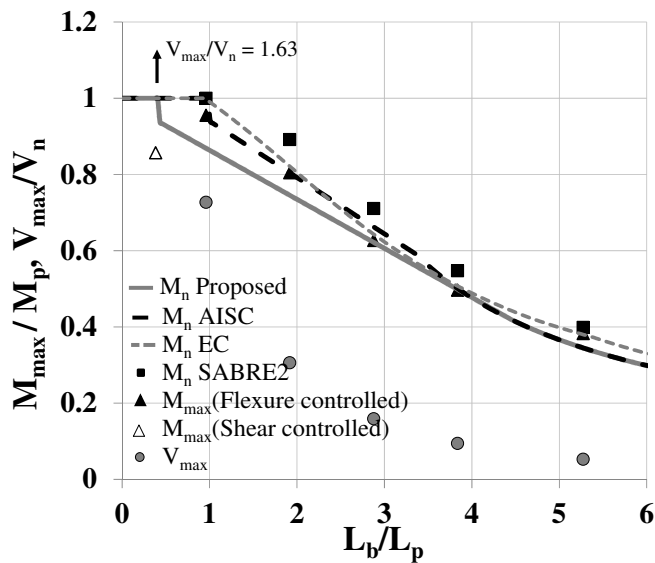
(b) W14x68

Figure 7-13: LTB curves for concentrated load acting at mid-span, acting at top flange, SS edge conditions

The following observations are made from Figure 7-13, for the case with top flange loading.

1. The proposed LTB curve predicts the simulation data fairly well for the W21x44 (narrow flange) section, and predicts smaller than simulation strengths for the W14x68 (wider flange) section.

2. Once again, Eurocode provides the best fit to the test simulation data.

Figure 7-14 shows the plots for the concentrated load acting on the bottom flange. The C_b calculated from Equation 7.3 is 1.8 and is higher than the value calculated for loading at the centroid.

The following observations can be made from Figure 7-14 for bottom flange loading.

1. The proposed and current AISC curves are almost coincidental, similar to the loading cases with linear moment diagrams that have high values of C_b.

2. It is evident that the recommended value of C_b for bottom flange loading is unconservative in the elastic LTB region for W14x68. This is consistent with the observation made by Helwig et al. (1997) that the expression for C_b tends to be unconservative for bottom flange loading when L_b/h is larger than 15. They also noted that Equation 7.3 becomes conservative for a similar top flange loading (as corroborated by Figure 7-13 (b)).

In view of the above observation, it is advisable to use a value of $C_b = 1.13$ (calculated for shear center loading) without accounting for additional benefits from bottom flange loading.

(a) W21x44

(b) W14x68
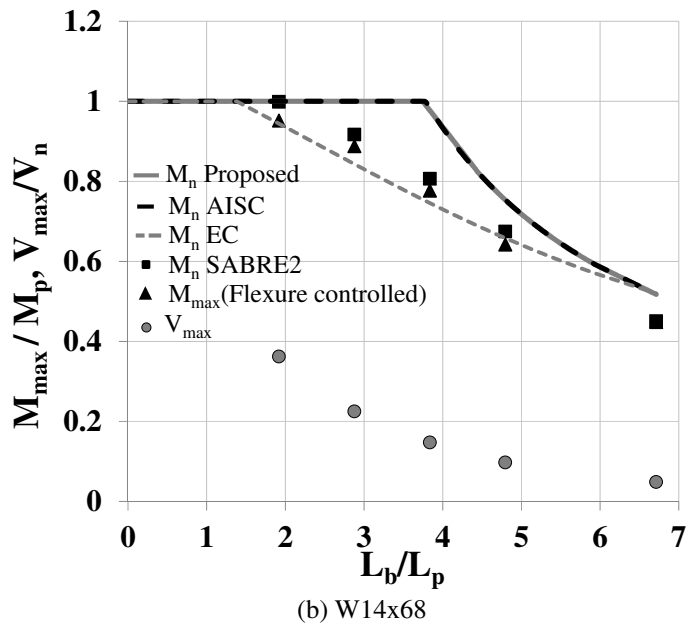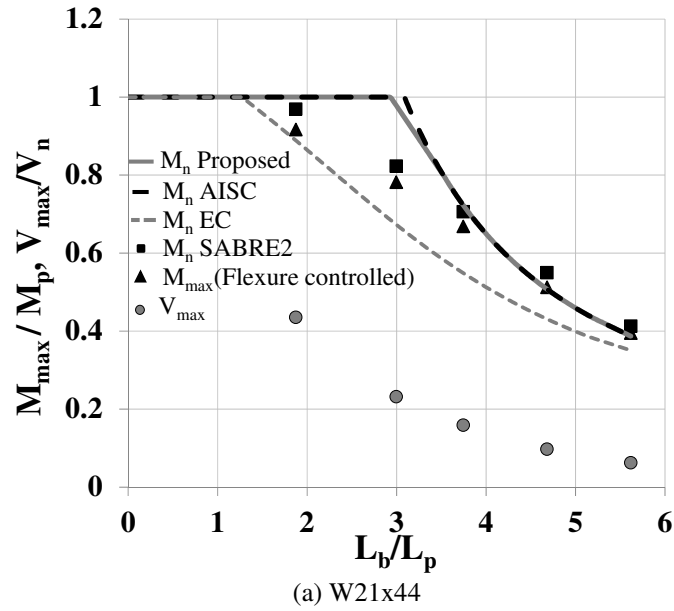
Figure 7-14: LTB curves for concentrated load acting at mid-span, acting at bottom flange, SS edge conditions

7.2 Modified LTB Equation

It is established in Section 7.1.2, that the design curves (both proposed and current) tend to be optimistic in predicting the inelastic LTB strengths when the beams are subjected to transverse loading, such that the maximum moment within the beam is away from the

location of the lateral brace. This is also corroborated by the fact that the Eurocode LTB equation which does not scale the inelastic LTB strength for uniform moment by C_b correlates better with the test simulation data. It is also observed in Section 7.1.1 that the proposed equation gives satisfactory results when there is a linear moment gradient with no transverse loading within the unbraced segment (the maximum moment is at the location of the lateral brace), and it is less than 10% higher than simulation data for the extreme cases when C_b is 1.75. Based on these observations, a simple modification to the inelastic LTB curve (AISC Equation F2-2) is proposed,

$$M_n = f_1 C_b \left[M_p - \left(M_p - f_1 F_{yr} S_x \right) \left(\frac{L_b - L_p}{L_r - L_p} \right) \right] \leq M_p \qquad (7.4)$$

where,

$f_1 = 1$ (when the maximum moment is at the brace location), and

$\quad = 1/C_b$ (when the maximum moment is away from the brace location)

The current Specification equation is modified by multiplying C_b and F_{yr} by the factor f_1. The modified inelastic LTB equation in Equation 7.4 does not change the equations for the linear moment diagrams discussed in Section 7.1.1, and it greatly improves the correlation of the proposed curve with the FE test simulation data for Cases c and d with transverse loading, as shown in Figures 7-15 through 7-18.

(a) W21x44 (b) W14x68
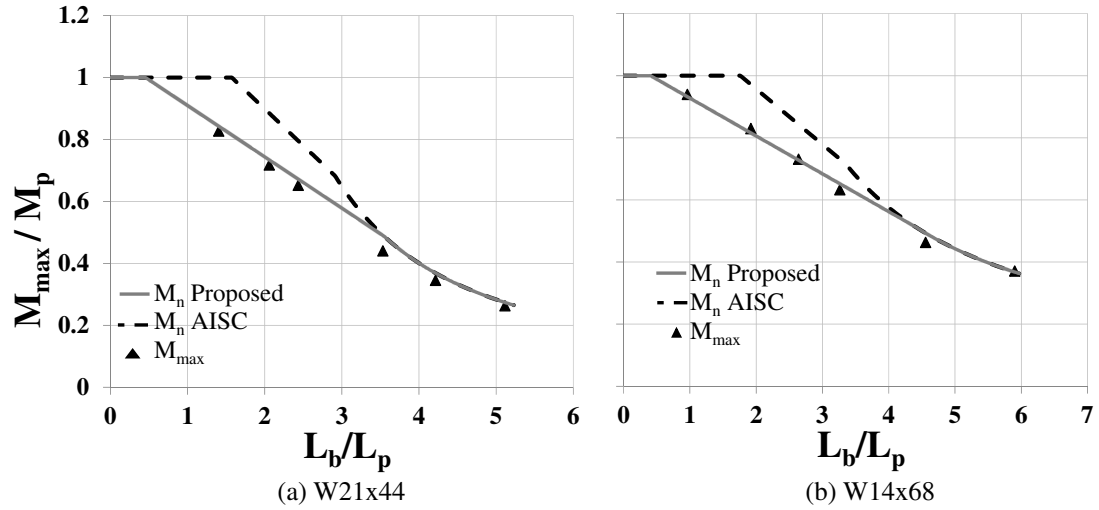
Figure 7-15: Comparison of test data with modified LTB curves for Case c in Table 7-1

(a) W21x44 (b) W14x68
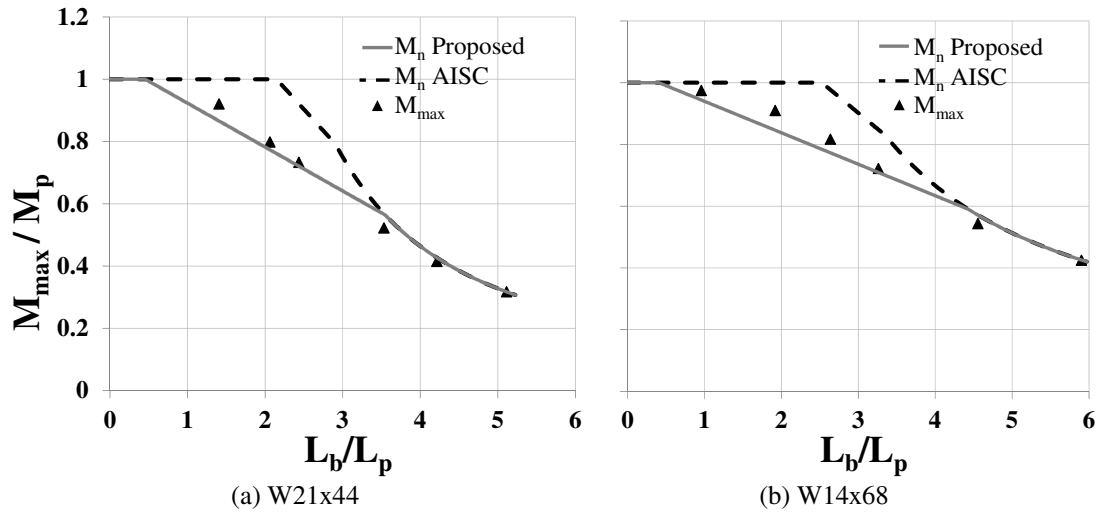
Figure 7-16: Comparison of test data with modified LTB curves for Case d-1 in Table 7-1

163
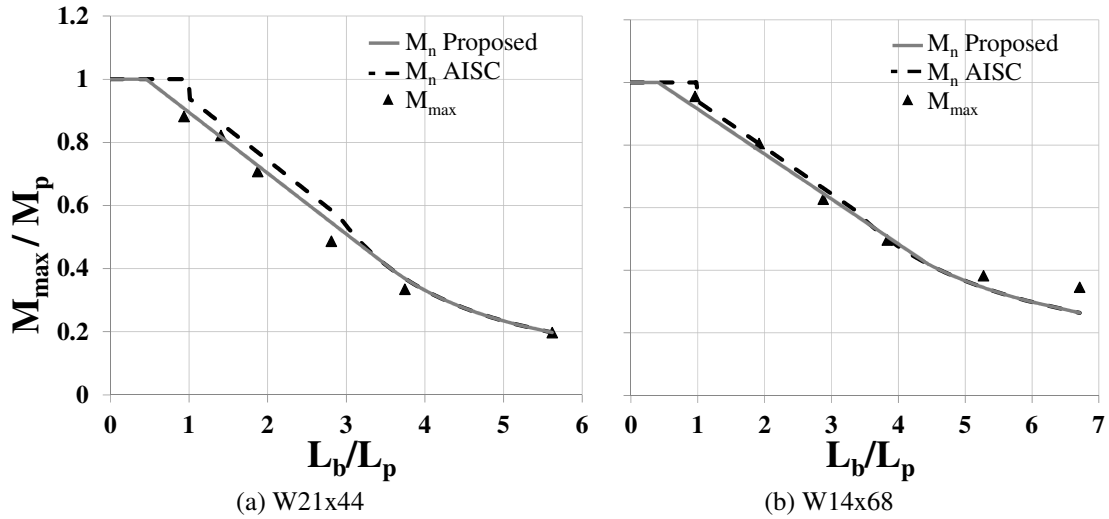
Figure 7-17: Comparison of test data with modified LTB curves for Case d-2 in Table 7-1
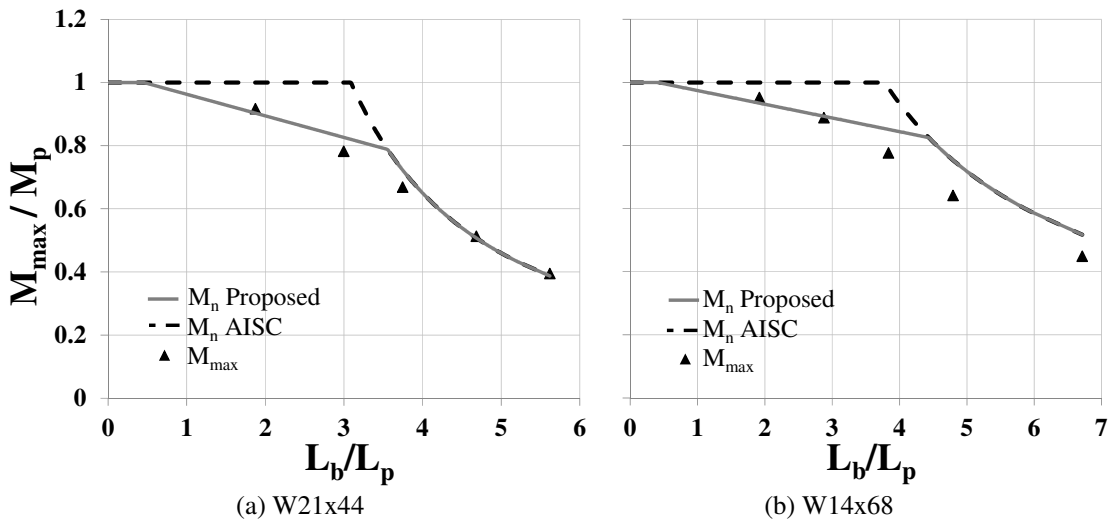
Figure 7-18: Comparison of test data with modified LTB curves for Case d-3 in Table 7-1

From the above figures, it is apparent that the modification to the inelastic LTB equation recommended by Equation 7.4 predicts the test data for the transverse loading cases with reasonable accuracy. These loading conditions result in the location of the maximum moment within the span, and away from the brace location (at the ends). It is also observed from Figure 7-17 that the proposed model predicts higher strengths with the modification factor, f_1 for top flange loading, and brings the curve closer to the simulation

data. The following sections of the chapter discuss moment gradient studies on noncompact and slender web cross-sections.

7.3 Welded Noncompact and Slender Web Beams Subjected to Linear Moment Gradient

The three linear moment diagrams indicated in Section 7.1.1 are also used for the studies on noncompact and slender web plate girders. Eleven cross-sections in Table 6-14 are marked as members studied for LTB responses of welded beams subjected to moment gradient loading. These girders are G1, G3, G5, G9, G13, G37, G44, G45, G46, G47 and G49. These girders are chosen to represent cross-sections that encompass noncompact webs, slender webs with compact and noncompact flanges and different web depths in compression. Out of these girders, G37, G44 and G45 are omitted for the studies on reverse curvature (C_b = 2.3), as they have flanges that do not meet AASHTO requirements for compression flanges. The slender flanges are in tension for the moment gradient loadings with C_b = 1.3 and C_b = 1.75.

7.3.1 Noncompact and Slender Web Girders Subjected to Linear Moment Gradient with C_b = 1.3

Figures 7-19 through 7-21 show the plots for three girders, that are a selection of doubly-symmetric and singly-symmetric cross-sections with noncompact webs and slender webs for C_b = 1.3 (β = 0.5 in Figure 7-1). The plots for other girders can be found in Appendix B. These plots show that the proposed model predicts the simulation data with good accuracy for all the flexure controlled data points. It is seen that the shears attained

by the girders barring the first two data points for the small unbraced lengths, are very low, and are not considered to cause M-V interaction.
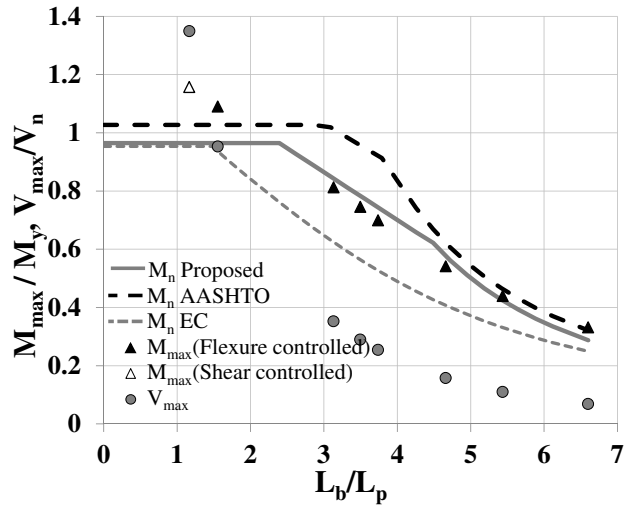
Figure 7-19: LTB curves for linear moment diagram with C_b = 1.3, girder G1 in Table 6-14
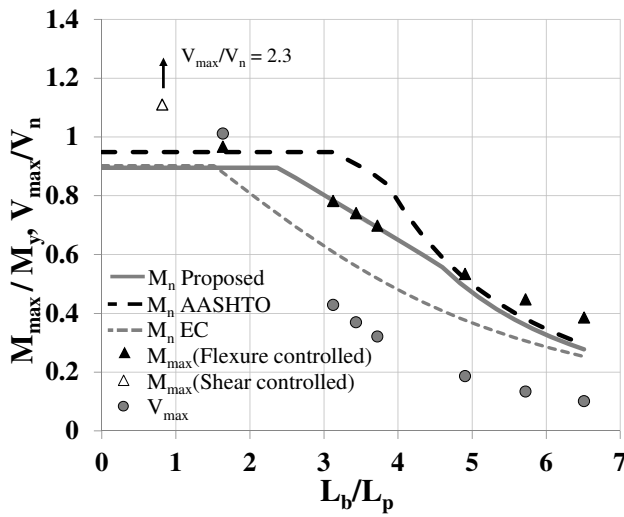
Figure 7-20: LTB curves for linear moment diagram with C_b = 1.3, girder G9 in Table 6-14
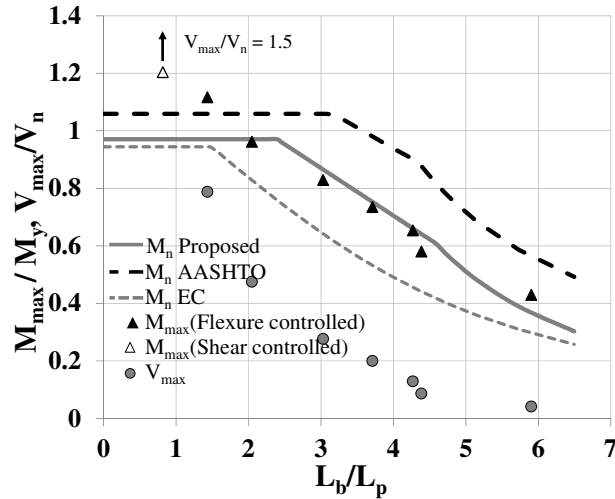
Figure 7-21: LTB curves for linear moment diagram with C_b = 1.3, girder G49 in Table 6-14

7.3.2 Noncompact and slender web girders subjected to linear moment gradient with C_b = 1.75 and 2.3

Figures 7-22 through 7-24 show plots for three girders for a moment gradient case with C_b = 1.75. In these cases with higher levels of moment gradient, the shears in the girders are also high. It is observed that the FE test simulation results fall well below the current and proposed design curves in the inelastic LTB regions.

In order to better understand the reasons for this behavior, results from SABRE2 are also included. It can be observed that SABRE2 predicts strengths that are higher than the results from ABAQUS with nominal imperfections and residual stresses, but lower than the proposed curves. While SABRE2 captures the effects of an "inelastic C_b", it does not account for any potential moment – shear (M-V) interaction effects.

An elliptical equation has traditionally been used to define moment-shear interaction in plate girders. An equation of the form

$$\left(\frac{M}{M_n}\right)^2 + \left(\frac{V}{V_n}\right)^2 \le 1.0 \tag{7.5}$$

167

is used to calculate the moment capacity when moment-shear interaction is considered. Equation 7.5 is similar to the M-V interaction equation used in AISI (2014).

The moment capacity calculated thus is included on Figures 7-22 and 7-23, and labeled as M_n Interaction. The moment-shear interaction check is not considered important in the case of Girder G49 in Figure 7-24, where it is shown that the shears in the girder are low. It is observed from Figure 7-24 that although M-V interaction is not a concern for G49, there is an influence of "inelastic C_b" and the simulations strengths are smaller than the proposed LTB equation.
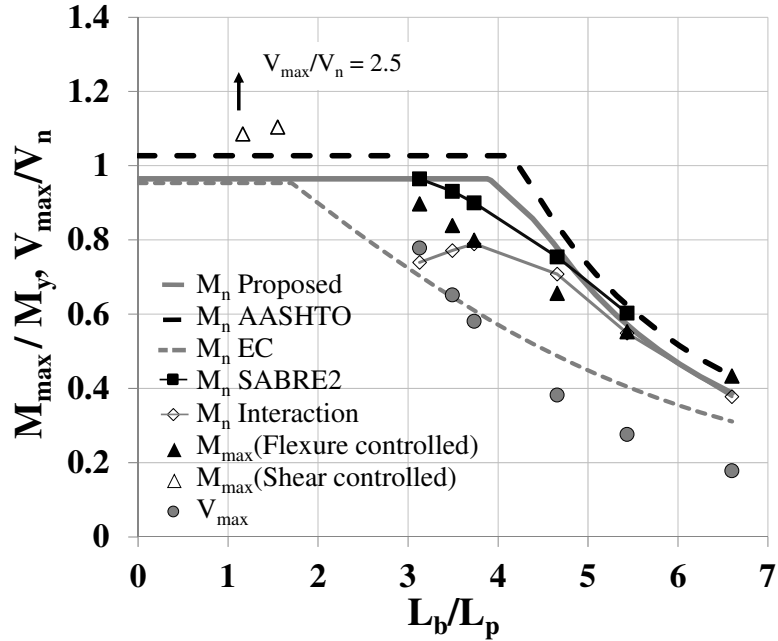
Figure 7-22: LTB curves for linear moment diagram with C_b = 1.75, girder G1 in Table 6-14
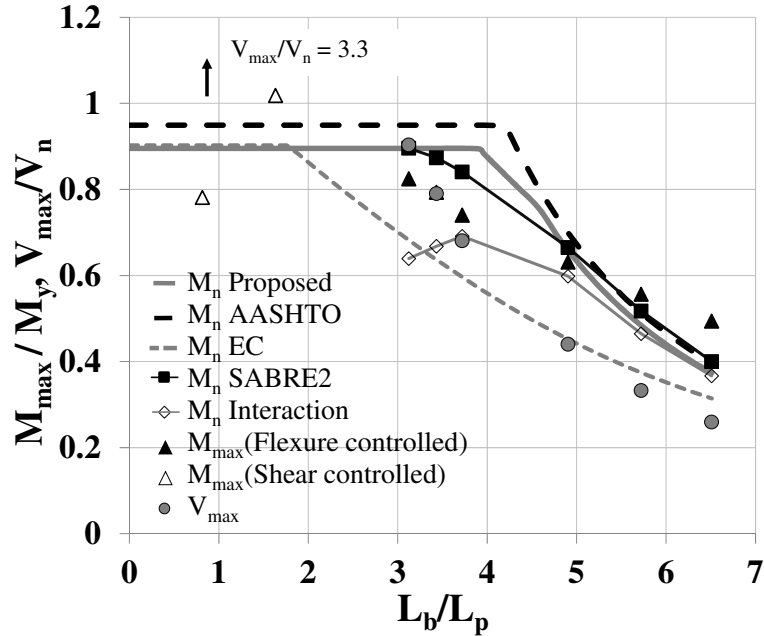
Figure 7-23: LTB curves for linear moment diagram with C_b = 1.75, girder G9 in Table 6-14
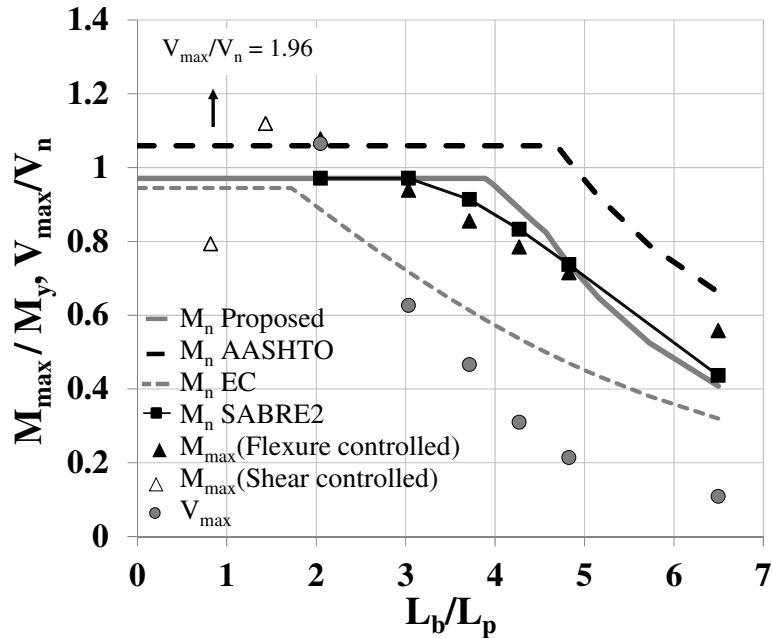
Figure 7-24: LTB curves for linear moment diagram with C_b = 1.75, girder G49 in Table 6-14

Figure 7-25 shows a similar set of curves for girder G1 in full reverse curvature, with C_b = 2.3. The shears for this moment gradient are even higher than previously seen. In Figure 7-25, only the two data points with the longest KL_b are flexure-controlled, while the

169

rest are shear-controlled. Tables in Appendix B clearly indicate the controlling limit state (shear or flexure) for each of the data points.
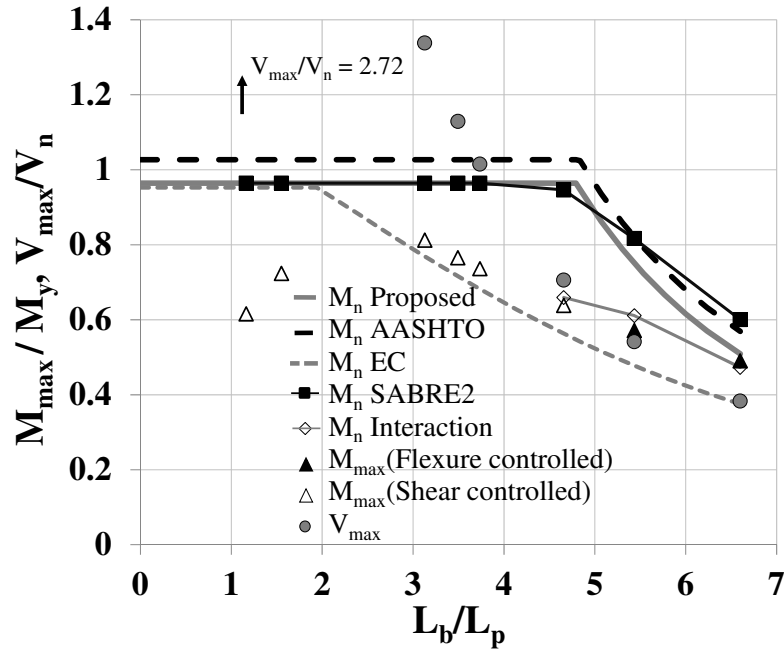
Figure 7-25: LTB curves for linear moment diagram with C_b = 2.3, girder G1 in Table 6-14

From the above figures, it is evident that for slender webs (G1 and G9), shear influences the flexure capacity to some extent. The reasons for smaller predictions in the noncompact web girder G49 are explained by the influence of "inelastic C_b", corroborated by the results from SABRE2. Moreover, it is observed that FE test simulations of G1 and G9 with closely spaced transverse stiffeners predict capacities (not shown) almost identical to those of SABRE2. The closely spaced transverse stiffeners increase the shear capacities of the girders, while also reducing potential web distortion.

It is found that the behavior of slender web plate girders under high moment-high shear is complex and the strengths are influenced by several factors. M-V interaction and inelastic C_b are the key factors that reduce the strengths of slender web girders. Web distortional effects may also influence the strengths of such members.

7.4 Summary

The following are the key conclusions from the work conducted in this chapter for unstiffened girders subjected to moment gradient loading, with the flexure limit state controlled by LTB.

1. The proposed LTB model in Chapter 6 matches closely with the test simulation strengths for moment gradient, for compact web rolled beams with linear moment diagrams. A modification factor on the LTB resistance equation is recommended for beams with maximum moment away from the brace locations, which is shown to greatly improve the correlation of test data with the proposed equation. However, it is recommended that further studies be conducted with similar transverse loading conditions on noncompact and slender web sections.

2. An "inelastic C_b" effect is shown to influence the girder strength in the inelastic LTB region for compact web and noncompact web sections. This effect is captured by rigorous inelastic buckling solutions from SABRE2 using a stiffness reduction approach based on the proposed equation.

3. It is seen that the expressions in the current Specifications for computation of C_b are optimistic for girders that have warping fixity at either or both ends. In the case of warping restraint, the Specifications allow the use of an effective length factor, K in the calculation of the LTB strengths. The combination of $K < 1$ and the C_b from torsionally simply-supported boundary conditions results in unconservative predictions of the girder strengths. It is shown that the equations from Johnston (1976) and Galambos (1988) predict lower values of C_b. However, they are approximate solutions and do not address all possible boundary conditions and

loading cases. Computational tools with rigorous inelastic buckling solutions such as SABRE2 can account for "inelastic C_b" and end restraint effects for various loading conditions.

4. It is seen that M-V interaction, and possibly web distortion influence the flexural strengths of slender web girders when subjected to high moment and high shear loading. While the theoretical aspects of the problem have been discussed in this chapter, it is worth noting that it is unlikely that bridge girders will be designed with no intermediate transverse stiffeners for such long unbraced lengths as considered in this research. Hence, in practical situations, it is possible that this kind of extreme loading is not witnessed, and the shear capacities will be higher due to intermediate transverse stiffeners or cross-frames. The intermediate transverse stiffeners also reduce the likelihood of web distortion.

The following chapters discuss the LTB resistance of longitudinally stiffened girders, for both uniform bending and moment gradient cases in the context of the proposed LTB equations from Chapters 6 and 7.

CHAPTER 8

LATERAL TORSIONAL BUCKLING RESISTANCE OF STRAIGHT LONGITUDINALLY STIFFENED GIRDERS

In this chapter, various design parameters are evaluated for their impact on the flexural capacity of longitudinally stiffened girders at the LTB limit state. A range of unbraced lengths is tested to assess the behavior of the longitudinal stiffeners as well as the application of the proposed yield limit state R_b prediction model and the proposed LTB equations, as part of the calculation of the flexural resistance for longitudinally stiffened girders governed by LTB. Only uniform bending is considered in this chapter. Moment gradient is treated separately in the following chapter.

8.1 Test Setup

The test setup for the lateral torsional buckling studies is the same as that for the yield limit state studies shown in Figure 4-1. However, the unbraced lengths of the test specimens are varied. This allows evaluation of the impact of the longitudinal stiffener on the flexural capacity of girders subjected to the yield, inelastic LTB, and elastic LTB limit states. The test fixtures are assumed to provide torsionally and laterally fixed boundary conditions at each end of the test specimen, i.e., the value of K in KL_b is taken as 0.5 in estimating the LTB resistances by various potential nominal strength equations. Similar to the test setup in Section 4.3, the flange and web plates of the end fixtures are significantly larger than the plate thicknesses of the test specimens; therefore, this is an accurate estimate of K. The length L_b is taken as the distance between the connection points to the end fixtures

(i.e., no lateral bracing is provided within the length of the test specimens, but lateral bracing is provided at the ends of the test specimens).

In accordance with the findings in Chapter 6, the magnitudes of imperfection used for FE modeling are one half of the imperfections discussed in Section 3.6, with an additional flange sweep of magnitude $L_b/2000$. There is not sufficient data to estimate the general imperfections found in longitudinally stiffened girders at various unbraced lengths. Hence, a comparison of the strengths obtained when using the full AWS tolerance on web imperfection and flange sweep as initial geometric imperfections, and full Best-fit Prawel residual stresses along with one half of the imperfections and residual stress magnitudes is presented. The sweep in the longitudinal stiffener is taken as $d_o/400$, which is the same as in the tests at the yield limit state in Chapter 4.

Given the fixity at both ends of the unbraced length, a flange sweep imperfection of magnitude $L_b/2000$, amounts to a smaller net imperfection between the inflection points of the unbraced length. Only compact flange girders are studied in this Chapter.

8.2 Case Studies

The cases defined in Table 8-1 are assessed as part of the parametric studies discussed in this chapter. The unbraced length is different for each of these cases. The different KL_b values shown in the table belong to different ranges of the AASHTO LTB curve depending on the girder dimensions (particularly the b_{fc}/D ratio) for a given test. In general, Case 1 has an effective unbraced length near the transition between the yield plateau and the inelastic lateral torsional buckling regions as defined by AASHTO (i.e., at the length $KL_b = L_p$). Cases 2 and 3 have effective unbraced lengths within the inelastic LTB range. Case 4 has an effective unbraced length near the length L_r on the current AASHTO LTB curve,

but located in either the inelastic or elastic LTB region depending on the girder dimensions. Cases 5 and 6 are comprised of studies with effective unbraced lengths well within the elastic range of the AASHTO LTB resistance curve.

Table 8-1: Case studies for straight longitudinally stiffened girders at the LTB limit state

Case	KL_b (in) $d_o/D =1$	KL_b (in) $d_o/D =2$
1	225	300
2	375	450
3	525	600
4	675	750
5	825	900
6	975	1050
7	1125[a]	1350

a. Unbraced length studied only for girders with D/t$_w$ = 300, and D/b$_{fc}$ = 5, 4

For each of the above cases, the following parameters are held constant:

- $D = 150$ inches,

- $d_s/D_c = 0.4$,

- Longitudinal stiffeners sized based on the minimum requirements from the AASHTO LRFD Specifications as explained in Section 2.8, and

- 9.5 x 0.75 inch transverse stiffeners, which satisfy the minimum requirements from the AASHTO LRFD Specifications for all of the girders tested.

The following parameters are varied:

- $D_c/D = 0.5, 0.625$ and 0.75,

- $D/t_w = 200, 240$ and 300, and

- $b_{fc} = D/6, D/5$, and $D/4$.

- t_{fc} = 1.5, 1.75, 2.25 in corresponding to the different values of compression flange widths.

A total of 357 test girders are studied in this chapter.

8.3 Proposed Model

A slightly varied form of the existing AASHTO LTB equations is proposed in Chapter 6. This model, with the modifications discussed below to address the influence of longitudinal web stiffening, is proposed in this research as one method that captures the test simulation results for longitudinally stiffened girders with improved accuracy. As per the recommendations, the LTB strength curve uses a shorter plateau length of $L_p = 0.63 r_t \sqrt{E/F_y}$, and a smaller maximum stress level for elastic LTB of F_{yr} = 0.5 F_{yc}. Furthermore, for the longitudinally stiffened plate girders considered in this research, the "plateau" resistance used with these equations is calculated by multiplying the yield moment capacity by R_{bPr} from the proposed model discussed in Section 4.7.

In addition to the above, the bend-buckling stress of the longitudinally stiffened web, F_{crw}, is calculated using the AASHTO LRFD Article 6.10.1.9.2 provisions. If this stress is less than F_{yr} = 0.5 F_{yc}, the unbraced length at which the nominal elastic buckling stress F_{nc} is equal to F_{crw} is determined. The value F_{crw} is the stress level at which R_b effectively becomes equal to 1.0, and the corresponding unbraced length is referred to here as L_1. The inelastic LTB resistance of the longitudinally stiffened plate girder is then determined by linearly interpolating between the plateau strength (using the factor R_{bPr}) at L_p and the point (L_1, F_{crw}).

Conversely, if F_{crw} is greater than F_{yr} = 0.5F_{yc}, the inelastic LTB resistance is obtained by linearly interpolating between $(L_p, R_{bPr}F_{yc})$ and $(L_r, 0.5F_{yc})$, where L_r is defined here as

the length at which the theoretical elastic LTB strength is equal to $F_{yr} = 0.5F_{yc}$ (note that the current AASHTO provisions define L_r as the length corresponding to $F_{yr} = 0.7F_{yc}$ for homogeneous slender web plate girders).

For compression flange stress levels below the smaller of the values F_{crw} or $0.5F_{yc}$, the elastic buckling equation in the current AASHTO Specifications, with $R_b = 1$ is used to compute the LTB resistance.

8.4 Results and Evaluation of Proposed Model

Figures 8-1 through 8-3 compare the FE test simulation data to the current AASHTO LRFD and Eurocode predictions as well as to the above proposed model for several tests with $d_o/D = 1$. These figures show comparisons between the data obtained using the imperfections as per the full AWS tolerances and the full Best-Fit Prawel residual stresses, and with half of the AWS tolerances as imperfections and half Best-Fit Prawel residual stresses. In these figures, M_{max} refers to the flexural capacity obtained from FE test simulations, M_n EC refers to the capacity calculated using the Eurocode EN 1993-1-1 (CEN 2005) and EN 1993-1-5 (CEN 2006a) provisions, M_n $AASHTO$ (R_b based on F_{yc}) is the capacity computed using the current AASHTO provisions including R_b as calculated by AASHTO, as well as using the elastic section modulus that includes the longitudinal stiffener, M_n $AASHTO$ ($R_b = 1.0$) is the same calculation but taking $R_b = 1.0$, and M_n $Proposed$ is the result from the proposed model described in Section 8.3. In these figures, the data points that correspond to the "plateau resistance" are obtained from the results in Chapter 4.

177
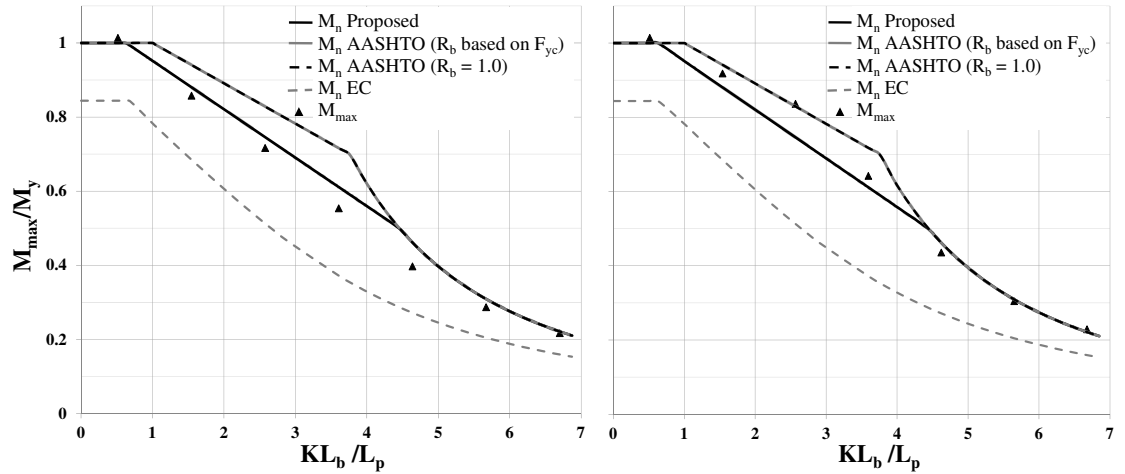
Figure 8-1: Flexural capacity comparing AASHTO, Eurocode and FE simulations, $D/t_w = 240$, $D_c/D = 0.5$, $D/b_{fc} = 6$, $d_o/D = 1$ with full AWS imperfections and Best-fit Prawel residual stress (Left) and half AWS imperfections and half Best-fit Prawel residual stress (right)

Figure 8-1 shows results for a girder that has a value of $R_{bAASHTO} = 1.0$ ($R_{bAASHTO}$ is equal to 1.0 here because the longitudinal stiffener increases the bend-buckling stress F_{crw} to a value greater than the compression flange stress at the strength limit for all unbraced lengths).

Figures 8-2 and 8-3 show results for slender web longitudinally stiffened girders with $R_{bAASHTO} < 1.0$. It can be observed from Figure 8-2 that at the point (L_1, $F_{crw}S_{xc}$), the M_n *AASHTO ($R_b = 1.0$)* curve tends to over-predict the LTB resistance of the girders obtained from the test simulations. One can observe that the proposed model is also somewhat unconservative near this point, since the proposed model and the above AASHTO model both correspond to the theoretical elastic LTB resistance (with J taken equal to zero) at (L_1, F_{crw}). This over-prediction by the proposed model is greatly reduced in the plots on the right that correspond to half the AWS tolerances used as imperfections, and one-half Best-fit Prawel residual stresses. This behavior is expected based on the results presented in Chapter 6. Furthermore, the proposed model still slightly over predicts the test simulation results for shorter unbraced lengths within the inelastic LTB for higher values of initial

geometric imperfections. The M_n *AASHTO* (R_b based on F_{yc}) curve gives a closer prediction to the test simulation results in the vicinity of $KL_b = L_1$. However, this is largely because a single R_b is calculated conservatively by taking the compression flange stress as F_{yc} and then used throughout this curve. The M_n *AASHTO* (R_b based on F_{yc}) curve is significantly conservative for short effective unbraced lengths.
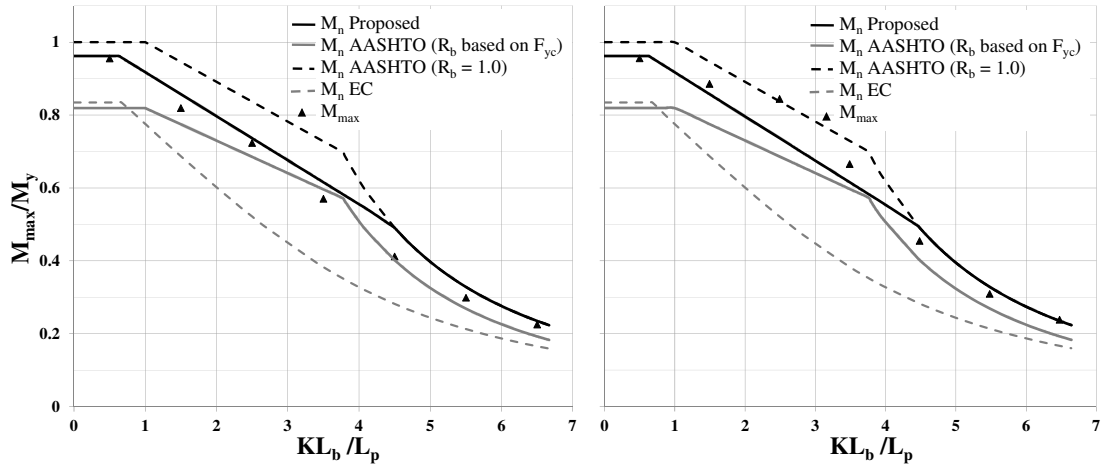
Figure 8-2: Flexural capacity comparing AASHTO, Eurocode and FE simulations, $D/t_w = 300$, $D_c/D = 0.5$, $D/b_{fc} = 6$, $d_o/D = 1$ with full AWS imperfections and Best-fit Prawel residual stress (Left) and half AWS imperfections and half Best-fit Prawel residual stress (right)
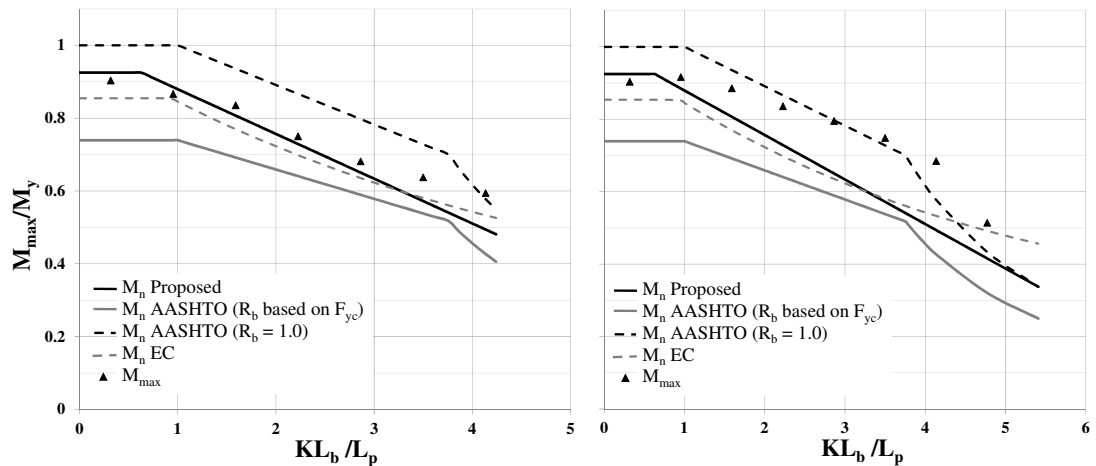
Figure 8-3: Flexural capacity comparing AASHTO, Eurocode and FE simulations, $D/t_w = 300$, $D_c/D = 0.75$, $D/b_{fc} = 4$, $d_o/D = 1$ with full AWS imperfections and Best-fit Prawel residual stress (Left) and half AWS imperfections and half Best-fit Prawel residual stress (right)

In the case of singly-symmetric girders having a large tension flange (and hence a large D_c/D), the AASHTO LRFD and proposed equations are highly conservative for large KL_b values when $R_{bAASHTO} < 1.0$ as shown in Figure 8-3. This is due to the AASHTO and AISC based assumption that, due to the slender web and potential distortional lateral buckling, the St. Venant torsional stiffness GJ provides no help to the LTB resistance. The AASHTO equations neglect the contribution from St. Venant torsion in calculating the elastic buckling stress for all slender web I-sections. This is a conservative approximation for the girders with large tension flanges studied in this research. For these girders, it is notable that the FE predictions compare closely with the calculations based on Eurocode, which include the St. Venant torsional stiffness contribution to the LTB resistance.

It is important to note that the above behavior for large tension flanges may not always be the case. Due to the cross-section distortional deflection of the web, the influence of GJ on I-girder LTB resistances can be substantially reduced (White and Jung 2007). However, for longitudinally stiffened girders having relatively close spacing of the intermediate transverse stiffeners, the frame action of the transverse stiffeners tends to limit the amount and impact of the distortional deflections of the web. In order to assess the influence of frame action on the flexural capacities of these girders, studies are conducted on a larger panel aspect ratio of $d_o/D = 2.0$.

Figures 8-4 through 8-6 show the LTB resistance curves along with the simulation data for girders with $d_o/D = 2.0$. These plots show that the proposed model gives the best results for doubly-symmetric girders. While the proposed model appears to be conservative in the inelastic LTB region, they give excellent correlation in the elastic LTB region for doubly-symmetric girders. Figure 8-6 is an indication that the web distortion effects are not

significant enough at $d_o/D = 2.0$, and the proposed model is still conservative at large

unbraced lengths for singly-symmetric girders with large tension flanges.
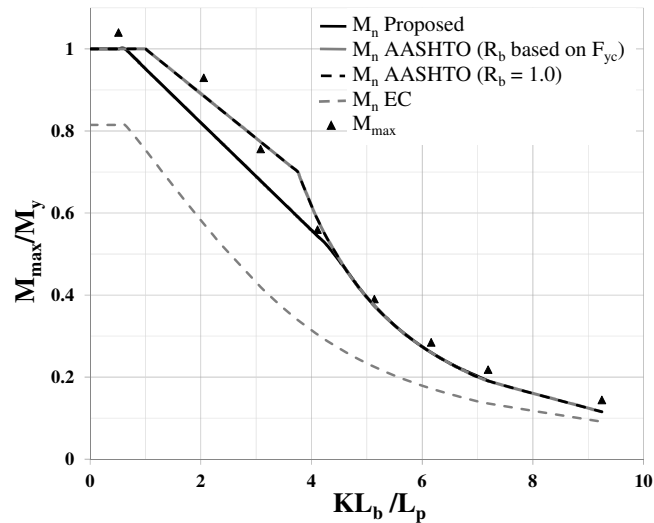
Figure 8-4: Flexural capacity comparing AASHTO, Eurocode and FE simulations, $D/t_w = 240$, $D_c/D = 0.5$, $D/b_{fc} = 6$, $d_o/D = 2$ with half AWS imperfections and half Best-fit Prawel residual stress
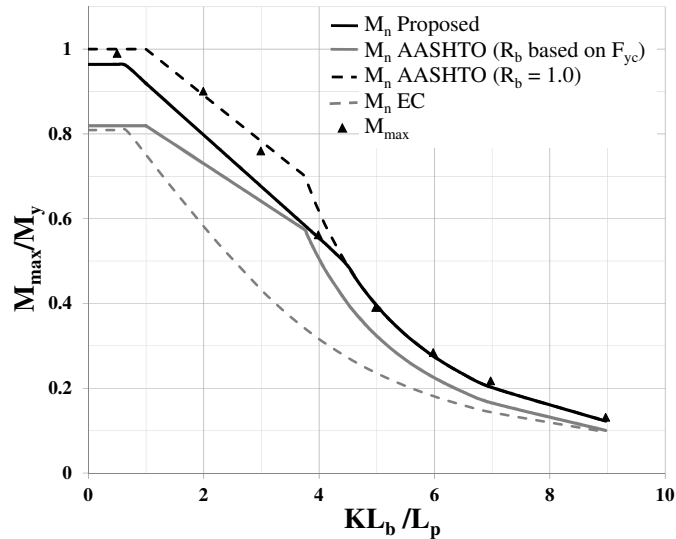
Figure 8-5: Flexural capacity comparing AASHTO, Eurocode and FE simulations, $D/t_w = 300$, $D_c/D = 0.5$, $D/b_{fc} = 6$, $d_o/D = 2$ with half AWS imperfections and half Best-fit Prawel residual stress
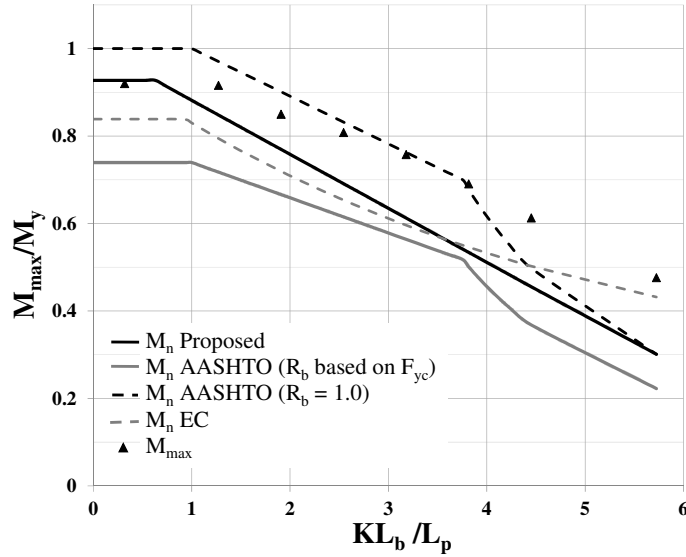
Figure 8-6: Flexural capacity comparing AASHTO, Eurocode and FE simulations, $D/t_w = 300$, $D_c/D = 0.75$, $D/b_{fc} = 4$, $d_o/D = 2$ with half AWS imperfections and half Best-fit Prawel residual stress

In addition, the above plots indicate that, in many cases, the Eurocode is conservative in its prediction of the LTB resistances of longitudinally stiffened girders obtained from the test simulations conducted in this research. This is due largely to the assumption of larger flange residual stresses in similar underlying test simulations conducted in the research leading to the Eurocode provisions (Greiner and Kaim 2001; Roberts and Narayanan 1988). The best estimate of the FE test simulation results conducted in this research is obtained using the proposed model. The complete set of results are presented in Appendix C. These plots show trends similar to those illustrated in Figures 8-1 through 8-6.

8.4.1 Summary of Results for Doubly-Symmetric Girders

Tables 8-2 and 8-3 summarize the moment capacities obtained for all the doubly-symmetric girders ($D_c/D = 0.5$) for the panel aspect ratios of 1.0 and 2.0, evaluated in the LTB test simulations, while also addressing how well the AASHTO, Eurocode, and proposed model compare to the simulation data (M_{max}). It is observed that the proposed

182

model described in Section 8.3 performs better than the current AASHTO and Eurocode

equations in predicting the simulation-based flexural capacities of these girders.

Table 8-2: Statistics for 9 longitudinally stiffened girders with d_o/D =1, D_c/D = 0.5

(a) KL_b = 225 in

Statistical Parameter	$M_{max}/M_{nProposed}$	$M_{max}/M_{nAASHTO}$	M_{max}/M_{nEC}
Mean	1.05	1.04	1.26
COV	0.02	0.06	0.06
Maximum	1.08	1.14	1.36
Minimum	1.03	0.98	1.15

(b) KL_b = 375 in

Statistical Parameter	$M_{max}/M_{nProposed}$	$M_{max}/M_{nAASHTO}$	M_{max}/M_{nEC}
Mean	1.11	1.07	1.46
COV	0.02	0.08	0.09
Maximum	1.15	1.23	1.63
Minimum	1.08	1.01	1.28

(c) KL_b = 525 in

Statistical Parameter	$M_{max}/M_{nProposed}$	$M_{max}/M_{nAASHTO}$	M_{max}/M_{nEC}
Mean	1.10	1.02	1.60
COV	0.03	0.09	0.08
Maximum	1.14	1.16	1.74
Minimum	1.04	0.88	1.43

(d) KL_b = 675 in

Statistical Parameter	$M_{max}/M_{nProposed}$	$M_{max}/M_{nAASHTO}$	M_{max}/M_{nEC}
Mean	1.04	1.00	1.63
COV	0.08	0.09	0.02
Maximum	1.14	1.13	1.69
Minimum	0.93	0.87	1.59

Table 8-2 (Continued): Statistics for 9 longitudinally stiffened girders with $d_o/D = 1$, $D_c/D = 0.5$

(e) $KL_b = 825$ in

Statistical Parameter	$M_{max}/M_{nProposed}$	$M_{max}/M_{nAASHTO}$	M_{max}/M_{nEC}
Mean	0.99	0.99	1.55
COV	0.07	0.08	0.05
Maximum	1.08	1.15	1.65
Minimum	0.90	0.92	1.44

(f) $KL_b = 975$ in

Statistical Parameter	$M_{max}/M_{nProposed}$	$M_{max}/M_{nAASHTO}$	M_{max}/M_{nEC}
Mean	1.00	1.03	1.51
COV	0.03	0.10	0.05
Maximum	1.06	1.24	1.60
Minimum	0.97	0.91	1.43

(g) $KL_b = 1125$ in (2 girders)

Statistical Parameter	$M_{max}/M_{nProposed}$	$M_{max}/M_{nAASHTO}$	M_{max}/M_{nEC}
Mean	0.97	1.11	1.47
COV	0.04	0.07	0.04
Maximum	1.00	1.17	1.51
Minimum	0.95	1.05	1.42

Table 8-3: Statistics for 9 longitudinally stiffened girders with $d_o/D = 2$, $D_c/D = 0.5$

(a) $KL_b = 300$ in

Statistical Parameter	$M_{max}/M_{nProposed}$	$M_{max}/M_{nAASHTO}$	M_{max}/M_{nEC}
Mean	1.12	1.09	1.45
COV	0.03	0.06	0.10
Maximum	1.18	1.23	1.67
Minimum	1.07	1.03	1.25

(b) $KL_b = 450$ in

Statistical Parameter	$M_{max}/M_{nProposed}$	$M_{max}/M_{nAASHTO}$	M_{max}/M_{nEC}
Mean	1.11	1.05	1.59
COV	0.01	0.07	0.11
Maximum	1.13	1.18	1.84
Minimum	1.08	0.98	1.37

(c) $KL_b = 600$ in

Statistical Parameter	$M_{max}/M_{nProposed}$	$M_{max}/M_{nAASHTO}$	M_{max}/M_{nEC}
Mean	1.09	1.03	1.72
COV	0.04	0.07	0.08
Maximum	1.12	1.12	1.93
Minimum	1.01	0.95	1.54

(d) $KL_b = 750$ in

Statistical Parameter	$M_{max}/M_{nProposed}$	$M_{max}/M_{nAASHTO}$	M_{max}/M_{nEC}
Mean	1.05	1.03	1.71
COV	0.06	0.09	0.04
Maximum	1.12	1.20	1.85
Minimum	0.98	0.92	1.65

Table 8-3 (Continued): Statistics for 9 longitudinally stiffened girders with $d_o/D = 2$, $D_c/D = 0.5$

(e) $KL_b = 900$ in

Statistical Parameter	$M_{max} / M_{nProposed}$	$M_{max} / M_{nAASHTO}$	M_{max} / M_{nEC}
Mean	1.04	1.04	1.65
COV	0.06	0.13	0.04
Maximum	1.19	1.26	1.77
Minimum	0.95	0.87	1.56

(f) $KL_b = 1050$ in

Statistical Parameter	$M_{max} / M_{nProposed}$	$M_{max} / M_{nAASHTO}$	M_{max} / M_{nEC}
Mean	1.03	1.09	1.57
COV	0.12	0.12	0.06
Maximum	1.24	1.31	1.73
Minimum	0.83	0.93	1.39

(g) $KL_b = 1350$ in

Statistical Parameter	$M_{max} / M_{nProposed}$	$M_{max} / M_{nAASHTO}$	M_{max} / M_{nEC}
Mean	1.11	1.17	1.47
COV	0.12	0.11	0.09
Maximum	1.37	1.37	1.71
Minimum	0.99	1.00	1.26

The following observations can be gleaned from the data presented in Tables 8-2 and 8-3:

1. The proposed model performs reasonably well for doubly-symmetric slender web girders. In general, this model gives slightly conservative predictions at smaller unbraced lengths in the inelastic LTB region, as compared to the AASHTO equations. This is due to the low values of initial geometric imperfections and residual stresses used in FE test simulations. As noted previously, an initial flange

sweep of $L_b/2000$ is close to $L_b/4000$ between the inflection points. The influence

of this low magnitude of imperfection is reflected in Figures 8-1 through 8-6, where

the simulation data indicate a relatively flat slope within the inelastic LTB region.

However, plots for twice the values of initial imperfections are also shown in

Figures 8-1 through 8-3, which indicate excellent correlation with the proposed

model in the inelastic range, albeit slightly unconservative at the region around L_r.

In view of these observations, it is reasonable to state that the proposed model is

safe to use for design in the presence of reasonable geometric imperfections within

AWS tolerances.

2. While the current AASHTO model is conservative for the yield limit state cases

   considered in Chapter 4, it tends to over-predict the capacities for the doubly-

   symmetric girders in the inelastic and the elastic regions of the LTB curve. The

   current AASHTO predictions are actually quite good for doubly-symmetric girders

   at the smallest unbraced length considered within the inelastic LTB range in these

   studies (KL_b = 225 inches and 300 inches, Tables 8-2 and 8-3).

   It is important to note that the $M_{nAASHTO}$ calculations here are based on the

   calculation of a single R_b using the compression flange yield strength, and the use

   of this R_b for all the unbraced lengths corresponding to a given girder cross-section

   is conservative. If separate larger R_b values are calculated for each of the unbraced

   lengths, as permitted by AASHTO LRFD Article C6.10.1.10.2, the current

   AASHTO LRFD predictions tend to increase for larger KL_b values within the

   inelastic buckling range, but not sufficiently large to capture the strengths indicated

   by FE test simulations.

3. The proposed model recognizes the fact that $R_b = 1$ at effective unbraced lengths long enough where the elastic LTB strength precedes web bend-buckling. This ensures that the proposed model is either an excellent prediction of elastic LTB strengths (for doubly-symmetric girders) or conservative (for singly-symmetric girders with large tension flanges) at large effective unbraced lengths.

8.4.2 Summary of Results for Singly-Symmetric Girders

Tables 8-4 through 8-7 show similar tables for the singly-symmetric girders ($D_c/D = 0.625$ and $D_c/D = 0.75$) studied in this research. The unbraced lengths encompass the inelastic and elastic regions of the proposed LTB curve. The data for tests in the plateau region are presented in Chapter 4.

Table 8-4: Statistics for 9 longitudinally stiffened girders with $d_o/D = 1$, $D_c/D = 0.625$

(a) $KL_b = 225$ in

Statistical Parameter	$M_{max}/M_{nProposed}$	$M_{max}/M_{nAASHTO}$	M_{max}/M_{nEC}
Mean	1.05	1.13	1.21
COV	0.01	0.10	0.04
Maximum	1.07	1.26	1.28
Minimum	1.03	0.96	1.11

(b) $KL_b = 375$ in

Statistical Parameter	$M_{max}/M_{nProposed}$	$M_{max}/M_{nAASHTO}$	M_{max}/M_{nEC}
Mean	1.12	1.18	1.36
COV	0.02	0.12	0.07
Maximum	1.17	1.40	1.48
Minimum	1.08	1.00	1.21

Table 8-4 (Continued): Statistics for 9 longitudinally stiffened girders with $d_o/D = 1$, $D_c/D = 0.625$

(c) $KL_b = 525$ in

Statistical Parameter	$M_{max}/M_{nProposed}$	$M_{max}/M_{nAASHTO}$	M_{max}/M_{nEC}
Mean	1.13	1.15	1.42
COV	0.03	0.12	0.05
Maximum	1.18	1.32	1.48
Minimum	1.07	0.93	1.32

(d) $KL_b = 675$ in

Statistical Parameter	$M_{max}/M_{nProposed}$	$M_{max}/M_{nAASHTO}$	M_{max}/M_{nEC}
Mean	1.10	1.18	1.39
COV	0.05	0.14	0.05
Maximum	1.17	1.45	1.46
Minimum	1.01	0.94	1.27

(e) $KL_b = 825$ in

Statistical Parameter	$M_{max}/M_{nProposed}$	$M_{max}/M_{nAASHTO}$	M_{max}/M_{nEC}
Mean	1.10	1.23	1.30
COV	0.06	0.16	0.09
Maximum	1.19	1.53	1.46
Minimum	0.98	0.96	1.17

(f) $KL_b = 975$ in

Statistical Parameter	$M_{max}/M_{nProposed}$	$M_{max}/M_{nAASHTO}$	M_{max}/M_{nEC}
Mean	1.15	1.33	1.24
COV	0.07	0.17	0.09
Maximum	1.31	1.71	1.40
Minimum	1.06	1.02	1.11

Table 8-4 (Continued): Statistics for 9 longitudinally stiffened girders with $d_o/D = 1$, $D_c/D = 0.625$

(f) $KL_b = 1125$ in (2 girders)

Statistical Parameter	$M_{max}/M_{nProposed}$	$M_{max}/M_{nAASHTO}$	M_{max}/M_{nEC}
Mean	1.07	1.36	1.19
COV	0.12	0.18	0.02
Maximum	1.16	1.54	1.21
Minimum	0.98	1.19	1.17

Table 8-5: Statistics for 9 longitudinally stiffened girders with $d_o/D = 2$, $D_c/D = 0.625$

(a) $KL_b = 300$ in

Statistical Parameter	$M_{max}/M_{nProposed}$	$M_{max}/M_{nAASHTO}$	M_{max}/M_{nEC}
Mean	1.12	1.20	1.37
COV	0.03	0.10	0.08
Maximum	1.17	1.37	1.55
Minimum	1.08	1.05	1.21

(b) $KL_b = 450$ in

Statistical Parameter	$M_{max}/M_{nProposed}$	$M_{max}/M_{nAASHTO}$	M_{max}/M_{nEC}
Mean	1.12	1.16	1.43
COV	0.02	0.12	0.07
Maximum	1.15	1.37	1.55
Minimum	1.08	0.98	1.26

(c) $KL_b = 600$ in

Statistical Parameter	$M_{max}/M_{nProposed}$	$M_{max}/M_{nAASHTO}$	M_{max}/M_{nEC}
Mean	1.11	1.18	1.47
COV	0.03	0.12	0.03
Maximum	1.15	1.38	1.52
Minimum	1.06	0.96	1.38

Table 8-5 (Continued): Statistics for 9 longitudinally stiffened girders with d_o/D =2, D_c/D = 0.625

(d) KL_b = 750 in

Statistical Parameter	$M_{max}/M_{nProposed}$	$M_{max}/M_{nAASHTO}$	M_{max}/M_{nEC}
Mean	1.12	1.23	1.42
COV	0.06	0.15	0.04
Maximum	1.24	1.54	1.48
Minimum	1.04	0.99	1.32

(e) KL_b = 900 in

Statistical Parameter	$M_{max}/M_{nProposed}$	$M_{max}/M_{nAASHTO}$	M_{max}/M_{nEC}
Mean	1.15	1.30	1.34
COV	0.09	0.19	0.06
Maximum	1.36	1.67	1.44
Minimum	1.04	0.95	1.23

(f) KL_b =1050 in

Statistical Parameter	$M_{max}/M_{nProposed}$	$M_{max}/M_{nAASHTO}$	M_{max}/M_{nEC}
Mean	1.19	1.41	1.27
COV	0.13	0.18	0.05
Maximum	1.49	1.80	1.36
Minimum	1.03	1.06	1.17

(g) KL_b = 1350 in

Statistical Parameter	$M_{max}/M_{nProposed}$	$M_{max}/M_{nAASHTO}$	M_{max}/M_{nEC}
Mean	1.37	1.62	1.18
COV	0.15	0.19	0.03
Maximum	1.76	2.09	1.22
Minimum	1.14	1.21	1.12

Table 8-6: Statistics for 9 longitudinally stiffened girders with $d_o/D =1$, $D_c/D = 0.75$

(a) $KL_b = 225$ in

Statistical Parameter	$M_{max}/M_{nProposed}$	$M_{max}/M_{nAASHTO}$	M_{max}/M_{nEC}
Mean	1.05	1.30	1.16
COV	0.01	0.08	0.05
Maximum	1.07	1.51	1.25
Minimum	1.03	1.18	1.08

(b) $KL_b = 375$ in

Statistical Parameter	$M_{max}/M_{nProposed}$	$M_{max}/M_{nAASHTO}$	M_{max}/M_{nEC}
Mean	1.17	1.41	1.31
COV	0.04	0.11	0.07
Maximum	1.23	1.71	1.44
Minimum	1.10	1.25	1.15

(c) $KL_b = 525$ in

Statistical Parameter	$M_{max}/M_{nProposed}$	$M_{max}/M_{nAASHTO}$	M_{max}/M_{nEC}
Mean	1.23	1.47	1.35
COV	0.05	0.12	0.08
Maximum	1.32	1.77	1.50
Minimum	1.15	1.26	1.20

(d) $KL_b = 675$ in

Statistical Parameter	$M_{max}/M_{nProposed}$	$M_{max}/M_{nAASHTO}$	M_{max}/M_{nEC}
Mean	1.33	1.71	1.35
COV	0.08	0.25	0.10
Maximum	1.53	2.37	1.55
Minimum	1.21	1.30	1.22

Table 8-6 (Continued): Statistics for 9 longitudinally stiffened girders with $d_o/D = 1$, $D_c/D = 0.75$

(e) $KL_b = 825$ in

Statistical Parameter	$M_{max}/M_{nProposed}$	$M_{max}/M_{nAASHTO}$	M_{max}/M_{nEC}
Mean	1.52	2.07	1.34
COV	0.15	0.30	0.11
Maximum	1.96	2.91	1.54
Minimum	1.31	1.36	1.16

(f) $KL_b = 975$ in

Statistical Parameter	$M_{max}/M_{nProposed}$	$M_{max}/M_{nAASHTO}$	M_{max}/M_{nEC}
Mean	1.72	2.46	1.28
COV	0.21	0.32	0.11
Maximum	2.35	3.54	1.47
Minimum	1.32	1.59	1.10

(f) $KL_b = 1125$ in (2 girders)

Statistical Parameter	$M_{max}/M_{nProposed}$	$M_{max}/M_{nAASHTO}$	M_{max}/M_{nEC}
Mean	1.52	2.22	1.24
COV	0.27	0.39	0.22
Maximum	1.81	2.84	1.43
Minimum	1.24	1.60	1.05

Table 8-7: Statistics for 9 longitudinally stiffened girders with $d_o/D = 2$, $D_c/D = 0.75$

(a) $KL_b = 300$ in

Statistical Parameter	$M_{max}/M_{nProposed}$	$M_{max}/M_{nAASHTO}$	M_{max}/M_{nEC}
Mean	1.13	1.39	1.31
COV	0.03	0.10	0.08
Maximum	1.20	1.65	1.43
Minimum	1.08	1.23	1.15

(b) $KL_b = 450$ in

Statistical Parameter	$M_{max}/M_{nProposed}$	$M_{max}/M_{nAASHTO}$	M_{max}/M_{nEC}
Mean	1.16	1.40	1.34
COV	0.04	0.11	0.07
Maximum	1.22	1.69	1.47
Minimum	1.10	1.23	1.18

(c) $KL_b = 600$ in

Statistical Parameter	$M_{max}/M_{nProposed}$	$M_{max}/M_{nAASHTO}$	M_{max}/M_{nEC}
Mean	1.23	1.54	1.36
COV	0.04	0.18	0.09
Maximum	1.30	1.99	1.54
Minimum	1.16	1.26	1.24

(d) $KL_b = 750$ in

Statistical Parameter	$M_{max}/M_{nProposed}$	$M_{max}/M_{nAASHTO}$	M_{max}/M_{nEC}
Mean	1.34	1.80	1.32
COV	0.12	0.27	0.10
Maximum	1.66	2.51	1.50
Minimum	1.22	1.27	1.18

Table 8-7 (Continued): Statistics for 9 longitudinally stiffened girders with $d_o/D = 2$, $D_c/D = 0.75$

(e) $KL_b = 900$ in

Statistical Parameter	$M_{max}/M_{nProposed}$	$M_{max}/M_{nAASHTO}$	M_{max}/M_{nEC}
Mean	1.52	2.11	1.27
COV	0.18	0.32	0.11
Maximum	2.01	3.02	1.44
Minimum	1.24	1.36	1.10

(f) $KL_b = 1050$ in

Statistical Parameter	$M_{max}/M_{nProposed}$	$M_{max}/M_{nAASHTO}$	M_{max}/M_{nEC}
Mean	1.73	2.50	1.21
COV	0.23	0.31	0.11
Maximum	2.39	3.57	1.39
Minimum	1.29	1.63	1.05

(g) $KL_b = 1350$ in

Statistical Parameter	$M_{max}/M_{nProposed}$	$M_{max}/M_{nAASHTO}$	M_{max}/M_{nEC}
Mean	2.27	3.30	1.14
COV	0.26	0.33	0.12
Maximum	3.28	4.76	1.33
Minimum	1.58	2.10	1.02

The following observations can be gleaned from the data presented in Tables 8-4 through 8-7:

4. The current AASHTO LRFD equations can severely under-predict the true strength in the case of singly-symmetric girders, especially at longer unbraced lengths in the elastic buckling range. The mean professional factor ($M_{max}/M_{nAASHTO}$) for $D_c/D = 0.625$ varies between 1.13 and 1.62, and the COV varies between 0.10 and 0.19. The mean professional factor ($M_{max}/M_{nAASHTO}$) for $D_c/D = 0.75$ varies between 1.3

and 3.3, and the COV varies between 0.08 and 0.33. The larger means and COVs are for the longer unbraced lengths. It is evident that neglecting J in computing the elastic unbraced lengths is overly pessimistic for cross-sections with larger tension flanges. However, including J and using the form of the proposed or current LTB strength equations, will result in a gross over-prediction of the inelastic LTB strength of such girders.

5. The proposed model provides a better prediction with a mean professional factor ($M_{max}/M_{nProposed}$) that varies between 1.05 and 1.37, and a COV that varies between 0.01 and 0.15 for $D_c/D = 0.625$. The mean professional factor ($M_{max}/M_{nProposed}$) for $D_c/D = 0.75$ varies between 1.05 and 2.27, and the COV varies between 0.01 and 0.26.

6. The current AASHTO model under-predicts the capacity for several reasons. The first is that AASHTO's current calculation of R_b is highly conservative for singly-symmetric girders as discussed in Section 4.6. The second is the fact that the AASHTO elastic LTB equations neglect the St Venant torsional stiffness (GJ) contribution to the buckling strength. These factors combine to make the current AASHTO predictions significantly conservative for these cases.

7. The proposed model eliminates the conservatism associated with the first of the above reasons. However, it does not address the second reason. As discussed previously, one must be cautious in counting upon the contribution from GJ for slender web members. However, it is expected that for the close transverse stiffener spacing typically used in longitudinally stiffened girders (even when the d_o/D limit

is extended to 2.0), the assumption of $J = 0$ in writing the LTB resistances tends to be generally conservative.

8. For the singly-symmetric girders studied in this research, the above conservative approach of taking $J = 0$ in the elastic LTB prediction is justified due to lack of better characterization of web distortion effects.

Based on all the data in Tables 8-2 through 8-7, one can observe that the Eurocode model is more conservative than both the current AASHTO and the proposed models. However, the under-prediction of the Eurocode model is consistent across various unbraced lengths for both doubly and singly-symmetric girders. This conservatism is largely due to two reasons:

1. For slender web girders with unbraced lengths sufficiently short such that the yield limit state governs, the Eurocode cross-section model (Section 2.9) is conservative compared to the model proposed in Section 4.7 (which provides an accurate characterization of the girder yield limit state resistances in the test simulations conducted in Chapter 3).

2. The residual stress pattern considered for slender web I-girders in the Eurocode developments is more severe than that considered in this research.

8.5 Summary

The following are the key conclusions from the studies conducted in this Chapter.

1. The proposed model described in Section 8.3 performs better than the current AASHTO model because R_{bPr} is a better estimate of the true cross-section behavior

than $R_{bAASHTO}$, and the model provides a better estimate of the resistance within the inelastic buckling range.

2. The proposed model does not penalize girders with long unbraced lengths by scaling the resistance by R_b. Instead, it allows the use of $R_b = 1.0$ when LTB precedes web bend-buckling.

3. The proposed model tends to be overly conservative for larger unbraced lengths in cases of singly-symmetric girders with large tension flanges. However, it is expected that most bridge girders will fall in the inelastic LTB range for design. It is expected that cross-frames and other bracing systems will reduce the unbraced lengths such that the long unbraced lengths are typically of no concern in the final constructed condition. In the extreme case that such a design is deemed necessary, the proposed model is conservative, and safe for design.

CHAPTER 9

RESISTANCE OF STRAIGHT GIRDERS SUBJECTED TO

COMBINED BENDING AND SHEAR

Loadings involving high moment and high shear can be particularly important in the negative moment regions of continuous-span bridges. The test simulations presented in this chapter are designed to evaluate the shear and bending resistances within this realm, considering cases where the flexural resistance is governed by the yield limit state or the LTB limit state in longitudinally stiffened girders. In evaluating the tests with flexure controlled by compression flange yielding, LTB and flange local buckling (FLB) are ruled out by the selection of the lateral brace spacing and the compression flange width-to-thickness ratio. The proposed yield limit state model (Section 4.7) predicts a higher flexural capacity compared to the current AASHTO provisions. It is important to ascertain whether the use of the proposed model results in any moment-shear strength interaction. The proposed LTB model in Section 8.3 is used to study the behavior of longitudinally stiffened girders under moment gradient when flexure is controlled by LTB limit state.

The current AASHTO LRFD provisions neglect the presence of longitudinal stiffeners in predicting the shear resistance of longitudinally stiffened girders. Conversely, Cooper (1965) proposed a model where the shear resistances of the individual web sub-panels are computed separately using Basler's equations (shear resistance equations in AASHTO LRFD) and then simply added to determine the shear resistance of the entire web. Both the current simpler AASHTO LRFD model and Cooper's model are considered for the calculation of the girder shear resistances in the evaluations presented on tests with flexure

controlled by compression flange yield. It is demonstrated that the AASHTO shear equations perform as well or better than Cooper's model for the longitudinally stiffened girders. Based on this conclusion, only the AASHTO shear equations are considered for the moment gradient studies with LTB flexure limit state discussed later in the chapter.

AASHTO Equation 6.10.9.3.2-1 requires a check on the ratio of the web area to the average flange area of the plate girder, and accordingly requires the use of either the true Basler equation or the full tension field action in computing the shear capacity of plate girders. This method is used for all the shear capacity calculations in this research. The AASHTO LRFD provisions use the true Basler or the complete tension field action equations, as appropriate, considering the full web panel, neglecting any assistance from the longitudinal stiffener. Conversely, the implementation of Cooper's model uses the same AASHTO LRFD equations for each of the separate sub-panels.

9.1 High Shear-High Moment Loading with Flexure Controlled by Yield Limit State

9.1.1 Test Setup

The behavior under high-shear high-moment loading is studied herein using three-point bending tests as shown in Figure 9-1. The setup for these tests is similar to that used by Cooper (1965). The end panels and the bearing and transverse stiffeners are designed such that failure occurs in the interior panel next to the mid-span load in all the tests. The web thickness used in the end panels is 1.25 in, resulting in a web slenderness ratio of 120. This is constant in all test simulations. The residual stress patterns applied in these tests are the same as those explained in Section 3.5. The imperfection pattern 2, previously selected for

200

the test studies in Chapters 4 and 8, is also used here. This initial imperfection is applied to the interior panel on one side of the load.
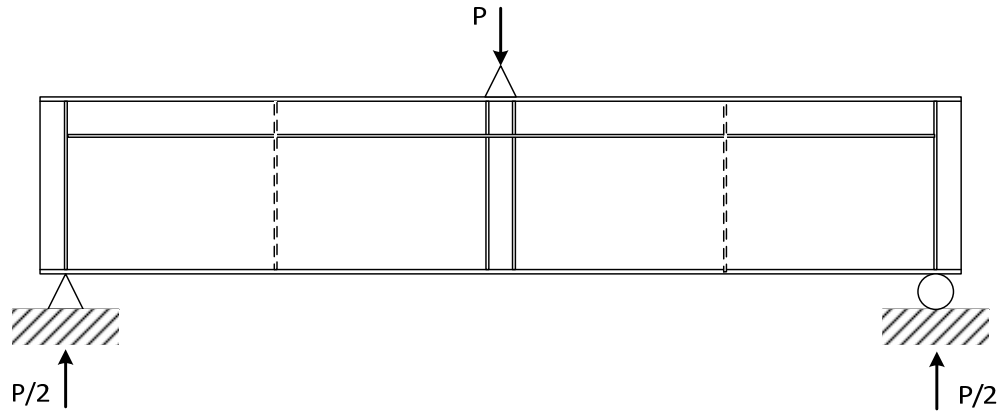
Figure 9-1: Test setup for high shear and high bending moment (yield limit state)

9.1.2 Case Studies

A total of 123 distinct tests are simulated in this research to evaluate the behavior under high shear and high bending moment. Lateral braces are located such that LTB is not a mode of failure. The following are the variables considered in these studies:

- $D/t_w = 300$, 240, and 200

- $d_o/D = 1.25$, 1.5, and 2.0

- $b_{fc} = $ D/6, D/5, and D/4

- $t_{fc} = 1.5$, 1.75, and 2.25 corresponding to the different values of b_{fc}

- $D_c/D = 0.5$, 0.625, and 0.75

- A_l /A_{wc}

- I_l

- $d_s/D_c = 0.40$ and 0.533

In addition to the variation of the above parameters, the overall girder lengths are varied such that the test girders have configurations that range from panels that fail in shear when

the applied moment is approximately 60% of the recommended moment capacity prediction ($R_{bPr}M_y$) to panels that fail in flexure when the applied shear is approximately 60% of the predicted shear capacity based on the AASHTO shear equations ($V_{nAASHTO}$). The largest number of the test simulations are conducted with loadings and geometries such that, approximately, the girders reach their flexural capacity (governed by the yield limit state), and shear capacity (including tension field action and calculated per the AASHTO LRFD Specifications) simultaneously. It may be noted that it is in the above ranges of the moments and shears that we expect the highest potential influence of moment-shear strength interaction, if any.

Six different girder cases considered in these studies are defined in Table 9-1. These cases include two values of d_o/D, 1.25 and 1.5. Subsequent studies focus on the effect of extending the current AASHTO limits on d_o/D to 2.0 for longitudinally stiffened girders. The end panel lengths shown in Table 9-1 are selected to provide a desired overall length of the girders. Two positions of the longitudinal stiffener through the web depth are studied – one at 0.4 D_c and the other at 0.533 D_c. The value 0.533 D_c is closer to 0.5D, which theoretically maximizes the girder web shear capacity (however, it should be noted that D_c varies from 0.5 to 0.75D in these studies, and thus the longitudinal stiffener for this case is not necessarily close to the web mid-depth). Table 9-1 shows the relative position of the longitudinal stiffener with respect to the depth of the web (d_s/D_c) for all the different girder web depths in compression used in the FE test simulations. The area and moment of inertia of the stiffener are provided per the minimum AASHTO requirements, as explained in Section 2.8. They vary as a function of d_o/D and D/t_w. The moment-to-shear ratios are varied by changing the overall girder length, i.e., the moment to shear ratio in the tests

(*M/V*) is equal to one-half of the overall girder length. These values are shown in the right-most column of Table 9-1.

Table 9-1: Case studies for straight girders subjected to high shear combined with high bending moment

Case	d_o/D IP^a	d_o/D EP^a	d_s/D_c	d_s/D $D_c/D=$ 0.5	d_s/D $D_c/D=$ 0.625	d_s/D $D_c/D=$ 0.75	M/V
1	1.5	1.5	0.40	0.20	0.25	0.30	3.0D
2	1.25	0.75	0.53	0.27	0.33	0.40	2.0D
3	1.5	0.5	0.53	0.27	0.33	0.40	2.0D
4	1.5	3	0.53	0.27	0.33	0.40	4.5D
5	2.0	0.75	0.53	0.27	0.33	0.40	2.75D
6	2.0	2.25	0.53	0.27	0.33	0.40	4.25D

a. IP = Interior Panel, EP = End panel

9.1.3 Results for Cases 1 Through 4

The FE test simulation strengths for Cases 1 through 4 are compared to the governing strengths from the current AASHTO shear resistance model, Cooper's shear resistance model, and the recommended flexural yield strength model in Tables 9-2 through 9-5. Cases 5 and 6 are discussed separately in Section 9.1.4. The term V_{max} is the maximum shear achieved in the FE test simulations, $V_{nCooper}$ is the shear capacity calculated as per Cooper's (1965) recommendations (but using the true Basler or the Basler complete tension field action shear strengths as specified per the current AASHTO LRFD provisions), and $V_{nAASHTO}$ is the shear capacity calculated as per the current AASHTO LRFD provisions. The term M_{max} is the maximum moment achieved in the test simulations. The test strengths are moment controlled (i.e., the flexural yield strength as per the proposed R_b governs) when $M_{max}/R_{bPr}M_y$ is greater than $V_{max}/V_{nAASHTO}$ or $V_{max}/V_{nCooper}$. Otherwise, the tests are

203

shear controlled. The governing shear or flexural strength ratios are bolded in the table. Since this study is considering two different shear resistance models, the values in more than one column are bolded for some of the tests, indicating that one strength governs when the AASHTO shear resistance model is employed and another governs when Cooper's shear resistance model is employed.

Table 9-2: Comparison of the test simulation load capacities to the governing strengths from the AASHTO shear resistance model, Cooper's shear resistance model, and the recommended flexural yield strength model (Case1)

D/b_{fc}	D_c/D	$D/t_w = 300$			$D/t_w = 240$			$D/t_w = 200$		
		$V_{max}/V_{nCooper}$	$V_{max}/V_{nAASHTO}$	$M_{max}/R_{bPr}M_y$	$V_{max}/V_{nCooper}$	$V_{max}/V_{nAASHTO}$	$M_{max}/R_{bPr}M_y$	$V_{max}/V_{nCooper}$	$V_{max}/V_{nAASHTO}$	$M_{max}/R_{bPr}M_y$
	0.5	0.94*	0.77	**1.10**	0.80	0.67	**1.13**	0.69	0.88	**1.18**
6	0.625	0.76	0.79	**1.09**	0.64	0.72	**1.13**	0.59	0.66	**1.15**
	0.75	0.85	0.82	**1.10**	0.66	0.72	**1.12**	0.58	0.68	**1.17**
	0.5	0.86	0.93	**1.03**	0.76	0.82	**1.09**	0.84	0.72	**1.14**
5	0.625	0.92	0.97	**1.03**	0.78	0.87	**1.10**	0.70	0.78	**1.12**
	0.75	1.04	1.00	**1.05**	0.81	0.89	**1.10**	0.68	0.80	**1.12**
	0.5	**0.95**	**1.04**	0.76	**0.96**	**1.04**	0.95	0.91	0.99	**1.09**
4	0.625	**1.04**	**1.08**	0.78	**0.95**	**1.07**	0.93	0.92	1.03	**1.05**
	0.75	**1.25**	**1.20**	0.85	**1.06**	**1.16**	1.00	0.91	1.06	**1.07**

*_Bolded values are the governing strength ratios given the use of one or both shear resistance models._

Table 9-3: Comparison of the test simulation load capacities to the governing strengths from the AASHTO shear resistance model, Cooper's shear resistance model, and the recommended flexural yield strength model (Case2)

D/b_{fc}	D_c/D	$D/t_w = 300$			$D/t_w = 240$			$D/t_w = 200$		
		$V_{max}/V_{nCooper}$	$V_{max}/V_{nAASHTO}$	$M_{max}/R_{bPr}M_y$	$V_{max}/V_{nCooper}$	$V_{max}/V_{nAASHTO}$	$M_{max}/R_{bPr}M_y$	$V_{max}/V_{nCooper}$	$V_{max}/V_{nAASHTO}$	$M_{max}/R_{bPr}M_y$
	0.5	**1.17***	0.89	**0.94**	0.98	0.85	**1.06**	0.83	0.79	**1.06**
6	0.625	**1.00**	0.89	**0.92**	0.82	0.84	**1.01**	0.71	0.81	**1.07**
	0.75	**1.15**	0.97	**0.98**	0.92	0.89	**1.05**	0.74	0.90	**1.02**
	0.5	**0.97**	**0.95**	0.77	0.89	**0.96**	**0.93**	1.00	0.93	**1.00**
5	0.625	**1.08**	**0.97**	0.76	**0.95**	**0.97**	0.91	0.84	0.94	**1.00**
	0.75	**1.30**	**1.10**	0.85	**1.08**	**1.05**	0.96	**0.85**	**1.05**	0.82
	0.5	**1.02**	**1.00**	0.53	**0.99**	**1.05**	0.69	**0.97**	**1.08**	0.81
4	0.625	**1.17**	**1.05**	0.54	**1.06**	**1.09**	0.69	0.97	**1.17**	0.86
	0.75	**1.46**	**1.24**	0.63	**1.24**	**1.20**	0.75	1.06	**1.24**	**1.08**

Bolded values are the governing strength ratios given the use of one or both shear resistance models.

Table 9-4: Comparison of the test simulation load capacities to the governing strengths from the AASHTO shear resistance model, Cooper's shear resistance model, and the recommended flexural yield strength model (Case3)

D/b_{fc}	D_c/D	$D/t_w = 300$			$D/t_w = 240$			$D/t_w = 200$		
		$V_{max}/V_{nCooper}$	$V_{max}/V_{nAASHTO}$	$M_{max}/R_{bPr}M_y$	$V_{max}/V_{nCooper}$	$V_{max}/V_{nAASHTO}$	$M_{max}/R_{bPr}M_y$	$V_{max}/V_{nCooper}$	$V_{max}/V_{nAASHTO}$	$M_{max}/R_{bPr}M_y$
	0.5	**0.96***	**0.98**	0.92	**1.04**	0.95	**1.06**	0.88	**1.24**	1.08
6	0.625	**1.10**	**1.01**	0.92	0.91	0.98	**1.04**	0.78	**0.91**	1.09
	0.75	-	-	-	1.02	1.02	**1.07**	0.80	**0.93**	1.09
5	0.5	**1.01**	**1.03**	0.73	-	-	-	-	-	-
	0.625	-	-	-	**1.00**	**1.08**	0.90	-	-	-
4	0.5	-	-	-	-	-	-	**1.00**	**1.14**	0.80

Bolded values are the governing strength ratios given the use of one or both shear resistance models.

Table 9-5: Comparison of the test simulation load capacities to the governing strengths from the AASHTO shear resistance model, Cooper's shear resistance model, and the recommended flexural yield strength model (Case4)

D/b_{fc}	D_c/D	$D/t_w = 300$			$D/t_w = 240$		
		$V_{max}/$ $V_{nCooper}$	$V_{max}/$ $V_{nAASHTO}$	$M_{max}/$ $R_{bPr}M_y$	$V_{max}/$ $V_{nCooper}$	$V_{max}/$ $V_{nAASHTO}$	$M_{max}/$ $R_{bPr}M_y$
	0.5	**0.90***	0.91	**0.97**	-	-	-
4	0.625	**1.03**	0.95	**0.99**	0.76	0.81	**1.04**
	0.75	**1.13**	0.98	**1.01**	-	-	-

*Bolded values are the governing strength ratios given the use of one or both shear resistance models.

Figures 9-2 and 9-3 summarize the above results for the girders with $D/t_w = 300$ for the two respective shear resistance models. Figures 9-4 and 9-5 do the same for the girders with $D/t_w = 240$, and Figures 9-6 and 9-7 show the results for the girders with $D/t_w = 200$. Each of the figures label some of the data points from the test simulations as moment controlled and others as shear controlled. It is important to note that some of the tests are moment controlled when one shear resistance is employed, and shear controlled when the other shear resistance model is employed. Tables 9-6 through 9-8 provide the statistics for the governing strength ratios in the above plots.
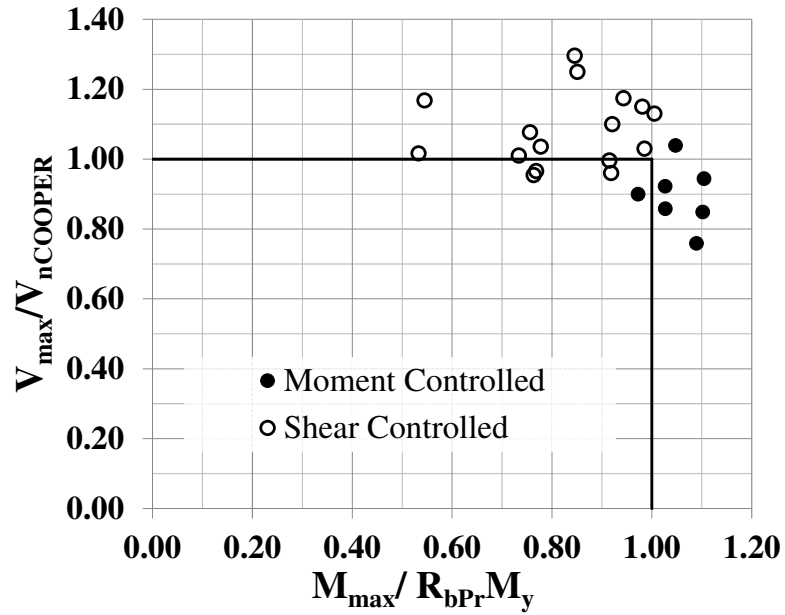
Figure 9-2: *$V_{max}/V_{nCooper}$* **versus** *$M_{max}/R_{bPr}M_y$* **for high-moment high-shear tests with** *D/t_w* **= 300 (Cases 1 through 4)**
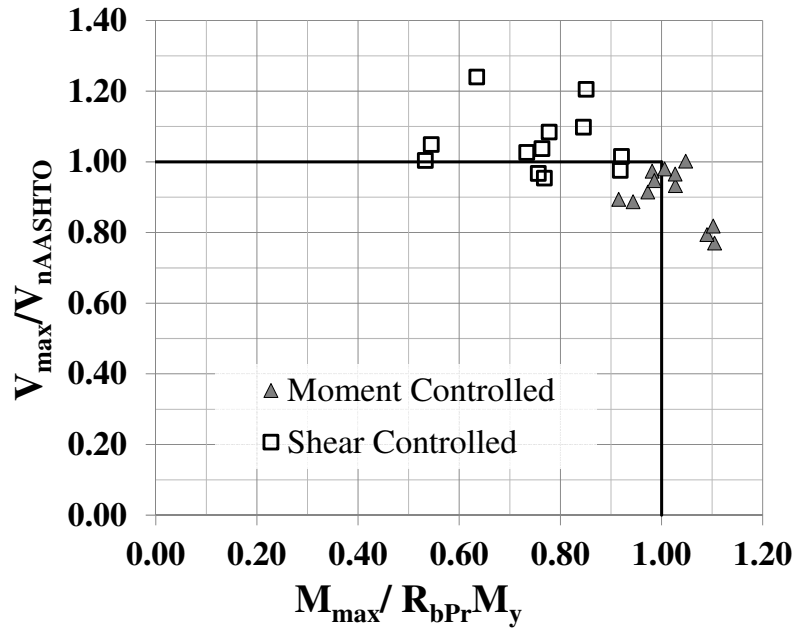
Figure 9-3: *$V_{max}/V_{nAASHTO}$* **versus** *$M_{max}/R_{bPr}M_y$* **for high-moment high-shear tests with** *D/t_w* **= 300 (Cases 1 through 4)**
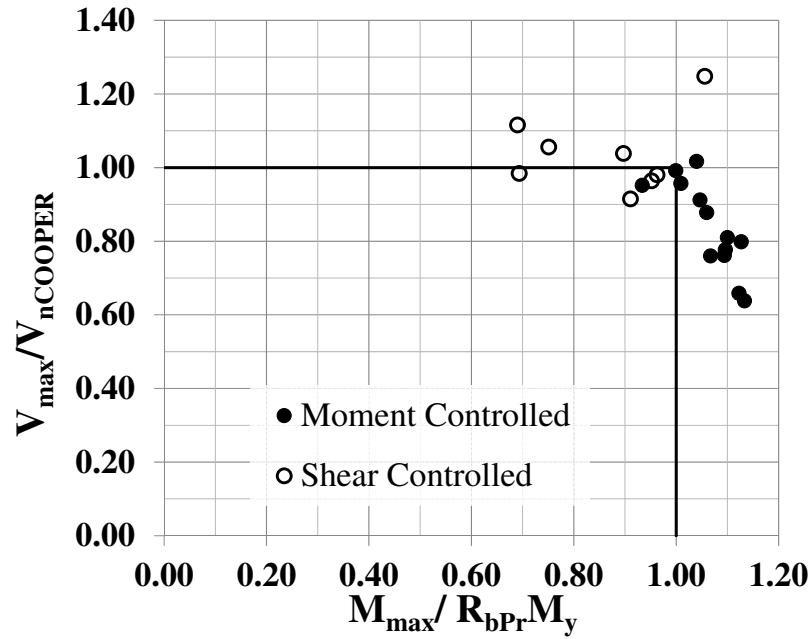
Figure 9-4: *V$_{max}$/V$_{nCooper}$* **versus** *M$_{max}$/R$_{bPr}$M$_y$* **for high-moment high-shear tests with** *D/t$_w$* = 240 **(Cases 1 through 4)**
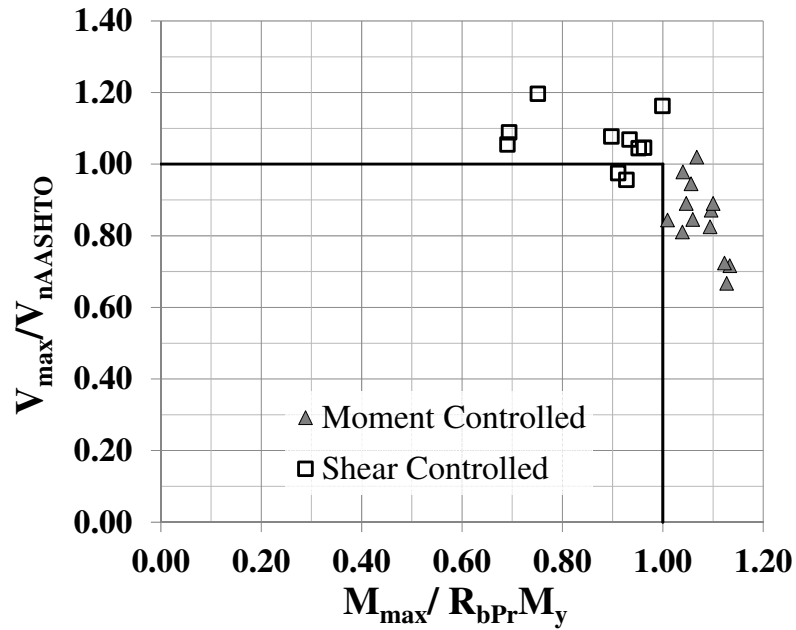
Figure 9-5: *V$_{max}$/V$_{nAASHTO}$* **versus** *M$_{max}$/R$_{bPr}$M$_y$* **for high-moment high-shear tests with** *D/t$_w$* = 240 **(Cases 1 through 4)**
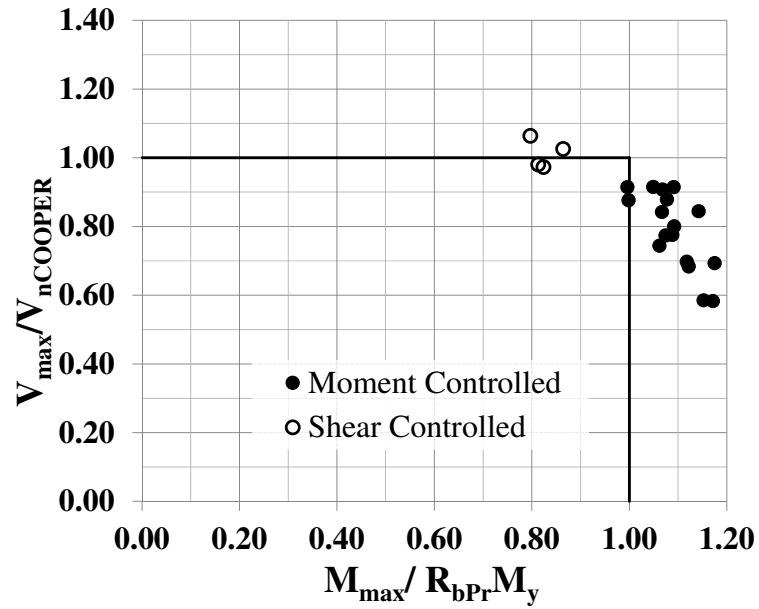
Figure 9-6: $V_{max}/V_{nCooper}$ **versus** $M_{max}/R_{bPr}M_y$ **for high-moment high-shear tests with** $D/t_w = 200$ **(Cases 1 through 4)**
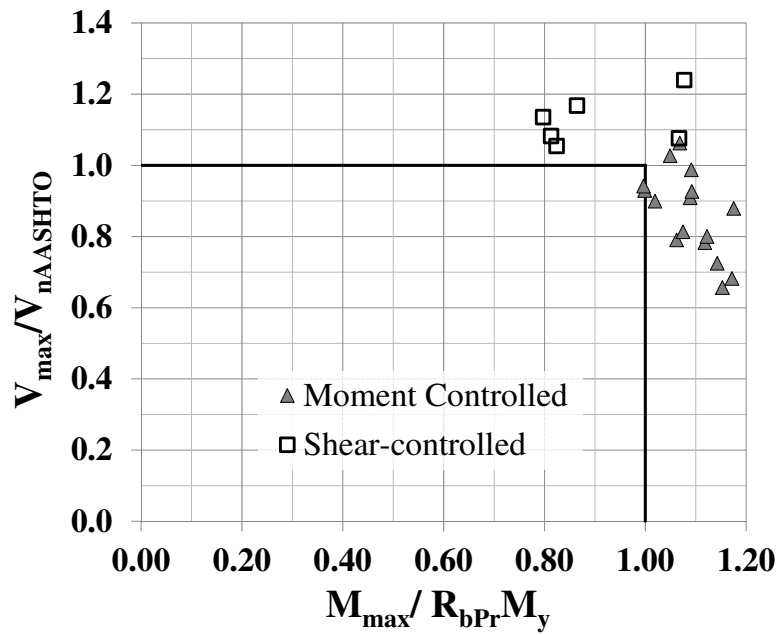
Figure 9-7: $V_{max}/V_{nAASHTO}$ **versus** $M_{max}/R_{bPr}M_y$ **for high-moment high-shear tests with** $D/t_w = 200$ **(Cases 1 through 4)**

Table 9-6: Statistics for the high-moment high-shear tests (Cases 1 through 4) with $D/t_w = 300$

Statistical Parameter	AASHTO		Cooper	
	Moment Controlled (12 tests) $M_{max}/R_{bPr}M_y$	Shear Controlled (12 tests) $V_{max}/V_{nAASHTO}$	Moment Controlled (7 tests) $M_{max}/R_{bPr}M_y$	Shear Controlled (17 tests) $V_{max}/V_{nCooper}$
Mean	1.02	1.05	1.05	1.10
COV	0.06	0.09	0.05	0.12
Maximum	1.10	1.24	1.10	1.46
Minimum	0.92	0.95	0.97	0.95
Median	1.02	1.03	1.05	1.08

Table 9-7: Statistics for the high-moment high-shear tests (Cases 1 through 4) with $D/t_w = 240$

Statistical Parameter	AASHTO		Cooper	
	Moment Controlled (13 tests) $M_{max}/R_{bPr}M_y$	Shear Controlled (10 tests) $V_{max}/V_{nAASHTO}$	Moment Controlled (14 tests) $M_{max}/R_{bPr}M_y$	Shear Controlled (9 tests) $V_{max}/V_{nCooper}$
Mean	1.08	1.07	1.07	1.04
COV	0.04	0.07	0.05	0.09
Maximum	1.13	1.20	1.13	1.25
Minimum	1.01	0.96	0.93	0.95
Median	1.07	1.06	1.06	1.00

Table 9-8: Statistics for the high-moment high-shear tests (Cases 1 through 4) with $D/t_w = 200$

Statistical Parameter	AASHTO		Cooper	
	Moment Controlled (16 tests)	Shear Controlled (6 tests)	Moment Controlled (17 tests)	Shear Controlled (5 tests)
	$M_{max}/R_{bPr}M_y$	$V_{max}/V_{nAASHTO}$	$M_{max}/R_{bPr}M_y$	$V_{max}/V_{nCooper}$
Mean	1.09	1.13	1.09	1.01
COV	0.05	0.06	0.05	0.04
Maximum	1.18	1.25	1.18	1.06
Minimum	1.00	1.05	1.00	0.97
Median	1.09	1.11	1.09	1.00

The following observations can be gleaned from these high-moment high-shear strength studies:

- On average, the AASHTO model gives the better prediction of the shear controlled tests for $D/t_w = 300$, but the Cooper model gives a slightly better prediction of the shear controlled tests for $D/t_w = 240$ and 200. However, the mean predictions by both models are reasonably good. The AASHTO model has the smaller coefficient of variation (COV) for $D/t_w = 300$ and 240, and the COV ranges from 0.09 to 0.06 for the three categories of web slenderness. Cooper's model has a COV that ranges from 0.12 for $D/t_w = 300$ to 0.04 for $D/t_w = 200$. There does not appear to be any major compelling reason to implement the more involved calculations of Cooper's model.

- Usage of the AASHTO shear resistance model, rather than Cooper's model, results in 5 additional tests becoming moment controlled for the girders with $D/t_w = 300$, and one less test being moment controlled for the girders with $D/t_w = 240$ and 200. For the girders with $D/t_w = 300$ that shift from shear controlled to moment

controlled, the corresponding flexural strength ratio ($M_{max}/R_{bPr}M_y$) is only slightly larger than 0.9. However, this strength ratio is within the scatter band of the results discussed in Section 4.7 for the proposed flexural yield limit state model. Therefore, these lower flexural strength ratios are considered to be acceptable.

- In Chapter 4, the proposed flexural resistance model for the yield limit state is developed based on uniform bending load conditions. It can be concluded from Figures 9-2 to 9-7 that this model may also be used for loading conditions where the flexural capacity is governed by the yield limit state, including combination with high shear loads.

- One can observe, generally, that there is a relatively large dispersion in the shear strength ratios. This dispersion is representative of past observations in research on transversely-stiffened I-girders without longitudinal stiffeners (White and Barker 2008; White et al. 2008).

It should be noted that although Cooper's model idealizes the separate web sub-panels as each developing a separate tension field, this type of behavior is not observed in any of the cases studied in this research. Cooper employed longitudinal stiffeners with larger rigidities than those required by AASHTO provisions for the shear tests. Figure 9-8 shows an example failure mode corresponding to Case 3 with $D/t_w = 300$, $D_c/D = 0.5$ and $D/b_{fc} = 5$. The contours in the figure correspond to the von Mises stresses at the mid-thickness of the plates, and the bright red contours indicate regions that have yielded. One can see that the tension fields essentially run through the longitudinal stiffeners, at least for the minimum size longitudinal stiffeners per AASHTO LRFD employed in this study. Figure 9-9 shows a comparable result, but where the flexural response is more dominant.

Particularly when one of the sub-panels has a small depth compared to its width, it is
unrealistic to assume development of two separate tension fields in the sub-panels.
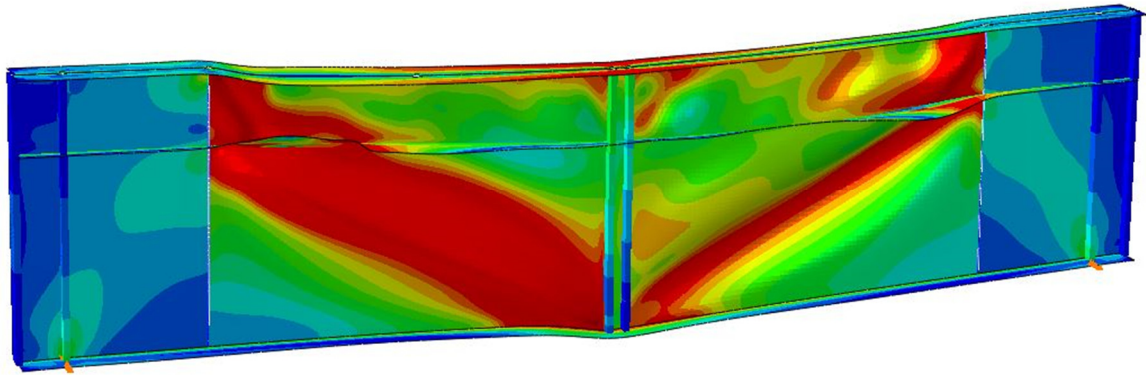
Figure 9-8: Typical failure mode for the high-moment high-shear tests, Case 3 with $D/t_w = 300$, $D_c/D = 0.5$ and $D/b_{fc} = 5$.
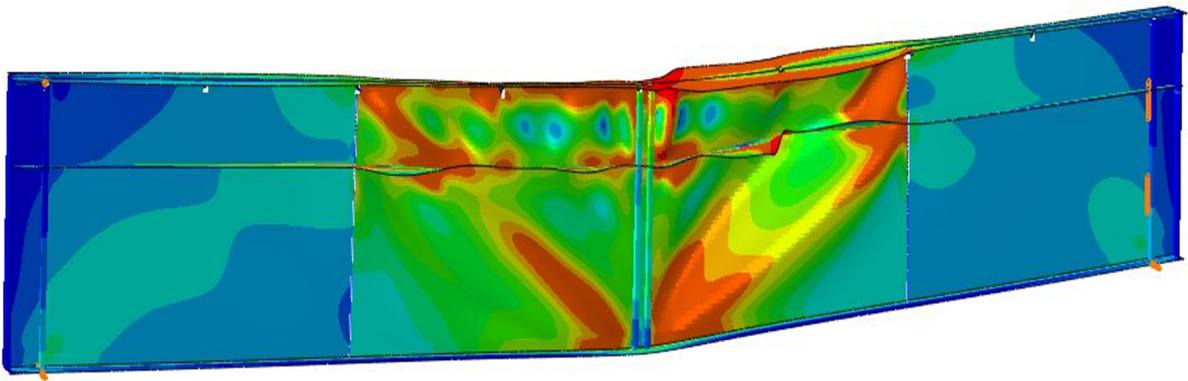
Figure 9-9: Typical failure mode for the high-moment high-shear tests, Case 1 with $D/t_w = 240$, $D_c/D = 0.75$ and $D/b_{fc} = 5$.

9.1.4 Evaluation of Strength Predictions for High-Moment High-Shear Cases with Panel Aspect Ratios Exceeding the Current AASHTO Limits (Cases 5 and 6)

It is of interest to consider whether the proposed models can be extended to girders with panel aspect ratios d_o/D up to 2.0. The proposed model for calculating R_b is independent of the panel aspect ratio, d_o. Hence the moment capacity $R_{bPr}M_y$ calculated for any test girder will remain the same in the event of increasing the panel aspect ratio to 2 (AASHTO currently restricts this value to 1.5). However, the AASHTO shear resistance equations are a function of d_o and the shear capacity of a girder can be expected to decrease with an increase in the panel aspect ratio.

Tables 9-9 and 9-10 compare the FE test simulation strengths for girder tests with d_o/D = 2.0 to the governing strengths from the AASHTO shear resistance model, Cooper's shear resistance model, and the recommended flexural yield strength model. The tests girders consist of two different configurations with different M/V values as indicated in the rows in Table 9-1 corresponding to Cases 5 and 6. Figures 9-10 and 9-11 summarize these results for the girders with D/t_w = 300 for the two respective shear strength models. Figures 9-12 and 9-13 do the same for the girders with D/t_w = 240, and Figures 9-14 and 9-15 show the results for girders with D/t_w = 200.

Table 9-9: Comparison of the test simulation load capacities to the governing strengths from the AASHTO shear resistance model, Cooper's shear resistance model, and the recommended flexural yield strength model for girders with $d_o/D = 2.0$ (Case 5)

D/b_{fc}	D_c/D	$D/t_w = 300$			$D/t_w = 240$			$D/t_w = 200$		
		$V_{max}/V_{nCooper}$	$V_{max}/V_{nAASHTO}$	$M_{max}/R_{bPr}M_y$	$V_{max}/V_{nCooper}$	$V_{max}/V_{nAASHTO}$	$M_{max}/R_{bPr}M_y$	$V_{max}/V_{nCooper}$	$V_{max}/V_{nAASHTO}$	$M_{max}/R_{bPr}M_y$
6	0.5	**1.12***	1.01	1.01	0.94	0.87	**1.03**	0.80	**1.14**	**1.05**
	0.625	0.89	**1.01**	**0.96**	0.76	0.94	**1.03**	0.69	0.85	**1.04**
	0.75	**1.04**	**1.07**	1.00	0.79	0.96	**1.03**	0.66	0.86	**1.03**
5	0.5	**0.97**	**1.13**	0.87	0.92	**1.08**	**1.01**	0.98	0.94	**1.04**
	0.625	**1.00**	**1.13**	0.83	0.91	**1.12**	**0.98**	0.83	**1.02**	**1.02**
	0.75	**1.13**	**1.17**	0.85	0.95	**1.15**	**0.99**	0.80	**1.04**	1.02
4	0.5	**1.03**	**1.21**	0.62	**1.08**	**1.27**	0.81	1.07	**1.25**	0.98
	0.625	**1.06**	**1.20**	0.60	**1.02**	**1.25**	0.77	1.05	**1.29**	0.93
	0.75	**1.23**	**1.27**	0.63	**1.08**	**1.30**	0.79	1.03	**1.34**	0.95

Bolded values are the governing strength ratios given the use of one or both shear resistance models

Table 9-10: Comparison of the test simulation load capacities to the governing strengths from the AASHTO shear resistance model, Cooper's shear resistance model, and the recommended flexural yield strength model for girders with $d_o/D = 2.0$ (Case 6)

D/b_{fc}	D_c/D	$D/t_w = 300$			$D/t_w = 240$			$D/t_w = 200$		
		$V_{max}/V_{nCooper}$	$V_{max}/V_{nAASHTO}$	$M_{max}/R_{bPr}M_y$	$V_{max}/V_{nCooper}$	$V_{max}/V_{nAASHTO}$	$M_{max}/R_{bPr}M_y$	$V_{max}/V_{nCooper}$	$V_{max}/V_{nAASHTO}$	$M_{max}/R_{bPr}M_y$
6	0.5	0.75	0.68	**1.05***	0.62	0.57	**1.04**	0.52	0.74	**1.07**
	0.625	0.62	0.71	**1.03**	0.50	0.62	**1.05**	0.45	0.55	**1.05**
	0.75	0.70	0.72	**1.04**	0.54	0.65	**1.09**	0.44	0.57	**1.06**
5	0.5	0.73	0.86	**1.02**	0.62	0.72	**1.04**	0.64	0.61	**1.05**
	0.625	0.78	0.89	**1.01**	0.62	0.77	**1.04**	0.54	0.67	**1.04**
	0.75	0.91	0.94	**1.05**	0.65	0.78	**1.04**	0.53	0.68	**1.04**
4	0.5	**0.96**	**1.13**	0.90	0.88	**1.03**	**1.02**	0.74	0.86	**1.05**
	0.625	**1.00**	**1.13**	0.88	0.88	**1.08**	**1.03**	0.76	0.94	**1.05**
	0.75	**1.16**	**1.20**	0.92	0.93	**1.12**	**1.05**	0.73	0.95	**1.05**

Bolded values are the governing strength ratios given the use of one or both shear resistance models
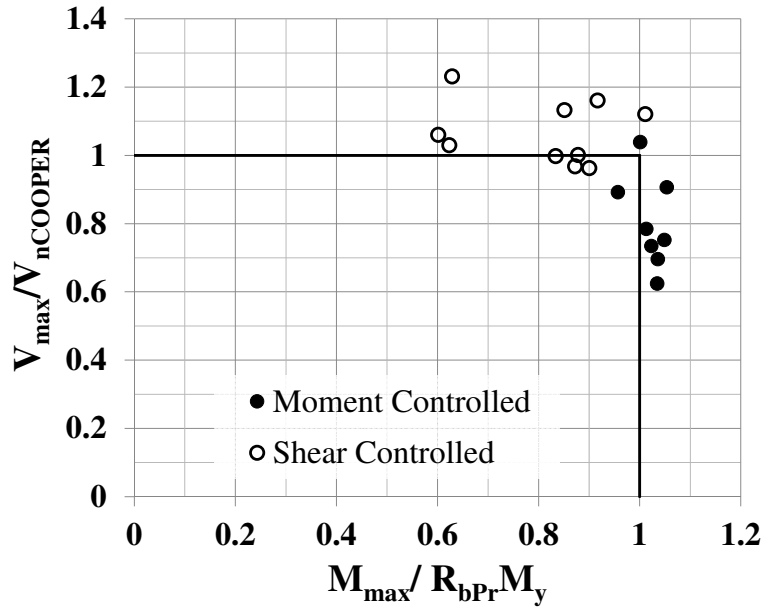
Figure 9-10: $V_{max}/V_{nCooper}$ **versus** $M_{max}/R_{bPr}M_y$ **for high-moment high-shear tests with** $d_o/D = 2$ **and** D/t_w **= 300**
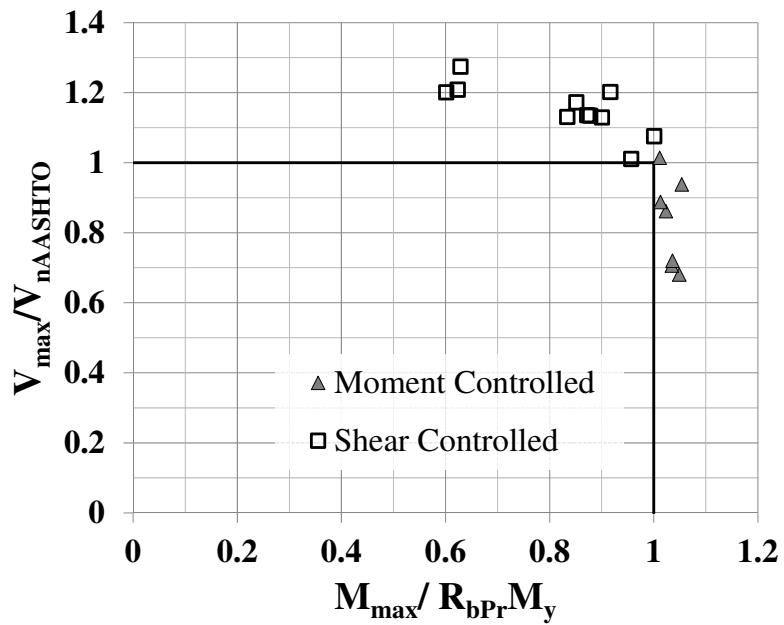
Figure 9-11: $V_{max}/V_{nAASHTO}$ **versus** $M_{max}/R_{bPr}M_y$ **for high-moment high-shear tests with** $d_o/D = 2$ **and** $D/t_w = 300$
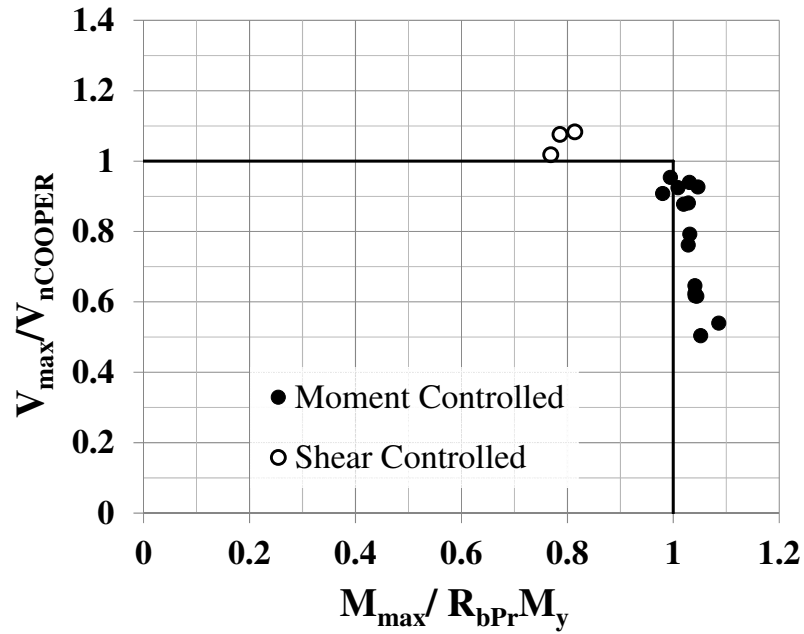
Figure 9-12: $V_{max}/V_{nCooper}$ versus $M_{max}/R_{bPr}M_y$ for high-moment high-shear tests with $d_o/D = 2$ and D/t_w $= 240$
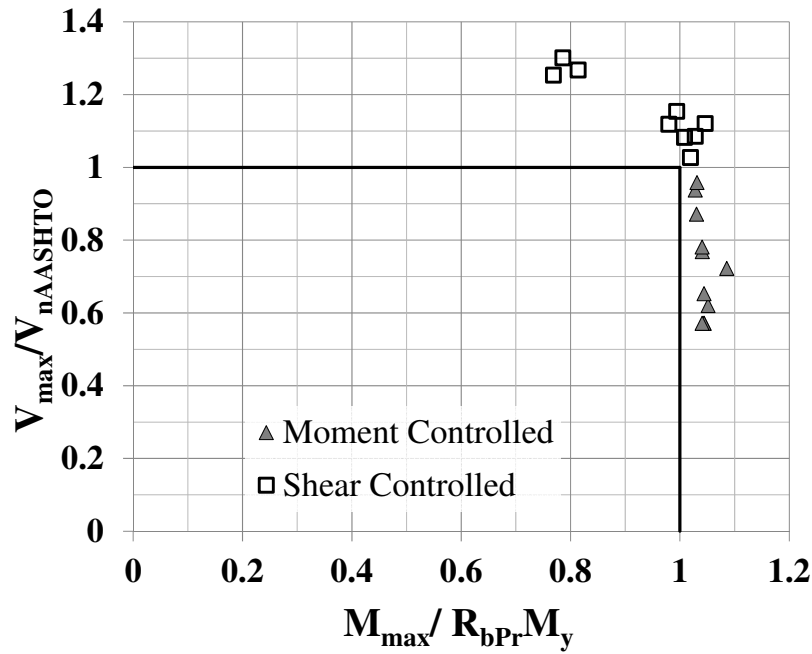
Figure 9-13: $V_{max}/V_{nAASHTO}$ versus $M_{max}/R_{bPr}M_y$ for high-moment high-shear tests with $d_o/D = 2$ and $D/t_w = 240$
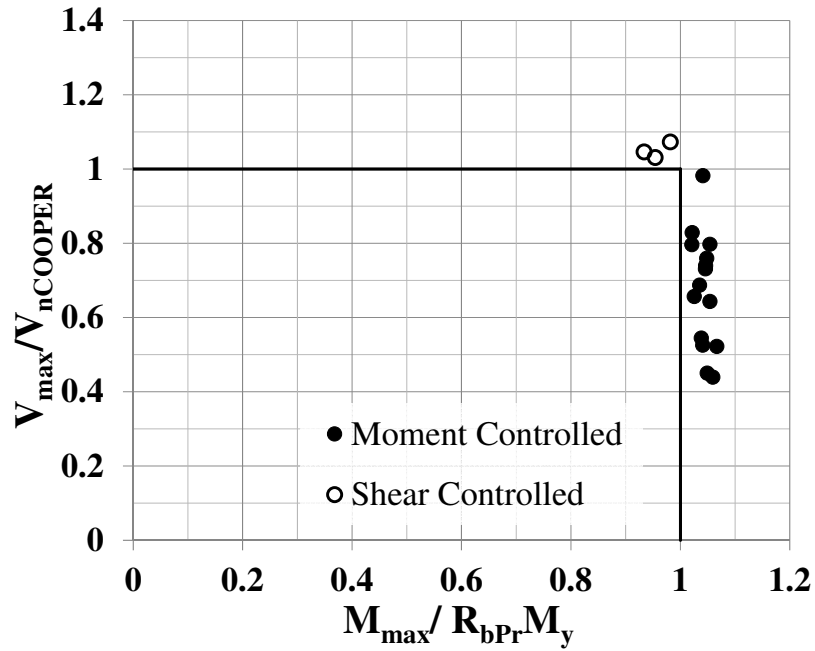
Figure 9-14: *V_max*/*V_nCooper* versus *M_max*/*R_bPr*M_y* for high-moment high-shear tests with *d_o*/D = 2 and *D*/*t_w* = 200
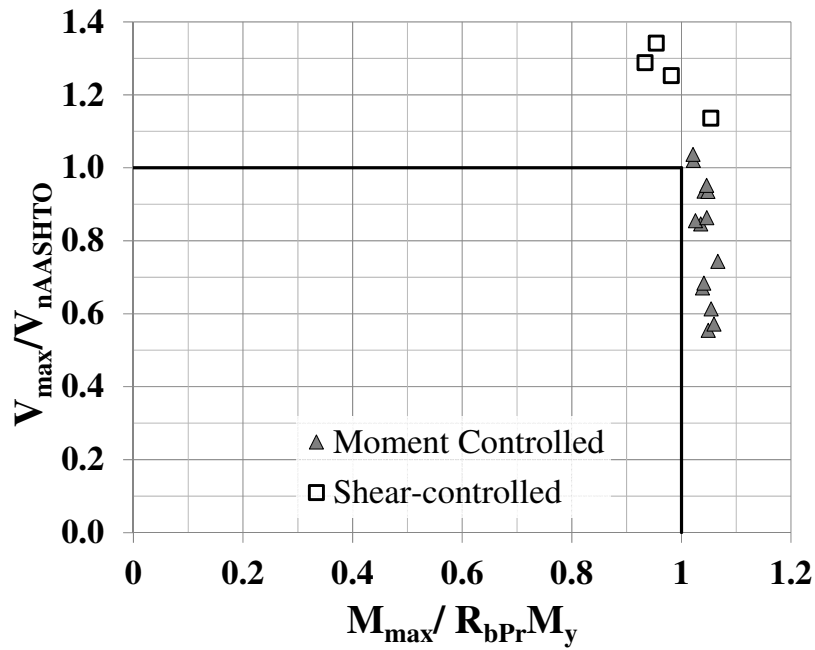
Figure 9-15: *V_max*/*V_nAASHTO* versus *M_max*/*R_bPr*M_y* for high-moment high-shear tests with *d_o*/D = 2 and *D*/*t_w* = 200

Tables 9-11 through 9-13 provide the statistics for the governing strength ratios in the above plots. The following observations can be made from these tests:

- Unlike the behavior in Cases 1 through 4, on average, Cooper's model gives the better prediction of the shear controlled tests for girders of all web slenderness ratios for $d_o/D = 2.0$, while the AASHTO equations are conservative. However, the mean predictions by both models are reasonably good. The AASHTO model has the smaller coefficient of variation (COV) for $D/t_w = 300$, and the COV varies from 0.07 ($D/t_w = 300$) to 0.10 ($D/t_w = 200$). Cooper's model has a COV that ranges from 0.08 for $D/t_w = 300$ to 0.02 for $D/t_w = 200$. Like before, the prediction of shear capacity by Cooper's model improves with lower web slenderness ratios.

- Usage of the AASHTO shear resistance model, rather than Cooper's model, results in six fewer tests becoming moment controlled for the girders with $D/t_w = 240$, and two less tests being moment controlled for the girders with $D/t_w = 200$. No shifting in the predicted type of failure occurs for $D/t_w = 300$. For the girders with $D/t_w = 240$ that shift from moment controlled to shear controlled, the data points fall outside the block, which indicate the conservative nature of the AASHTO shear resistance equations.

- It can be concluded from Figures 9-10 to 9-15 that the prediction model proposed in Section 4.7 may be used also for girders with panel aspect ratio of 2, which is larger than the current AASHTO limit of 1.5, in loading conditions where the flexural capacity is governed by the yield limit state, including combination with high shear loads.

Table 9-11: Statistics for AASHTO and Cooper shear prediction models for $D/t_w = 300$ and $d_o/D = 2$ (Cases 5 and 6)

Statistical Parameter	AASHTO		Cooper	
	Moment Controlled (6 tests)	Shear Controlled (12 tests)	Moment Controlled (7 tests)	Shear Controlled (11 tests)
	$M_{max}/R_{bPr}M_y$	$V_{max}/V_{nAASHTO}$	$M_{max}/R_{bPr}M_y$	$V_{max}/V_{nCooper}$
Mean	1.03	1.14	1.02	1.06
COV	0.01	0.07	0.03	0.08
Maximum	1.05	1.27	1.05	1.23
Minimum	1.01	1.01	0.96	0.96
Median	1.04	1.13	1.03	1.04

Table 9-12: Statistics for AASHTO and Cooper shear prediction models for $D/t_w = 240$ and $d_o/D = 2$ (Cases 5 and 6)

Statistical Parameter	AASHTO		Cooper	
	Moment Controlled (9 tests)	Shear Controlled (9 tests)	Moment Controlled (15 tests)	Shear Controlled (3 tests)
	$M_{max}/R_{bPr}M_y$	$V_{max}/V_{nAASHTO}$	$M_{max}/R_{bPr}M_y$	$V_{max}/V_{nCooper}$
Mean	1.04	1.16	1.03	1.06
COV	0.02	0.08	0.02	0.03
Maximum	1.09	1.30	1.09	1.08
Minimum	1.03	1.03	0.98	1.02
Median	1.04	1.12	1.03	1.08

Table 9-13: Statistics for AASHTO and Cooper shear prediction models for $D/t_w = 200$ and $d_o/D = 2$ (Cases 5 and 6)

Statistical Parameter	AASHTO		Cooper	
	Moment Controlled (13 tests)	Shear Controlled (5 tests)	Moment Controlled (15 tests)	Shear Controlled (3 tests)
	$M_{max}/R_{bPr}M_y$	$V_{max}/V_{nAASHTO}$	$M_{max}/R_{bPr}M_y$	$V_{max}/V_{nCooper}$
Mean	1.04	1.21	1.04	1.05
COV	0.01	0.10	0.01	0.02
Maximum	1.07	1.34	1.07	1.07
Minimum	1.02	1.04	1.02	1.03
Median	1.05	1.25	1.05	1.05

9.2 Moment Gradient Studies with Flexure Controlled by LTB Limit State

In this section, the behavior of longitudinally stiffened girders under moment gradient when the flexure limit state is controlled by LTB is studied.

9.2.1 Test Setup

It is shown in Chapter 8 that the proposed LTB model is adequate or conservative in predicting the test simulation strengths for uniform bending depending on the magnitude of initial geometric imperfections used. It is also shown in Chapter 7 for unstiffened girders that linear moment gradient with the ratio of end moment = 0.5, and $C_b = 1.3$ has low shear, and that the proposed LTB model predicts FE test data very well, with negligible moment-shear interaction. It is also demonstrated in Chapter 7 that moment-shear interaction begins to influence the girder flexural resistance for slender web girders with high shear. In view of the above observations, longitudinally stiffened girders are studied in this section for linear moment diagrams with no moment at one end, and an applied moment at the other, i.e. $\beta = 0$ in Figure 7-1, and $C_b = 1.75$.

The test setup is a longitudinally stiffened girder with fork boundary conditions as shown in Figure 7-1. There are no intermediate lateral braces. A small number of uniform bending studies on longitudinally stiffened girders with fork boundary conditions are first conducted to establish that the results concur with those obtained from the test setup with end fixtures for equivalent effective unbraced lengths in Chapter 4. The test setup with fork boundary conditions is chosen for its ease of modeling. Moment gradient cases with transverse loading are not considered.

9.2.2 Case Studies

It is shown in the studies in Section 9.1, and subsequently in this section that the current AASHTO LRFD shear resistance equations are sufficient in predicting the shear capacities of longitudinally stiffened girders. The objective of this study is to assess behavior of girders under high-moment high-shear, and potential M-V interaction. It is observed that wider flanges result in increasing the LTB strengths such that shear is the controlling limit state even at long unbraced lengths. Hence, only slender web girders with narrow flanges are chosen for this study.

Six girders with panel aspect ratio, $d_o/D = 1$, $d_s/D_c = 0.4$, and unbraced lengths shown in Table 9-14 are chosen for the moment gradient studies. The girder parameters are as follows:

- $D/t_w = 300, 240$
- $D/b_{fc} = 6$
- $D_c/D = 0.5, 0.625, 0.75$
- $t_{fc} = 1.5$

Table 9-14: Case studies for longitudinally stiffened girders subjected to moment gradient

Case	L_b (in) $d_o/D = 1$
1	450
2	600
3	750
4	900
5	1050

9.2.3 Results for Moment Gradient Studies at LTB Limit State

Figures 9-16 through 9-21 show plots that compare the current and proposed LTB resistance equations along with the FE test simulation strengths. V_{max} is the ratio of the shear capacity obtained in the FE test simulation to the AASHTO shear strength. V_n is the design shear strength of the girder as per the AASHTO shear resistance equations. The data points representing flexure controlled and shear controlled tests are indicated clearly in the figures. For example, in Figure 9-16, the first two data points are shear controlled, and the last three data points are flexure controlled.
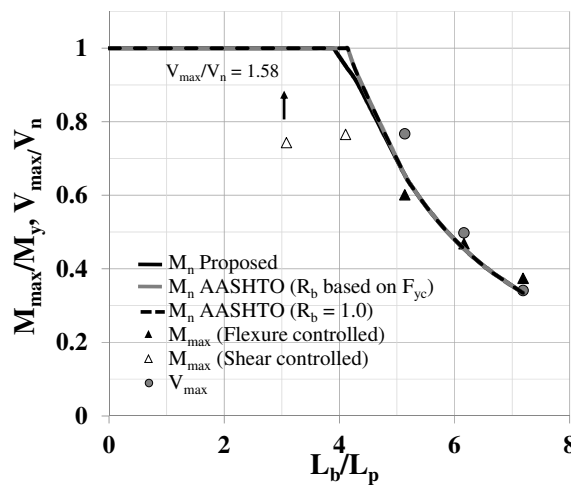
Figure 9-16: LTB curves for linear moment diagram with $C_b = 1.75$, $D/t_w = 240$, $D/b_{fc} = 6$, $D_c/D = 0.5$
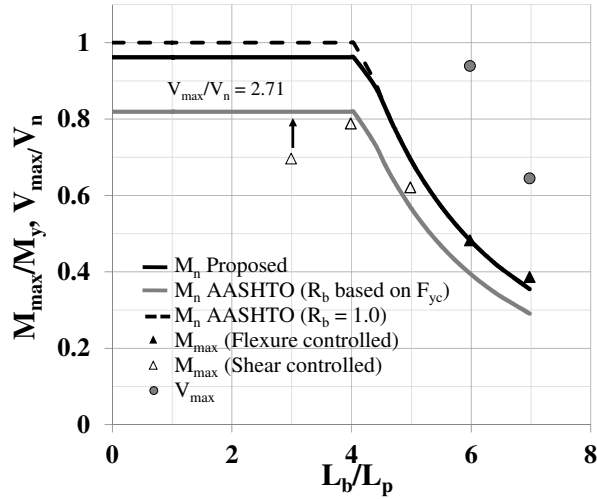
Figure 9-17: LTB curves for linear moment diagram with C_b = 1.75, D/t_w = 300, D/b_{fc} =6, D_c/D = 0.5
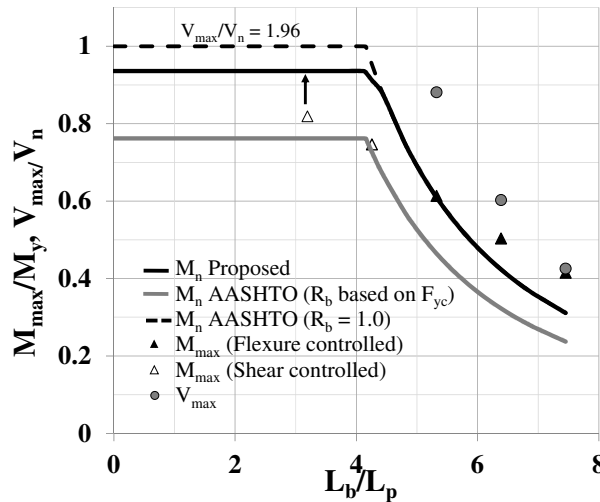
Figure 9-18: LTB curves for linear moment diagram with C_b = 1.75, D/t_w = 240, D/b_{fc} =6, D_c/D = 0.625
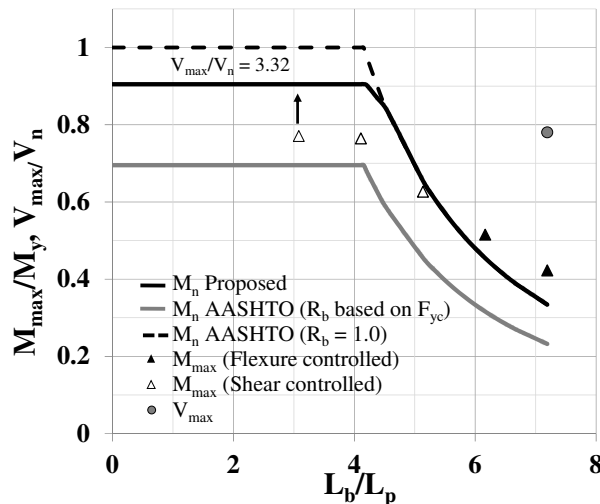
Figure 9-19: LTB curves for linear moment diagram with C_b = 1.75, D/t_w = 300, D/b_{fc} =6, D_c/D = 0.625

224
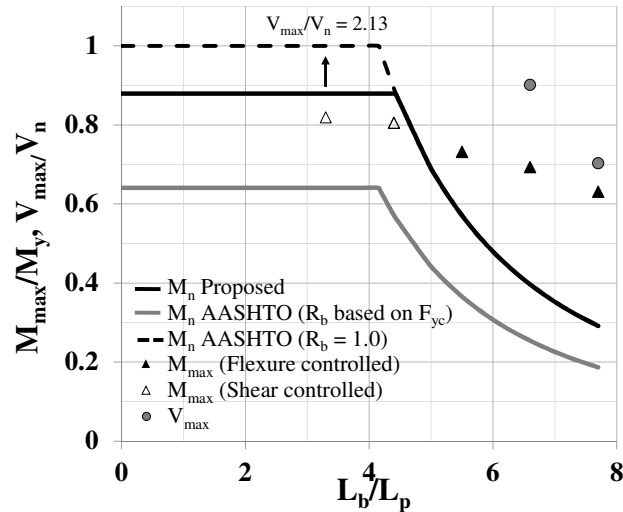
Figure 9-20: LTB curves for linear moment diagram with $C_b = 1.75$, $D/t_w = 240$, $D/b_{fc} = 6$, $D_c/D = 0.75$
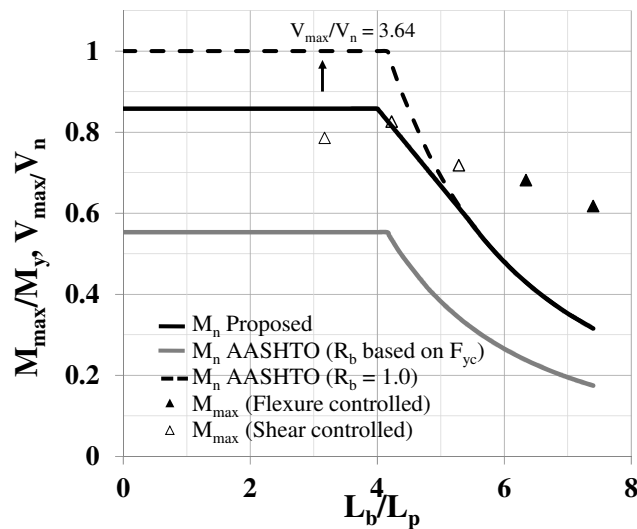
Figure 9-21: LTB curves for linear moment diagram with $C_b = 1.75$, $D/t_w = 300$, $D/b_{fc} = 6$, $D_c/D = 0.75$

The following can be gleaned from the above figures.

1. The shear capacities attained by the longitudinally stiffened girders equal or exceed the theoretical shear capacity as per AASHTO shear equations. The data points for V_{max} for some of the shorter unbraced lengths are not shown on the above plots because they are in the order of 1.6 to 3 times V_n *AASHTO*. The shear capacities in the earlier part of the chapter are not as large where the moment gradient within the critical unbraced length is much smaller. This suggests that in the presence of steep

moment gradients, there is higher postbuckling shear capacity in longitudinally stiffened girders. This precludes any potential moment–shear interaction.

2. In case of flexure controlled tests, it is evident that the trends observed are consistent with those reported in Section 8.4. The LTB strengths of the proposed model give excellent correlation with FE test data for doubly-symmetric girders (Figures 9-16 and 9-17), while tending to be increasingly conservative for singly-symmetric cross-sections with increasing web depths in compression (Figures 9-18 through 9-21). As explained in Section 8.4.2, this is largely due to the resistance equations discounting contribution from the St.Venant torsional resistance, which is higher for girders with larger tension flanges (larger D_c).

3. It is observed that the proposed LTB equation for longitudinally stiffened girders which use the full elastic LTB strength of the cross-section (neglecting J), with R_b = 1.0 for longer unbraced lengths is a good estimate even when the strengths are multiplied by C_b.

4. It is observed, as in the case of the LTB studies under uniform bending in Chapter 8 that the current AASHTO resistance equation is overly conservative despite the magnification factor (C_b) of 1.75 on the design moment resistance. This stems from the poor prediction of R_b for longitudinally stiffened girders in the current Specifications.

9.3 Summary

The following are the key conclusions from the work presented in this chapter.

1. The AASHTO shear equations are adequate or conservative in predicting the shear resistance of longitudinally stiffened girders. Although the proposed R_b model

increases the bending capacity of the girder, it does not cause moment-shear interaction. This is established via combined bending and shear studies with flexure controlled by the yield limit state, as well as the LTB limit state.

2. It is shown that the maximum allowable transverse stiffener spacing can be increased to at least 2.0D from the current limit of 1.5D.

3. It appears from the results presented in Section 9.2.3 that the inelastic LTB region is virtually indistinguishable except in the case of extremely singly-symmetric cross-sections (E.g. $D_c/D = 0.75$, $D/t_w = 300$), and hence the proposed LTB model for longitudinally stiffened girders in Section 8.3 with regard to the interpolation in the inelastic LTB region does not come into play. However, bridge girders are often designed where situations with "near uniform moment" may be encountered. In such cases, the proposed LTB model provides better strength predictions, i.e. it is beneficial to incorporate the modified form of the LTB equations for longitudinally stiffened girders in Section 8.3, as well as use the proposed R_b model.

CHAPTER 10

FLEXURAL RESISTANCE OF HYBRID LONGITUDINALLY

STIFFENED GIRDERS

In this chapter, the proposed R_b model for homogenous girders is expanded in scope to allow the calculation of R_b for hybrid girders. Hybrid girders refer to girders with lower strength web plates than the compression flange. These studies are restricted to girders with longitudinal stiffeners of the same strength as the web plates.

The early yielding of the web and stiffener raises the question as to whether the longitudinal stiffener column can continue to carry stresses until the compression flange begins to yield. It is demonstrated in Section 6.7 that early yielding of the web does not significantly affect the lateral stability of the compression flange. It is also validated in Chapter 5 that using the proposed R_b model in conjunction with the current FLB equations in the Specifications is adequate and usually conservative. Hence the studies in this chapter are limited to two objectives. The first goal is to ensure that the R_b model for homogenous girders can be extended to hybrid girders without loss of generality. In doing so, the extended model functions as a combined model for R_h and R_b, i.e. it simultaneously captures the effects of web postbuckling and the different yield strengths of the flange and web plates. The shear strength of the girder is principally derived from the web, which has a lower yield strength than the flange, and hence theoretically the same shear strength as an equivalent homogenous girder. The flexural capacity from the combined model for R_h and R_b is however increased with respect to the current AASHTO equations. Thus evaluating potential moment-shear strength interaction constitutes the second aim of this

228

chapter. The recommended increased transverse stiffener spacing to $2.0D$ in Section 9.1.4 is also evaluated for hybrid girders.

10.1 AASHTO Provisions for Hybrid Girders

The provisions for longitudinal stiffener are listed in Section 2.8. The minimum rigidity requirements are not a function of the longitudinal stiffener yield strength F_{ys}. The slenderness limit of the stiffener (b_l/t_s) is a function of F_{ys} but is not influenced by the different yield strengths of the stiffener and the compression flange. The AASHTO minimum radius of gyration, r, is however greatly increased for girders with lower stiffener yield strength than the compression flange. It is worthwhile to note that in the studies on homogenous girders, the requirement on r seldom controls, and it is typically the stiffness requirement, I_l that controls the longitudinal stiffener design.

Also, as explained in Section 6.7, the plateau strength is calculated as $R_bR_hF_{yc}$, where R_h is the hybrid factor, calculated as per AASHTO Equation 6.10.1.10.1.

10.2 Uniform Bending Tests on Hybrid Longitudinally Stiffened Girders

10.2.1 FE Modeling

The test setup for uniform bending is the same as that used for homogenous girders, shown in Figure 4-1. The flanges of the girder have yield strengths of 70 ksi, while the web, longitudinal and transverse stiffeners have yield strengths of 50 ksi. The geometric imperfections and residual stresses are the same as those used in Chapter 4 for homogenous girders.

10.2.2 Case Studies

The eight cases defined in Table 10-1 are assessed as part of the parametric studies. Each case corresponds to a specific web panel aspect ratio (d_o/D), and a specific ratio of the depth of the longitudinal stiffener relative to the depth of the web in compression (d_s/D_c). As in Chapter 4, the parameters D_c/D, D/t_w, and b_{fc} and t_{fc} are varied as follows for each of the cases:

- D_c/D = 0.5, 0.625 and 0.75,

- D/t_w = 200, 240 and 300, and

- b_{fc} = $D/6$, $D/5$ and $D/4$.

- t_{fc} = 1.75, 2.0, and 2.5 corresponding to different values of b_{fc}.

Table 10-1: Case studies for straight hybrid girders at yield limit state

Case	d_o/D	Longitudinal Stiffener	d_s/D_c
1	1	AASHTO min	0.40
2	1.5	AASHTO min	0.40
2a	1.5	AASHTO min for Homogenous Girders	0.40
3*	1.0	AASHTO min	0.27
4*	1.0	AASHTO min	0.53
5	2	AASHTO min	0.40
6*	2	AASHTO min	0.27
7*	2	AASHTO min	0.53

. Only girders with D/t_w =300 are studied in these cases

Seven cases with three different panel aspect ratios, 1.0, 1.5 and 2.0 are studied. Selected studies are also performed for different stiffener positions through the web depth for panel aspect ratios 1.0 and 2.0. In these cases (Cases 3, 4, 6 and 7), only girders with D/t_w = 300 are studied. These studies are aimed at ensuring that the behavior of the girders

at ultimate load and the recommended provisions remain applicable for various positions of the longitudinal stiffener.

Case 2 is studied twice, once with the minimum size stiffeners as per the requirement when $F_{ys} < F_{yc}$, and a second time, for stiffeners sized as per $F_{ys} = F_{yc} = 50$ ksi, i.e the same stiffeners used in Case 2 of Table 4-1. The Case 2a study is designed in order to evaluate the validity of the stringent requirements on the radius of gyration of the longitudinal stiffener column for girders with $F_{ys} < F_{yc}$, and the repercussions of designing the stiffeners by treating the girder as if it were homogenous. The longitudinal stiffeners of Case 2 are approximately 2.75 times stiffer than the ones in Case 2a. The stiffeners in Case 2a do not meet the "r" requirement in AASHTO Specifications.

It must be noted that the penalty on radius of gyration for such girders result in disproportionately large longitudinal stiffeners for larger panel aspect ratios. For example, for a girder with $d_o/D = 2$, $D/t_w = 300$, the stiffener size required is 16.5 x 1.45 inches in order to satisfy the AASHTO provisions for stiffener sizing. The width of this longitudinal stiffener is equal to or greater than the projecting compression flange width in most reasonably proportioned girders. In such instances, it may be more economical to use thicker webs and reduce the transverse stiffener spacing. However, these results are included here for the purpose of discussion.

A total of 117 girders are studied for uniform bending of hybrid longitudinally stiffened girders.

10.2.3 Results

This section discusses the results obtained from the uniform bending studies on hybrid girders.

10.2.3.1 Evaluation of the requirement on radius of gyration limit for $F_{ys} < F_{yc}$

The results for Case 2 and Case 2a are presented in Table 10-2. It is evident that the strengths obtained by the girders with the more rigid stiffeners in Case 2 are 1 to 7% higher than the equivalent girders in Case 2a.

However, the primary reason behind the radius of gyration requirement is to prevent the premature flexural buckling of the longitudinal stiffener column, i.e. to prevent lateral displacement of the web at construction loads and service load conditions. Figure 10-1 shows the load vs displacement for two girders at the mid-span of the member at the location of the longitudinal stiffener.

Table 10-2: Comparison of R_{bFEA} for Case 2 vs. Case 2a

b_{fc}	D_c/D	$D/t_w = 300$		$D/t_w = 240$		$D/t_w = 200$	
		Case 2	Case 2a	Case 2	Case 2a	Case 2	Case 2a
	0.5	0.91	0.86	0.92	0.91	0.94	0.94
D/6	0.625	0.87	0.81	0.90	0.84	0.92	0.88
	0.75	0.84	0.77	0.84	0.79	0.88	0.82
	0.5	0.97	0.90	0.93	0.93	0.93	0.95
D/5	0.625	0.88	0.86	0.92	0.88	0.94	0.89
	0.75	0.86	0.82	0.87	0.82	0.89	0.84
	0.5	0.99	0.93	0.95	0.93	0.94	0.96
D/4	0.625	0.92	0.90	0.92	0.91	0.96	0.92
	0.75	0.91	0.87	0.91	0.87	0.93	0.88
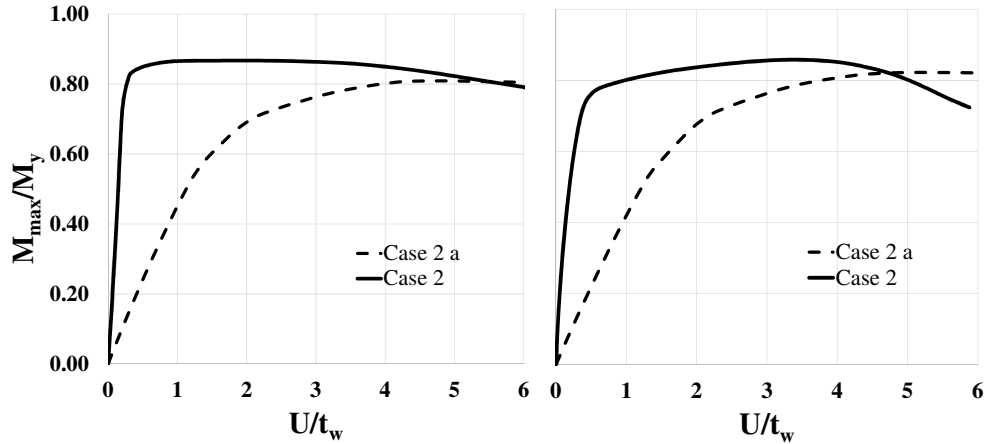
Figure 10-1: Normalized lateral web displacement at location of longitudinal stiffener versus M/M_y for Cases 2 and 2a for $D/t_w = 300$ and $D_c/D = 0.625$, $D/b_{fc} = 6$ (left), $D_c/D = 0.75$, $D/b_{fc} = 5$ (right)

From the above figure, it is evident that ignoring the lower yield strength of the longitudinal stiffener as compared to the yield strength of the compression flange does not provide acceptable displacement control even at lower load levels. The load-deflection responses for other girders are similar in nature. It is also observed from the load-deflection responses in Figure 10-1 that the minimum stiffener size that satisfies the criteria for "r" holds a near zero line of lateral deflection at the location of the stiffener almost up to the point of ultimate load, and that the deflections increase rapidly beyond this point. It is reasonable to conclude based on these limited studies that the AASHTO requirement for the radius of gyration (Equation 6.10.11.3.3-2), which penalizes the stiffness requirement on lower strength stiffeners, is justified albeit conservative.

10.2.3.2 Impact of girder panel aspect ratio and stiffener rigidity on girder strength

It is established from Table 10-2 and Figure 10-1 that the capacity of the girder increases by as much as 7% when a stiffener of three times the rigidity is used. It is concluded in Section 4.6.4 that the panel aspect ratio, d_o/D does not directly influence the girder strength. However the lateral stiffness requirement of the longitudinal stiffener column increases directly as a function of d_o/D. Hence, larger values of d_o/D requires the

233

use of more rigid stiffeners. Table 10-3 shows the results for Cases 1, 2, and 5 which have increasing stiffener rigidity.

The results for doubly-symmetric girders for $d_o/D = 2$ (Case 5) are omitted because of unreliable FE test data, where convergence issues are encountered. FE simulations for these cases with large stiffener sizes for the larger values of d_o/D have convergence issues because the stiffener is much more rigid in the lateral direction than the adjoining web, and there is difficulty in developing the required stress levels in the longitudinal stiffener column. It is observed from the results presented in Table 10-3 that increasing stiffener rigidity results in an increase in the girder strength, as in the case of homogenous girders discussed in Section 4.6.5.

$R_{bAASHTO}$ is independent of d_o/D and longitudinal stiffener dimensions, and is the same for all three cases for a given girder cross-section. It is interesting to observe that, where AASHTO predicts an R_b of 1 for doubly-symmetric girders with D/t_w of 200, and the stiffener located at the optimum position for flexure ($d_s/D_c = 0.4$), the FE test data predicts strengths which are 5 to 8% lower. In contrast, FE test simulations of homogenous girders with the same girder dimensions, achieve higher strengths than the yield moment of the girders. This is because M_y for the hybrid girders in the definition for R_{bFEA} (M_{max}/M_y) is taken as $S_{xc}F_{yc}$, although the web plate has a lower yield strength. $R_{bAASHTO}$ is less than 1.0 for alternate stiffener positions ($d_s/D_c = 0.27, 0.53$) for the same girder and stiffener dimensions.

Table 10-3: Comparison of R_{bFEA} and $R_{bAASHTO}$ for Cases 1, 2 and 5

(a) $D/t_w = 300$

b_{fc}	D_c/D	R_{bFEA}			$R_{bAASHTO}$
		Case 1	Case 2	Case 5	
	0.5	0.89	0.91	-	0.82
D/6	0.625	0.83	0.87	0.90	0.70
	0.75	0.78	0.84	0.86	0.57
	0.5	0.92	0.97	-	0.85
D/5	0.625	0.87	0.88	0.91	0.76
	0.75	0.83	0.86	0.87	0.64
	0.5	0.94	0.99	-	0.90
D/4	0.625	0.91	0.92	0.93	0.83
	0.75	0.88	0.91	0.90	0.74

(b) $D/t_w = 240$

b_{fc}	D_c/D	R_{bFEA}			$R_{bAASHTO}$
		Case 1	Case 2	Case 5	
	0.5	0.89	0.92	-	0.86
D/6	0.625	0.82	0.90	0.93	0.75
	0.75	0.77	0.84	0.86	0.64
	0.5	0.91	0.93	-	0.88
D/5	0.625	0.86	0.92	0.94	0.80
	0.75	0.81	0.87	0.87	0.70
	0.5	0.94	0.95	-	0.92
D/4	0.625	0.90	0.92	0.95	0.85
	0.75	0.87	0.91	0.92	0.78

(c) $D/t_w = 200$

b_{fc}	D_c/D	R_{bFEA}			$R_{bAASHTO}$
		Case 1	Case 2	Case 5	
	0.5	0.92	0.94	-	1.00
D/6	0.625	0.83	0.92	0.93	0.80
	0.75	0.78	0.88	0.88	0.70
	0.5	0.93	0.93	-	1.00
D/5	0.625	0.86	0.94	0.93	0.83
	0.75	0.81	0.89	0.89	0.75
	0.5	0.95	0.94	-	1.00
D/4	0.625	0.90	0.96	0.94	0.88
	0.75	0.86	0.93	0.90	0.81

10.2.3.3 Impact of longitudinal stiffener position through the web depth

The impact of the location of the longitudinal stiffener through the web depth is discussed in Section 4.6.6 for homogenous girders. As before, the impact of the stiffener position through the web depth on the girder strength is negligible for hybrid girders. The strength only marginally increases for girders with lower positions of the stiffener. The girders continue to take load until the longitudinal stiffener column develops stresses significant enough to cause its failure. Hence, a lower position of the stiffener delays the formation of these stresses due to lower major axis stresses and smaller lateral deformations.

Tables 10-4 and 10-5 show the comparisons for cases with $d_o/D = 1$ and 2 with stiffeners placed at the optimum location, and above and below this location for girders with $D/t_w = 300$.

Table 10-4: Comparison of R_{bFEA} for Cases 1, 3 and 4 for girders with $D/t_w = 300$

b_{fc}	D_c/D	R_{bFEA}		
		Case 1	Case 3	Case 4
	0.5	0.89	0.89	0.91
$D/6$	0.625	0.83	0.82	0.86
	0.75	0.78	0.78	0.81
	0.5	0.92	0.92	0.93
$D/5$	0.625	0.87	0.85	0.89
	0.75	0.83	0.82	0.88
	0.5	0.94	0.93	0.96
$D/4$	0.625	0.91	0.90	0.94
	0.75	0.88	0.88	0.89

Table 10-5: Comparison of R_{bFEA} and $R_{bAASHTO}$ for Cases 5, 6 and 7 for girders with $D/t_w = 300$

b_{fc}	D_c/D	R_{bFEA}		
		Case 5	Case 6	Case 7
D/6	0.625	0.90	0.84	0.90
	0.75	0.86	0.84	0.86
D/5	0.625	0.91	0.90	0.95
	0.75	0.87	-	0.89
D/4	0.625	0.93	0.90	0.95
	0.75	0.90	-	0.92

10.3 Proposed Model for Evaluating Postbuckling resistance of Hybrid Longitudinally Stiffened Girders

It is observed that the stress distribution patterns and the failure modes observed for hybrid girders are similar to those of homogenous longitudinally stiffened girders. Figure 10-2 shows a typical test specimen of hybrid longitudinally stiffened girders at failure. The lightly shaded regions indicate portions of the girder that have yielded. It can be seen that the compression flange and the region around the stiffener and the web have yielded. There may or may not be yielding in the tension portion of the cross-section. This is similar in nature to the failure mode in Figure 4-2.
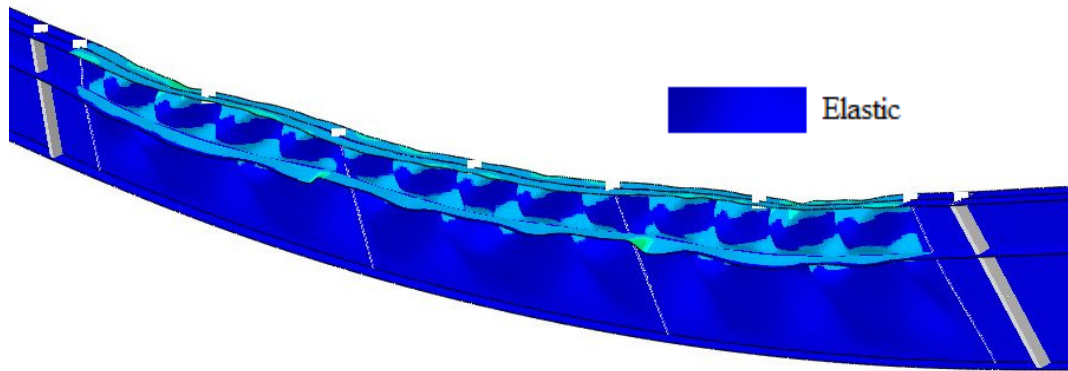
Figure 10-2: Typical failure mode of hybrid longitudinally stiffened girder

Figure 10-3 shows the average normal stresses through the mid-thickness of the hybrid girder web for girders with $D/t_w = 300$, Case1. Other girders for other cases possess similar stress distributions at failure. Again, as in Figure 4-11, the stress distributions are nearly identical for different flange widths, but differ in nature for different web depths in compression. It is observed that the neutral axis has shifted very little from the elastic neutral axis of the cross-section including the stiffener area.
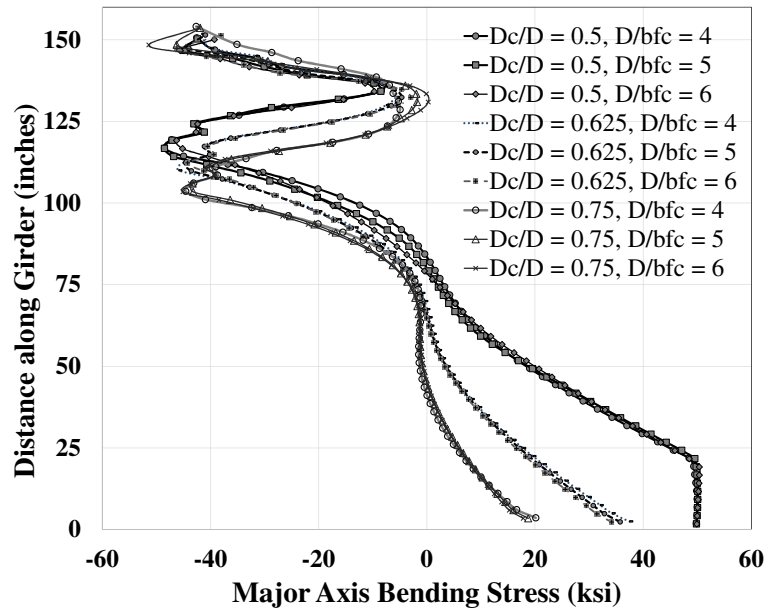
Figure 10-3: Major axis bending stresses in the web, girders with $D/t_w = 300$

Furthermore, it is observed in all cases that the compression flange stress at failure is 70 ksi which is the yield stress of the flange plate (not shown in figure). Figure 10-2 indicates yielding in the compression flange. Based on these observations, the proposed model in Section 4.7 is expanded to hybrid girders as shown in Figure 10-4.
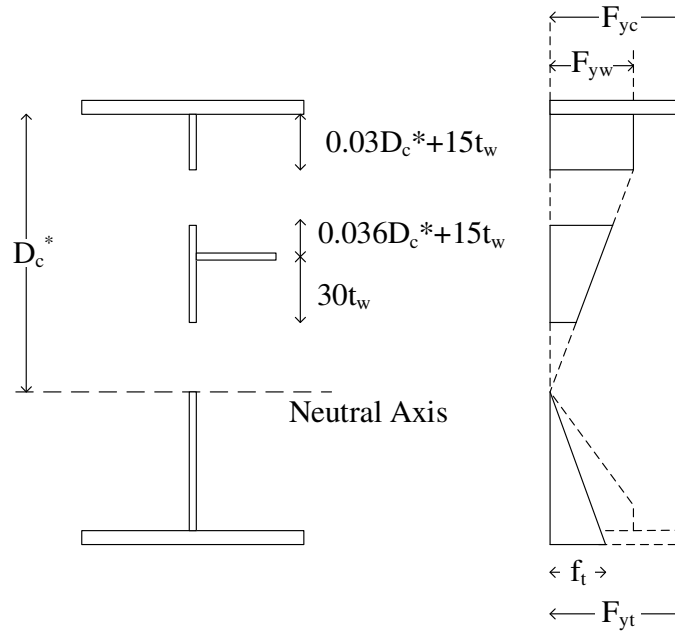
Figure 10-4: Proposed cross section model and stress distribution for hybrid girders

The cross-section model shown above for hybrid girders is essentially the same as that shown in Figure 4-10 for homogenous girders. The effective cross-section widths are the same as in homogenous girders. This figure recognizes that F_{yc} and F_{yt} are greater than F_{yw}. The neutral axis is located based on equilibrium and strain compatibility. The extreme tension stresses in the cross-section may or may not be at yield depending on the cross-section dimensions. As shown in Figure 10-3, the extreme tension stresses tend to be smaller as the web depth in compression becomes larger.

Figure 10-5 compares the moment capacities obtained in the FE test simulations to the proposed and AASHTO strength predictions. $M_{nAASHTO}$ is calculated as $R_b R_h M_{yc}$, where as $M_{nProposed}$ is calculated as $R_b P_r M_{yc}$, where R_{bPr} is calculated as per Figure 10-4.The R_{bPr} for hybrid girders is a combined load shedding and hybrid factor.

It is observed from Figure 10-5 that the proposed model predicts the simulation data with great accuracy. The greatest discrepancy with AASHTO model is for singly-

symmetric cross-sections with large web depths in compression. However, even for doubly-symmetric cross-sections with $D/t_w = 300$, the savings from using the proposed model can be as high as 20% for $d_o/D = 1$. These savings will be higher when more rigid stiffeners are used, or for larger d_o/D.
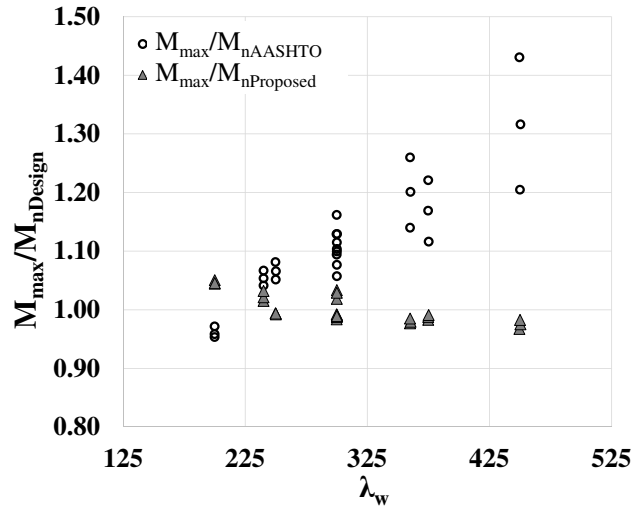
(a) Case 1
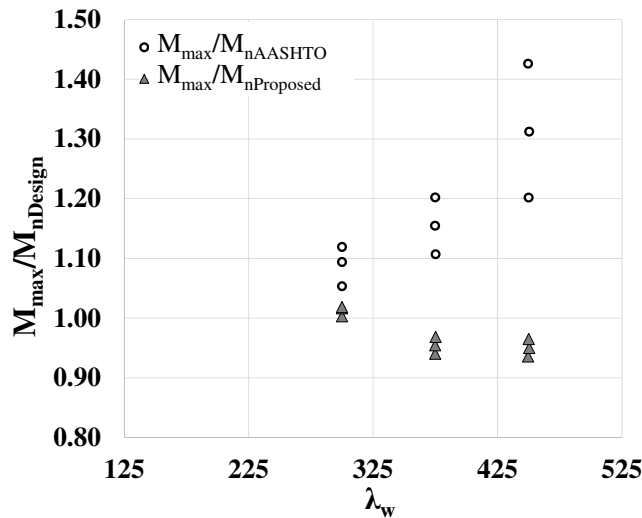
(b) Case 3

Figure 10-5: Comparison of $M_{nProposed}$ with $M_{nAASHTO}$ for Cases 1, 3 and 4

240
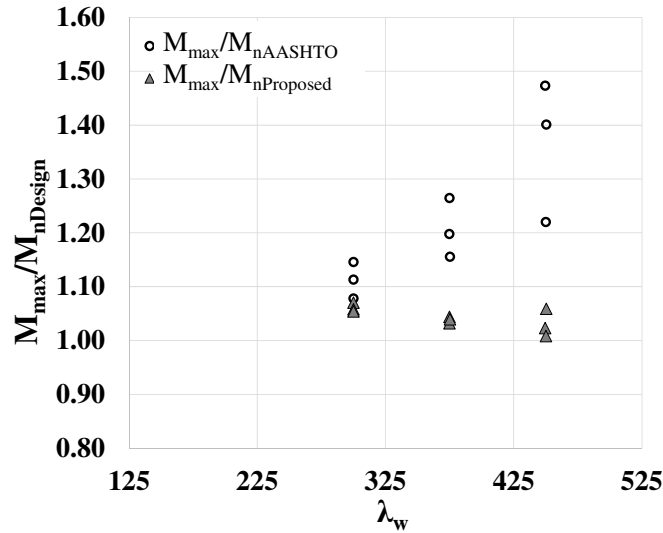
(c) Case 4

Figure 10-5 (Continued): Comparison of $M_{nProposed}$ with $M_{nAASHTO}$ for Cases 1, 3 and 4

It is also observed from the above figure that the proposed model is slightly optimistic for girders with stiffeners located above the optimum depth for flexure (Case 3), and slightly conservative for stiffener positions below the optimum depth (Case 4).

Table 10-6 shows the statistics for the hybrid girders tested in this Chapter for uniform bending at the compression flange yield limit state. It is seen that the recommended model gives excellent correlation with test data.

Table 10-6: Statistics for R_{bFEA}/R_{bPr} for straight hybrid girders at yield limit state

Statistical Parameter	R_{bFEA}/R_{bPr}
Mean	1.03
Coefficient of Variation	0.04
Maximum	1.11
Minimum	0.94
Median	1.03

10.4 High-Moment High-Shear Tests on Hybrid Longitudinally Stiffened Girders

As explained previously, it is essential to verify that the increased design flexural capacity of longitudinally stiffened girders does not lead to scenarios of moment-shear strength interaction. In order to corroborate the lack of significant moment-shear interaction in steel girders, selected tests are conducted.

Three-point bending tests similar to that shown in Figure 9-1 are used to setup the high-moment high-shear studies in this section. The material properties, residual stresses and geometric imperfections are the same as those used in Section 10.2.1. The critical base imperfection pattern is modeled in one of the interior panels adjacent to the applied load.

10.4.1 Case Studies

The girder cross-section parameters are varied as in Section 9.1.2. As in the case of homogenous girders, the overall girder lengths are varied such that the test girders have configurations that range from panels that fail in shear when the applied moment is approximately 60% of the recommended moment capacity prediction ($R_{bPr}M_y$) to panels that fail in flexure when the applied shear is approximately 60% of the predicted shear capacity based on the AASHTO shear equations ($V_{nAASHTO}$). This range of the moments and shears is expected to be more prone to moment-shear strength interaction, if any.

Six different girder cases considered in these studies are defined in Table 10-7 and constitute a total of 162 girders. These cases include two values of d_o/D, 1.50 and 2.0. Two positions of the longitudinal stiffener through the web depth are studied – one at 0.4 D_c and the other at 0.533 D_c. Table 10-7 shows the relative position of the longitudinal stiffener with respect to the depth of the web (d_s/D_c) for all the different girder web depths in compression used in the FE test simulations. The area and moment of inertia of the stiffener

are provided per the minimum AASHTO requirements, as listed in Section 2.8. The moment to shear ratio in the tests (*M/V*) is equal to one-half of the overall girder length, and shown in the right-most column of Table 10-7. The end panels are designed with a web thickness of 3 inches, such that D/t_w is 50 for these panels.

Cases 5 and 6 are identical to Cases 3 and 4 aside from the position of the longitudinal stiffener. The longitudinal stiffener is placed farther along the web from the compression flange in Cases 5 and 6.

Cases 4 and 6 are designed with two interior panels and an end panel on either side of the load, such that there are a total of six panels in the girder. However, the first interior panel from the end support is designed with the same web thickness and d_o/D as the end panel, so that the interior panel adjacent to the load, with high moment and high shear is the critical panel. For the purpose of discussion, and in context of Table 10-7, the first interior panel is referred to as an end panel, and the critical interior panel as interior panel.

Table 10-7: Case studies for hybrid girders subjected to high shear combined with high bending moment

Case	d_o/D IP[a]	d_o/D EP[a]	d_s/D_c	d_s/D $D_c/D=$ 0.5	d_s/D $D_c/D=$ 0.625	d_s/D $D_c/D=$ 0.75	M/V
1	1.5	1.5	0.40	0.20	0.25	0.30	3.0 *D*
2	1.5	2.5	0.40	0.20	0.25	0.30	4.0 *D*
3	2.0	2.0	0.40	0.20	0.25	0.30	4.0 *D*
4	2.0	2.0[b]	0.40	0.20	0.25	0.30	6.0 *D*
5	2.0	2.0	0.53	0.27	0.33	0.40	4.0 *D*
6	2.0	2.0[b]	0.53	0.27	0.33	0.40	6.0 *D*

a. IP = Interior Panel, EP = End panel
b. Two "End panels" and one interior panel on either side of the load

10.4.2 Results

The FE test simulation strengths for Cases 1 and 2 are compared to the governing strengths from the current AASHTO shear resistance model. Cooper's shear resistance model for longitudinally stiffened girders is not discussed for hybrid girders, as it has been demonstrated that they do not offer a substantial improvement over the AASHTO shear resistance equations. The terms V_{max} and M_{max} are the maximum shear and maximum moment achieved in the FE test simulations, and $V_{nAASHTO}$ is the shear capacity calculated as per the current AASHTO LRFD provisions. The test strengths are moment controlled (i.e., recommended flexural yield strength with R_{bPr} governs) when $M_{max}/R_{bPr}M_y$ is greater than $V_{max}/V_{nAASHTO}$. Otherwise, the tests are shear controlled. The governing shear or flexural strength ratios are bolded in the table.

Tables 10-8 through 10-13 show the results for Cases 1-6. It is seen that in an all of these simulations, the ratio of test capacity over the design capacity is greater than 1.0. This indicates that moment-shear interaction is not a concern with the current AASHTO shear strength equations and the proposed model for the flexural capacity.

It is also observed by comparing Tables 10-10 and 10-12 and Tables 10-11 and 10-13 that the lower position of the longitudinal stiffener through the web causes a trivial increase in the girder capacity. This can be attributed to the slightly higher shear capacity in the shorter bottom panels.

Table 10-8: Comparison of the test simulation load capacities to the governing strengths from the AASHTO shear resistance model, and the recommended flexural yield strength model (Case 1)

D/b_{fc}	D_c/D	$D/t_w = 300$		$D/t_w = 240$		$D/t_w = 200$	
		$V_{max}/V_{nAASHTO}$	$M_{max}/R_{bPr}M_y$	$V_{max}/V_{nAASHTO}$	$M_{max}/R_{bPr}M_y$	$V_{max}/V_{nAASHTO}$	$M_{max}/R_{bPr}M_y$
6	0.5	**1.02**	0.98	0.94	**1.12**	**1.21**	1.16
	0.625	**1.05**	0.94	0.99	**1.09**	0.90	**1.15**
	0.75	**1.12**	0.98	1.03	**1.10**	0.92	**1.16**
5	0.5	**1.06**	0.79	**1.06**	0.99	1.00	**1.11**
	0.625	**1.09**	0.76	**1.09**	0.93	1.05	**1.06**
	0.75	**1.19**	0.81	**1.18**	0.99	**1.10**	1.09
4	0.5	**1.12**	0.57	**1.12**	0.72	**1.12**	0.87
	0.625	**1.17**	0.55	**1.16**	0.68	**1.17**	0.83
	0.75	**1.33**	0.61	**1.29**	0.75	**1.26**	0.88

* Bolded values are the governing strength ratios given the use of one or both shear resistance models.

Table 10-9: Comparison of the test simulation load capacities to the governing strengths from the AASHTO shear resistance model, and the recommended flexural yield strength model (Case 2)

D/b_{fc}	D_c/D	$D/t_w = 300$		$D/t_w = 240$		$D/t_w = 200$	
		$V_{max}/V_{nAASHTO}$	$M_{max}/R_{bPr}M_y$	$V_{max}/V_{nAASHTO}$	$M_{max}/R_{bPr}M_y$	$V_{max}/V_{nAASHTO}$	$M_{max}/R_{bPr}M_y$
6	0.5	0.87	**1.12**	0.73	**1.15**	0.93	**1.17**
	0.625	0.91	**1.07**	0.78	**1.13**	0.70	**1.17**
	0.75	0.95	**1.10**	0.80	**1.13**	0.71	**1.17**
5	0.5	**1.01**	1.00	0.91	**1.12**	0.78	**1.14**
	0.625	**1.04**	0.95	0.95	**1.07**	0.84	**1.12**
	0.75	**1.11**	0.99	0.98	**1.09**	0.85	**1.12**
4	0.5	**1.09**	0.73	**1.08**	0.91	1.05	**1.08**
	0.625	**1.13**	0.70	**1.12**	0.88	**1.08**	1.01
	0.75	**1.26**	0.77	**1.21**	0.93	**1.15**	1.06

* Bolded values are the governing strength ratios given the use of one or both shear resistance models.

Table 10-10: Comparison of the test simulation load capacities to the governing strengths from the AASHTO shear resistance model, and the recommended flexural yield strength model (Case 3)

D/b_{fc}	D_c/D	$D/t_w = 300$		$D/t_w = 240$		$D/t_w = 200$	
		$V_{max}/V_{nAASHTO}$	$M_{max}/R_{bPr}M_y$	$V_{max}/V_{nAASHTO}$	$M_{max}/R_{bPr}M_y$	$V_{max}/V_{nAASHTO}$	$M_{max}/R_{bPr}M_y$
6	0.5	1.08	**1.10**	0.91	**1.16**	1.15	**1.17**
	0.625	**1.10**	1.01	1.02	**1.16**	0.86	**1.18**
	0.75	**1.15**	1.04	1.04	**1.17**	0.88	**1.18**
5	0.5	**1.16**	0.92	1.11	**1.11**	0.94	**1.15**
	0.625	**1.16**	0.83	**1.15**	1.04	1.04	**1.14**
	0.75	**1.22**	0.86	**1.22**	1.08	1.08	**1.17**
4	0.5	**1.21**	0.66	**1.23**	0.86	**1.21**	1.04
	0.625	**1.23**	0.61	**1.27**	0.79	**1.23**	0.95
	0.75	**1.33**	0.64	**1.31**	0.81	**1.29**	0.98

[*] *Bolded values are the governing strength ratios given the use of one or both shear resistance models.*

Table 10-11: Comparison of the test simulation load capacities to the governing strengths from the AASHTO shear resistance model, and the recommended flexural yield strength model (Case 4)

D/b_{fc}	D_c/D	$D/t_w = 300$		$D/t_w = 240$		$D/t_w = 200$	
		$V_{max}/V_{nAASHTO}$	$M_{max}/R_{bPr}M_y$	$V_{max}/V_{nAASHTO}$	$M_{max}/R_{bPr}M_y$	$V_{max}/V_{nAASHTO}$	$M_{max}/R_{bPr}M_y$
6	0.5	0.76	**1.16**	0.61	**1.15**	0.77	**1.18**
	0.625	0.85	**1.16**	0.69	**1.16**	0.59	**1.19**
	0.75	0.85	**1.14**	0.70	**1.16**	0.60	**1.20**
5	0.5	0.96	**1.14**	0.77	**1.15**	0.64	**1.16**
	0.625	1.03	**1.10**	0.85	**1.14**	0.70	**1.14**
	0.75	1.05	**1.10**	0.86	**1.13**	0.73	**1.17**
4	0.5	**1.16**	0.94	1.08	**1.11**	0.89	**1.13**
	0.625	**1.17**	0.85	**1.13**	1.05	0.97	**1.11**
	0.75	**1.24**	0.89	**1.17**	1.08	0.99	**1.11**

[*] *Bolded values are the governing strength ratios given the use of one or both shear resistance models.*

Table 10-12: Comparison of the test simulation load capacities to the governing strengths from the AASHTO shear resistance model, and the recommended flexural yield strength model (Case 5)

D/b_{fc}	D_c/D	$D/t_w = 300$		$D/t_w = 240$		$D/t_w = 200$	
		$V_{max}/V_{nAASHTO}$	$M_{max}/R_{bPr}M_y$	$V_{max}/V_{nAASHTO}$	$M_{max}/R_{bPr}M_y$	$V_{max}/V_{nAASHTO}$	$M_{max}/R_{bPr}M_y$
6	0.5	1.09	**1.16**	1.08	**1.11**	1.11	**1.19**
	0.625	**1.12**	1.10	**1.13**	1.05	0.85	**1.24**
	0.75	**1.17**	1.12	**1.17**	1.08	0.85	**1.23**
5	0.5	**1.17**	0.96	0.89	**1.19**	0.93	**1.17**
	0.625	**1.19**	0.90	0.99	**1.21**	1.03	**1.19**
	0.75	**1.23**	0.91	0.99	**1.19**	1.04	**1.18**
4	0.5	**1.23**	0.68	1.12	**1.16**	**1.26**	1.10
	0.625	**1.24**	0.63	**1.18**	1.13	**1.27**	1.03
	0.75	**1.33**	0.67	**1.22**	1.14	**1.34**	1.06

* Bolded values are the governing strength ratios given the use of one or both shear resistance models.

Table 10-13: Comparison of the test simulation load capacities to the governing strengths from the AASHTO shear resistance model, and the recommended flexural yield strength model (Case 6)

D/b_{fc}	D_c/D	$D/t_w = 300$		$D/t_w = 240$		$D/t_w = 200$	
		$V_{max}/V_{nAASHTO}$	$M_{max}/R_{bPr}M_y$	$V_{max}/V_{nAASHTO}$	$M_{max}/R_{bPr}M_y$	$V_{max}/V_{nAASHTO}$	$M_{max}/R_{bPr}M_y$
6	0.5	0.74	**1.17**	0.60	**1.18**	0.74	**1.19**
	0.625	0.82	**1.19**	0.67	**1.21**	0.56	**1.23**
	0.75	0.82	**1.16**	0.67	**1.19**	0.57	**1.21**
5	0.5	0.94	**1.15**	0.76	**1.16**	0.62	**1.17**
	0.625	1.01	**1.14**	0.84	**1.19**	0.70	**1.20**
	0.75	1.02	**1.13**	0.84	**1.16**	0.70	**1.18**
4	0.5	**1.17**	0.97	1.08	**1.14**	0.88	**1.15**
	0.625	**1.19**	0.91	**1.14**	1.11	0.96	**1.15**
	0.75	**1.25**	0.93	**1.17**	1.12	0.97	**1.14**

* Bolded values are the governing strength ratios given the use of one or both shear resistance models.

Figure 10-6 shows the results in Tables 10-8 and 10-9 for Cases 1 and 2 with $d_o/D = 1.5$. It is clear that all data points are outside of the "interaction zone".
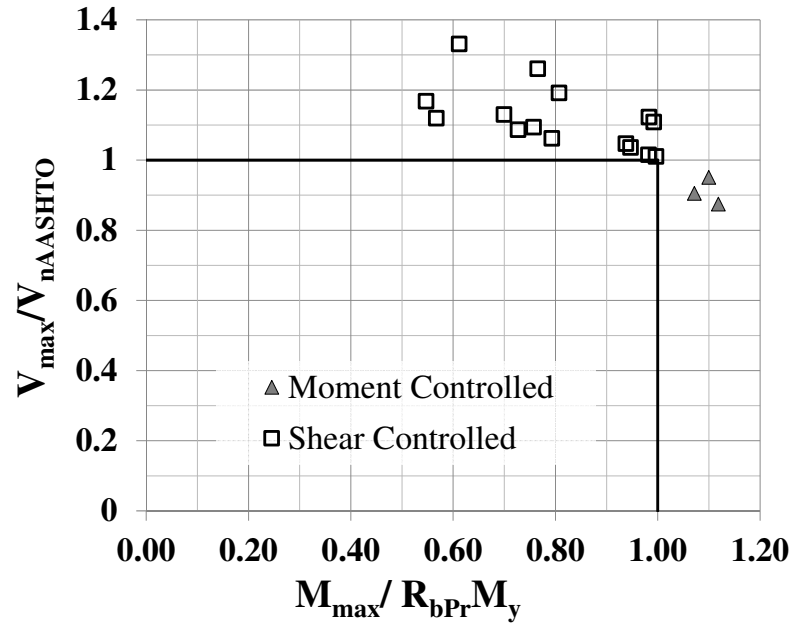
(a) $D/t_w = 300$
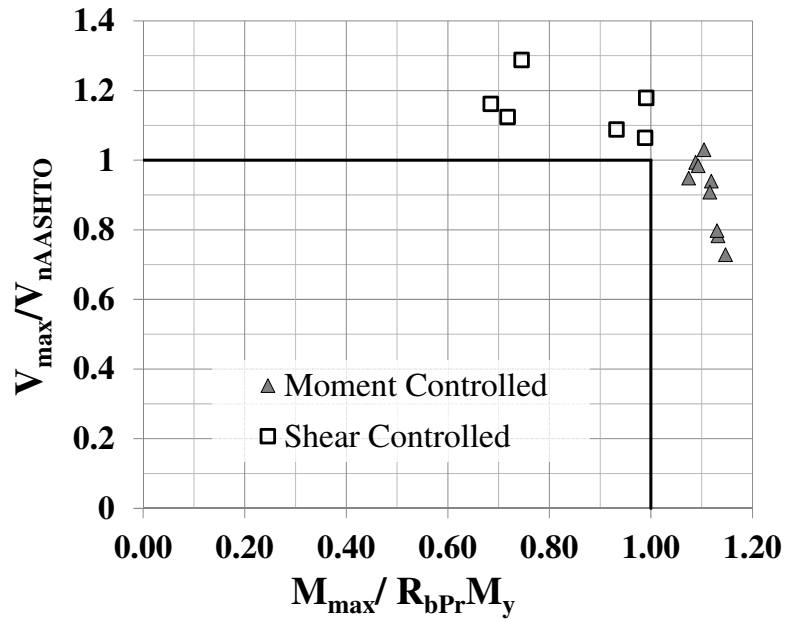
(b) $D/t_w = 240$

Figure 10-6: $V_{max}/V_{nAASHTO}$ **versus** $M_{max}/R_{bPr}M_y$ **for high-moment high-shear tests (Cases 1 and 2)**
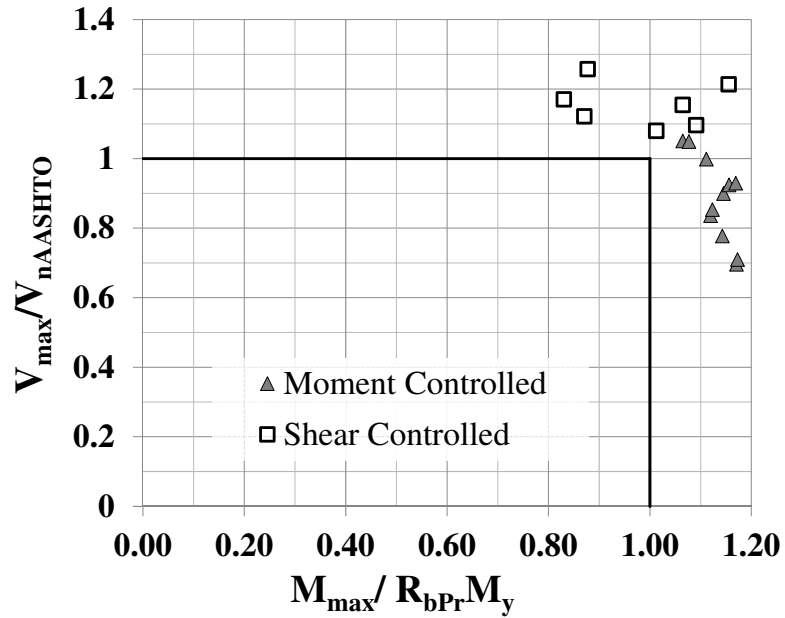
(c) $D/t_w = 200$

Figure 10-6 (Continued): $V_{max}/V_{nAASHTO}$ **versus** $M_{max}/R_{bPr}M_y$ **for high-moment high-shear tests (Cases 1 and 2)**

Figure 10-7 shows a typical failure mode of hybrid longitudinally stiffened girder subject to high moment-high shear loading. The lighter shade indicates regions that have yielded. It is evident that there is a clear development of a single tension field through the stiffener. There is also extensive yielding in the compression flange at the region of maximum moment near the center of the girder and in the top panel of the web. The tension field in the web continues to develop until the compression flange is yielded sufficiently such that it cannot help develop the shear forces any further.

Figure 10-7: Typical failure mode for hybrid girder with high moment-high shear

249

Table 10-14 shows the statistics for the 162 girders tested for high moment- high shear and high shear-high moment. It is observed that the mean of the professional factors and the minimum values for both the moment controlled and shear controlled tests are greater than 1.0. The COV for the moment controlled tests are lower (0.03) than the COV for the shear controlled tests (0.06). However, the results are conservative, and the shear strengths of the girders are beneficially influenced by the higher strength flanges, although the resistance equations do not account for that.

Table 10-14: Statistics for the high-moment high-shear hybrid girder tests (Cases 1 - 6)

Statistical Parameter	$D/t_w = 300$		$D/t_w = 240$		$D/t_w = 200$	
	Moment Controlled (17 tests) $M_{max}/R_{bPr}M_y$	Shear Controlled (37 tests) $M_{max}/R_{bPr}M_y$	Moment Controlled (31 tests) $M_{max}/R_{bPr}M_y$	Shear Controlled (23 tests) $V_{max}/V_{nAASHTO}$	Moment Controlled (41 tests) $M_{max}/R_{bPr}M_y$	Shear Controlled (13 tests) $V_{max}/V_{nAASHTO}$
Mean	1.13	1.17	1.15	1.19	1.16	1.21
COV	0.03	0.07	0.03	0.06	0.03	0.06
Maximum	1.19	1.33	1.21	1.33	1.24	1.34
Minimum	1.07	1.01	1.07	1.06	1.06	1.08
Median	1.14	1.17	1.15	1.18	1.17	1.21

10.5 Experimental Verification of the Proposed R_b Model

Results from selected experimental tests in the literature are compared against the proposed cross-section model. Tests by Cooper (1965; 1967) and Owen et al. (1970) are chosen to test the efficacy of the proposed model in predicting the experimental test results. These tests have web and flange plates of nearly equal yield strengths.

10.5.1 Evaluation of Cooper (1965; 1967)

Cooper tested girders LB2-LB5 and reported results in 1965, where he observed no benefits from the longitudinal stiffener in the postbuckling capacity. From Table 10-15, it appears the AASHTO provides a better prediction of the test capacities reported by Cooper than the proposed model. However, Cooper observed in a later publication in 1967 by means of an additional test LB6 that longitudinal stiffeners when sized adequately achieve their ultimate strengths with almost no stress redistribution in the web. It is found that the longitudinal stiffener sizes used in tests LB2 to LB5 have at least 20% larger b_l/t_s than the current AASHTO limits that are intended to prevent local buckling of the stiffener. Cooper observed that the failure of the girders was preceded by failure of the longitudinal stiffeners. The proposed model predicts higher strengths than the reported results for these tests because it only works under the assumption that the stiffeners are sized as per the AASHTO requirements which includes a maximum stiffener slenderness (b_l/t_s). It is observed that for LB6, where AASHTO ignores the contribution of the longitudinal stiffener, the proposed model predicts a strength 13% higher than AASHTO, and equal to the reported value.

Table 10-15: Comparison of $R_{bExperiment}$ with $R_{bAASHTO}$ and $R_{bProposed}$ from Cooper's Tests

Girder	D/t_w	$R_{bReported}$	$R_{bAASHTO}$	$R_{bProposed}$
LB2*	444	0.88	0.85	0.95
LB3*	447	0.89	0.85	0.96
LB4*	447	0.90	0.85	0.96
LB5*	447	0.91	0.85	0.96
LB6	408	0.95	0.82	0.95

* Longitudinal stiffeners do not satisfy AASHTO requirements

10.5.2 Evaluation of Owen et al. (1970)

Table 10-16 compares the results from the tests conducted by Owen, et.al. It is observed that for this high slenderness, the proposed model is 5 to 12% conservative. This is due to the simplified expressions for the effective widths in the model. The test TG 4-1 had a longitudinal stiffener that is twice the minimum rigidity requirement in AASHTO and only half the maximum slenderness. Girders TG 1-1 and TG 2-1 had stiffeners that were much less rigid, but also more stocky. It is clear that the reported strength for TG 4-1 is higher due to the more rigid stiffener. AASHTO on the other hand predicts strengths that are 30 to 38% lower than the reported results.

It is also interesting to observe that despite the high web slenderness used in these tests (750), the girders achieve almost the full compression flange yield strength on account of using the longitudinal stiffeners. The proposed model recommends effective web widths as a function of the web depth in compression, based on the studies conducted in this research, where D/t_w is limited to 300. This is a clear indicator that there is enormous potential for using longitudinally stiffened girders with higher web slenderness, and achieve much larger strengths than currently predicted by AASHTO.

Table 10-16: Comparison of $R_{bExperiment}$ with $R_{bAASHTO}$ and $R_{bProposed}$ from Owen et.al

Girder	D/t_w	$R_{bReported}$	$R_{bAASHTO}$	$R_{bProposed}$
TG 1-1	750	0.96	0.66	0.91
TG 2-1	750	0.99	0.66	0.91
TG 4-1	750	1.03	0.66	0.91

10.6 Summary

The following are the key recommendations and findings from the research on hybrid longitudinally stiffened girders.

1. The improved R_b model for homogenous girders proposed previously is expanded to serve as a combined R_b and R_h model for hybrid longitudinally stiffened girders.

2. The model is expanded to hybrid girders without changing any key element of the model for homogenous girders.

3. The proposed model is evaluated for potential moment shear interaction effects and is in fact found to be conservative under moment gradient effects. This indicates the contribution of the higher strength compression flange in developing post-buckling shear strength.

4. Although the tests in this chapter preclude LTB and FLB, it can be surmised from the results in Chapters 5, 6 and 8 that the proposed R_b model is conservative for FLB and that the proposed LTB model works as well for hybrid girders. The recommendations in this chapter are expected to satisfy other limit states.

5. The comparisons with experimental results indicate that AASHTO model is clearly conservative when stiffeners are proportioned such that premature failure of the longitudinal stiffeners are avoided. It is seen that the proposed model predicts strengths that are much higher and closer to the reported experimental values than the current Specifications. It however tends to be conservative for larger web slenderness than those considered in this research. This is because the proposed expressions for effective panel widths are functions of the web depths in compression.

CHAPTER 11

PRELIMINARY STUDIES ON CURVED LONGITUDINALLY

STIFFENED GIRDERS AT YIELD LIMIT STATE

In this chapter, parametric studies are conducted on curved homogenous girders with single longitudinal stiffeners. The principal parameter varied in addition to those varied in the earlier straight girder studies is the curvature parameter

$$Z = \frac{0.95d_o^2}{Rt_w} \tag{11.1}$$

(as defined by AASHTO). These studies are aimed at understanding the influence of horizontal curvature on the ultimate flexural capacity of longitudinally stiffened plate girders, with a focus on cases where the girder flexural capacity is governed by the yield limit state and where the girder flange lateral bending in relatively small.

11.1 Constant Test Parameters

The following parameters are held constant in all these tests.

1. The yield stress of all plated elements, F_y is 50 ksi.

2. The depth of web panel, D is 150 inches.

3. A single size for all of the transverse stiffeners is designed to meet the AASHTO (2014) requirements for all of the tests. The transverse stiffeners are sized at 12.5 x 0.8 inches.

4. The width-to-thickness ratio, b_l/t_s, of the longitudinal stiffeners is set at the AASHTO (2014) maximum limit, $0.48\sqrt{E/F_{ys}}$.

5. The width of the compression flange is taken as $b_{fc} = D/3$.

11.2 Variable Test Parameters

To understand the influence of longitudinal stiffeners on the flexural capacity of horizontally curved girders, the following design parameters are varied to create a comprehensive suite of parametric studies to study the curved girder response at the yield limit state.

1. D/t_w = 300, 240, and 200

2. d_o/D = 0.75, 1.0, 1.5, and 2.0

3. D_c/D = 0.5, 0.625, and 0.75

4. A_l/A_{wc}, varied as explained below

5. I_l, varied as explained below

6. R

where:

R = radius of curvature of girder

The parameters A_l/A_{wc} and I_l are varied by designing the longitudinal stiffener sizes to meet the minimum requirements as per AASHTO. These requirements are the same as described in Section 2.8, except that an additional curvature factor, Z, is applied to the rigidity requirement. Therefore, these parameters are varied as a function of d_o/D and D/t_w. The radius, R, is varied by placing limits on the AASHTO curvature parameter, Z, which is applied to the longitudinal stiffener rigidity. AASHTO limits this to a value of 10. The studies evaluate the effect of Z up to a value of 15.

11.3 Test Setup

The test setup for the curved girders is the same as that for straight girders as shown in Figure 3-1 except that a horizontal curvature is introduced. The curvature is constant along the length of the test setup. The girders are braced out of plane at top and bottom flanges at each of the transverse stiffener locations in the test specimens.

11.4 Case Studies

The studies are conducted on four groups of tests with different panel aspect ratios ranging from 0.75 to 2.0. The case studies are summarized in Table 11-1. Each of these cases is further subdivided into several tests with different radii, resulting in different curvature parameters. For instance, Case 1 is a set of parametric studies for $d_o/D = 1$, with D_c/D, D/t_w, and d_o/R as variable parameters. Similar to the straight girder studies, the depth of the stiffener location is always at $0.4D_c$, which has been established as the theoretical optimum stiffener location for flexure. Cases 1a, 1b, and 1c are the same girders with different radii. The suffix i and o indicate that the longitudinal stiffener is placed on the inside (towards the center) or outside (away from the center) of the curve. Cases 2, 3, and 4 are studies with $d_o/D = 1.5$, 2, and 0.75 respectively. Similar to Case 1, each of these cases are also subdivided into several cases based on their radii. However, Cases 2, 3 and 4 are only analyzed with the longitudinal stiffener on the inside of the curve as a result of the observations from Case 1. The longitudinal stiffener sizes for each girder in each case are designed such that they are just sufficient to satisfy the corresponding AASHTO design criteria. A single size transverse stiffener (12.5 x 0.8 inches) is used for all the analyses, which satisfies the minimum size requirement from AASHTO for all the girders in all cases. The compression flanges of the test panels are compact, and are braced such that

256

FLB and LTB, according to the AASHTO LRFD provisions, does not govern any of the resistances in the studies presented in this section. To assess directly the importance of curvature of the web in on postbuckling flexural response, Cases 1 and 4 are also analyzed as straight girders and the results are presented.

A total of 162 different girders are studied in this chapter.

Table 11-1: Case studies for curved girders at yield limit state

Case	d_o/D	R (ft)	d_o/R
1a-i	1	1500.00	0.01
1a-i2	1	1500.00	0.01
1a-o	1	1500.00	0.01
1b-i	1	500.00	0.025
1b-o	1	500.00	0.025
1c-i	1	312.50	0.04
1c-o	1	312.50	0.04
2a-i	1.5	1875.00	0.01
2b-i	1.5	815.22	0.023
2c-i	1.5	535.71	0.035
3a-i	2	1666.67	0.015
3b-i	2	1000.00	0.025
4a-i	0.75	208.33	0.045
4b-i	0.75	144.23	0.065

11.5 Calculation of R_{bFEA}

R_{bFEA} for the curved girder studies is computed as M_{max}/M_{nPr}, where M_{max} is the maximum moment reached at the maximum load capacity in the FE test simulations, and M_{nPr} is the theoretical moment capacity of the girder computed using the one third rule:

$$f_b + \frac{1}{3} f_l = R_b F_{yc} \tag{11.2}$$

$$\frac{M_{max}}{S_{xc}} + \frac{1}{3} \frac{M_{max} L_b^2}{12RD\left(b_{fc}^2 t_{fc}/6\right)} = R_b F_{yc} \tag{11.3}$$

$$M_{max} \left[1 + \frac{1}{3} \frac{L_b^2 S_{xc}}{12RD\left(b_{fc}^2 t_{fc}/6\right)}\right] = R_b F_{yc} S_{xc} \tag{11.4}$$

$$M_{max} \left[1 + \frac{1}{3} \frac{L_b^2 S_{xc}}{12RD\left(b_{fc}^2 t_{fc}/6\right)}\right] = R_b M_{yc} \tag{11.5}$$

$$R_{bFEA} = \frac{M_{max}}{M_{yc}} \left[1 + \frac{1}{3} \frac{L_b^2 S_{xc}}{12RD\left(b_{fc}^2 t_{fc}/6\right)}\right] \tag{11.6}$$

To determine M_{max}, M_{max}/S_{xc} is substituted for f_b and the elastic flange lateral bending stress, f_l is estimated using the equation

$$f_l = \frac{M_{lat}}{b_{fc}^2 t_{fc}/6} \tag{11.7}$$

where

$$M_{lat} = \frac{M_{max} L_b^2}{12RD} \tag{11.8}$$

The unbraced length L_b for each case is the same as the transverse stiffener spacing, i.e. the girders are braced at every stiffener/cross frame location. In the tests presented in this chapter, the flange lateral bending stresses f_l are a small fraction (1% to 5%) of the overall flexural stresses in the compression flange. Therefore, the maximum reduction in the

major-axis bending resistance due to the flange lateral bending is only in the order of 2% in these studies. The primary emphasis in these tests is on the influence of the horizontal curvature on the longitudinal stiffener behavior.

11.6 Synthesis of Results

All the FE results for the 162 tests associated with the cases from Table 11-1 are presented in Tables 11-3 through 11-10.

11.6.1 Evaluation of Critical Side of Curvature for Base Imperfection

The base imperfection pattern used in the parametric studies for curved girders is the same as that used in the straight girder studies. However, to check the influence of applying this imperfection on the convex or concave side of the curve, a sensitivity study on Case 1a-i is performed. The imperfection is applied on the opposite side of the stiffener in Case 1a-i while it is applied on the same side of the stiffener in Case 1a-i2. As previously described, the suffix i indicates that the longitudinal stiffener is placed on the side of the girder that is towards the center of the curve. Table 11-2 compares the results obtained from the two cases. It may be concluded that the effect of the direction of the base imperfection pattern is minimal. However, the strengths of the girders are slightly smaller when the imperfection is applied on the same side as the stiffener, i.e., when the stiffener imperfection is the direction of the side of the web having the longitudinal stiffener. In all remaining studies, the base imperfection is applied on the same side as the longitudinal stiffener.

Table 11-2: R_{bFEA} for girders with web imperfection applied on different sides of the curve

D/t_w	D_c/D	Case 1a -i	Case 1a -i2
300	0.5	0.9948	0.9933
	0.625	0.9809	0.9715
	0.75	0.9564	0.9472
240	0.5	1.0177	1.0065
	0.625	0.9926	0.9760
	0.75	0.9524	0.9490
200	0.5	1.0413	1.0227
	0.625	1.0028	0.9924
	0.75	0.9698	0.9611

11.6.2 Relative Performance of AASHTO, Eurocode and FE Test Simulations

Table 11-3 shows a comparison of R_{bFEA} with $R_{bAASHTO}$ and R_{bEC}. The relative behavior of the curved girder models is similar to the behavior observed in the straight girder studies. Similar to the previous studies, the Eurocode predictions are closer to the FE simulation results, and the AASHTO predictions are more conservative for higher values of D_c/D. The Eurocode calculations are presented only for Case1a-i because all other cases display the same trends in their behavior with respect to values predicted by AASHTO and FE. The prediction of R_b using the proposed model from Section 0 is evaluated in Section 11.7.

Table 11-3: Comparison of $R_{bAASHTO}$, R_{bEC} and R_{bFEA} (Case 1a – i)

(a) $Dc/D = 0.5$

D/t_w	$R_{bAASHTO}$	R_{bEC}	R_{bFEA}	$R_{bFEA}/R_{bAASHTO}$	R_{bFEA}/R_{bEC}
300	0.93	0.94	0.99	1.06	1.06
240	1.00	0.94	1.02	1.02	1.08
200	1.00	0.95	1.04	1.04	1.10

(b) $Dc/D = 0.625$

D/t_w	$R_{bAASHTO}$	R_{BEC}	R_{bFEA}	$R_{bFEA}/R_{bAASHTO}$	R_{bFEA}/R_{bEC}
300	0.88	0.92	0.98	1.11	1.06
240	0.90	0.92	0.99	1.10	1.08
200	1.00	0.92	1.00	1.00	1.09

(c) $Dc/D = 0.75$

D/t_w	$R_{bAASHTO}$	R_{BEC}	R_{bFEA}	$R_{bFEA}/R_{bAASHTO}$	R_{bFEA}/R_{bEC}
300	0.82	0.90	0.96	1.16	1.06
240	0.85	0.90	0.95	1.12	1.06
200	0.87	0.90	0.97	1.11	1.08

11.6.3 Comparison of Girders With and Without Longitudinal Web Stiffener

Table 11-4 compares the results between stiffened and unstiffened girders for the two cases that have the sharpest radii. This helps in quantifying the effect of the longitudinal stiffeners in contributing to the overall flexural capacity of curved girders. The table clearly shows that the curved girders attain an improvement in strength when they are longitudinally stiffened as opposed to the slender web girders with no longitudinal stiffeners. It is also clear that a greater value of D_c/D is detrimental to the capacity of the girder, and the more slender the web, the smaller the capacity.

Table 11-4: Comparison of R_{bFEA} of plate girders with and without longitudinal stiffeners

D/t_w	D_c/D	Case 4a-i	Case 4a-no LS	Case 4b-i	Case 4b-no LS
300	0.5	1.01	0.98	1.02	0.99
	0.625	0.98	0.95	0.99	0.96
	0.75	0.96	0.93	0.97	0.94
240	0.5	1.03	0.98	1.03	0.99
	0.625	0.99	0.95	1.00	0.96
	0.75	0.97	0.92	0.98	0.93
200	0.5	1.05	0.98	1.05	0.99
	0.625	1.01	0.94	1.02	0.96
	0.75	0.98	0.92	0.99	0.93

11.6.4 Evaluation of Relative Efficacy of Longitudinal Stiffener When Placed Inside or Outside of the Curvature

Table 11-5 compares the simulation results for Case 1 when the longitudinal stiffener is placed towards (inside) or away (outside) from the center of curvature. While the girder appears to have a slight increase in capacity when the longitudinal stiffener is placed on the outside of the curve, it is important to note that AASHTO requirements for the minimum required longitudinal stiffener rigidity are different depending on the side of web where the stiffener is placed. The required stiffener rigidity is larger when the stiffener is placed on the outside of the curve. Based on the behavior in straight girders, and on the results presented in this chapter, it is reasonable to surmise that the side of the web where the stiffener is placed has little bearing on the overall flexural capacity of the girder when the AASHTO rules are applied for the stiffener rigidity.

Table 11-5: Effect of side of the web at which the longitudinal stiffener is placed (inside or outside) on R_{bFEA}

D/t_w	D_c/D	Case 1a -i	Case 1a -o	Case 1b-i	Case 1b-o	Case 1c-i	Case 1c-o
300	0.5	0.9948	1.0013	1.0137	1.0202	1.0149	1.0225
	0.625	0.9809	0.9703	0.9808	0.9987	0.9916	1.0087
	0.75	0.9564	0.9486	0.9735	0.9783	0.9787	0.9862
240	0.5	1.0177	1.0243	1.0290	1.0310	1.0338	1.0368
	0.625	0.9926	0.9908	0.9987	1.0147	1.0082	1.0237
	0.75	0.9524	0.9629	0.9691	0.9853	0.9908	0.9985
200	0.5	1.0413	1.0356	1.0492	1.0449	1.0553	1.0478
	0.625	1.0028	1.0178	1.0211	1.0323	1.0316	1.0443
	0.75	0.9698	0.9853	0.9856	1.0039	1.0004	1.0155

11.6.5 Influence of Degree of Curvature on Ultimate Strength

Tables 11-6 through 11-9 show the effect of the curvature on the flexural capacity of the girders for different panel aspect ratios. In all these tables, it may be observed that the capacity of the girder increases with decreasing R. This is likely due to the increase in the longitudinal stiffener size required for the increased curvature. To scrutinize the above observation further, 11-10 compares Cases 1 and 4 with and without horizontal curvature. It is important to note that, the flange width in all these studies is one-third of the depth of the girder, and ranges between one-third to one half of the lateral unbraced length. This limits the flange lateral bending stress to a maximum of 5% of the compression flange yield stress. The capacities (indicated by R_{bFEA}) are nearly the same in most cases (within 1 to 2%) which leads to the conclusion that the horizontal curvature has no significant effect on the flexural capacity when the base flexural capacity is governed by the yield limit state and when flange lateral bending stresses are small.

Table 11-6: Effect of degree of curvature on R_{bFEA} (d_o/D =1)

D/t_w	D_c/D	Case 1a –i (R = 1250 ft)		Case 1b-i (R = 500 ft)		Case 1c-i (312.5 ft)	
		b_l x t_s (in)	R_{bFEA}	b_l x t_s (in)	R_{bFEA}	b_l x t_s (in)	R_{bFEA}
300	0.5	7.2 x 6.3	0.99	7.86 x 0.68	0.99	8.32 x 0.72	0.99
	0.625	7.2 x 6.3	0.98	7.86 x 0.68	0.98	8.32 x 0.72	0.99
	0.75	7.2 x 6.3	0.96	7.86 x 0.68	0.97	8.32 x 0.72	0.98
240	0.5	8.32 x 0.72	1.02	9.01 x 0.78	1.03	9.36 x 0.81	1.03
	0.625	8.32 x 0.72	0.99	9.01 x 0.78	0.99	9.36 x 0.81	1.01
	0.75	8.32 x 0.72	0.95	9.01 x 0.78	0.97	9.36 x 0.81	0.99
200	0.5	9.36 x 0.81	1.04	9.94 x 0.86	1.05	10.4 x 0.9	1.05
	0.625	9.36 x 0.81	1.00	9.94 x 0.86	1.02	10.4 x 0.9	1.03
	0.75	9.36 x 0.81	0.97	9.94 x 0.86	0.98	10.4 x 0.9	1.00

Table 11-7: Effect of degree of curvature on R_{bFEA} (d_o/D =1.5)

D/t_w	D_c/D	Case 2a –i (R = 1875 ft)		Case 2b-i (R = 815.22 ft)		Case 2c-i (R = 535.71 ft)	
		b_l x t_s (in)	R_{bFEA}	b_l x t_s (in)	R_{bFEA}	b_l x t_s (in)	R_{bFEA}
300	0.5	9.59 x 0.83	1.01	10.51 x 0.91	1.02	11.21 x 0.97	1.02
	0.625	9.59 x 0.83	0.98	10.51 x 0.91	0.99	11.21 x 0.97	1.00
	0.75	9.59 x 0.83	0.95	10.51 x 0.91	0.97	11.21 x 0.97	0.98
240	0.5	11 x 0.955	1.03	11.9 x 1.03	1.03	12.6 x 1.095	1.04
	0.625	11 x 0.955	1.00	11.9 x 1.03	1.01	12.6 x 1.095	1.04
	0.75	11 x 0.955	0.97	11.9 x 1.03	0.99	12.6 x 1.095	1.00
200	0.5	12.35 x 1.07	1.04	13.23 x 1.145	1.05	13.92 x 1.205	1.05
	0.625	12.35 x 1.07	1.04	13.23 x 1.145	1.06	13.92 x 1.205	1.06
	0.75	12.35 x 1.07	1.00	13.23 x 1.145	1.02	13.92 x 1.205	1.02

Table 11-8: Effect of degree of curvature on R_{bFEA} (d_o/D =2.0)

D/t_w	D_c/D	Case 3a –i (R = 1666.67 ft)		Case 3b-i (R = 1000 ft)	
		b_l x t_s (in)	R_{bFEA}	b_l x t_s (in)	R_{bFEA}
300	0.5	12.36 x 1.07	1.01	13.29 x 1.15	1.02
	0.625	12.36 x 1.07	0.99	13.29 x 1.15	1.01
	0.75	12.36 x 1.07	0.96	13.29 x 1.15	0.99
240	0.5	14.04 x 1.205	1.02	15 x 1.3	1.03
	0.625	14.04 x 1.205	1.02	15 x 1.3	1.04
	0.75	14.04 x 1.205	1.01	15 x 1.3	1.01
200	0.5	15.6 x 1.35	1.03	16.64 x 1.44	1.04
	0.625	15.6 x 1.35	1.06	16.64 x 1.44	1.07
	0.75	15.6 x 1.35	1.02	16.64 x 1.44	1.03

Table 11-9: Effect of degree of curvature on R_{bFEA} (d_o/D =0.75)

D/t_w	D_c/D	Case 4a –i (R = 208.33 ft)		Case 4b-i (R =144.23 ft)	
		b_l x t_s (in)	R_{bFEA}	b_l x t_s (in)	R_{bFEA}
300	0.5	6.7 x 0.58	1.01	7.06 x 0.611	1.02
	0.625	6.7 x 0.58	0.98	7.06 x 0.611	0.99
	0.75	6.7 x 0.58	0.96	7.06 x 0.611	0.97
240	0.5	7.62 x 0.66	1.03	7.97 x 0.69	1.03
	0.625	7.62 x 0.66	0.99	7.97 x 0.69	1.00
	0.75	7.62 x 0.66	0.97	7.97 x 0.69	0.98
200	0.5	8.49 x 0.735	1.05	8.9 x 0.77	1.05
	0.625	8.49 x 0.735	1.01	8.9 x 0.77	1.02
	0.75	8.49 x 0.735	0.98	8.9 x 0.77	0.99

Table 11-10: Comparison of R_{bFEA} for curved and straight configurations

D/t_w	D_c/D	Case 1a –i (curved)	Case 1a –s (straight)	Case 4a –i (curved)	Case 4a –s (straight)
	0.5	0.99	0.99	1.01	0.99
300	0.625	0.98	0.96	0.98	0.97
	0.75	0.96	0.94	0.96	0.95
	0.5	1.02	1.02	1.03	1.02
240	0.625	0.99	0.97	0.99	0.98
	0.75	0.95	0.95	0.97	0.96
	0.5	1.04	1.03	1.05	1.04
200	0.625	1.00	1.00	1.01	1.00
	0.75	0.97	0.97	0.98	0.97

11.7 Evaluation of Proposed Model

This section compares the results for the 162 girder models considered in this chapter against the prediction model presented in Figure 4-10. From Table 11-11, it is evident that the same cross-section model proposed for the straight girders may be used for curved girders when the base flexural capacity is governed by the yield limit state and when lateral bending stresses are within 5% of the compression flange yield stress. To study girders that are subjected to higher lateral bending stresses, it is necessary to consider the LTB limit state, which is beyond the scope of the current study.

Table 11-11: Performance of R_{bPr} in comparison to R_{bFEA} for Curved Girders

Statistical Parameter	R_{bFEA}/R_{bPr}
Mean	1.02
Coefficient of Variation	0.02
Maximum	1.07
Minimum	0.99
Median	1.02

CHAPTER 12

SUMMARY OF FINDINGS AND RECOMMENDATIONS FOR

FUTURE WORK

12.1 Summary of Studies Conducted in This Research

The following are the primary studies conducted in this research.

1. The web postbuckling flexural capacity of homogenous longitudinally stiffened girders is evaluated at the yield limit state, and a cross-section model is proposed. The studies are later expanded to include hybrid girders.

2. This cross-section model is validated for use with the current FLB equations in the Specifications.

3. The study of the LTB limit state is rendered more complex due to the disconnect observed between FE test simulations and the LTB resistance equations in the Specifications. An in-depth study of unstiffened compact web rolled beams and noncompact web and slender web girders is carried out to determine the appropriate initial geometric imperfections and residual stresses for FE test simulations to provide correlation with experimental data. Minor modifications to the current AISC/ AASHTO LTB resistance equations are also proposed based on uniform bending tests.

   These recommendations are further validated for moment gradient loading. The proposed LTB resistance equations are then extended to include longitudinally stiffened girders.

4. Homogenous longitudinally stiffened girders are then evaluated for loading with combined bending and shear loading. The current AASHTO provisions regarding the maximum transverse stiffener spacing are examined, and it is determined that the limit may be increased. Potential moment-shear strength interaction is gaged for both homogenous and hybrid girders under high moment-high shear loading. Flexural limit states include both compression flange yield and LTB.

5. Preliminary studies are conducted on curved longitudinally stiffened girders at the yield limit state.

12.2 Key Contributions in This Research

The following are the key contributions of this research.

12.2.1 Proposed Model for Postbuckling Flexural Resistance of Longitudinally Stiffened Girders

1. A cross-section model is proposed in Section 4.7 which can be used to calculate the ultimate moment capacity of a longitudinally stiffened girder. The salient FEtures of the proposed model are:

   a. The stress distribution and effective panel widths for the compression side of the girder are provided.

   b. The depth of neutral axis, D_c^*, is calculated based on an interative computation that satisfies both compatibility and equilibrium.

   c. The effective widths in the various sub-panels are taken as simple linear functions of D_c^* and t_w. This is an advantage over the Eurocode model, which involves more extensive calculations to determine the plate effective widths.

d. An alternate simplified model is provided that can be used when A_l/A_w is less than 0.15, which provides 3 to 5% higher strengths than the exact model. This computation is simpler to use because the depth of the neutral axis can simply be taken as the elastic neutral axis of the gross cross-section and the compression stress over all effective portions of the web is equal to the yield stress of the web. The tension stresses can be calculated using the above depth of neutral axis, based on the assumption of a linear strain variation through the cross-section depth, and satisfying equilibrium.

e. The flexural capacity of the girder at the yield limit state, M_{nPr} is calculated by integrating the idealized stress distribution over the cross-section, using elementary principles of mechanics. The load shedding factor, R_{bPr}, is evaluated as M_{nPr}/M_y, and is limited to a maximum value of 1.0.

2. It is established that the proposed model used in conjunction with the FLB equations for noncompact flanges is satisfactory in predicting the capacities of these types of girders. Slender flanges are not studied in this research because AASHTO prohibits their use in bridge girders by limiting the maximum flange slenderness to 12.0.

3. The model originally provided for homogenous girders is expanded to predict the flexural capacity of hybrid girders without changing any component of the original model. This model serves as a combined R_b and R_h model for hybrid longitudinally stiffened girders, and it is not required to compute the hybrid factor independently for the computation of flexural resistance.

4. It is noteworthy that while this procedure of calculating R_{bPr} is more elaborate than the simple equation in the current AASHTO LRFD, the savings can be substantial. It is possible to obtain up to 60% more capacity by this calculation for both homogenous and hybrid girders for girders with high web depths in compression and narrow flanges ($D_c/D = 0.75$, $D/b_{fc} = 6$, $D/t_w = 300$). The least savings obtained are in the order of 10% for doubly-symmetric girders with $D/t_w = 300$, and $D/b_{fc} = 4$. The savings increase up to 20% for identical girders with $D/b_{fc} = 6$. However, for cases where AASHTO recommends that R_b be taken as 1.0, the proposed and the current equations are identical.

12.2.2 Proposed Modifications to LTB Equations

1. Based on extensive sensitivity studies considering experimental tests and various rolled and welded type plate girder sections, the use of one half of the AWS fabrication tolerances are recommended as the initial geometric imperfections to be used in FE test simulations. This constitutes using $L_b/2000$ as the flange sweep, and $D/300$ for the web out-of-flatness for unstiffened girders, and a flange tilt which is the smaller of 1/8 in or $b_{fc}/200$. The web out-of-flatness is $D/134$ for longitudinally stiffened girders. This is to be combined with one-half Lehigh residual stresses for rolled beams and one-half Best-fit Prawel residual stresses for welded plate girders.

2. A smaller plateau length $L_p = 0.63 r_t \sqrt{E/F_y}$, and a smaller $F_{yr} = 0.5F_y$ are recommended within the AISC and AASHTO LTB equations based on uniform bending studies. The current Specification provisions allow a longer plateau length for rolled beams, which cannot be justified based on simulations. The current LTB

design equations also limit the value of F_{yr} to be the smaller of $0.7F_{yc}$ or F_{yw}, but not less than $0.5F_{yc}$. The proposed equations simplify the equations by providing a single value of L_p and a single value of F_{yr} for all types of cross-sections.

3. The recommendations based on uniform bending studies are also evaluated for applicability to moment gradient loading.

   a. It is observed that behavior of beams with transverse loading within the unbraced length is different from girders with linear moment gradient loading with no transverse loading. This is principally due to the location of the maximum moment with respect to the brace point. A modification factor to the inelastic LTB equation is proposed which addresses this discrepancy, as explained in detail in Section 7.2. Further studies on noncompact and slender web sections with transverse loading are required to validate the proposed equation.

   b. The C_b equations defined in the AISC and AASHTO are based on elastic buckling solutions. Scaling of the entire inelastic LTB curve by a C_b based on elastic buckling solutions often gives predictions higher than the FE test simulation data, especially for cross-sections that have narrower flanges compared to web depths. In other words, an "inelastic C_b" effect is observed. This behavior is corroborated by rigorous inelastic buckling solutions in SABRE2 which are based on the proposed LTB equations.

   c. The C_b equations in the current Specifications are based on the assumption of torsionally simply-supported end conditions. It is shown in this research that warping fixity at either or both ends combined with an effective length factor,

$K < 1$ results in an over-prediction of FE test data in the elastic LTB region of the curve. With greater warping fixity, the K value is smaller and the discrepancy with the test data is larger. Further research is required to assess the influence of warping rigidity on the moment modification factor.

d. Moment-shear interaction is not observed for compact web rolled beams, but is observed to be a concern for slender web unstiffened girders. A combination of moment-shear interaction and an "inelastic C_b" effects, along with potential web distortion leads to lower strengths in FE test simulations as compared to the current or proposed equations. It is noted that an interaction equation of the form similar to the equations in the Specifications for cold-formed steel, AISI (2014) gives reasonable predictions of test data in such situations.

4. The LTB equations are extended to longitudinally stiffened girders as detailed in Section 8.3. This model recognizes that the load shedding factor, R_b need not be used as a factor on the LTB resistance equations, if LTB precedes web bend-buckling. The proposed model allows R_b to be taken as 1.0 if the LTB strength of the girder is smaller than the web buckling strength, F_{crw}. AASHTO allows the computation of R_b based on the compression flange stress, but does not include this additional test for the relative magnitude of F_{crw} and the elastic buckling stress. This is a more optimistic approach to the LTB resistances of longitudinally stiffened girders than the current AASHTO provisions.

12.2.3 Proposed Modifications to Noncompact Web Slenderness Limit

In course of the studies conducted on unstiffened girders, it is observed that the current noncompact web slenderness limit, λ_{rw} in AASHTO and AISC is optimistic for cross-sections with narrow flanges. By recognizing that the relative areas of the flanges and the web influence the web buckling strength of the cross-section, an improved equation for λ_{rw} is developed in Section 6.6.

12.2.4 Increased Transverse Stiffener Spacing for Longitudinally Stiffened Girders

1. It is observed that the longitudinal stiffeners do not contribute significantly to the shear strength of the girders, and that the current AASHTO shear strength provisions compare reasonably well with FE simulation results. The shear strength model recommended by Cooper (1965) is evaluated along with the current AASHTO shear strength model and no compelling reasons are found for the use of Cooper's model. That is, there are cases where Cooper's model gives some modest improvements relative to the current AASTHO equations, but there are also cases where the AASHTO model performs somewhat better than Cooper's model.

2. It is demonstrated that the strengths are predicted accurately to conservatively without considering moment-shear strength interaction. The results for high moment-high shear tests fall within the scatter-band of results observed by other researchers (White et al. 2008) for transversely stiffened girders.

3. Furthermore, it is shown that the current AASHTO limit of 1.5 on the panel aspect ratio (d_o/D) can be increased safely to 2.0 for both homogenous and hybrid girders.

4. The proposed R_b model and proposed LTB equations for longitudinally stiffened girders are shown to be valid for moment gradient loading.

12.2.5 Studies on Curved Longitudinally Stiffened Girders

The proposed yield limit state model is also evaluated for its applicability with respect to horizontally curved girders with short unbraced lengths, subjected to uniform bending, and where the flange lateral bending stresses are small. It is observed that the yield limit state model performs well, and that curvature of web has negligible effect on the overall flexural capacity of the girder at small values of the flange lateral bending stresses.

12.3 Recommendations for Future Work

The research conducted to date is a comprehensive study of the flexural resistance of I-girders. The studies have encompassed various limit states and loading conditions. However, there are areas that merit further investigation, some of which are listed below.

1. The behavior of girders with more than one longitudinal stiffener needs to be studied. This will allow the use of girders with more slender webs, and expand the possibilities of design.

2. The behavior of girders with lower strength longitudinal stiffeners than the web plate may be studied.

3. Some Moment-Shear interaction was observed for unstiffened slender web girders in Section 7.3, but it merits further research.

4. It is recommended that further studies be conducted on the appropriate C_b to use in the inelastic LTB region, and for conditions with warping fixity at the girder ends. It is apparent that computational tools such as SABRE2 using stiffness reduction

factors are advantageous over theoretical expressions that may be limited in scope with regard to end restraints and loading conditions.

5. It is recommended that moment gradient effects for unstiffened noncompact and slender web plate girders and longitudinally stiffened plate girders be studied with transverse loading within the unbraced length.

6. The behavior of horizontally curved longitudinally stiffened girders under LTB limit state should be investigated. The applicability of the one-third rule for the compression flange resistance needs to be investigated thoroughly in the context of longitudinally stiffened girders. An increase in the limits of the curvature parameter, Z is also a potential area of research.

APPENDIX A

ADDITIONAL RESULTS FOR LTB OF UNSTIFFENED GIRDERS

SUBJECTED TO UNIFORM BENDING

This section provides the complete set of results for all rolled beams, and homogenous and hybrid welded type plate girders discussed in Chapter 6.These girders are subjected to uniform bending.

Table A-1 lists the results for rolled beams, while Tables A-2 through A-15 list the results for homogenous and hybrid welded girders.

The tables are followed by figures that graphically represent the same data.

Table A-1: Test simulation results and comparison with proposed and AISC equations for rolled beams subjected to uniform moment

W21x44	L_b (inches)	26.7	40.1	53.4	87.6	121.8	156.0	187.2	218.4	273.0
	M_{max}/M_p	0.97	0.92	0.89	0.69	0.59	0.47	0.37	0.30	0.22
	M_{max}/M_{nPr}	0.98	0.97	0.98	0.89	0.88	0.87	0.85	0.88	0.89
	M_{max}/M_{nAISC}	0.97	0.92	0.89	0.80	0.80	0.79	0.85	0.88	0.89
W14x68	L_b (inches)	52.1	78.2	104.3	186.7	269.2	351.6	421.9	492.2	615.3
	M_{max}/M_p	0.97	0.94	0.90	0.76	0.65	0.54	0.46	0.40	0.34
	M_{max}/M_{nPr}	0.98	0.99	0.98	0.93	0.92	0.91	0.92	0.96	1.04
	M_{max}/M_{nAISC}	0.97	0.94	0.90	0.86	0.86	0.86	0.93	0.96	1.04
W10x30	L_b (inches)	29.0	43.6	58.1	103.1	148.2	193.2	231.8	270.5	338.1
	M_{max}/M_p	1.00	0.97	0.94	0.83	0.72	0.58	0.48	0.41	0.34
	M_{max}/M_{nPr}	1.01	1.02	1.03	1.03	1.03	0.98	0.98	1.03	1.07
	M_{max}/M_{nAISC}	1.00	0.97	0.94	0.95	0.96	0.93	0.98	1.01	1.07
W16x31	L_b (inches)	24.8	37.2	49.6	80.6	111.7	142.8	171.4	199.9	249.9
	M_{max}/M_p	0.97	0.94	0.90	0.78	0.67	0.53	0.41	0.33	0.25
	M_{max}/M_{nPr}	0.99	1.00	1.01	0.99	1.00	0.95	0.92	0.97	0.96
	M_{max}/M_{nAISC}	0.97	0.94	0.90	0.89	0.91	0.86	0.92	0.94	0.96
W14x90	L_b (inches)	90.6	135.9	181.2	290.8	400.4	510.0	612.0	714.0	892.5
	M_{max}/M_p	0.97	0.95	0.91	0.84	0.74	0.65	0.56	0.49	0.43
	M_{max}/M_{nPr}	1.00	1.01	1.02	1.05	1.07	1.08	1.11	1.17	1.26
	M_{max}/M_{nAISC}	1.00	0.97	0.94	0.95	0.98	1.02	1.07	1.12	1.26

Table A-2: Test simulation results and comparison with proposed and AASHTO equations for plate girders subjected to uniform moment, Girders G1 – G5

G1	L_b (inches)	64.1	96.1	216.4	304.7	481.2	577.4	673.7	842.1		
	M_{max}/M_y	0.94	0.91	0.77	0.66	0.49	0.41	0.34	0.25		
	M_{max}/M_{nPr}	0.97	0.96	0.93	0.89	0.87	0.86	0.97	1.12		
	$M_{max}/M_{nAASHTO}$	0.91	0.89	0.81	0.76	0.70	0.80	0.89	1.01		
G2	L_b (inches)	72.0	108.0	144.0	242.8	341.9	440.9	540.0	648.0	756.0	944.9
	M_{max}/M_y	0.94	0.93	0.92	0.80	0.76	0.66	0.55	0.43	0.35	0.25
	M_{max}/M_{nPr}	1.12	1.11	1.11	0.96	1.01	1.01	0.96	0.90	0.98	1.10
	$M_{max}/M_{nAASHTO}$	1.00	0.99	0.98	0.85	0.87	0.84	0.77	0.84	0.90	0.99
G3	L_b (inches)	157.0	235.5	314.0	530.2	746.5	962.7	1179.0	1414.8	1650.5	2063.2
	M_{max}/M_y	1.05	1.03	1.02	0.94	0.86	0.76	0.63	0.49	0.39	0.27
	M_{max}/M_{nPr}	1.03	1.02	1.05	1.06	1.08	1.08	1.01	0.93	0.93	0.98
	$M_{max}/M_{nAASHTO}$	1.03	1.01	1.00	0.99	0.99	0.96	0.87	0.89	0.93	0.98
G4	L_b (inches)	154.3	231.5	308.6	521.2	733.8	946.3	1158.9	1390.7	1622.5	2028.1
	M_{max}/M_y	1.03	1.02	1.01	0.93	0.85	0.75	0.61	0.48	0.37	0.27
	M_{max}/M_{nPr}	1.17	1.16	1.15	1.06	1.07	1.07	1.00	0.92	0.94	1.00
	$M_{max}/M_{nAASHTO}$	1.10	1.09	1.08	1.00	0.98	0.96	0.86	0.89	0.94	1.00
G5	L_b (inches)	68.5	102.8	137.0	231.4	325.8	420.2	514.6	617.5	720.4	900.5
	M_{max}/M_y	0.90	0.89	0.88	0.83	0.74	0.66	0.55	0.43	0.34	0.24
	M_{max}/M_{nPr}	1.01	1.01	1.04	1.08	1.07	1.08	1.04	0.98	1.05	1.16
	$M_{max}/M_{nAASHTO}$	0.96	0.95	0.94	0.96	0.93	0.91	0.84	0.94	1.00	1.10

Table A-3: Test simulation results and comparison with proposed and AASHTO equations for plate girders subjected to uniform moment, Girders G6 – G10

G6	L_b (inches)	65.9	98.8	131.7	222.4	313.2	403.9	494.6	593.5	692.4	865.6
	M_{max}/M_y	0.86	0.86	0.85	0.78	0.72	0.63	0.54	0.42	0.33	0.23
	M_{max}/M_{nPr}	1.13	1.12	1.12	1.03	1.05	1.06	1.04	0.96	1.04	1.14
	$M_{max}/M_{nAASHTO}$	1.01	1.01	1.00	0.92	0.91	0.88	0.83	0.91	0.99	1.08
G7	L_b (inches)	160.8	241.2	321.6	543.1	764.6	986.1	1207.6	1449.2	1690.7	2113.3
	M_{max}/M_y	1.00	0.99	0.97	0.90	0.84	0.76	0.62	0.48	0.38	0.27
	M_{max}/M_{nPr}	1.02	1.03	1.05	1.07	1.12	1.14	1.08	0.98	1.05	1.16
	$M_{max}/M_{nAASHTO}$	1.02	1.02	1.00	1.00	1.02	1.00	0.91	0.98	1.05	1.16
G8	L_b (inches)	158.8	238.2	317.5	536.3	754.9	973.7	1192.4	1441.1	1681.3	2101.6
	M_{max}/M_y	0.99	0.98	0.97	0.90	0.83	0.75	0.61	0.47	0.37	0.26
	M_{max}/M_{nPr}	1.17	1.16	1.15	1.07	1.11	1.13	1.07	0.98	1.04	1.15
	$M_{max}/M_{nAASHTO}$	1.11	1.10	1.08	1.00	1.01	1.00	0.90	0.98	1.04	1.15
G9	L_b (inches)	60.6	90.9	121.2	204.7	288.2	371.6	455.2	546.2	637.2	796.6
	M_{max}/M_y	0.87	0.84	0.82	0.75	0.69	0.62	0.54	0.45	0.37	0.29
	M_{max}/M_{nPr}	0.98	0.95	0.96	0.97	1.00	1.00	1.00	1.00	1.12	1.35
	$M_{max}/M_{nAASHTO}$	0.92	0.88	0.87	0.85	0.86	0.83	0.80	0.94	1.10	1.32
G10	L_b (inches)	68.0	102.1	136.1	229.8	323.5	417.2	510.9	613.1	715.3	894.1
	M_{max}/M_y	0.84	0.83	0.82	0.76	0.70	0.62	0.55	0.45	0.38	0.29
	M_{max}/M_{nPr}	1.08	1.06	1.06	0.99	1.00	1.01	1.02	1.00	1.14	1.34
	$M_{max}/M_{nAASHTO}$	0.96	0.95	0.94	0.88	0.86	0.84	0.82	0.94	1.07	1.26

Table A-4: Test simulation results and comparison with proposed and AASHTO equations for plate girders subjected to uniform moment, Girders G11 – G15

G11	L_b (inches)	153.2	229.9	306.5	517.6	728.7	939.8	1150.8	1381.0	1611.2	2014.0
	M_{max}/M_y	0.99	0.98	0.97	0.90	0.83	0.76	0.65	0.52	0.43	0.33
	M_{max}/M_{nPr}	1.01	1.02	1.04	1.07	1.10	1.12	1.10	1.06	1.17	1.39
	$M_{max}/M_{nAASHTO}$	1.01	1.00	0.99	0.99	1.00	0.99	0.93	1.05	1.17	1.39
G12	L_b (inches)	150.1	225.2	300.3	507.1	713.9	920.7	1127.5	1352.9	1578.4	1973.0
	M_{max}/M_y	0.95	0.96	0.95	0.89	0.82	0.74	0.63	0.51	0.42	0.32
	M_{max}/M_{nPr}	1.12	1.14	1.13	1.06	1.08	1.11	1.08	1.04	1.15	1.36
	$M_{max}/M_{nAASHTO}$	1.06	1.08	1.06	0.99	0.99	0.98	0.92	1.03	1.15	1.36
G13	L_b (inches)	65.4	98.1	130.8	220.9	310.9	401.0	491.1	589.3	687.5	859.4
	M_{max}/M_y	0.83	0.81	0.80	0.74	0.68	0.61	0.54	0.44	0.35	0.26
	M_{max}/M_{nPr}	1.03	1.03	1.05	1.07	1.10	1.12	1.13	1.08	1.20	1.38
	$M_{max}/M_{nAASHTO}$	0.98	0.96	0.95	0.94	0.95	0.93	0.90	1.02	1.13	1.31
G14	L_b (inches)	62.5	93.8	125.0	211.1	297.3	383.4	469.5	563.4	657.3	821.6
	M_{max}/M_y	0.77	0.76	0.76	0.71	0.66	0.59	0.51	0.43	0.35	0.26
	M_{max}/M_{nPr}	1.15	1.13	1.12	1.05	1.09	1.10	1.09	1.09	1.20	1.40
	$M_{max}/M_{nAASHTO}$	1.01	1.00	0.99	0.93	0.93	0.91	0.87	1.02	1.13	1.31
G15	L_b (inches)	157.8	236.7	315.5	532.9	750.2	967.5	1184.9	1421.8	1658.8	2073.5
	M_{max}/M_y	0.97	0.95	0.94	0.87	0.82	0.74	0.63	0.50	0.40	0.30
	M_{max}/M_{nPr}	1.03	1.03	1.06	1.08	1.12	1.15	1.11	1.05	1.14	1.33
	$M_{max}/M_{nAASHTO}$	1.03	1.02	1.01	1.01	1.02	1.01	0.94	1.04	1.14	1.33

Table A-5: Test simulation results and comparison with proposed and AASHTO equations for plate girders subjected to uniform moment, Girders G16 – G20

G16	L_b (inches)	155.4	233.1	310.8	524.8	738.9	952.9	1167.0	1400.4	1633.8	2042.2
	M_{max}/M_y	0.94	0.94	0.93	0.86	0.81	0.73	0.62	0.49	0.39	0.29
	M_{max}/M_{nPr}	1.17	1.17	1.15	1.08	1.12	1.15	1.11	1.05	1.14	1.32
	$M_{max}/M_{nAASHTO}$	1.10	1.10	1.09	1.01	1.02	1.01	0.94	1.05	1.14	1.32
G17	L_b (inches)	60.6	90.9	121.2	204.7	288.2	371.7	455.2	546.2	637.2	796.5
	M_{max}/M_y	0.80	0.76	0.75	0.69	0.64	0.57	0.50	0.43	0.37	0.30
	M_{max}/M_{nPr}	0.98	0.95	0.97	0.98	1.02	1.03	1.05	1.10	1.28	1.64
	$M_{max}/M_{nAASHTO}$	0.92	0.87	0.86	0.85	0.87	0.84	0.84	1.02	1.20	1.53
G18	L_b (inches)	68.0	102.1	136.1	229.8	323.5	417.2	510.9	613.1	715.3	894.1
	M_{max}/M_y	0.77	0.76	0.75	0.70	0.65	0.58	0.51	0.44	0.37	0.31
	M_{max}/M_{nPr}	1.09	1.06	1.06	1.00	1.03	1.04	1.07	1.11	1.30	1.70
	$M_{max}/M_{nAASHTO}$	0.96	0.94	0.93	0.87	0.87	0.86	0.86	1.04	1.22	1.59
G19	L_b (inches)	153.2	229.9	306.5	517.6	728.7	939.8	1150.8	1381.0	1611.2	2014.0
	M_{max}/M_y	0.95	0.94	0.93	0.87	0.81	0.73	0.64	0.53	0.45	0.37
	M_{max}/M_{nPr}	1.01	1.02	1.04	1.07	1.11	1.14	1.14	1.13	1.31	1.69
	$M_{max}/M_{nAASHTO}$	1.01	1.00	0.99	1.00	1.01	1.00	0.96	1.13	1.31	1.69
G20	L_b (inches)	150.1	225.2	300.3	507.1	713.9	920.7	1127.5	1352.9	1578.4	1973.0
	M_{max}/M_y	0.90	0.92	0.91	0.85	0.79	0.72	0.63	0.52	0.45	0.37
	M_{max}/M_{nPr}	1.13	1.16	1.14	1.08	1.11	1.14	1.15	1.16	1.35	1.75
	$M_{max}/M_{nAASHTO}$	1.05	1.08	1.06	1.00	1.00	0.99	0.96	1.14	1.33	1.73

Table A-6: Test simulation results and comparison with proposed and AASHTO equations for plate girders subjected to uniform moment, Girders G21 – G25

G21	L_b (inches)	65.4	98.1	130.8	220.9	310.9	401.0	491.1	589.3	687.5	859.4
	M_{max}/M_y	0.76	0.75	0.74	0.68	0.64	0.57	0.51	0.41	0.34	0.26
	M_{max}/M_{nPr}	1.11	1.10	1.13	1.15	1.20	1.22	1.25	1.24	1.39	1.68
	$M_{max}/M_{nAASHTO}$	1.03	1.01	1.00	1.00	1.01	1.00	0.99	1.16	1.30	1.57
G22	L_b (inches)	62.5	93.8	125.0	211.1	297.3	383.4	469.5	563.4	657.3	821.6
	M_{max}/M_y	0.71	0.70	0.69	0.65	0.61	0.55	0.48	0.40	0.33	0.26
	M_{max}/M_{nPr}	1.23	1.21	1.20	1.14	1.19	1.21	1.23	1.26	1.43	1.73
	$M_{max}/M_{nAASHTO}$	1.07	1.05	1.05	0.98	1.00	0.98	0.97	1.17	1.32	1.60
G23	L_b (inches)	157.8	236.7	315.5	532.9	750.2	967.5	1184.9	1421.8	1658.8	2073.5
	M_{max}/M_y	0.93	0.92	0.91	0.85	0.80	0.72	0.61	0.49	0.40	0.31
	M_{max}/M_{nPr}	1.05	1.06	1.08	1.10	1.16	1.18	1.16	1.10	1.24	1.49
	$M_{max}/M_{nAASHTO}$	1.05	1.04	1.03	1.03	1.05	1.04	0.98	1.10	1.24	1.49
G24	L_b (inches)	155.4	233.1	310.8	524.8	738.9	952.9	1167.0	1400.4	1633.8	2042.2
	M_{max}/M_y	0.90	0.90	0.89	0.83	0.78	0.71	0.61	0.49	0.40	0.31
	M_{max}/M_{nPr}	1.19	1.20	1.18	1.11	1.16	1.19	1.17	1.13	1.26	1.53
	$M_{max}/M_{nAASHTO}$	1.12	1.13	1.11	1.04	1.05	1.05	0.99	1.13	1.26	1.53
G25	L_b (inches)	82.8	124.1	165.5	279.5	393.5	507.5	621.5	745.8	870.1	1088.0
	M_{max}/M_y	0.98	0.98	0.97	0.89	0.80	0.70	0.57	0.45	0.35	0.25
	M_{max}/M_{nPr}	1.01	1.02	1.05	1.06	1.06	1.06	0.99	0.92	1.00	1.11
	$M_{max}/M_{nAASHTO}$	0.96	0.95	0.95	0.94	0.92	0.89	0.81	0.86	0.92	0.99

Table A-7: Test simulation results and comparison with proposed and AASHTO equations for plate girders subjected to uniform moment, Girders G26 – G30

G26	L_b (inches)	79.7	119.5	159.3	269.0	378.7	488.5	598.2	717.8	837.4	1046.8
	M_{max}/M_y	0.94	0.95	0.94	0.87	0.77	0.68	0.56	0.44	0.35	0.25
	M_{max}/M_{nPr}	1.12	1.13	1.12	1.05	1.03	1.03	0.98	0.91	0.99	1.10
	$M_{max}/M_{nAASHTO}$	1.00	1.01	1.00	0.93	0.89	0.87	0.79	0.85	0.91	0.99
G27	L_b (inches)	110.9	166.3	221.7	374.4	527.1	679.7	832.4	998.9	1165.4	1456.8
	M_{max}/M_y	1.02	1.02	1.01	0.92	0.83	0.73	0.60	0.46	0.36	0.26
	M_{max}/M_{nPr}	1.02	1.04	1.06	1.06	1.08	1.08	1.01	0.93	0.99	1.10
	$M_{max}/M_{nAASHTO}$	0.99	1.00	0.98	0.97	0.96	0.93	0.84	0.88	0.92	0.99
G28	L_b (inches)	107.8	161.7	215.6	364.1	512.5	661.0	809.5	971.4	1133.3	1416.6
	M_{max}/M_y	0.97	0.99	0.99	0.90	0.82	0.72	0.59	0.46	0.36	0.25
	M_{max}/M_{nPr}	1.14	1.15	1.16	1.06	1.08	1.07	1.00	0.93	0.99	1.10
	$M_{max}/M_{nAASHTO}$	1.04	1.05	1.06	0.96	0.95	0.92	0.83	0.88	0.92	1.00
G29	L_b (inches)	82.8	124.1	165.5	279.5	393.5	507.5	621.5	745.8	870.1	1087.6
	M_{max}/M_y	0.89	0.88	0.87	0.82	0.73	0.66	0.55	0.45	0.37	0.28
	M_{max}/M_{nPr}	0.99	1.00	1.03	1.07	1.07	1.09	1.07	1.08	1.21	1.43
	$M_{max}/M_{nAASHTO}$	0.93	0.92	0.92	0.93	0.90	0.89	0.87	1.01	1.13	1.34
G30	L_b (inches)	79.7	119.5	159.3	269.0	378.7	488.5	598.2	717.8	837.4	1046.8
	M_{max}/M_y	0.85	0.84	0.84	0.80	0.70	0.63	0.53	0.44	0.36	0.27
	M_{max}/M_{nPr}	1.08	1.08	1.08	1.03	1.02	1.05	1.03	1.06	1.18	1.40
	$M_{max}/M_{nAASHTO}$	0.96	0.96	0.96	0.91	0.87	0.87	0.85	1.00	1.12	1.33

Table A-8: Test simulation results and comparison with proposed and AASHTO equations for plate girders subjected to uniform moment, Girders G31 – G35

G31	L_b (inches)	110.8	166.3	221.7	374.4	527.1	679.7	832.4	998.9	1165.4	1456.8
	M_{max}/M_y	0.94	0.94	0.94	0.86	0.79	0.71	0.59	0.48	0.39	0.29
	M_{max}/M_{nPr}	1.00	1.01	1.05	1.07	1.09	1.11	1.08	1.07	1.19	1.40
	$M_{max}/M_{nAASHTO}$	0.97	0.97	0.97	0.97	0.96	0.95	0.90	1.04	1.16	1.37
G32	L_b (inches)	107.8	161.7	215.6	364.1	512.5	661.0	809.5	971.4	1133.3	1416.6
	M_{max}/M_y	0.88	0.89	0.89	0.84	0.76	0.68	0.58	0.46	0.38	0.28
	M_{max}/M_{nPr}	1.11	1.12	1.12	1.06	1.08	1.10	1.07	1.07	1.19	1.39
	$M_{max}/M_{nAASHTO}$	1.00	1.01	1.01	0.95	0.94	0.92	0.89	1.03	1.14	1.34
G33	L_b (inches)	82.8	124.1	165.5	279.5	393.5	507.5	621.5	745.8	870.1	1087.6
	M_{max}/M_y	0.82	0.81	0.81	0.76	0.68	0.61	0.53	0.44	0.38	0.31
	M_{max}/M_{nPr}	0.98	0.99	1.02	1.07	1.07	1.11	1.10	1.19	1.39	1.79
	$M_{max}/M_{nAASHTO}$	0.92	0.91	0.91	0.94	0.91	0.91	0.93	1.13	1.31	1.69
G34	L_b (inches)	79.7	119.5	159.3	269.0	378.7	488.5	598.2	717.8	837.4	1046.8
	M_{max}/M_y	0.78	0.77	0.77	0.74	0.65	0.59	0.51	0.43	0.37	0.31
	M_{max}/M_{nPr}	1.08	1.08	1.08	1.05	1.05	1.08	1.09	1.19	1.40	1.83
	$M_{max}/M_{nAASHTO}$	0.96	0.95	0.95	0.92	0.89	0.88	0.92	1.12	1.32	1.71
G35	L_b (inches)	110.8	166.3	221.7	374.4	527.1	679.7	832.4	998.9	1165.4	1456.8
	M_{max}/M_y	0.88	0.88	0.88	0.81	0.75	0.68	0.58	0.47	0.41	0.34
	M_{max}/M_{nPr}	1.01	1.02	1.07	1.09	1.12	1.16	1.15	1.19	1.39	1.79
	$M_{max}/M_{nAASHTO}$	0.96	0.96	0.97	0.97	0.97	0.97	0.96	1.14	1.33	1.71

Table A-9: Test simulation results and comparison with proposed and AASHTO equations for plate girders subjected to uniform moment, Girders G36 – G40

G36	L_b (inches)	107.8	161.7	215.6	364.1	512.5	661.0	809.5	971.4	1133.3	1416.6
	M_{max}/M_y	0.83	0.83	0.83	0.79	0.72	0.64	0.56	0.47	0.40	0.33
	M_{max}/M_{nPr}	1.11	1.11	1.12	1.08	1.11	1.13	1.14	1.21	1.41	1.84
	$M_{max}/M_{nAASHTO}$	0.99	1.00	1.00	0.95	0.95	0.94	0.96	1.15	1.34	1.75
G37	L_b (inches)	66.0	99.0	132.0	222.8	313.7	404.6	495.5	594.6	693.7	867.1
	M_{max}/M_y	0.98	0.98	0.97	0.88	0.79	0.69	0.57	0.44	0.35	0.25
	M_{max}/M_{nPr}	1.24	1.23	1.21	1.10	1.02	1.01	0.95	0.89	0.96	1.07
	$M_{max}/M_{nAASHTO}$	1.10	1.09	1.08	0.98	0.90	0.87	0.79	0.85	0.91	0.99
G38	L_b (inches)	73.8	110.7	147.7	249.4	351.1	452.7	554.4	665.3	776.2	970.3
	M_{max}/M_y	0.97	0.97	0.97	0.88	0.79	0.69	0.57	0.44	0.35	0.25
	M_{max}/M_{nPr}	1.19	1.19	1.19	1.09	1.03	1.02	0.96	0.89	0.96	1.07
	$M_{max}/M_{nAASHTO}$	1.07	1.07	1.07	0.98	0.90	0.87	0.80	0.86	0.91	0.99
G39	L_b (inches)	84.7	127.1	169.6	286.2	403.0	519.7	636.5	763.8	891.1	1113.8
	M_{max}/M_y	0.99	0.99	0.99	0.90	0.81	0.72	0.59	0.45	0.36	0.25
	M_{max}/M_{nPr}	1.25	1.25	1.25	1.12	1.04	1.03	0.96	0.89	0.91	0.99
	$M_{max}/M_{nAASHTO}$	1.12	1.12	1.12	1.01	0.93	0.90	0.82	0.87	0.91	0.99
G40	L_b (inches)	81.6	122.4	163.2	275.7	388.1	500.5	612.9	735.5	858.1	1072.7
	M_{max}/M_y	0.97	0.98	0.89	0.89	0.80	0.70	0.58	0.45	0.36	0.25
	M_{max}/M_{nPr}	1.20	1.21	1.11	1.11	1.04	1.03	0.97	0.90	0.96	1.07
	$M_{max}/M_{nAASHTO}$	1.08	1.09	0.99	1.00	0.92	0.89	0.81	0.86	0.92	0.99

Table A-10: Test simulation results and comparison with proposed and AASHTO equations for plate girders subjected to uniform moment, Girders G41 – G45

G41	L_b (inches)	112.7	169.0	225.3	380.5	535.7	690.9	846.1	1015.4	1184.6	1480.8
	M_{max}/M_y	1.01	1.01	0.87	0.90	0.83	0.74	0.60	0.46	0.36	0.26
	M_{max}/M_{nPr}	1.13	1.13	0.98	1.02	1.05	1.05	0.98	0.90	0.93	0.99
	$M_{max}/M_{nAASHTO}$	1.13	1.13	0.98	1.01	0.96	0.93	0.84	0.88	0.93	0.99
G42	L_b (inches)	109.8	164.7	219.6	370.8	475.0	522.0	673.2	824.4	1154.2	1442.7
	M_{max}/M_y	0.99	1.00	0.99	0.87	0.87	0.82	0.73	0.59	0.36	0.25
	M_{max}/M_{nPr}	1.16	1.17	1.16	1.02	1.06	1.05	1.05	0.98	0.93	1.00
	$M_{max}/M_{nAASHTO}$	1.11	1.12	1.11	0.97	0.97	0.95	0.92	0.83	0.93	1.00
G43	L_b (inches)	158.7	238.0	317.4	535.9	754.5	973.1	1191.7	1430.0	1668.3	2085.4
	M_{max}/M_y	0.98	0.98	0.96	0.90	0.85	0.76	0.62	0.48	0.38	0.27
	M_{max}/M_{nPr}	1.10	1.10	1.07	1.03	1.08	1.09	1.02	0.92	0.94	0.98
	$M_{max}/M_{nAASHTO}$	1.10	1.10	1.07	1.00	0.99	0.96	0.87	0.89	0.94	0.98
G44	L_b (inches)	156.2	234.4	312.5	527.7	742.9	958.1	1173.3	1408.0	1642.6	2053.3
	M_{max}/M_y	0.99	0.99	0.97	0.91	0.84	0.75	0.62	0.47	0.37	0.26
	M_{max}/M_{nPr}	1.13	1.13	1.11	1.04	1.07	1.08	1.01	0.92	0.94	1.00
	$M_{max}/M_{nAASHTO}$	1.11	1.11	1.09	1.02	0.98	0.96	0.86	0.89	0.94	1.00
G45	L_b (inches)	65.8	98.7	131.6	222.2	312.8	403.5	494.1	592.9	691.8	864.7
	M_{max}/M_y	1.08	1.05	1.03	0.92	0.79	0.69	0.57	0.46	0.37	0.27
	M_{max}/M_{nPr}	1.15	1.13	1.11	1.01	0.97	0.96	0.92	0.88	0.92	1.00
	$M_{max}/M_{nAASHTO}$	1.07	1.05	1.03	0.92	0.87	0.85	0.80	0.85	0.92	1.00

Table A-11: Test simulation results and comparison with proposed and AASHTO equations for plate girders subjected to uniform moment, Girders G46 – G50

G46	L_b (inches)	158.3	237.5	316.6	534.7	752.8	970.9	1189.0	1426.8	1664.5	2080.7
	M_{max}/M_y	1.00	0.99	0.98	0.88	0.85	0.77	0.64	0.50	0.40	0.29
	M_{max}/M_{nPr}	1.00	1.00	1.02	1.00	1.07	1.08	1.02	0.94	0.93	0.99
	$M_{max}/M_{nAASHTO}$	1.00	0.99	0.97	0.94	0.98	0.96	0.88	0.89	0.93	0.99
G47	L_b (inches)	63.8	95.9	127.8	215.8	303.8	391.8	479.9	575.8	671.8	839.8
	M_{max}/M_y	1.07	1.03	1.01	0.89	0.77	0.67	0.56	0.44	0.36	0.27
	M_{max}/M_{nPr}	1.00	0.98	1.00	0.97	0.94	0.93	0.89	0.87	0.91	1.00
	$M_{max}/M_{nAASHTO}$	0.94	0.91	0.89	0.86	0.83	0.82	0.78	0.84	0.91	1.00
G48	L_b (inches)	156.5	234.8	313.0	528.6	744.2	959.7	1175.3	1410.4	1645.4	2056.8
	M_{max}/M_y	1.04	1.05	1.05	0.96	0.86	0.77	0.64	0.51	0.41	0.30
	M_{max}/M_{nPr}	0.96	0.97	1.01	1.02	1.02	1.03	0.99	0.94	0.93	0.98
	$M_{max}/M_{nAASHTO}$	0.96	0.96	0.97	0.96	0.94	0.94	0.88	0.88	0.93	0.98
G49	L_b (inches)	60.4	90.6	120.7	203.9	287.0	370.2	453.4	544.0	634.7	793.4
	M_{max}/M_y	0.99	0.93	0.90	0.82	0.73	0.66	0.57	0.48	0.41	0.32
	M_{max}/M_{nPr}	1.02	0.97	0.98	0.97	0.97	0.99	0.98	0.99	1.15	1.41
	$M_{max}/M_{nAASHTO}$	0.93	0.88	0.85	0.83	0.81	0.79	0.76	0.74	0.80	0.86
G50	L_b (inches)	152.6	228.9	305.3	515.5	725.7	936.0	1146.2	1375.4	1604.7	2005.8
	M_{max}/M_y	1.05	1.04	1.02	0.95	0.86	0.78	0.67	0.56	0.47	0.37
	M_{max}/M_{nPr}	1.01	1.01	1.02	1.01	0.99	0.98	0.93	0.85	0.82	0.84
	$M_{max}/M_{nAASHTO}$	1.01	1.00	0.98	0.97	0.94	0.91	0.85	0.77	0.79	0.84

Table A-12: Test simulation results and comparison with proposed and AASHTO equations for plate girders subjected to uniform moment, Girders G51 – G55

G51	L_b (inches)	57.1	85.7	114.2	183.2	252.1	321.0	390.0	468.0	545.9	682.4
	M_{max}/M_y	1.03	0.98	0.94	0.81	0.71	0.62	0.52	0.42	0.34	0.25
	M_{max}/M_{nPr}	1.03	1.00	1.00	0.95	0.91	0.90	0.86	0.83	0.89	0.98
	$M_{max}/M_{nAASHTO}$	0.93	0.89	0.86	0.82	0.78	0.77	0.73	0.81	0.89	0.98
G52	L_b (inches)	53.7	80.6	107.4	172.3	237.1	301.9	366.8	440.1	513.5	641.9
	M_{max}/M_y	1.08	0.98	0.92	0.81	0.70	0.63	0.55	0.47	0.41	0.33
	M_{max}/M_{nPr}	1.08	1.00	0.98	0.94	0.91	0.92	0.93	0.96	1.13	1.42
	$M_{max}/M_{nAASHTO}$	0.95	0.86	0.82	0.78	0.74	0.73	0.71	0.70	0.75	0.82
G53	L_b (inches)	65.3	98.0	130.7	209.5	288.4	367.2	446.1	535.3	624.5	780.7
	M_{max}/M_y	1.03	0.97	0.93	0.84	0.74	0.66	0.58	0.49	0.42	0.34
	M_{max}/M_{nPr}	1.03	0.99	0.99	0.98	0.97	0.98	0.97	1.00	1.16	1.45
	$M_{max}/M_{nAASHTO}$	0.91	0.85	0.83	0.81	0.79	0.78	0.75	0.74	0.79	0.85
G54	L_b (inches)	162.6	243.9	325.2	521.4	717.6	913.8	1110.0	1332.0	1554.0	1942.6
	M_{max}/M_y	1.06	1.07	1.04	0.95	0.85	0.77	0.66	0.55	0.46	0.36
	M_{max}/M_{nPr}	0.99	1.02	1.03	1.01	0.98	0.97	0.92	0.87	0.84	0.92
	$M_{max}/M_{nAASHTO}$	0.97	0.98	0.96	0.94	0.91	0.89	0.84	0.78	0.86	0.92
G55	L_b (inches)	57.1	85.6	114.2	183.1	251.9	320.8	389.7	467.7	545.6	682.0
	M_{max}/M_y	1.02	0.96	0.93	0.81	0.70	0.62	0.52	0.42	0.34	0.25
	M_{max}/M_{nPr}	1.03	1.00	1.00	0.95	0.92	0.91	0.87	0.84	0.95	1.09
	$M_{max}/M_{nAASHTO}$	0.94	0.89	0.87	0.82	0.79	0.77	0.73	0.81	0.89	0.98

Table A-13: Test simulation results and comparison with proposed and AASHTO equations for plate girders subjected to uniform moment, Girders G56 – G60

G56	L_b (inches)	53.7	80.6	107.4	172.3	237.1	301.9	366.7	440.1	513.4	641.8
	M_{max}/M_y	1.05	0.95	0.90	0.79	0.68	0.62	0.54	0.46	0.40	0.32
	M_{max}/M_{nPr}	1.06	0.99	0.97	0.94	0.91	0.92	0.93	0.96	1.12	1.41
	$M_{max}/M_{nAASHTO}$	0.95	0.86	0.82	0.78	0.74	0.73	0.71	0.70	0.75	0.83
G57	L_b (inches)	163.8	245.7	327.6	525.3	723.0	920.7	1118.4	1342.1	1565.7	1957.2
	M_{max}/M_y	1.04	1.05	1.02	0.95	0.85	0.77	0.66	0.55	0.46	0.36
	M_{max}/M_{nPr}	0.99	1.02	1.02	1.02	1.00	0.98	0.93	0.87	0.84	0.91
	$M_{max}/M_{nAASHTO}$	0.97	0.98	0.96	0.95	0.92	0.90	0.85	0.78	0.86	0.91
G58	L_b (inches)	53.7	80.5	107.4	172.2	237.0	301.8	366.6	439.9	513.2	641.6
	M_{max}/M_y	1.10	1.00	0.94	0.82	0.71	0.64	0.56	0.48	0.41	0.34
	M_{max}/M_{nPr}	1.07	1.00	0.98	0.94	0.91	0.92	0.93	0.97	1.14	1.45
	$M_{max}/M_{nAASHTO}$	0.95	0.87	0.82	0.78	0.74	0.73	0.71	0.69	0.74	0.81
G59	L_b (inches)	161.8	242.6	323.5	518.7	713.9	909.1	1104.3	1325.2	1546.0	1932.6
	M_{max}/M_y	1.06	1.08	1.05	0.97	0.85	0.77	0.66	0.55	0.47	0.37
	M_{max}/M_{nPr}	0.98	1.02	1.03	1.02	0.97	0.96	0.92	0.86	0.84	0.91
	$M_{max}/M_{nAASHTO}$	0.95	0.97	0.95	0.95	0.90	0.88	0.84	0.78	0.86	0.91
G60	L_b (inches)	53.7	80.5	107.4	172.2	237.0	301.7	366.5	439.8	513.1	641.4
	M_{max}/M_y	0.98	0.90	0.85	0.75	0.65	0.60	0.53	0.45	0.39	0.31
	M_{max}/M_{nPr}	1.03	0.96	0.95	0.92	0.89	0.92	0.93	0.96	1.12	1.40
	$M_{max}/M_{nAASHTO}$	0.95	0.87	0.83	0.79	0.73	0.73	0.71	0.71	0.77	0.84

Table A-14: Test simulation results and comparison with proposed and AASHTO equations for plate girders subjected to uniform moment, Girders G61 – G65

G61	L_b (inches)	54.5	81.8	109.0	174.8	240.6	306.3	372.1	446.5	521.0	651.2
	M_{max}/M_y	0.96	0.88	0.84	0.74	0.64	0.60	0.53	0.45	0.38	0.30
	M_{max}/M_{nPr}	1.02	0.96	0.95	0.92	0.89	0.93	0.94	0.97	1.12	1.40
	$M_{max}/M_{nAASHTO}$	0.96	0.88	0.85	0.81	0.76	0.77	0.75	0.91	1.06	1.32
G62	L_b (inches)	60.0	150.0	250.0	300.0	350.0	430.0	600.0	800.0	60.0	150.0
	M_{max}/M_y	0.89	0.85	0.77	0.73	0.66	0.55	0.34	0.22	0.89	0.85
	M_{max}/M_{nPr}	0.99	1.03	1.07	1.08	1.06	1.00	1.00	1.14	0.99	1.03
	$M_{max}/M_{nAASHTO}$	0.96	0.93	0.94	0.93	0.89	0.79	0.96	1.10	0.96	0.93
G63	L_b (inches)	150.0	250.0	403.0	600.0	950.0	1203.0	1600.0	2100.0	150.0	250.0
	M_{max}/M_y	0.98	0.96	0.93	0.87	0.68	0.49	0.32	0.21	0.98	0.96
	M_{max}/M_{nPr}	1.01	1.03	1.07	1.12	1.11	1.00	1.10	1.26	1.01	1.03
	$M_{max}/M_{nAASHTO}$	1.01	0.99	1.00	1.02	0.95	0.97	1.10	1.26	1.01	0.99
G64	L_b (inches)	50.0	95.0	210.0	310.0	403.0	483.0	600.0	800.0	50.0	95.0
	M_{max}/M_y	0.83	0.78	0.70	0.65	0.54	0.45	0.34	0.24	0.83	0.78
	M_{max}/M_{nPr}	1.00	0.97	1.01	1.08	1.06	1.03	1.16	1.43	1.00	0.97
	$M_{max}/M_{nAASHTO}$	0.96	0.90	0.89	0.91	0.84	0.95	1.11	1.37	0.96	0.90
G65	L_b (inches)	67.9	115.0	270.0	330.0	405.0	479.0	600.0	800.0	67.9	115.0
	M_{max}/M_y	0.92	0.88	0.74	0.66	0.54	0.44	0.32	0.21	0.92	0.88
	M_{max}/M_{nPr}	0.98	0.99	1.02	1.00	0.95	0.90	1.00	1.17	0.98	0.99
	$M_{max}/M_{nAASHTO}$	0.93	0.89	0.74	0.67	0.55	0.45	0.33	0.22	0.93	0.89

Table A-15: Test simulation results and comparison with proposed and AASHTO equations for plate girders subjected to uniform moment, Girders G66 – G70

G66	L_b (inches)	120.0	240.0	553.0	700.0	1042.0	1230.0	1600.0	2100.0	120.0	240.0
	M_{max}/M_y	1.01	1.00	0.89	0.83	0.59	0.47	0.31	0.21	1.01	1.00
	M_{max}/M_{nPr}	1.00	1.03	1.07	1.10	1.00	0.93	0.97	1.04	1.00	1.03
	$M_{max}/M_{nAASHTO}$	1.00	0.99	0.88	0.82	0.58	0.46	0.31	0.21	1.00	0.99
G67	L_b (inches)	50.0	102.0	210.0	300.0	383.0	453.0	600.0	800.0	50.0	102.0
	M_{max}/M_y	0.88	0.79	0.70	0.64	0.54	0.46	0.33	0.24	0.88	0.79
	M_{max}/M_{nPr}	0.99	0.94	0.96	1.01	1.00	0.98	1.19	1.53	0.99	0.94
	$M_{max}/M_{nAASHTO}$	0.95	0.85	0.84	0.85	0.79	0.90	1.13	1.46	0.95	0.85
G68	L_b (inches)	60.0	120.0	250.0	300.0	454.0	537.0	650.0	800.0	60.0	120.0
	M_{max}/M_y	0.87	0.85	0.77	0.74	0.56	0.44	0.33	0.23	0.87	0.85
	M_{max}/M_{nPr}	1.02	1.04	1.10	1.12	1.09	0.99	1.06	1.15	1.02	1.04
	$M_{max}/M_{nAASHTO}$	0.99	0.97	0.98	0.98	0.88	0.95	1.03	1.12	0.99	0.97
G69	L_b (inches)	150.0	250.0	403.0	600.0	950.0	1230.0	1600.0	2100.0	150.0	250.0
	M_{max}/M_y	0.97	0.95	0.91	0.85	0.69	0.48	0.32	0.21	0.97	0.95
	M_{max}/M_{nPr}	1.02	1.04	1.07	1.12	1.14	0.98	1.09	1.23	1.02	1.04
	$M_{max}/M_{nAASHTO}$	1.02	1.00	1.00	1.02	0.98	0.98	1.09	1.23	1.02	1.00
G70	L_b (inches)	50.0	116.0	240.0	330.0	437.0	517.0	600.0	800.0	50.0	116.0
	M_{max}/M_y	0.81	0.78	0.72	0.65	0.55	0.44	0.36	0.24	0.81	0.78
	M_{max}/M_{nPr}	1.07	1.07	1.15	1.18	1.18	1.11	1.17	1.38	1.07	1.07
	$M_{max}/M_{nAASHTO}$	1.02	0.98	1.01	0.99	0.94	1.03	1.12	1.32	1.02	0.98

Figures A-1 through A-67 show the LTB curves along with FE test data for the 61 homogenous girders and the 9 hybrid girders, whose cross-sections are listed in Tables 6-14 and 6-20. The results for these girders are presented in Tables A-1 through A-15.
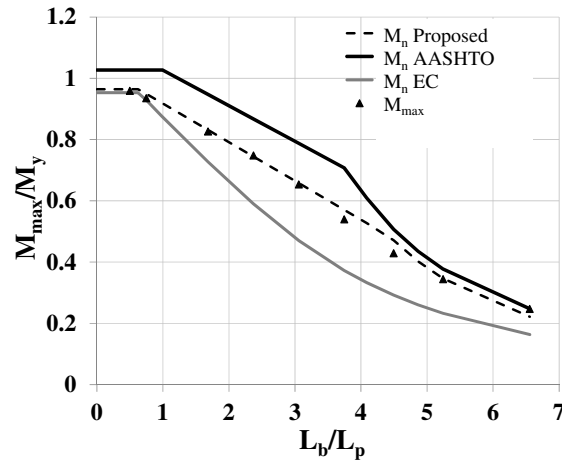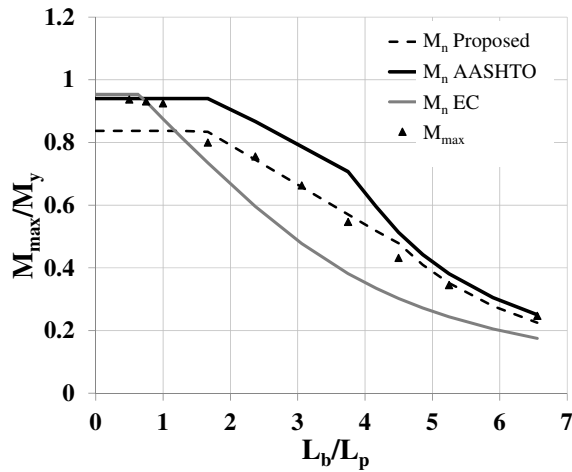

Figure A-1: LTB curves for G1
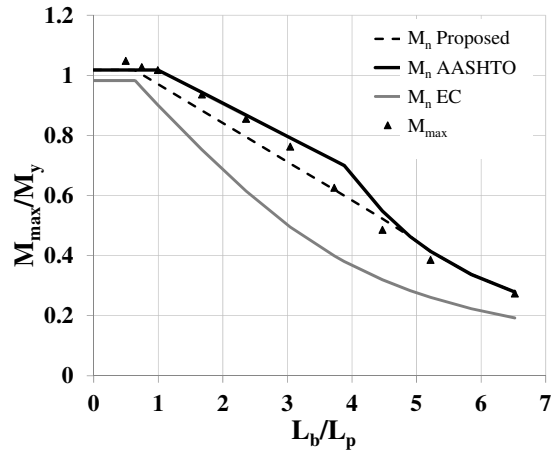

Figure A-2: LTB curves for G2
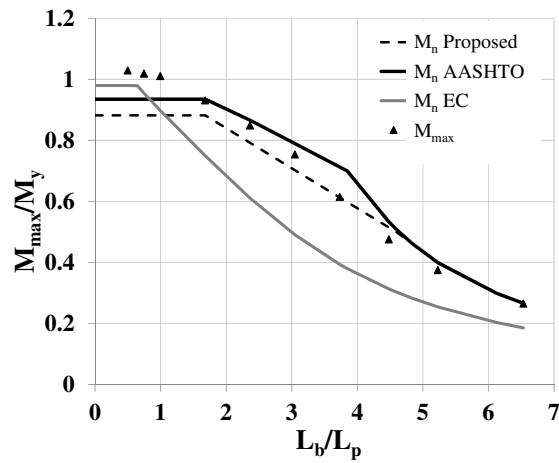
Figure A-3: LTB curves for G3
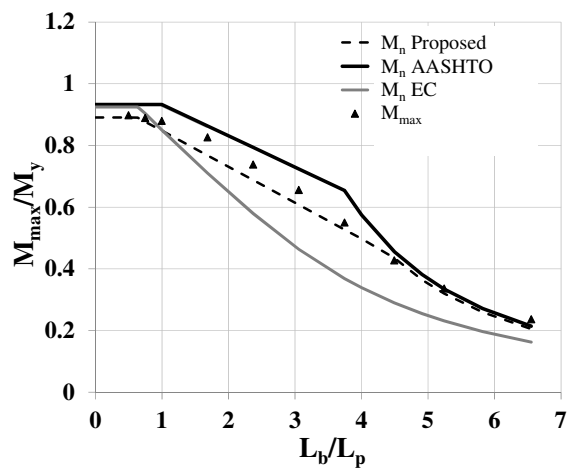

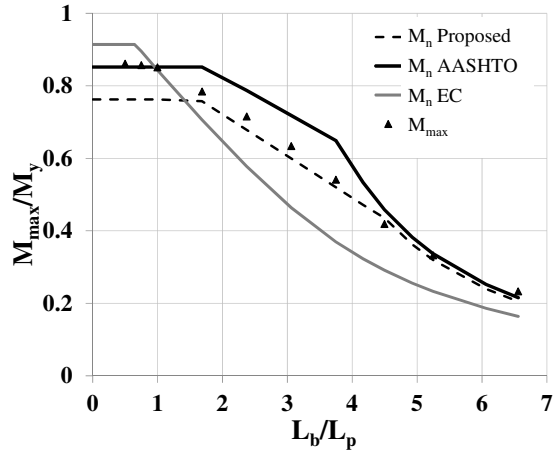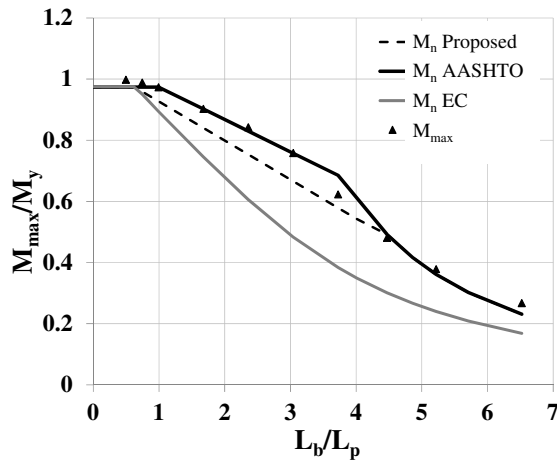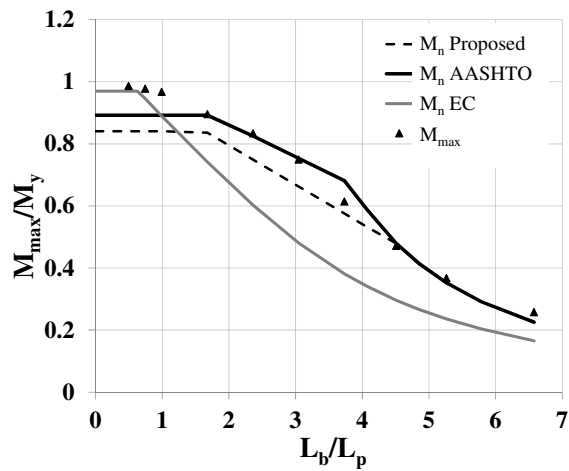**Figure A-4: LTB curves for G4**

Figure A-5: LTB curves for G5

293

Figure A-6: LTB curves for G6

Figure A-7: LTB curves for G7

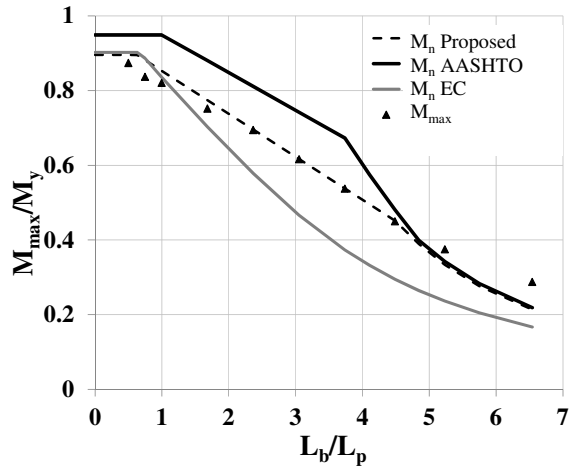**Figure A-8: LTB curves for G8**

294

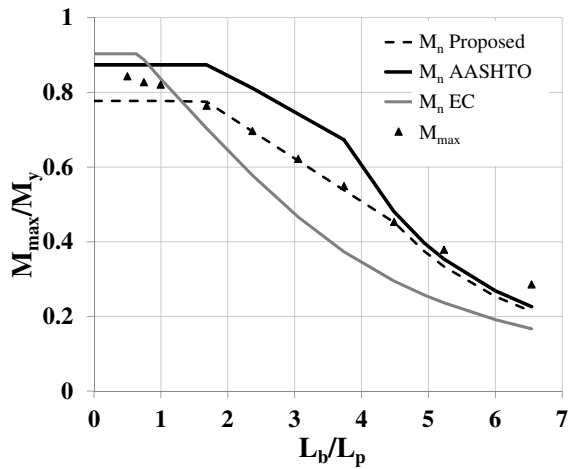**Figure A-9: LTB curves for G9**
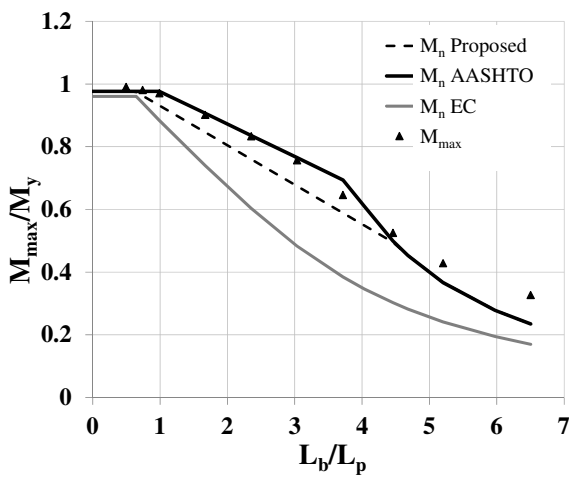

Figure A-10: LTB curves for G10

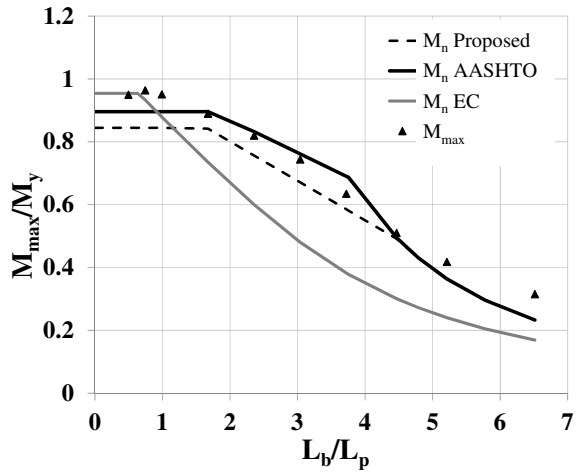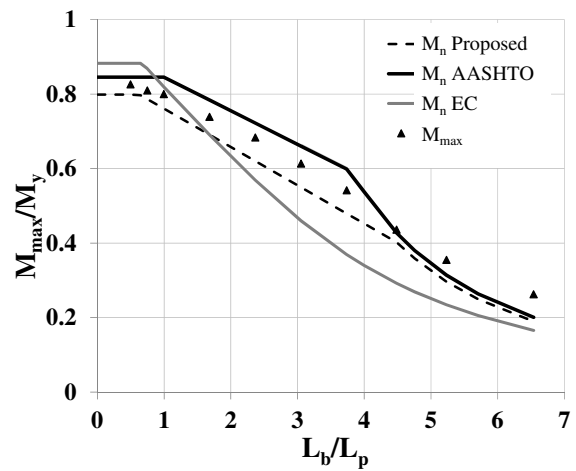**Figure A-11: LTB curves for G11**

Figure A-12: LTB curves for G12
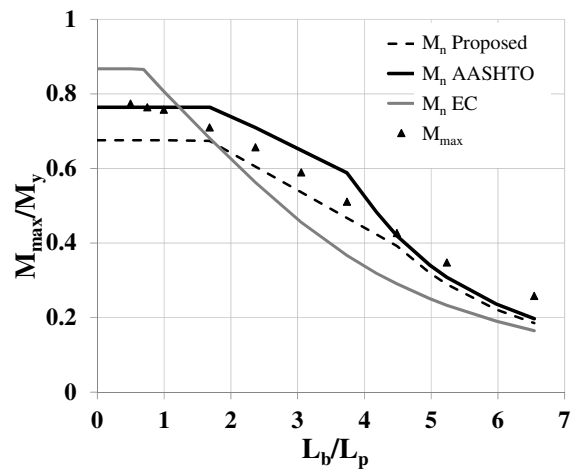

Figure A-13: LTB curves for G13

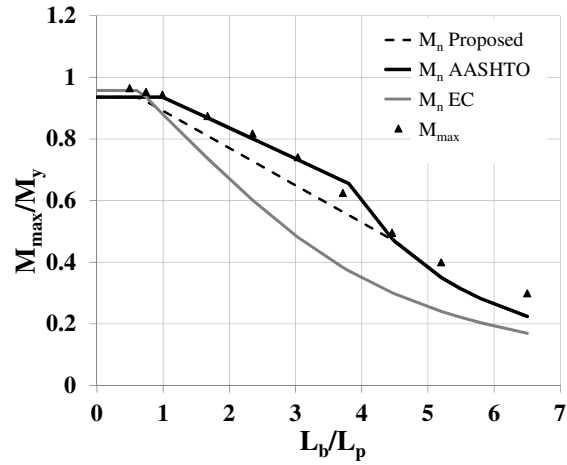**Figure A-14: LTB curves for G14**

296

Figure A-15: LTB curves for G15

Figure A-16: LTB curves for G16

Figure A-17: LTB curves for G17

297

Figure A-18: LTB curves for G18

Figure A-19: LTB curves for G19
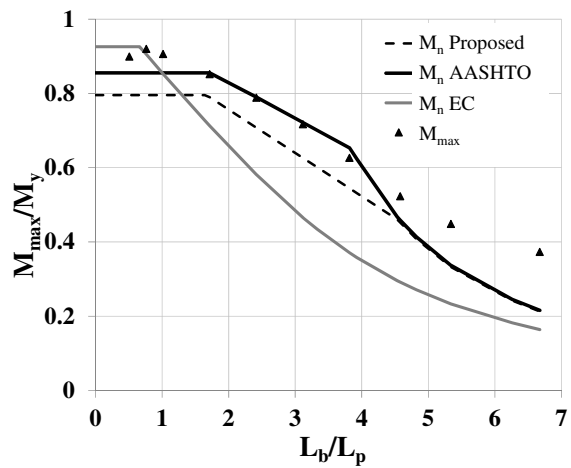
Figure A-20: LTB curves for G20

298

Figure A-21: LTB curves for G21
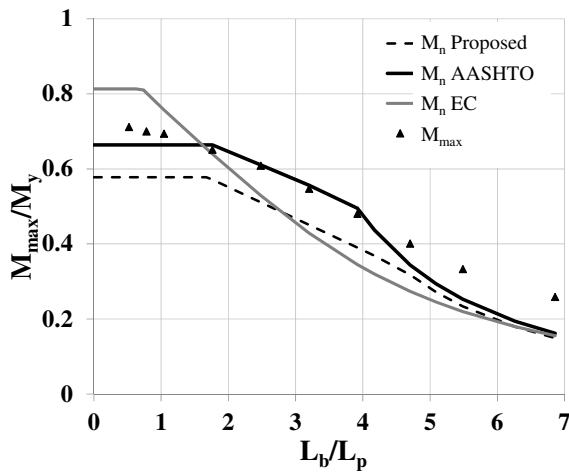
Figure A-22: LTB curves for G22

Figure A-23: LTB curves for G23

299
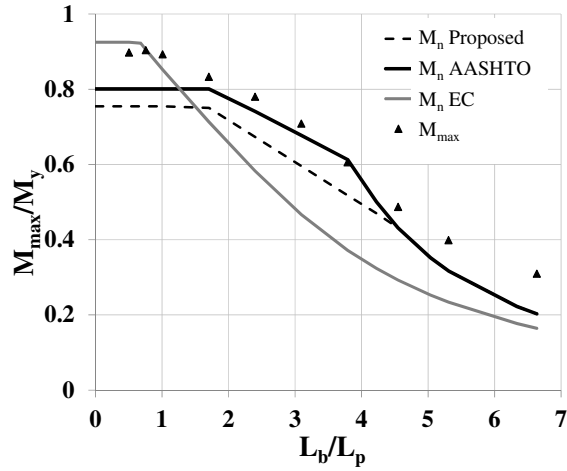
Figure A-24: LTB curves for G24
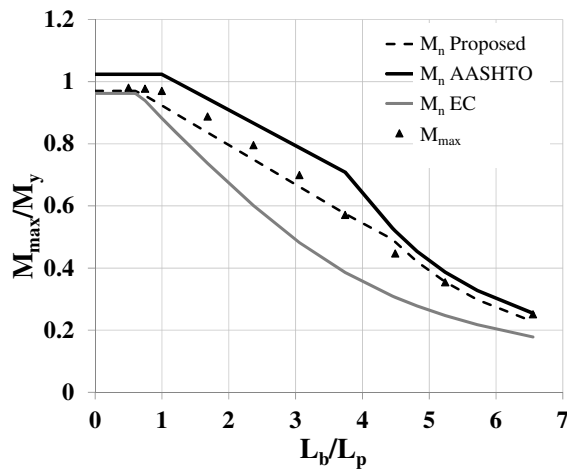
Figure A-25: LTB curves for G25
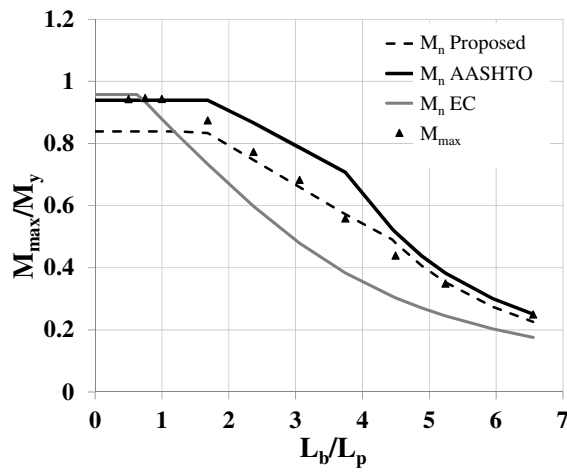
Figure A-26: LTB curves for G26

300
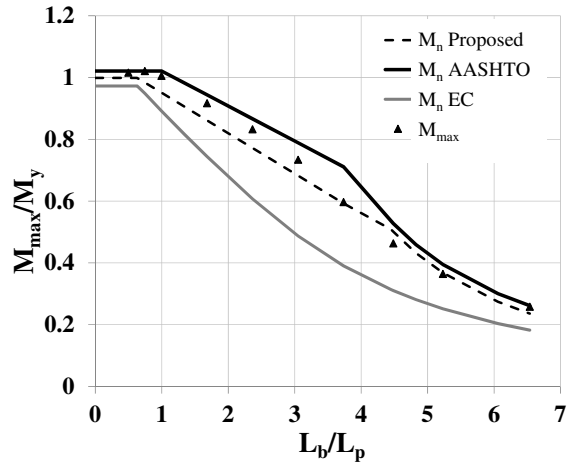
Figure A-27: LTB curves for G27
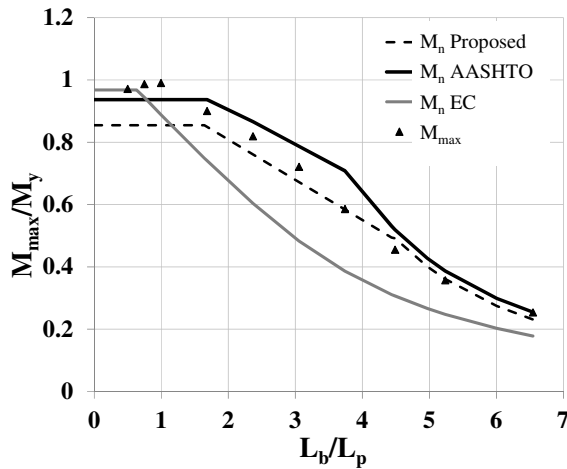
Figure A-28: LTB curves for G28
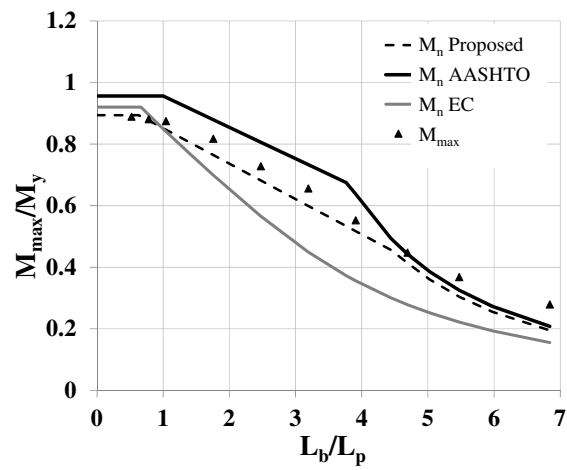
Figure A-29: LTB curves for G29

301

Figure A-30: LTB curves for G30
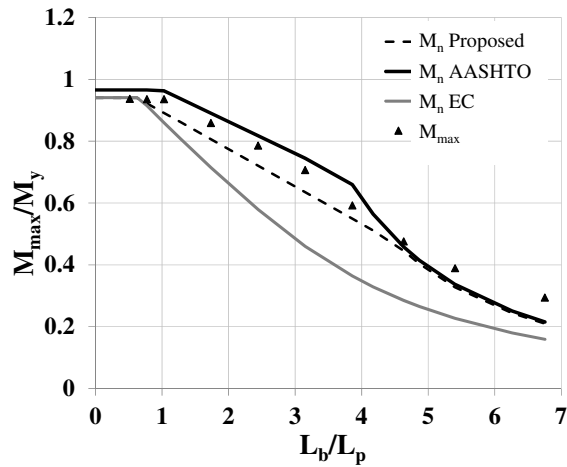
Figure A-31: LTB curves for G31
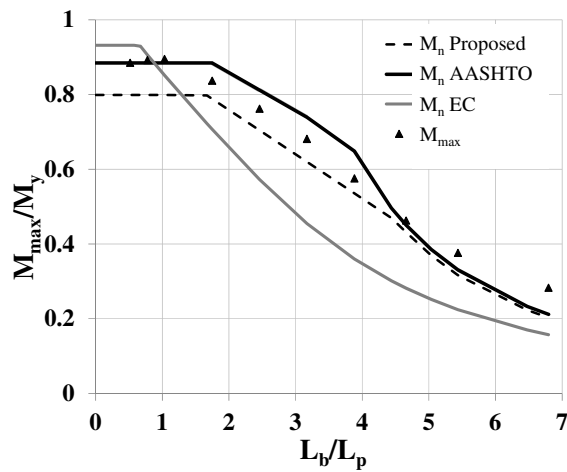
Figure A-32: LTB curves for G32

302
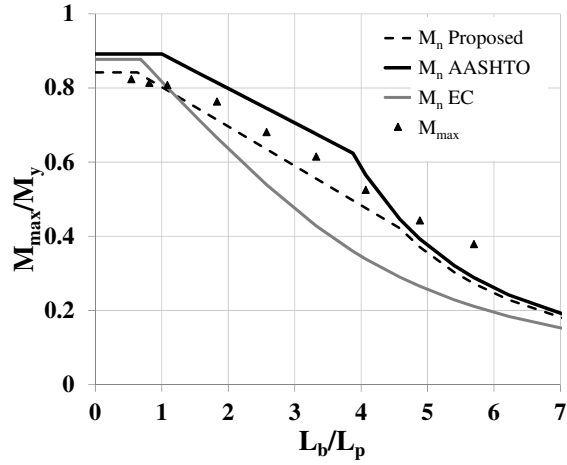
Figure A-33: LTB curves for G33
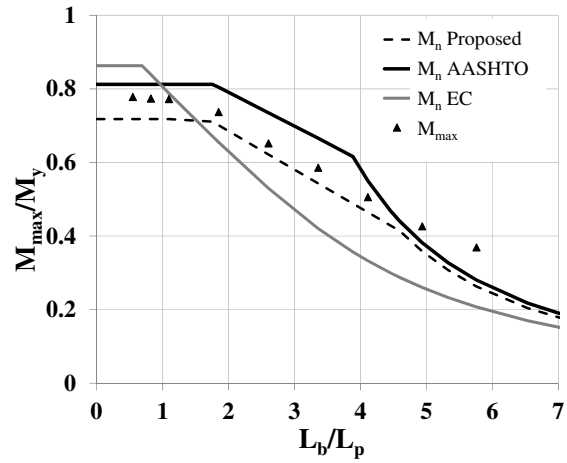
Figure A-34: LTB curves for G34
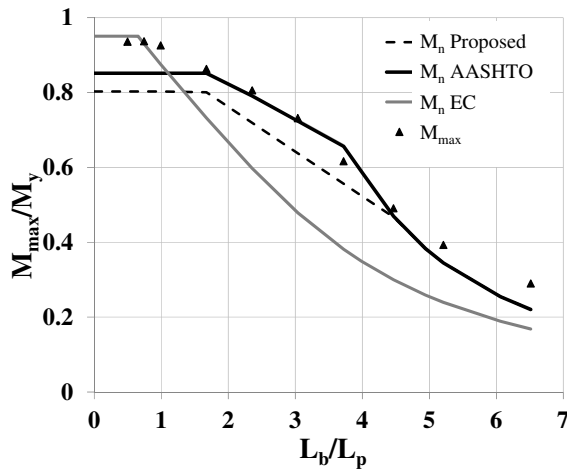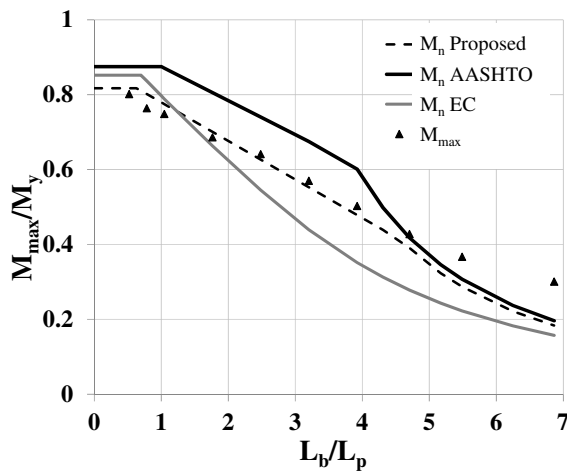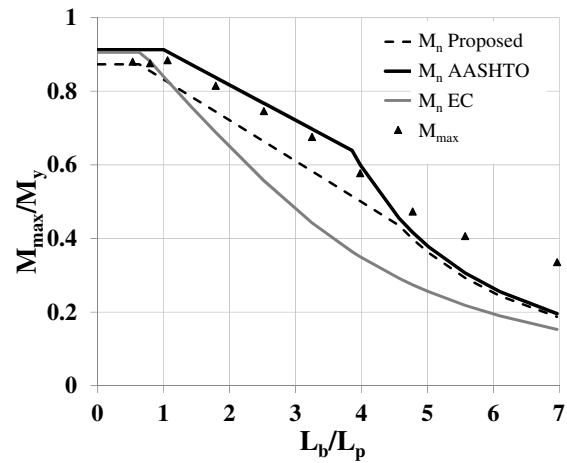

Figure A-35: LTB curves for G35

303
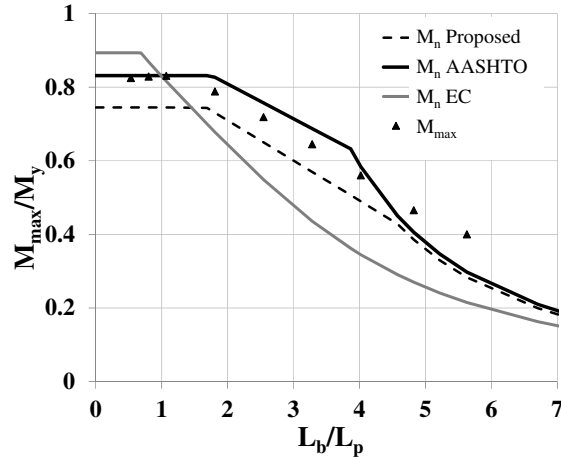
Figure A-36: LTB curves for G36
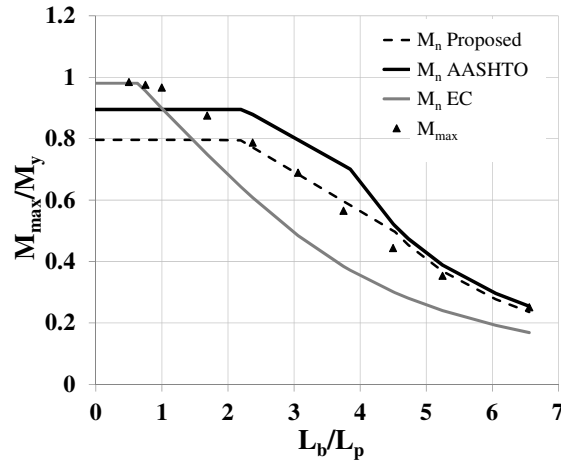
Figure A-37: LTB curves for G37
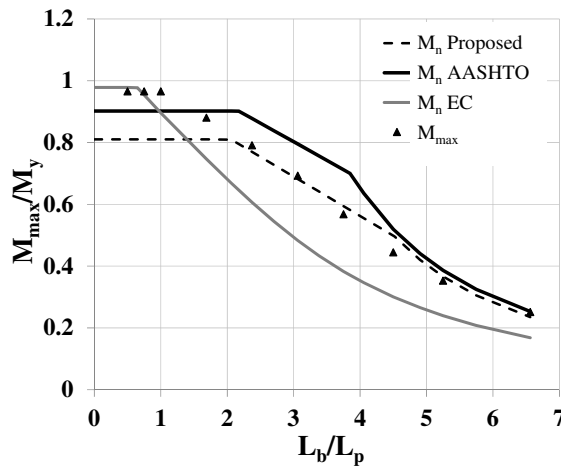
Figure A-38: LTB curves for G38

304
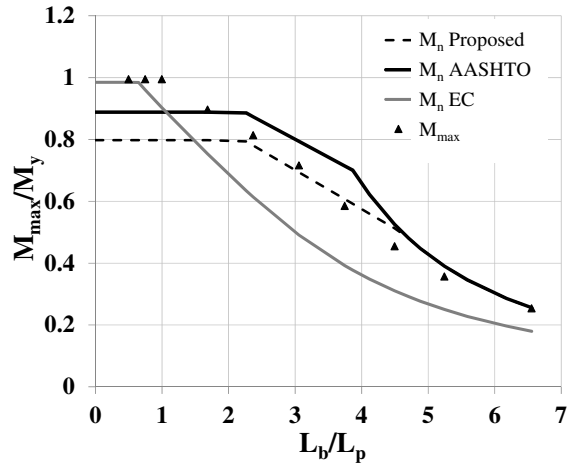
Figure A-39: LTB curves for G39
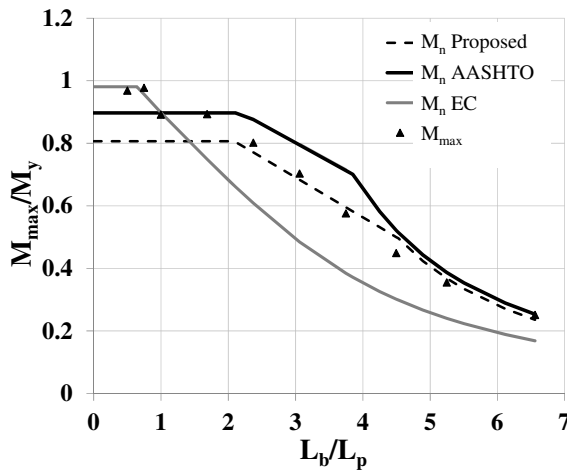
Figure A-40: LTB curves for G40
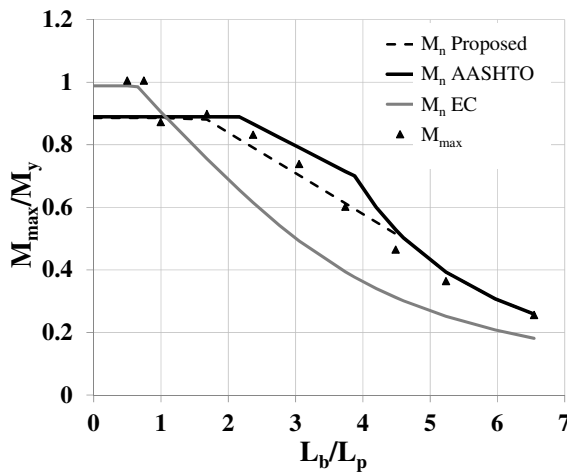
Figure A-41: LTB curves for G41

305
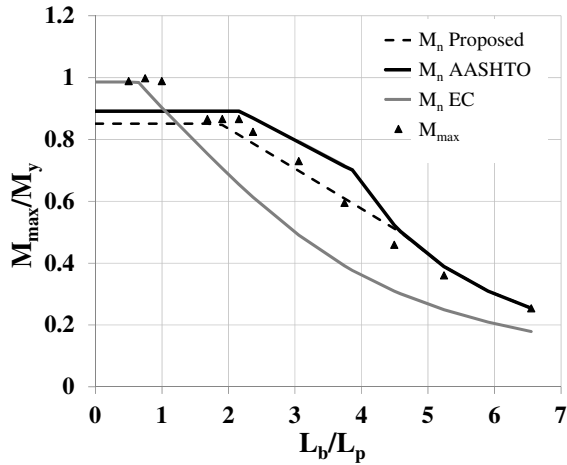
Figure A-42: LTB curves for G42
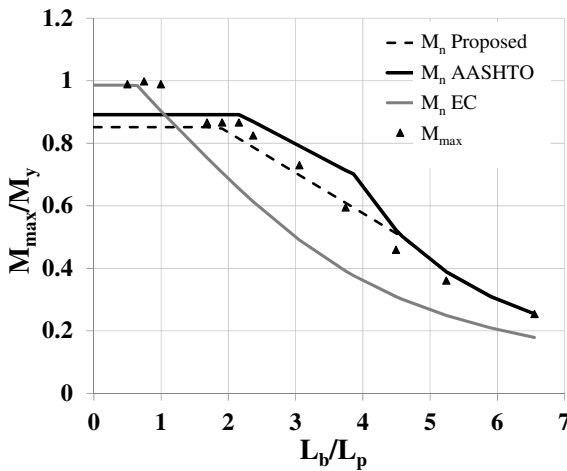
Figure A-43: LTB curves for G43
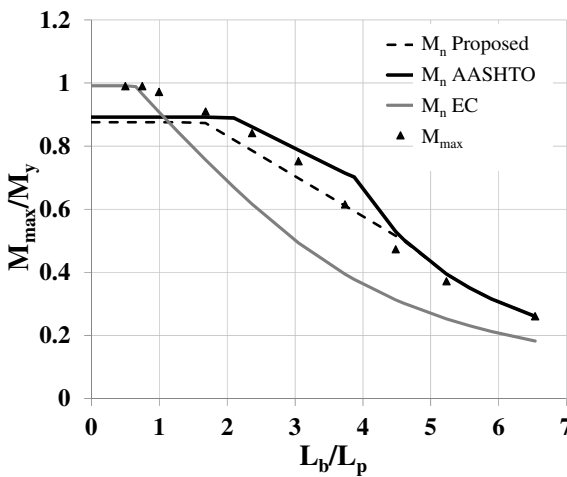
Figure A-44: LTB curves for G44

306
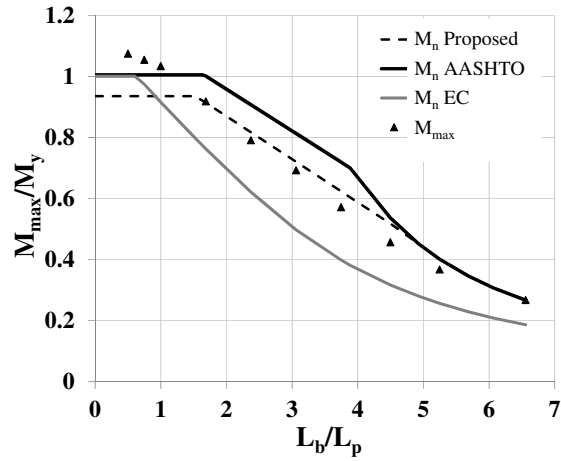
Figure A-45: LTB curves for G45
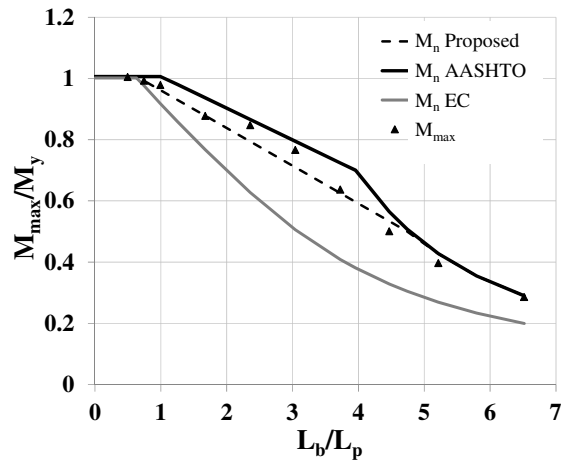
Figure A-46: LTB curves for G46
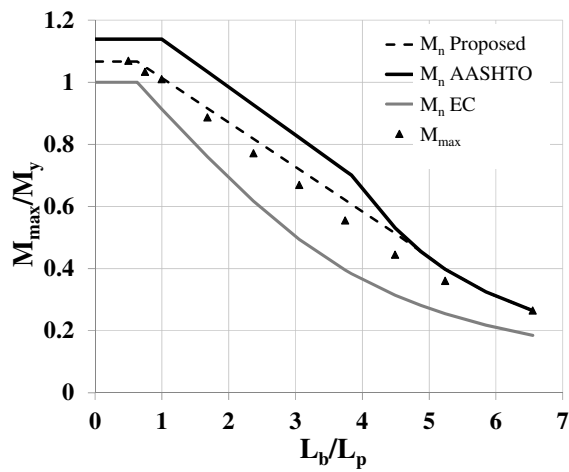
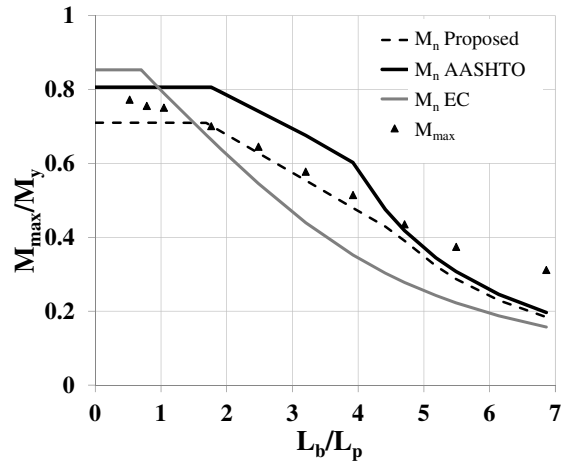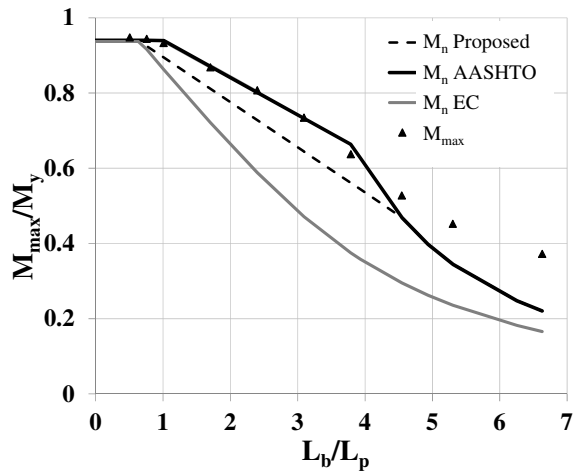**Figure A-47: LTB curves for G47**

307
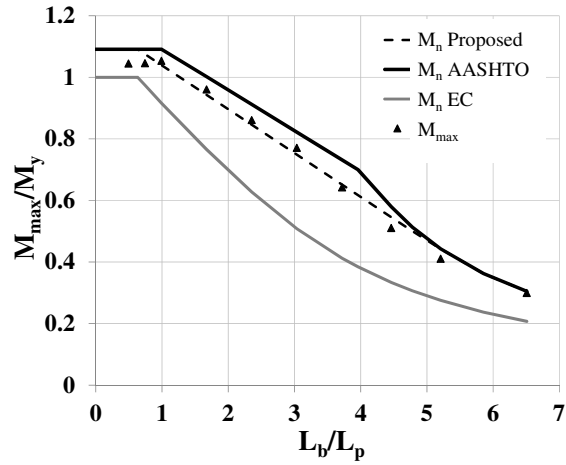
Figure A-48: LTB curves for G48
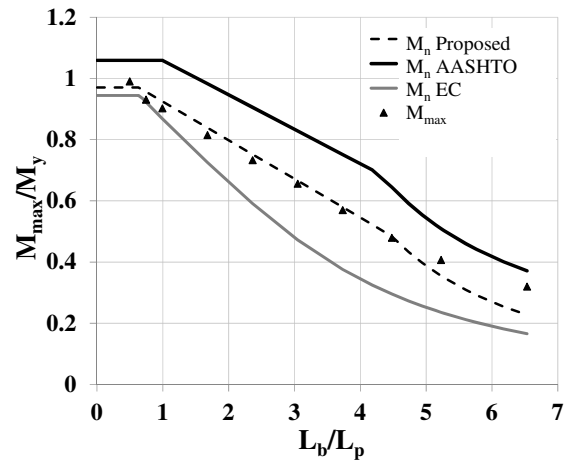
Figure A-49: LTB curves for G49
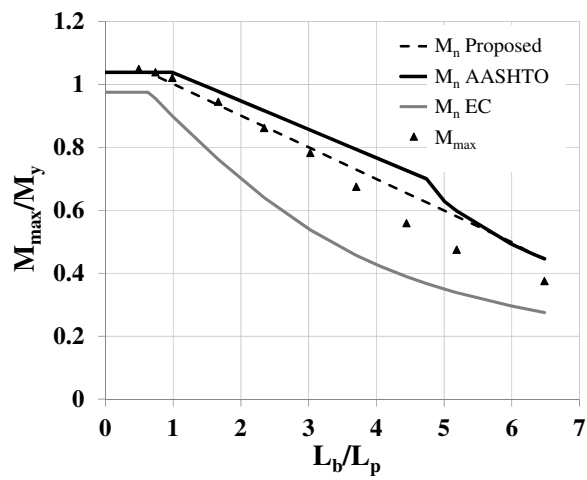
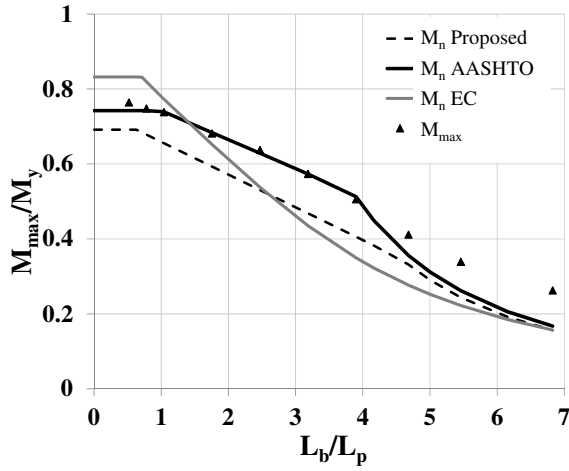**Figure A-50: LTB curves for G50**

308
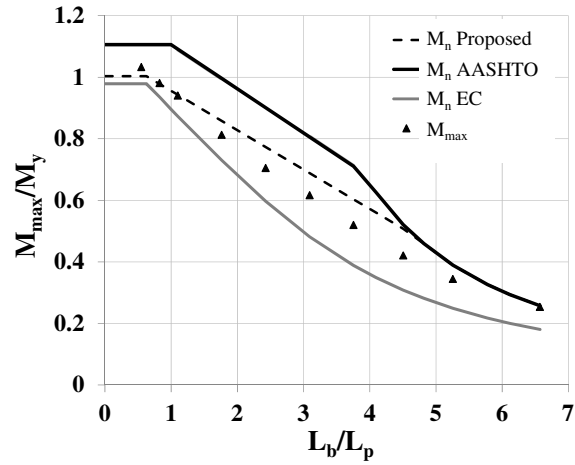
Figure A-51: LTB curves for G51
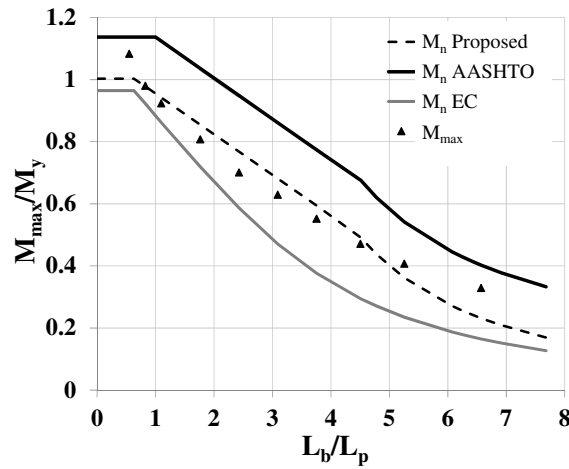
Figure A-52: LTB curves for G52
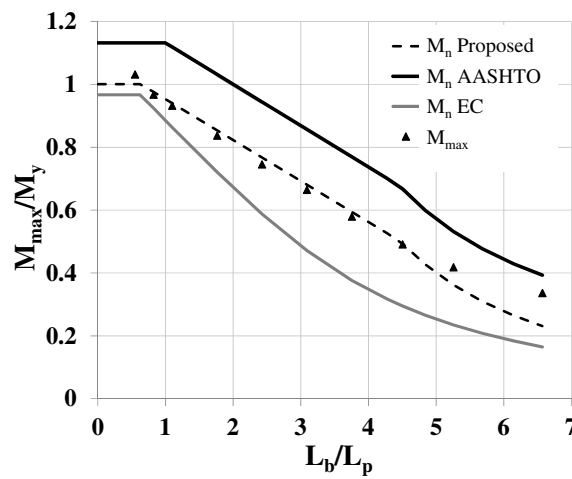
Figure A-53: LTB curves for G53

309
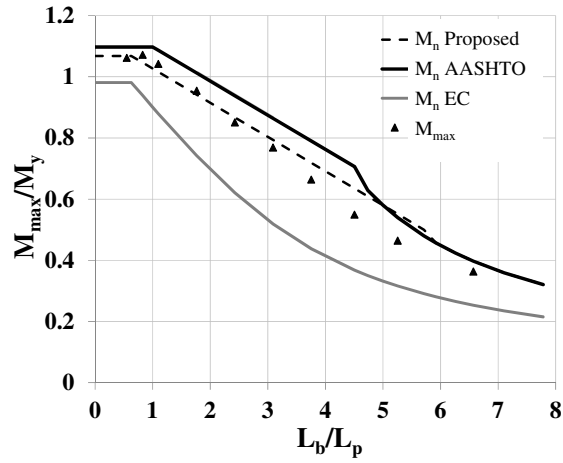
Figure A-54: LTB curves for G54
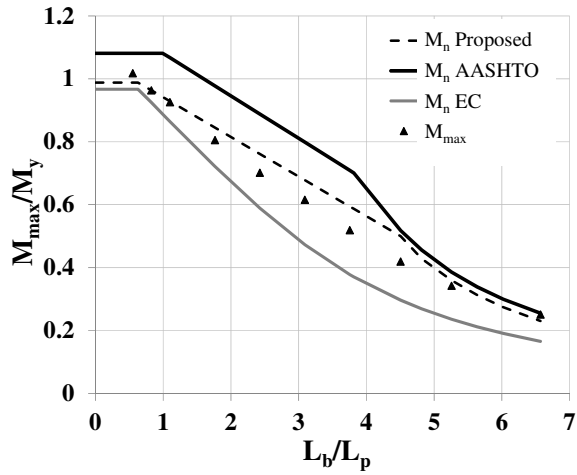
Figure A-55: LTB curves for G55
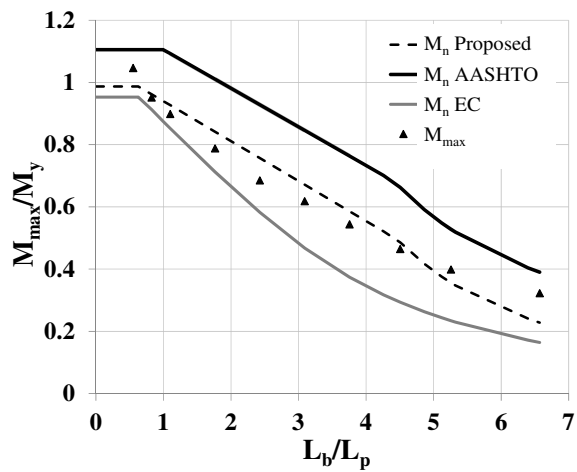
Figure A-56: LTB curves for G56

310
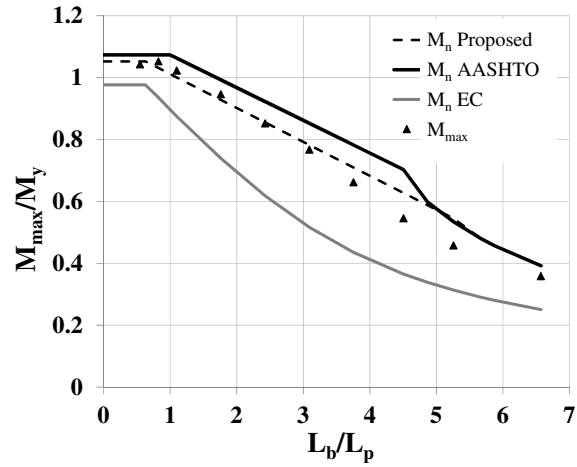
Figure A-57: LTB curves for G57
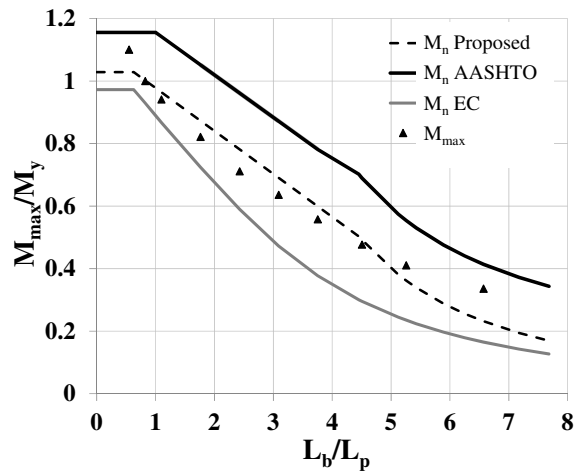
Figure A-58: LTB curves for G58
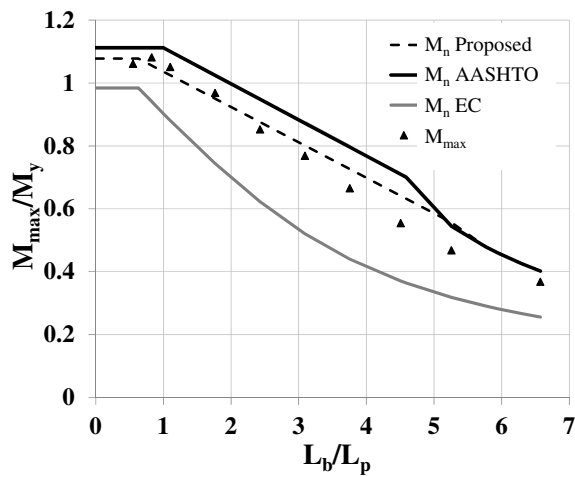
Figure A-59: LTB curves for G59

311
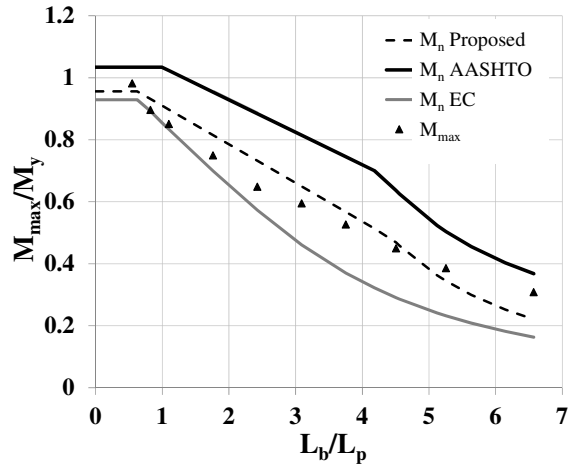
Figure A-60: LTB curves for G60
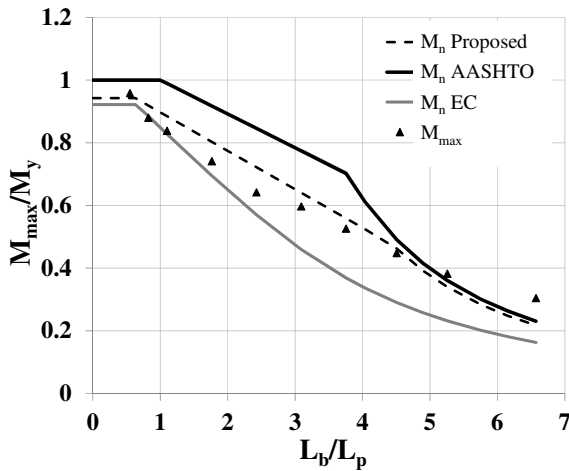
Figure A-61: LTB curves for G61
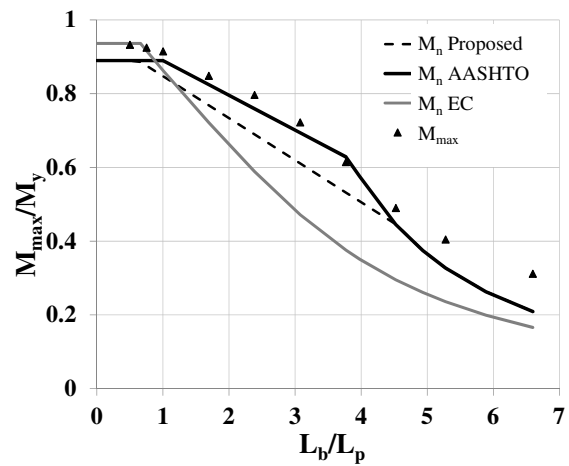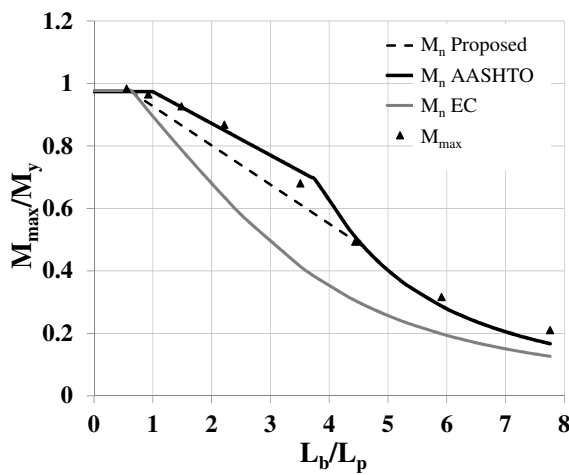

Figure A-62: LTB curves for G63

312
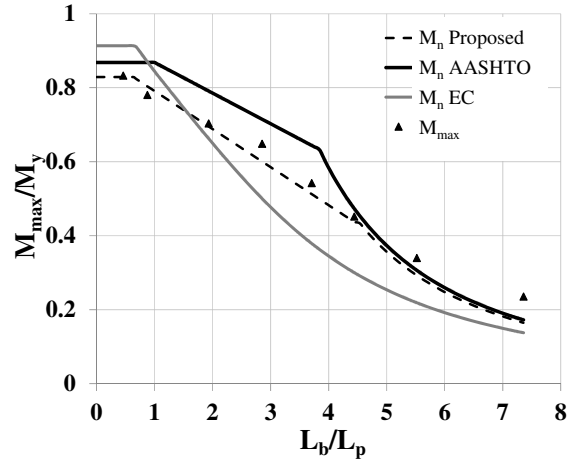
Figure A-63: LTB curves for G64

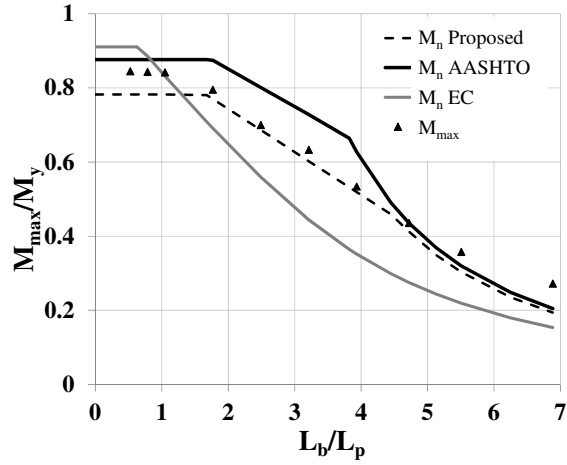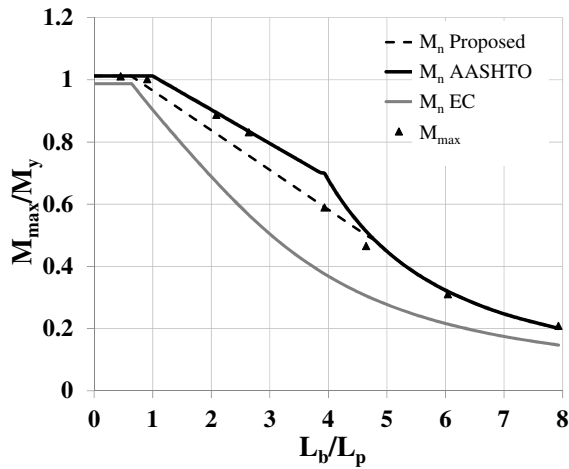**Figure A-64: LTB curves for G66**
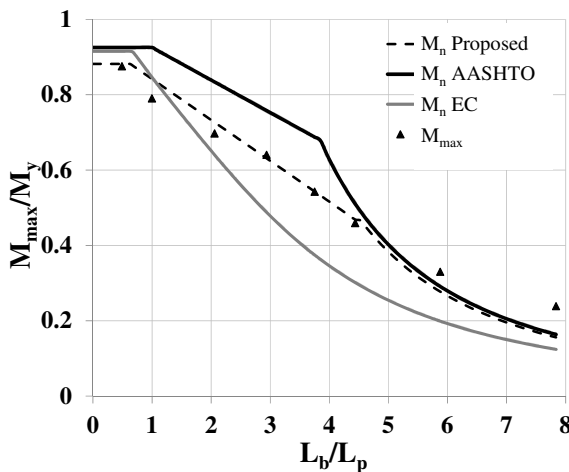
Figure A-65: LTB curves for G67

313
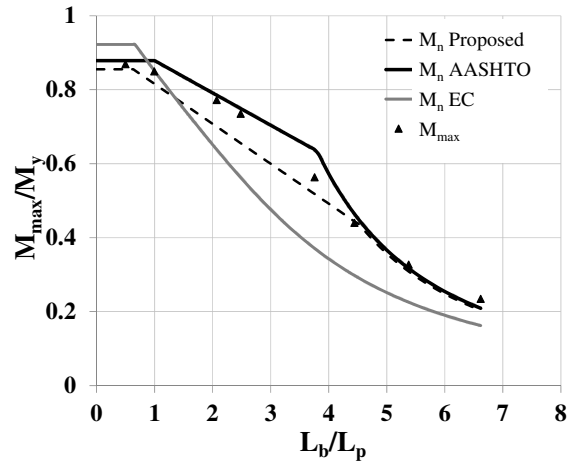
Figure A-66: LTB curves for G68
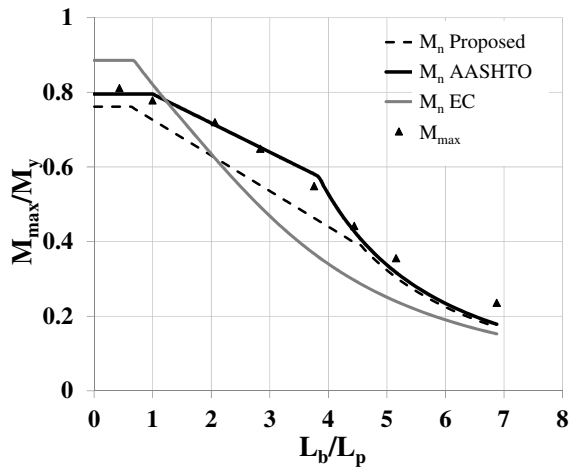
Figure A-67: LTB curves for G70

314

APPENDIX B

ADDITIONAL RESULTS FOR LTB OF UNSTIFFENED GIRDERS SUBJECTED TO MOMENT GRADIENT

This Appendix provides the complete set of results for rolled beams and welded type plate girders subjected to moment gradient. Results are provided for various linear moment gradient loading, and the transverse loading cases discussed in Chapter 7.

Table B-1 shows the results for rolled beams subjected to moment gradient, with $C_b =$ 1.3. Tables B-2 through B-4 list the results for welded type plate girders. Figures B1 through B8 show the LTB curves for welded plate girders with linear moment diagrams described in Section 7.1.1, and $C_b = 1.3$. Similarly, Tables B-5 through B-8 and Figures B9 through B-16 show the results for $C_b = 1.75$; and Tables B-9 through B-11 and Figures B-17 through B-23 show the results for $C_b = 2.3$. The moment gradient loading is as shown in Figure 7-1.

These results are followed by the transverse loading cases discussed in Section 7.1.2 for rolled beams. The results are listed in Tables B-12 through B-17.

These tables list $V_{max}/V_{nAASHTO}$ or V_{max}/V_{nAISC} for girders when the tests are shear controlled (i.e. the design of these members are controlled by the shear resistance equations rather than the flexural resistance equations in the Specifications) and M_{max}/M_{nPr} and M_{max}/M_{nAISC} or $M_{max}/M_{nAASHTO}$ when the tests are moment controlled. Some tables in which the shear ratio is not listed contain all flexure controlled tests.

Table B-1: Test simulation results and comparison with proposed and AISC equations for rolled beams subjected to moment gradient, $C_b = 1.3$

W21x44	L_b (inches)	50.0	75.0	110.0	130.0	188.5	225.0	273.0
	M_{max}/M_p	1.03	1.00	0.87	0.80	0.53	0.41	0.31
	M_{max}/M_{nPr}	1.03	1.00	0.95	0.96	0.94	0.97	0.99
	M_{max}/M_{nAISC}	1.03	1.00	0.87	0.87	0.94	0.97	0.99
W14x68	L_b (inches)	100.0	200.0	275.0	340.0	475.0	615.3	
	M_{max}/M_p	1.09	1.01	0.92	0.82	0.61	0.49	
	M_{max}/M_{nPr}	1.09	1.01	1.02	1.03	1.08	1.17	
	M_{max}/M_{nAISC}	1.09	1.01	0.96	0.97	1.08	1.17	
W10x30	L_b (inches)	103.1	150.0	175.0	200.0	258.0	300.0	338.1
	M_{max}/M_p	1.04	0.94	0.85	0.77	0.60	0.53	0.47
	M_{max}/M_{nPr}	1.04	1.04	1.04	1.04	1.07	1.12	1.16
	M_{max}/M_{nAISC}	1.04	0.97	0.98	1.00	1.07	1.12	1.16
W16x31	L_b (inches)	50.0	95.0	125.0	200.0	250.0		
	M_{max}/M_p	1.04	0.93	0.81	0.47	0.35		
	M_{max}/M_{nPr}	1.04	0.98	1.01	1.02	1.05		
	M_{max}/M_{nAISC}	1.04	0.93	0.91	1.02	1.05		
W14x90	L_b (inches)	250.0	470.0	500.0	650.0	750.0	892.5	1000.0
	M_{max}/M_p	1.12	0.95	0.84	0.68	0.61	0.52	0.47
	M_{max}/M_{nPr}	1.17	1.16	1.07	1.12	1.18	1.23	1.27
	M_{max}/M_{nAISC}	1.12	1.09	1.00	1.12	1.18	1.23	1.27

Table B-2: Test simulation results and comparison with proposed and AASHTO equations for plate girders subjected to moment gradient, $C_b = 1.3$, Girders G1, G3, G5, G9

	L_b (inches)	150.0	200.0	403.0	450.0	481.2	600.0	700.0	850.0
	M_{max}/M_y	1.16	1.09	0.81	0.75	0.70	0.54	0.44	0.33
G1	M_{max}/M_{nPr}		1.13	0.96	0.95	0.94	0.94	1.04	1.17
	$M_{max}/M_{nAASHTO}$		1.06	0.80	0.78	0.76	0.87	0.95	1.03
	$V_{max}/V_{nAASHTO}$	1.35							
	L_b (inches)	250.0	600.0	987.0	1178.0	1300.0	1600.0	1800.0	2000.0
	M_{max}/M_y	1.10	1.08	0.93	0.81	0.71	0.53	0.45	0.38
G3	M_{max}/M_{nPr}		1.06	1.02	0.99	0.96	0.93	0.97	0.99
	$M_{max}/M_{nAASHTO}$		1.06	0.92	0.86	0.86	0.93	0.97	0.99
	$V_{max}/V_{nAASHTO}$	2.04							
	L_b (inches)	100.0	350.0	430.0	480.0	514.6	600.0	700.0	800.0
	M_{max}/M_y	1.08	0.88	0.80	0.73	0.69	0.58	0.47	0.39
G5	M_{max}/M_{nPr}			1.02	1.01	1.00	0.98	1.06	1.14
	$M_{max}/M_{nAASHTO}$			0.85	0.83	0.81	0.91	1.01	1.08
	$V_{max}/V_{nAASHTO}$	4.38	1.02						
	L_b (inches)	100.0	200.0	382.0	420.0	455.2	600.0	700.0	796.5
	M_{max}/M_y	1.11	0.97	0.78	0.74	0.70	0.53	0.45	0.39
G9	M_{max}/M_{nPr}		1.08	1.00	1.01	1.01	1.09	1.25	1.39
	$M_{max}/M_{nAASHTO}$		1.02	0.82	0.82	0.80	1.03	1.18	1.31
	$V_{max}/V_{nAASHTO}$	2.32							

Table B-3: Test simulation results and comparison with proposed and AASHTO equations for plate girders subjected to moment gradient, C_b = 1.3, Girders G13, G37, G44, G45

G13	L_b (inches)	200.0	365.0	430.0	460.0	491.1	600.0	675.0	859.4
	M_{max}/M_y	0.93	0.78	0.72	0.72	0.69	0.56	0.48	0.36
	M_{max}/M_{nPr}		1.04	1.06	1.11	1.11	1.11	1.21	1.44
	$M_{max}/M_{nAASHTO}$		0.92	0.87	0.90	0.89	1.04	1.14	1.36
	$V_{max}/V_{nAASHTO}$	2.21							
G37	L_b (inches)	150.0	300.0	450.0	475.0	495.5	594.6	693.7	867.1
	M_{max}/M_y	1.17	1.00	0.81	0.77	0.74	0.59	0.48	0.35
	M_{max}/M_{nPr}	1.47	1.25	1.02	0.98	0.97	0.92	1.01	1.14
	$M_{max}/M_{nAASHTO}$	1.31	1.11	0.91	0.86	0.83	0.89	0.96	1.06
	$V_{max}/V_{nAASHTO}$								
G44	L_b (inches)	350.0	500.0	958.0	1000.0	1173.3	1408.0	1642.6	2053.3
	M_{max}/M_y	1.05	1.04	0.92	0.91	0.79	0.62	0.49	0.34
	M_{max}/M_{nPr}	1.20	1.19	1.05	1.04	1.00	0.93	0.96	1.02
	$M_{max}/M_{nAASHTO}$	1.18	1.17	1.03	1.02	0.89	0.91	0.96	1.02
	$V_{max}/V_{nAASHTO}$								
G45	L_b (inches)	131.6	222.2	312.8	475.0	494.1	550.0	691.8	864.7
	M_{max}/M_y	1.24	1.16	1.00	0.78	0.75	0.67	0.50	0.36
	M_{max}/M_{nPr}	1.33	1.24	1.07	0.94	0.93	0.92	0.96	1.05
	$M_{max}/M_{nAASHTO}$	1.24	1.15	1.00	0.82	0.81	0.84	0.96	1.05
	$V_{max}/V_{nAASHTO}$								

Table B-4: Test simulation results and comparison with proposed and AASHTO equations for plate girders subjected to moment gradient, C_b = 1.3, Girders G46, G47, G49

	L_b (inches)	316.6	534.7	752.8	970.9	1189.0	1426.8	1664.5	2080.7
	M_{max}/M_y	1.07	1.05	1.01	0.94	0.82	0.65	0.52	0.38
G46	M_{max}/M_{nPr}	1.06	1.04	1.00	1.02	1.01	0.94	0.95	1.01
	$M_{max}/M_{nAASHTO}$	1.06	1.04	1.00	0.93	0.88	0.89	0.95	1.01
	$V_{max}/V_{nAASHTO}$								
	L_b (inches)	100.0	200.0	370.0	391.8	479.9	575.8	671.8	839.8
	M_{max}/M_y	1.26	1.17	0.89	0.86	0.73	0.59	0.48	0.36
G47	M_{max}/M_{nPr}		1.10	0.92	0.92	0.90	0.88	0.93	1.04
	$M_{max}/M_{nAASHTO}$		1.03	0.81	0.80	0.78	0.86	0.93	1.04
	$V_{max}/V_{nAASHTO}$	1.29							
	L_b (inches)	100.0	175.0	250.0	370.2	453.4	521.4	589.36	793.4
	M_{max}/M_y	1.20	1.12	0.96	0.83	0.74	0.65	0.58	0.43
G49	M_{max}/M_{nPr}		1.15	0.99	0.96	0.98	0.99	1.06	1.42
	$M_{max}/M_{nAASHTO}$		1.05	0.91	0.78	0.75	0.71	0.77	0.87
	$V_{max}/V_{nAASHTO}$	1.49							
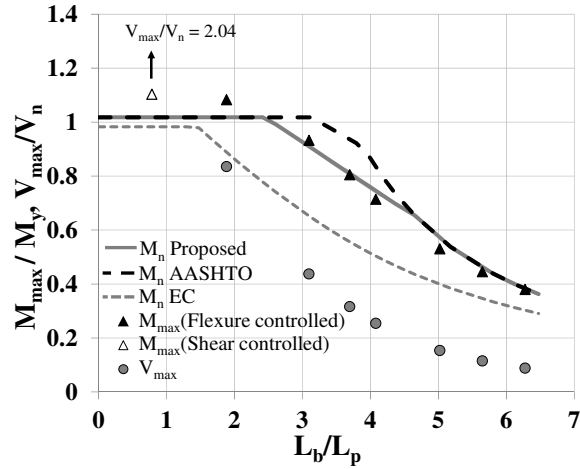
Figure B-1: LTB curves for G3, $C_b = 1.3$
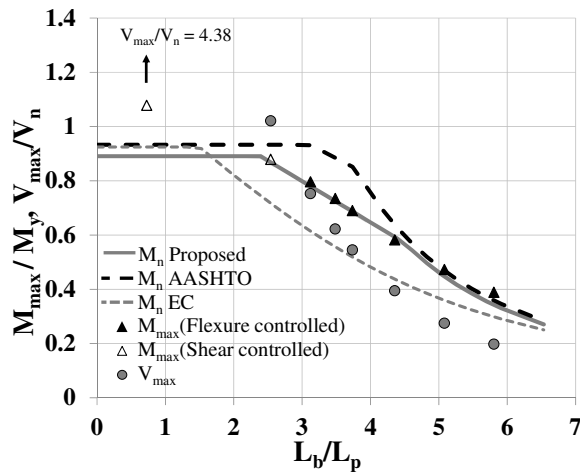
Figure B-2: LTB curves for G5, $C_b = 1.3$
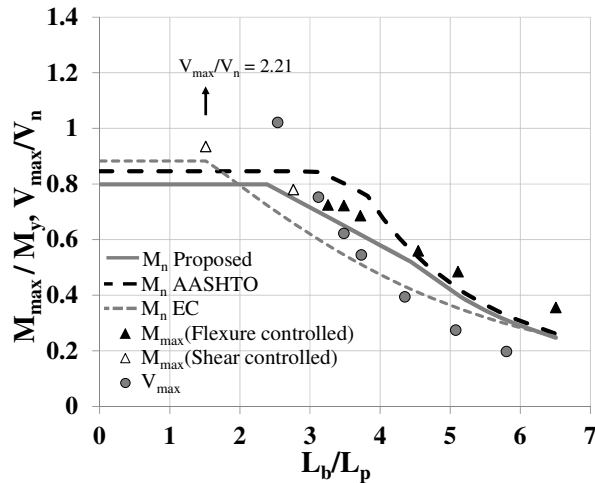
Figure B-3: LTB curves for G13, $C_b = 1.3$

320
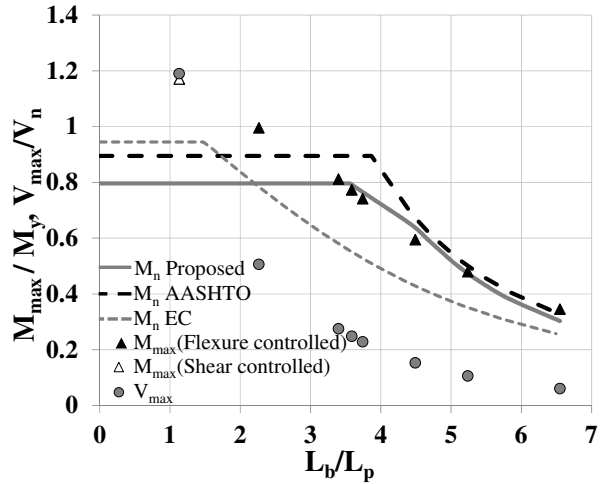
Figure B-4: LTB curves for G37, C_b = 1.3
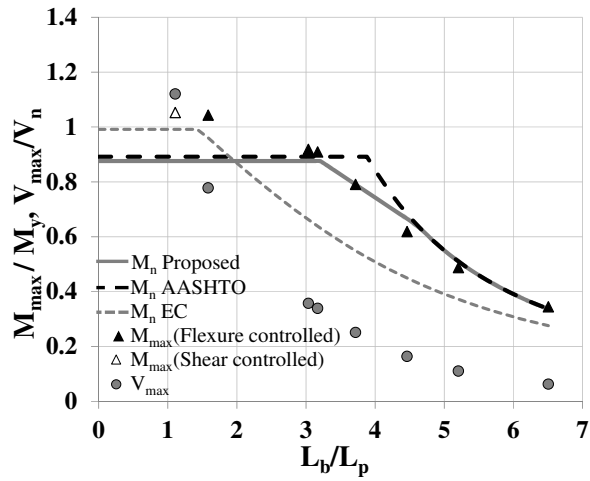
Figure B-5: LTB curves for G44, C_b = 1.3
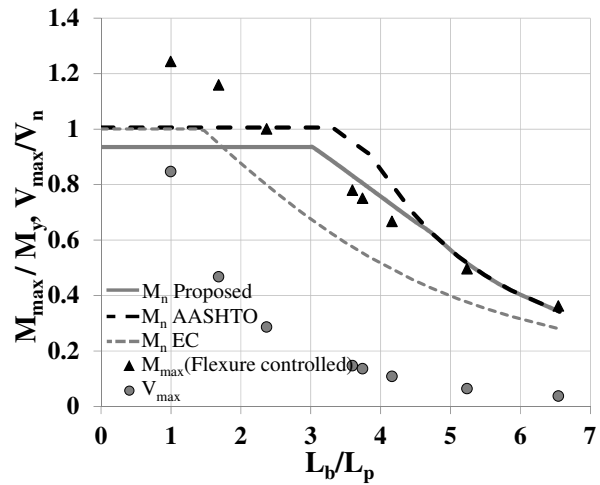
Figure B-6: LTB curves for G45, C_b = 1.3

321

Figure B-7: LTB curves for G46, $C_b = 1.3$

Figure B-8: LTB curves for G47, $C_b = 1.3$

322

Table B-5: Test simulation results and comparison with proposed and AISC equations for rolled beams subjected to moment gradient, $C_b = 1.75$

W21x44	L_b (inches)	75.0	130.0	150.0	188.5	225.0	273.0
	M_{max}/M_p	1.04	0.95	0.88	0.71	0.56	0.43
	M_{max}/M_{nPr}	1.04	0.95	0.88	0.94	0.98	1.01
	M_{max}/M_{nAISC}	1.04	0.95	0.88	0.94	0.98	1.01
W14x68	L_b (inches)	200.0	275.0	340.0	400.0	475.0	615.3
	M_{max}/M_p	1.08	1.04	0.99	0.92	0.80	0.64
	M_{max}/M_{nPr}	1.08	1.04	0.99	0.99	1.05	1.13
	M_{max}/M_{nAISC}	1.08	1.04	0.99	0.98	1.05	1.13
W10x30	L_b (inches)	103.1	200.0	258.0	300.0	338.1	
	M_{max}/M_p	1.12	0.97	0.80	0.70	0.62	
	M_{max}/M_{nPr}	1.12	0.97	1.06	1.10	1.13	
	M_{max}/M_{nAISC}	1.12	0.97	1.06	1.10	1.13	
W16x31	L_b (inches)	50.0	95.0	125.0	150.0	200.0	250.0
	M_{max}/M_p	1.09	1.04	0.97	0.88	0.64	0.48
	M_{max}/M_{nPr}	1.09	1.04	0.97	0.95	1.03	1.07
	M_{max}/M_{nAISC}	1.09	1.04	0.97	0.90	1.03	1.07
W14x90	L_b (inches)	250.0	500.0	650.0	750.0	892.5	1000.0
	M_{max}/M_p	1.03	0.99	0.88	0.79	0.68	0.62
	M_{max}/M_{nPr}	1.08	1.04	1.07	1.14	1.20	1.24
	M_{max}/M_{nAISC}	1.03	0.99	1.07	1.14	1.20	1.24

Table B-6: Test simulation results and comparison with proposed and AASHTO equations for plate girders subjected to moment gradient, $C_b = 1.75$, Girders G1, G3, G5, G9

	L_b (inches)	150.0	200.0	403.0	450.0	481.2	600.0	700.0	850.0
	M_{max}/M_y	1.09	1.10	0.90	0.84	0.80	0.66	0.55	0.43
G1	M_{max}/M_{nPr}			0.93	0.87	0.83	0.84	0.97	1.13
	$M_{max}/M_{nAASHTO}$			0.87	0.82	0.78	0.78	0.89	1.00
	$V_{max}/V_{nAASHTO}$	2.53	1.93						
	L_b (inches)	250.0	600.0	987.0	1178.0	1300.0	1600.0	1800.0	2000.0
	M_{max}/M_y	0.70	1.10	1.05	0.96	0.89	0.70	0.59	0.51
G3	M_{max}/M_{nPr}			1.03	0.94	0.89	0.91	0.96	1.00
	$M_{max}/M_{nAASHTO}$			1.03	0.94	0.87	0.91	0.96	1.00
	$V_{max}/V_{nAASHTO}$	2.58	1.70						
	L_b (inches)	100.0	350.0	430.0	480.0	514.6	600.0	700.0	800.0
	M_{max}/M_y	0.73	0.88	0.82	0.77	0.74	0.65	0.56	0.48
G5	M_{max}/M_{nPr}							0.93	1.04
	$M_{max}/M_{nAASHTO}$							0.89	0.99
	$V_{max}/V_{nAASHTO}$	5.91	2.05	1.55	1.31	1.17	0.89		
	L_b (inches)	100.0	200.0	382.0	420.0	455.2	600.0	700.0	796.5
	M_{max}/M_y	0.78	1.02	0.82	0.79	0.74	0.63	0.56	0.49
G9	M_{max}/M_{nPr}			0.92	0.89	0.83	0.96	1.15	1.32
	$M_{max}/M_{nAASHTO}$			0.87	0.84	0.78	0.90	1.08	1.25
	$V_{max}/V_{nAASHTO}$	3.27	2.13						

Table B-7: Test simulation results and comparison with proposed and AASHTO equations for plate girders subjected to moment gradient, $C_b = 1.75$, Girders G13, G37, G44, G45

G13	L_b (inches)	200.0	365.0	430.0	460.0	491.1	600.0	675.0	859.4
	M_{max}/M_y	0.85	0.76	0.72	0.70	0.74	0.63	0.56	0.44
	M_{max}/M_{nPr}							1.04	1.32
	$M_{max}/M_{nAASHTO}$							0.98	1.25
	$V_{max}/V_{nAASHTO}$	4.01	1.98	1.58	1.43	1.42	0.98		
G37	L_b (inches)	150.0	300.0	450.0	475.0	495.5	594.6	693.7	867.1
	M_{max}/M_y	1.11	1.08	0.91	0.88	0.85	0.72	0.61	0.45
	M_{max}/M_{nPr}		1.36	1.14	1.11	1.11	1.08	1.22	1.39
	$M_{max}/M_{nAASHTO}$		1.04	0.93	0.93	0.93	1.07	1.21	1.38
	$V_{max}/V_{nAASHTO}$	2.26							
G44	L_b (inches)	350.0	500.0	958.0	1000.0	1173.3	1408.0	1642.6	2053.3
	M_{max}/M_y	1.02	1.05	1.03	1.01	0.94	0.79	0.64	0.46
	M_{max}/M_{nPr}			1.17	1.15	1.18	1.19	1.26	1.38
	$M_{max}/M_{nAASHTO}$			1.10	1.09	1.01	1.16	1.26	1.38
	$V_{max}/V_{nAASHTO}$	2.17	1.57						
G45	L_b (inches)	131.6	222.2	312.8	475.0	494.1	550.0	691.8	864.7
	M_{max}/M_y	1.17	1.23	1.15	0.92	0.90	0.82	0.64	0.48
	M_{max}/M_{nPr}		1.31	1.23	1.11	1.12	1.13	1.24	1.41
	$M_{max}/M_{nAASHTO}$		1.12	1.05	0.97	0.97	1.03	1.24	1.41
	$V_{max}/V_{nAASHTO}$	1.59							

Table B-8: Test simulation results and comparison with proposed and AASHTO equations for plate girders subjected to moment gradient, $C_b = 1.75$, Girders G46, G47, G49

|									
G46	L_b (inches)	316.6	534.7	752.8	970.9	1189.0	1426.8	1664.5	2080.7
	M_{max}/M_y	1.02	1.07	1.06	1.04	0.97	0.85	0.70	0.52
	M_{max}/M_{nPr}		1.06	1.05	1.13	1.19	1.22	1.27	1.38
	$M_{max}/M_{nAASHTO}$		1.06	1.05	1.03	1.03	1.16	1.27	1.38
	$V_{max}/V_{nAASHTO}$	1.65							
G47	L_b (inches)	100.0	200.0	370.0	391.8	479.9	575.8	671.8	839.76
	M_{max}/M_y	0.98	1.22	1.03	1.00	0.88	0.74	0.62	0.48
	M_{max}/M_{nPr}			1.06	1.07	1.08	1.10	1.21	1.38
	$M_{max}/M_{nAASHTO}$			0.93	0.94	0.94	1.07	1.21	1.38
	$V_{max}/V_{nAASHTO}$	2.02	1.25						
G49	L_b (inches)	100.0	175.0	250.0	370.2	453.4	521.4	589.36	793.37
	M_{max}/M_y	0.79	1.12	1.08	0.94	0.86	0.78	0.71	0.56
	M_{max}/M_{nPr}			1.11	0.97	0.88	0.88	0.97	1.37
	$M_{max}/M_{nAASHTO}$			1.02	0.89	0.81	0.74	0.94	1.33
	$V_{max}/V_{nAASHTO}$	1.96	1.58						
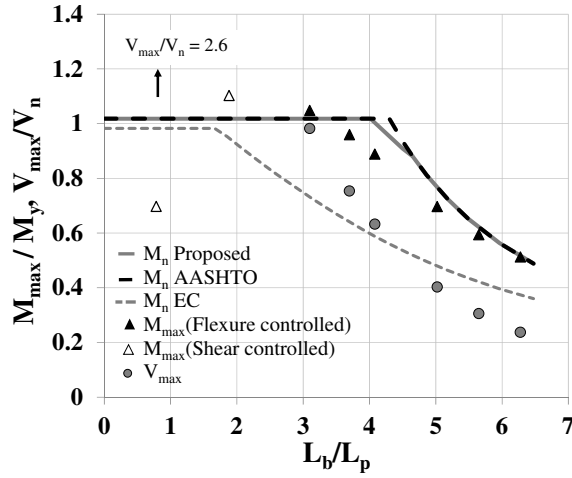
Figure B-9: LTB curves for G3, $C_b = 1.75$
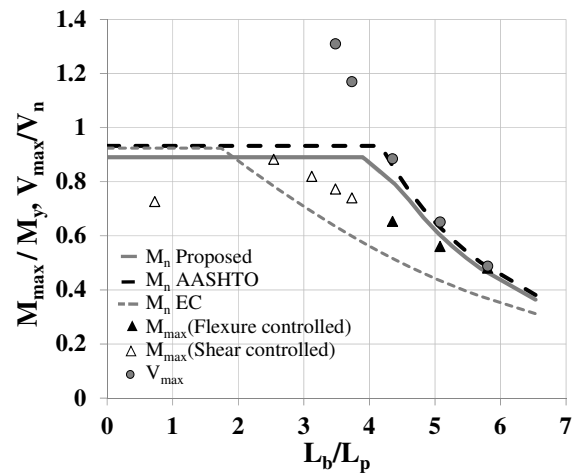
Figure B-10: LTB curves for G5, $C_b = 1.75$
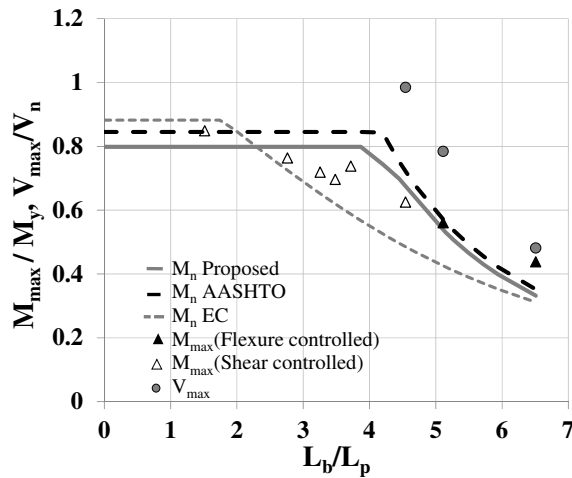
**Figure B-11: LTB curves for G13, $C_b = 1.75$**

327
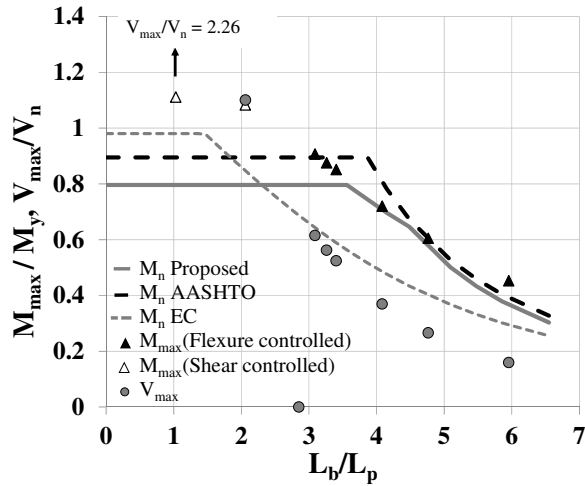
Figure B-12: LTB curves for G37, $C_b = 1.75$
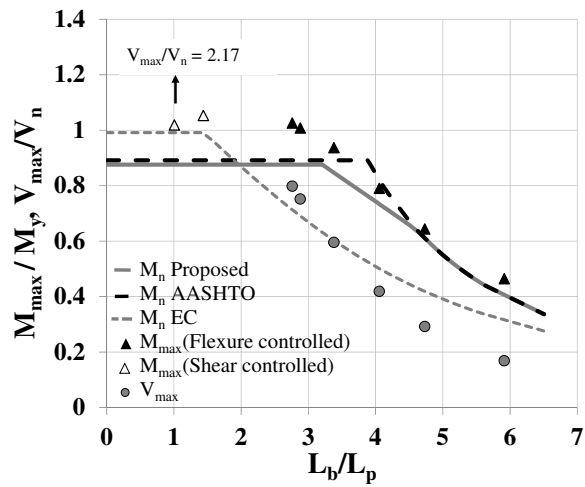
Figure B-13: LTB curves for G44, $C_b = 1.75$
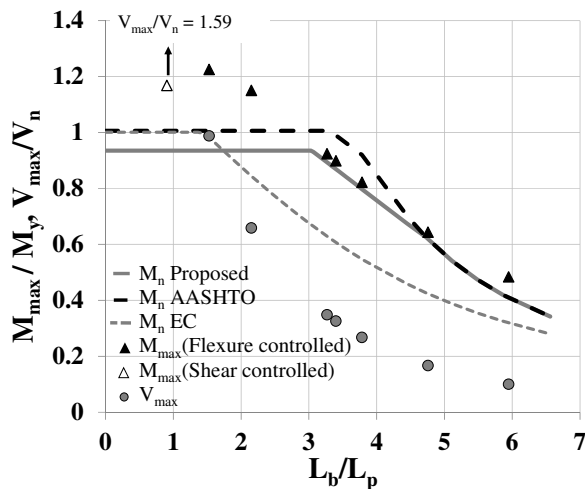
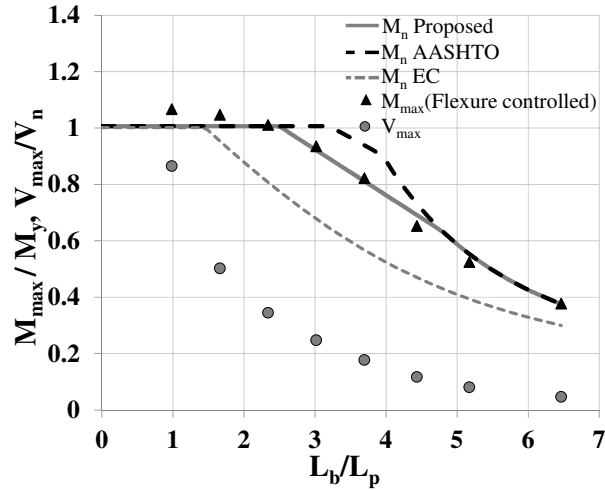**Figure B-14: LTB curves for G45, $C_b = 1.75$**

328

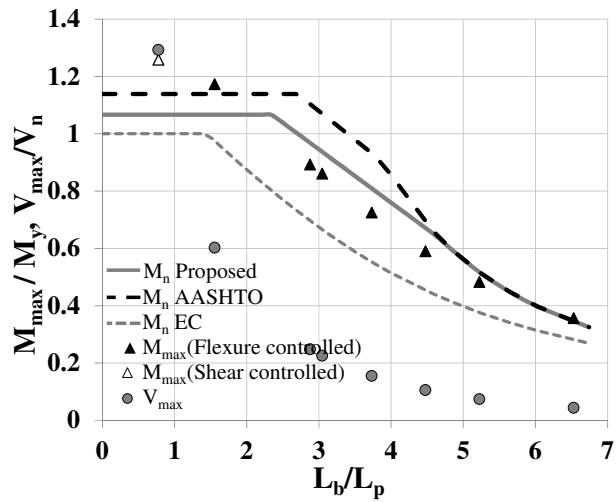**Figure B-15: LTB curves for G46, C_b = 1.75**

Figure B-16: LTB curves for G47, C_b = 1.75

329

Table B-9: Test simulation results and comparison with proposed and AISC equations for rolled beams subjected to moment gradient, $C_b = 2.3$

W21x44	L_b (inches)	75.0	130.0	188.5	225.0	273.0	
	M_{max}/M_p	1.11	1.06	0.96	0.82	0.64	
	M_{max}/M_{nPr}	1.11	1.06	0.96	1.09	1.15	
	M_{max}/M_{nAISC}	1.11	1.06	0.96	1.09	1.15	
W14x68	L_b (inches)	200.0	275.0	340.0	475.0	615.3	700.0
	M_{max}/M_p	1.16	1.13	1.10	1.05	0.90	0.80
	M_{max}/M_{nPr}	1.16	1.13	1.10	1.06	1.22	1.25
	M_{max}/M_{nAISC}	1.16	1.13	1.10	1.06	1.22	1.25
W10x30	L_b (inches)	103.1	200.0	258.0	300.0	338.1	400.0
	M_{max}/M_p	1.21	1.09	1.05	0.97	0.88	0.74
	M_{max}/M_{nPr}	1.21	1.09	1.05	1.16	1.20	1.23
	M_{max}/M_{nAISC}	1.21	1.09	1.05	1.16	1.20	1.23
W16x31	L_b (inches)	50.0	95.0	125.0	175.0	200.0	250.0
	M_{max}/M_p	1.15	1.11	1.07	1.01	0.93	0.72
	M_{max}/M_{nPr}	1.15	1.11	1.07	1.01	1.13	1.22
	M_{max}/M_{nAISC}	1.15	1.11	1.07	1.01	1.13	1.22
W14x90	L_b (inches)	500.0	650.0	750.0	892.5	1000.0	
	M_{max}/M_p	1.04	1.04	1.03	0.95	0.88	
	M_{max}/M_{nPr}	1.09	1.09	1.13	1.27	1.33	
	M_{max}/M_{nAISC}	1.04	1.04	1.13	1.27	1.33	

Table B-10: Test simulation results and comparison with proposed and AASHTO equations for plate girders subjected to moment gradient, $C_b = 2.3$, Girders G1, G3, G5, G9

	L_b (inches)	150.0	200.0	403.0	450.0	481.2	600.0	700.0	850.0	
	M_{max}/M_y	0.62	0.72	0.81	0.77	0.74	0.64	0.57	0.49	
G1	M_{max}/M_{nPr}							0.76	0.96	
	$M_{max}/M_{nAASHTO}$							0.70	0.86	
	$V_{max}/V_{nAASHTO}$	2.72	2.40	1.34	1.13	1.02	0.71			
	L_b (inches)	250.0	600.0	987.0	1178.0	1300.0	1600.0	1800.0	2000.0	
	M_{max}/M_y	0.35	0.73	1.04	0.95	0.91	0.79	0.72	0.65	
G3	M_{max}/M_{nPr}							0.88	0.96	
	$M_{max}/M_{nAASHTO}$							0.88	0.96	
	$V_{max}/V_{nAASHTO}$	2.60	2.24	1.95	1.49	1.29	0.92			
	L_b (inches)	100.0	350.0	430.0	480.0	514.6	600.0	700.0	800.0	
	M_{max}/M_y	0.37	0.76	0.73	0.69	0.66	0.60	0.53	0.48	
G5	M_{max}/M_{nPr}									
	$M_{max}/M_{nAASHTO}$									
	$V_{max}/V_{nAASHTO}$	6.03	3.51	2.75	2.33	2.09	1.62	1.24	0.98	
	L_b (inches)	100.0	200.0	382.0	420.0	455.2	575.0	600.0	700.0	796.5
	M_{max}/M_y	0.41	0.63	0.79	0.78	0.76	0.69	0.69	0.65	0.62
G9	M_{max}/M_{nPr}						1.19	1.30	1.67	2.05
	$M_{max}/M_{nAASHTO}$						1.12	1.22	1.58	1.93
	$V_{max}/V_{nAASHTO}$	3.39	2.64	1.74	1.55	1.40				

Table B-11: Test simulation results and comparison with proposed and AASHTO equations for plate girders subjected to moment gradient, C_b = 2.3, Girders G13, G46, G47, G49

G13	L_b (inches)	365.0	430.0	460.0	491.1	600.0	675.0	859.4	
	M_{max}/M_y	0.69	0.68	0.66	0.65	0.61	0.55	0.51	
	M_{max}/M_{nPr}							1.82	
	$M_{max}/M_{nAASHTO}$							1.72	
	$V_{max}/V_{nAASHTO}$	3.56	2.97	2.72	2.50	1.93	1.55		
G46	L_b (inches)	316.6	534.7	752.8	970.9	1189.0	1426.8	1664.5	2080.7
	M_{max}/M_y	0.52	0.80	0.92	0.93	0.89	0.82	0.74	0.59
	M_{max}/M_{nPr}				1.02	0.97	0.90	0.92	1.09
	$M_{max}/M_{nAASHTO}$				0.93	0.88	0.81	0.92	1.09
	$V_{max}/V_{nAASHTO}$	1.70	1.53	1.26					
G47	L_b (inches)	100.0	200.0	370.0	391.8	479.9	575.8	671.8	839.8
	M_{max}/M_y	0.50	0.81	0.95	0.93	0.84	0.76	0.68	0.57
	M_{max}/M_{nPr}					0.79	0.71	0.75	0.94
	$M_{max}/M_{nAASHTO}$					0.74	0.66	0.75	0.94
	$V_{max}/V_{nAASHTO}$	2.05	1.66	1.05	0.97				
G49	L_b (inches)	100.0	175.0	250.0	370.2	453.4	521.4	589.36	793.4
	M_{max}/M_y	0.41	0.63	0.83	0.94	0.90	0.87	0.84	0.74
	M_{max}/M_{nPr}					1.11	1.21	1.41	2.25
	$M_{max}/M_{nAASHTO}$					0.90	0.88	1.36	2.19
	$V_{max}/V_{nAASHTO}$	2.01	1.79	1.64	1.25				
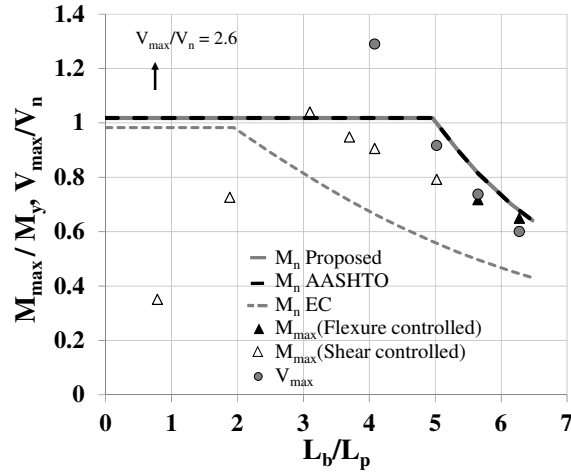
Figure B-17: LTB curves for G3, *C_b* = 2.3
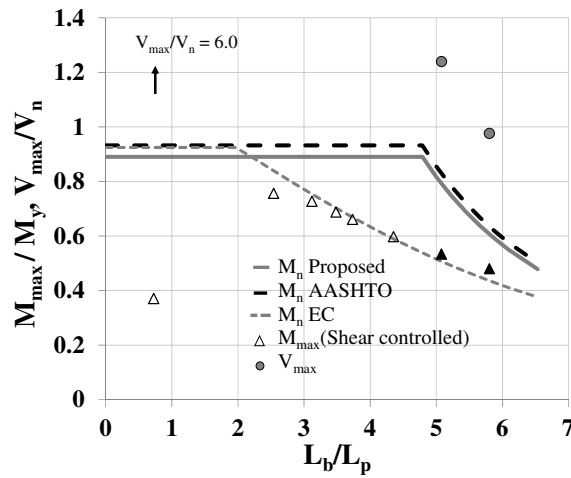
Figure B-18: LTB curves for G5, *C_b* = 2.3
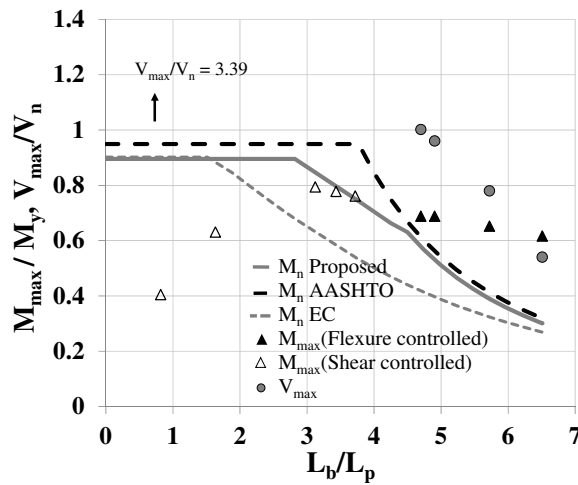
Figure B-19: LTB curves for G9, *C_b* = 2.3

333
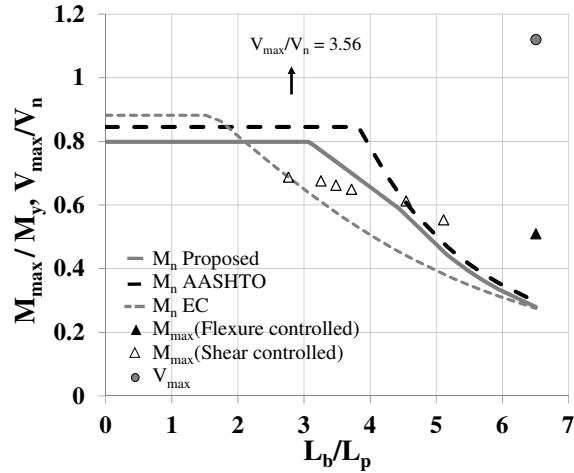
Figure B-20: LTB curves for G13, C_b = 2.3
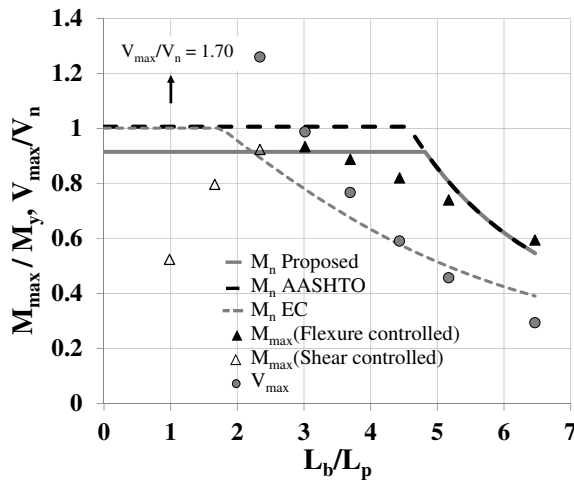
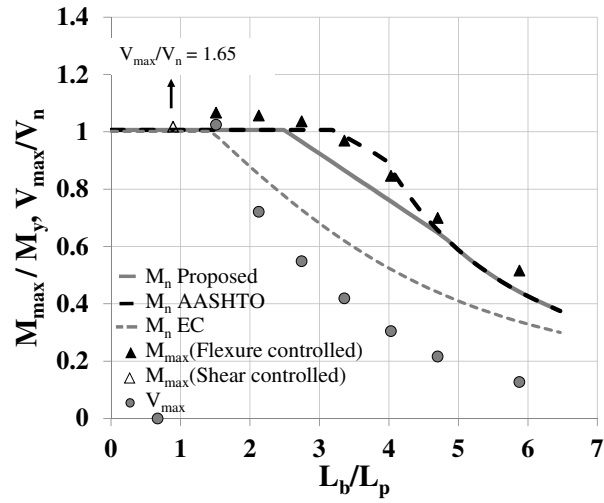**Figure B-21: LTB curves for G46, C_b = 2.3**

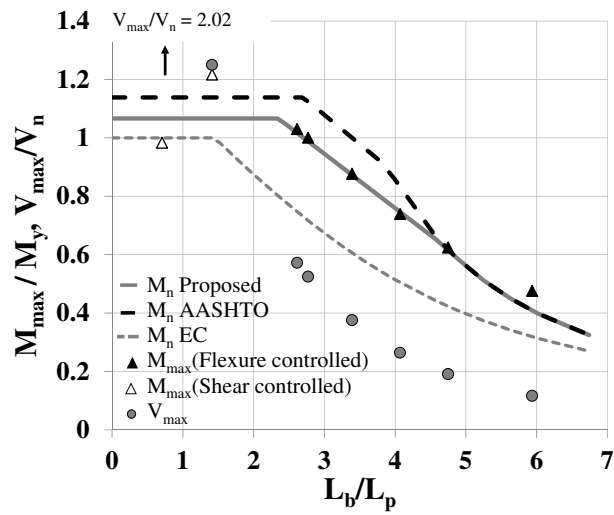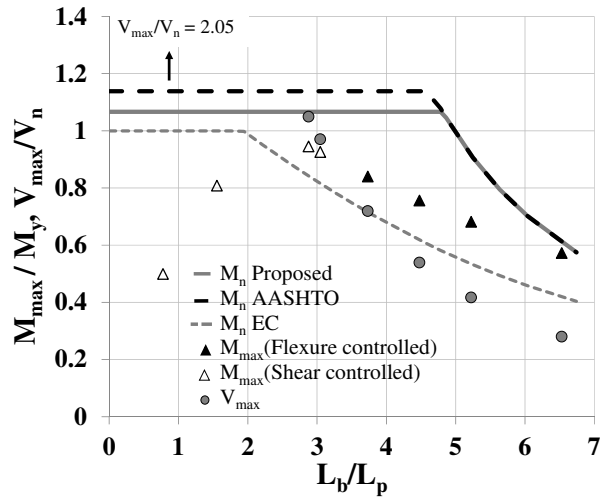**Figure B-22: LTB curves for G47, C_b = 2.3**

334
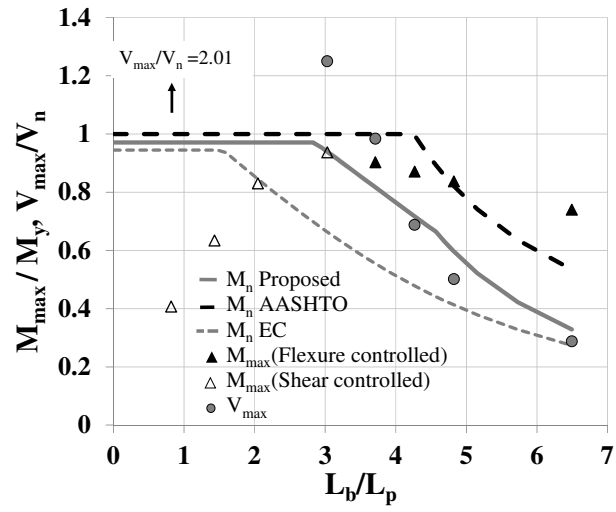
Figure B-23: LTB curves for G49, $C_b = 2.3$

Table B-12: Test simulation results and comparison with proposed and AISC equations for rolled beams subjected to transverse loading, Case a in Table 7-1

	L_b (inches)	200.0	300.0	400.0	550.0	650.0	800.0
W21x44	M_{max}/M_p	1.00	0.83	0.67	0.57	0.51	0.43
	M_{max}/M_{nPr}	1.00	0.83	0.72	1.01	1.15	1.27
	M_{max}/M_{nAISC}	1.00	0.56	0.72	1.12	1.55	2.17
	L_b (inches)	500.0	800.0	1000.0	1300.0	1600.0	
W14x68	M_{max}/M_p	1.04	0.88	0.82	0.74	0.68	
	M_{max}/M_{nPr}	1.04	0.88	0.84	1.02	1.17	
	M_{max}/M_{nAISC}	1.04	0.88	0.86	1.41	2.02	

Table B-13: Test simulation results and comparison with proposed and AISC equations for rolled beams subjected to transverse loading, Case b in Table 7-1

	L_b (inches)	200.0	252.0	300.0	400.0	550.0	650.0	800.0
W21x44	M_{max}/M_p	0.98	0.82	0.67	0.51	0.41	0.36	0.31
	M_{max}/M_{nPr}	0.98	0.83	0.89	1.06	1.31	1.43	1.60
	M_{max}/M_{nAISC}	0.98	0.82	0.89	1.06	1.31	1.43	1.60
	L_b (inches)	500.0	628.0	800.0	1000.0	1300.0	1600.0	
W14x68	M_{max}/M_p	0.98	0.83	0.73	0.63	0.50	0.41	
	M_{max}/M_{nPr}	0.98	0.84	0.97	1.07	1.13	1.16	
	M_{max}/M_{nAISC}	0.98	0.84	0.97	1.07	1.13	1.16	

Table B-14: Test simulation results and comparison with proposed and AISC equations for rolled beams subjected to transverse loading, Case c in Table 7-1

	L_b (inches)	50.0	75.0	110.0	130.0	188.5	225.0	273.0
	M_{max}/M_p	0.84	0.83	0.72	0.65	0.44	0.35	0.26
W21x44	M_{max}/M_{nPr}			0.90	0.90	0.90	0.94	0.96
	M_{max}/M_{nAISC}			0.81	0.82	0.90	0.94	0.96
	V_{max}/V_{nAISC}	1.60	1.05					
	L_b (inches)	100.0	200.0	275.0	340.0	475.0	615.3	
	M_{max}/M_p	0.94	0.83	0.73	0.63	0.46	0.37	
W14x68	M_{max}/M_{nPr}		0.92	0.93	0.91	0.94	1.01	
	M_{max}/M_{nAISC}		0.85	0.87	0.86	0.94	1.01	
	V_{max}/V_{nAISC}	1.43						

Table B-15: Test simulation results and comparison with proposed and AISC equations for rolled beams subjected to transverse loading, Case d-1 in Table 7-1

	L_b (inches)	50.0	75.0	110.0	130.0	188.5	225.0	273.0
	M_{max}/M_p	0.90	0.92	0.80	0.73	0.52	0.42	0.32
W21x44	M_{max}/M_{nPr}	0.96	1.06	1.03	1.02	0.92	0.97	1.00
	M_{max}/M_{nAISC}	0.90	0.92	0.80	0.80	0.92	0.97	1.00
	L_b (inches)	100.0	200.0	275.0	340.0	475.0	615.3	
	M_{max}/M_p	0.98	0.91	0.82	0.72	0.54	0.43	
W14x68	M_{max}/M_{nPr}	1.03	1.08	1.06	1.02	0.95	1.00	
	M_{max}/M_{nAISC}	0.98	0.91	0.84	0.85	0.95	1.00	

Table B-16: Test simulation results and comparison with proposed and AISC equations for rolled beams subjected to transverse loading, Case d-2 in Table 7-1

	L_b (inches)	24.0	50.0	75.0	100.0	150.0	200.0	300.0
	M_{max}/M_p	0.76	0.88	0.82	0.71	0.49	0.33	0.20
W21x44	M_{max}/M_{nPr}		0.97	1.01	0.97	0.89	0.91	1.00
	M_{max}/M_{nAISC}		0.88	0.95	0.92	0.83	0.91	1.00
	V_{max}/V_{nAISC}	1.50						
	L_b (inches)	40.0	100.0	200.0	300.0	400.0	550.0	700.0
	M_{max}/M_p	0.86	0.96	0.81	0.63	0.50	0.38	0.35
W14x68	M_{max}/M_{nPr}		1.04	1.03	0.97	0.98	1.11	1.31
	M_{max}/M_{nAISC}		0.96	1.00	0.95	0.99	1.11	1.31
	V_{max}/V_{nAISC}	1.63						

Table B-17: Test simulation results and comparison with proposed and AISC equations for rolled beams subjected to transverse loading, Case d-3 in Table 7-1

	L_b (inches)	100.0	160.0	200.0	250.0	300.0
	M_{max}/M_p	0.92	0.78	0.67	0.51	0.40
W21x44	M_{max}/M_{nPr}	1.02	0.95	0.93	1.01	1.02
	M_{max}/M_{nAISC}	0.92	0.78	0.93	1.01	1.02
	L_b (inches)	200.0	300.0	400.0	500.0	700.0
	M_{max}/M_p	0.95	0.89	0.78	0.64	0.45
W14x68	M_{max}/M_{nPr}	1.02	0.99	0.91	0.85	0.87
	M_{max}/M_{nAISC}	0.95	0.89	0.79	0.85	0.87

APPENDIX C

ADDITIONAL RESULTS FOR LTB OF LONGITUDINALLY

STIFFENED GIRDERS SUBJECTED TO UNIFORM BENDING

This section presents the complete set of results for longitudinally stiffened girders under uniform bending. Table C-1 lists the girder names for different cross-sections, and Tables C-2 to C-8 show the results for all girders considered for $d_o/D = 1$.

The tables are followed by Figures C-1 through C-24, which show the results for all girders with $d_o/D = 1$. Plots for girders LG2, LG3 and LG27 are shown in Chapter 8.

Table C-1: Designation of longitudinally stiffened girders

D_c/D	D/b_{fc}	D/t_w	Girder
0.5	6	200	LG1
		240	LG2
		300	LG3
	5	200	LG4
		240	LG5
		300	LG6
	4	200	LG7
		240	LG8
		300	LG9
0.625	6	200	LG10
		240	LG11
		300	LG12
	5	200	LG13
		240	LG14
		300	LG15
	4	200	LG16
		240	LG17
		300	LG18
0.75	6	200	LG19
		240	LG20
		300	LG21
	5	200	LG22
		240	LG23
		300	LG24
	4	200	LG25
		240	LG26
		300	LG27

Table C-2: Results from test simulations compared with proposed, AASHTO and Eurocode strength predictions for $d_o/D = 1$, $KL_b = 225$ inches

Girder	M_{max}/M_y	$M_{max}/M_{nProposed}$	$M_{max}/M_{nAASHTO}$	M_{max}/M_{nEC}
LG1	0.93	1.07	1.00	1.36
LG2	0.92	1.04	0.98	1.34
LG3	0.89	1.03	1.14	1.29
LG4	0.99	1.08	1.02	1.29
LG5	0.97	1.06	1.00	1.27
LG6	0.94	1.04	1.12	1.23
LG7	1.03	1.08	1.03	1.20
LG8	1.01	1.05	1.01	1.19
LG9	0.99	1.04	1.09	1.15
LG10	0.89	1.03	0.96	1.28
LG11	0.86	1.05	1.21	1.26
LG12	0.83	1.03	1.26	1.20
LG13	0.96	1.05	0.99	1.25
LG14	0.93	1.06	1.18	1.22
LG15	0.91	1.07	1.24	1.20
LG16	1.01	1.06	1.01	1.19
LG17	0.98	1.05	1.13	1.15
LG18	0.95	1.03	1.14	1.11
LG19	0.84	1.06	1.28	1.21
LG20	0.81	1.04	1.35	1.18
LG21	0.78	1.04	1.51	1.14
LG22	0.91	1.07	1.25	1.25
LG23	0.87	1.05	1.29	1.21
LG24	0.85	1.04	1.38	1.17
LG25	1.03	1.13	1.26	1.22
LG26	0.94	1.05	1.20	1.11
LG27	0.92	1.04	1.24	1.08

Table C-3: Results from test simulations compared with proposed, AASHTO and Eurocode strength predictions for $d_o/D = 1$, $KL_b = 375$ inches

Girder	M_{max}/M_y	$M_{max}/M_{nProposed}$	$M_{max}/M_{nAASHTO}$	M_{max}/M_{nEC}
LG1	0.83	1.12	1.01	1.63
LG2	0.84	1.12	1.01	1.63
LG3	0.84	1.15	1.23	1.62
LG4	0.89	1.11	1.01	1.46
LG5	0.89	1.10	1.01	1.46
LG6	0.89	1.11	1.17	1.43
LG7	0.98	1.11	1.04	1.32
LG8	0.96	1.10	1.02	1.32
LG9	0.94	1.08	1.11	1.28
LG10	0.81	1.12	1.00	1.46
LG11	0.82	1.17	1.32	1.48
LG12	0.81	1.16	1.40	1.44
LG13	0.89	1.11	1.02	1.38
LG14	0.88	1.14	1.24	1.37
LG15	0.85	1.11	1.27	1.32
LG16	0.97	1.11	1.04	1.30
LG17	0.94	1.10	1.17	1.26
LG18	0.91	1.08	1.17	1.21
LG19	0.83	1.23	1.46	1.38
LG20	0.81	1.21	1.56	1.36
LG21	0.78	1.22	1.71	1.30
LG22	0.90	1.20	1.37	1.44
LG23	0.85	1.15	1.39	1.38
LG24	0.83	1.15	1.48	1.33
LG25	0.96	1.15	1.26	1.25
LG26	0.91	1.11	1.25	1.19
LG27	0.89	1.10	1.28	1.15

Table C-4: Results from test simulations compared with proposed, AASHTO and Eurocode strength predictions for $d_o/D = 1$, $KL_b = 525$ inches

Girder	M_{max}/M_y	$M_{max}/M_{nProposed}$	$M_{max}/M_{nAASHTO}$	M_{max}/M_{nEC}
LG1	0.62	1.04	0.88	1.72
LG2	0.64	1.05	0.89	1.73
LG3	0.67	1.08	1.11	1.74
LG4	0.78	1.12	0.99	1.66
LG5	0.79	1.12	0.99	1.65
LG6	0.80	1.14	1.16	1.64
LG7	0.87	1.11	1.01	1.44
LG8	0.88	1.10	1.01	1.44
LG9	0.88	1.11	1.11	1.43
LG10	0.62	1.07	0.93	1.42
LG11	0.64	1.10	1.19	1.45
LG12	0.66	1.13	1.32	1.48
LG13	0.78	1.14	1.00	1.47
LG14	0.79	1.17	1.25	1.48
LG15	0.79	1.18	1.31	1.46
LG16	0.87	1.12	1.02	1.35
LG17	0.87	1.13	1.17	1.35
LG18	0.86	1.13	1.19	1.32
LG19	0.70	1.27	1.58	1.32
LG20	0.70	1.26	1.65	1.35
LG21	0.69	1.32	1.77	1.33
LG22	0.81	1.24	1.38	1.50
LG23	0.80	1.23	1.46	1.50
LG24	0.78	1.25	1.55	1.46
LG25	0.88	1.17	1.26	1.27
LG26	0.86	1.15	1.27	1.24
LG27	0.84	1.15	1.30	1.20

Table C-5: Results from test simulations compared with proposed, AASHTO and Eurocode strength predictions for d_o/D =1, KL_b = 675 inches

Girder	M_{max}/M_y	$M_{max}/M_{nProposed}$	$M_{max}/M_{nAASHTO}$	M_{max}/M_{nEC}
LG1	0.42	0.96	0.96	1.60
LG2	0.44	0.94	0.94	1.60
LG3	0.45	0.93	1.13	1.61
LG4	0.61	1.03	0.87	1.67
LG5	0.62	1.04	0.88	1.68
LG6	0.64	1.06	1.04	1.69
LG7	0.80	1.13	1.01	1.61
LG8	0.81	1.13	1.01	1.61
LG9	0.81	1.14	1.12	1.59
LG10	0.44	1.08	1.08	1.27
LG11	0.45	1.04	1.37	1.30
LG12	0.47	1.01	1.45	1.33
LG13	0.61	1.07	0.94	1.41
LG14	0.63	1.09	1.14	1.44
LG15	0.65	1.12	1.21	1.46
LG16	0.80	1.15	1.02	1.44
LG17	0.81	1.17	1.18	1.45
LG18	0.80	1.16	1.20	1.41
LG19	0.57	1.53	2.14	1.22
LG20	0.57	1.43	2.23	1.25
LG21	0.57	1.40	2.37	1.25
LG22	0.71	1.29	1.52	1.52
LG23	0.71	1.28	1.56	1.55
LG24	0.70	1.32	1.58	1.52
LG25	0.83	1.24	1.30	1.32
LG26	0.82	1.21	1.32	1.29
LG27	0.80	1.22	1.35	1.25

Table C-6: Results from test simulations compared with proposed, AASHTO and Eurocode strength predictions for $d_o/D = 1$, $KL_b = 825$ inches

Girder	M_{max}/M_y	$M_{max}/M_{nProposed}$	$M_{max}/M_{nAASHTO}$	M_{max}/M_{nEC}
LG1	0.29	1.01	1.01	1.50
LG2	0.30	0.98	0.98	1.49
LG3	0.31	0.94	1.15	1.44
LG4	0.44	0.94	0.94	1.56
LG5	0.45	0.92	0.92	1.56
LG6	0.45	0.90	1.04	1.52
LG7	0.67	1.07	0.92	1.65
LG8	0.68	1.08	0.93	1.65
LG9	0.67	1.06	1.01	1.60
LG10	0.32	1.19	1.19	1.17
LG11	0.33	1.14	1.50	1.18
LG12	0.33	1.07	1.53	1.17
LG13	0.46	1.06	1.06	1.29
LG14	0.47	1.03	1.28	1.31
LG15	0.47	0.98	1.29	1.29
LG16	0.69	1.13	0.96	1.45
LG17	0.70	1.14	1.12	1.46
LG18	0.69	1.12	1.13	1.41
LG19	0.49	1.96	2.75	1.16
LG20	0.49	1.81	2.82	1.18
LG21	0.47	1.61	2.91	1.16
LG22	0.62	1.51	1.99	1.50
LG23	0.62	1.42	2.03	1.54
LG24	0.60	1.39	2.01	1.49
LG25	0.79	1.34	1.36	1.37
LG26	0.79	1.31	1.40	1.36
LG27	0.75	1.31	1.39	1.29

Table C-7: Results from test simulations compared with proposed, AASHTO and Eurocode strength predictions for $d_o/D = 1$, $KL_b = 975$ inches

Girder	M_{max}/M_y	$M_{max}/M_{nProposed}$	$M_{max}/M_{nAASHTO}$	M_{max}/M_{nEC}
LG1	0.22	1.06	1.06	1.45
LG2	0.23	1.03	1.03	1.44
LG3	0.24	1.01	1.24	1.43
LG4	0.33	0.99	0.99	1.48
LG5	0.34	0.97	0.97	1.48
LG6	0.35	0.97	1.13	1.49
LG7	0.53	0.97	0.91	1.58
LG8	0.54	0.98	0.91	1.59
LG9	0.55	1.00	1.00	1.60
LG10	0.25	1.31	1.31	1.11
LG11	0.26	1.24	1.63	1.13
LG12	0.26	1.19	1.71	1.14
LG13	0.36	1.15	1.15	1.20
LG14	0.37	1.12	1.39	1.22
LG15	0.38	1.09	1.44	1.24
LG16	0.56	1.06	1.02	1.36
LG17	0.57	1.07	1.16	1.38
LG18	0.58	1.09	1.19	1.40
LG19	0.42	2.35	3.29	1.10
LG20	0.42	2.15	3.36	1.12
LG21	0.41	1.96	3.54	1.12
LG22	0.52	1.77	2.33	1.41
LG23	0.52	1.67	2.38	1.45
LG24	0.52	1.56	2.45	1.47
LG25	0.69	1.34	1.59	1.28
LG26	0.69	1.32	1.60	1.30
LG27	0.68	1.39	1.60	1.28

Table C-8: Results from test simulations compared with proposed, AASHTO and Eurocode strength predictions for $d_o/D = 1$, $KL_b = 1125$ inches

Girder	M_{max}/M_y	$M_{max}/M_{nProposed}$	$M_{max}/M_{nAASHTO}$	M_{max}/M_{nEC}
LG6	0.27	1.00	1.17	1.42
LG9	0.44	0.95	1.05	1.51
LG15	0.30	1.16	1.54	1.17
LG18	0.44	0.98	1.19	1.21
LG24	0.45	1.81	2.84	1.43
LG27	0.51	1.24	1.60	1.05

Figure C-1: Curves for LG1, *d_o/D* = 1

Figure C-2: Curves for LG4, *d_o/D* = 1
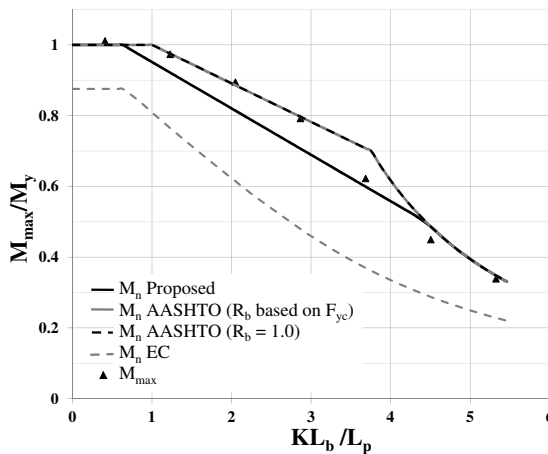
Figure C-3: Curves for LG5, *d_o/D* = 1

348
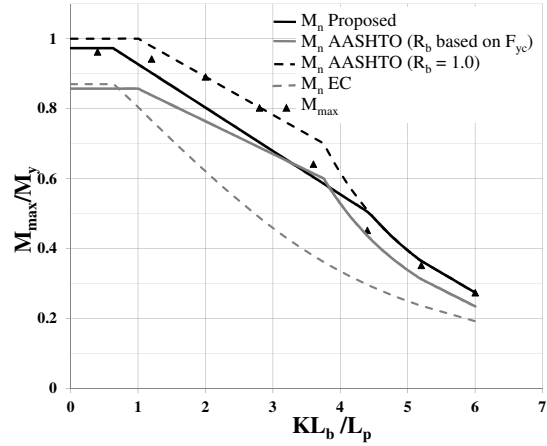
Figure C-4: Curves for LG6, do/D = 1
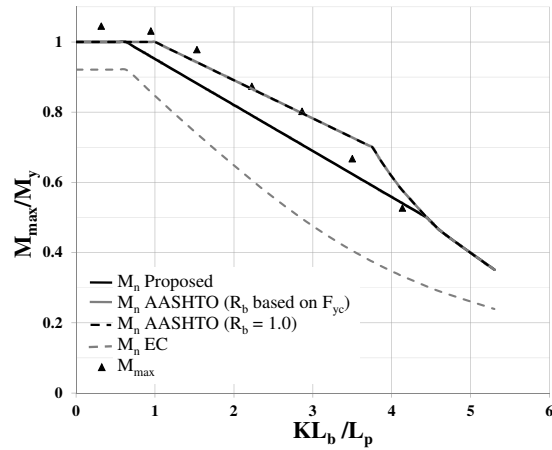
Figure C-5: Curves for LG7, d_o/D = 1
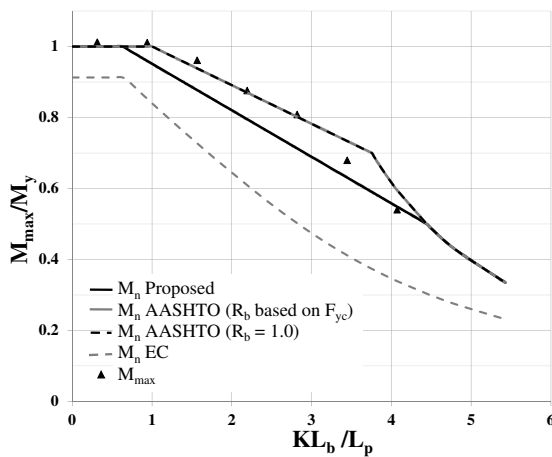
Figure C-6: Curves for LG8, d_o/D = 1

Figure C-7: Curves for LG9, $d_o/D = 1$

Figure C-8: Curves for LG10, $d_o/D = 1$

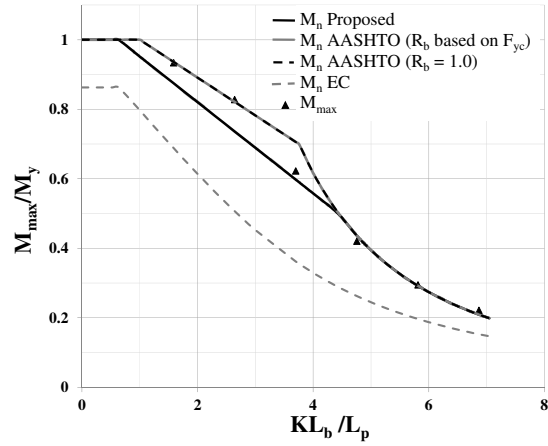**Figure C-9: Curves for LG11, $d_o/D = 1$**

350

Figure C-10: Curves for LG12, $d_o/D = 1$

Figure C-11: Curves for LG13, $d_o/D = 1$
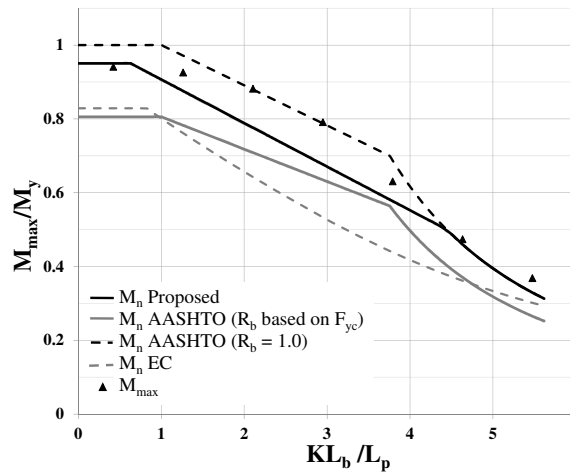
Figure C-12: Curves for LG14, $d_o/D = 1$

351
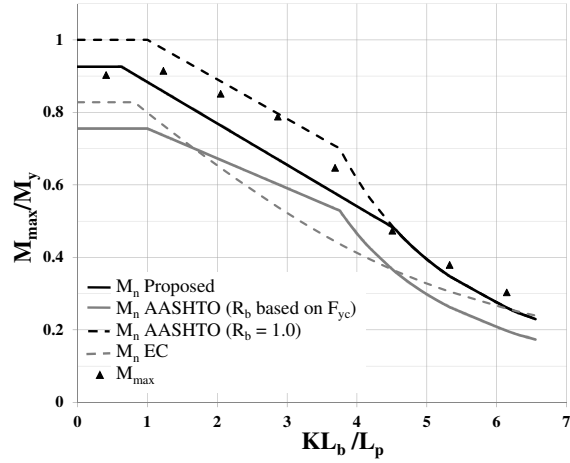
Figure C-13: Curves for LG15, $d_o/D = 1$
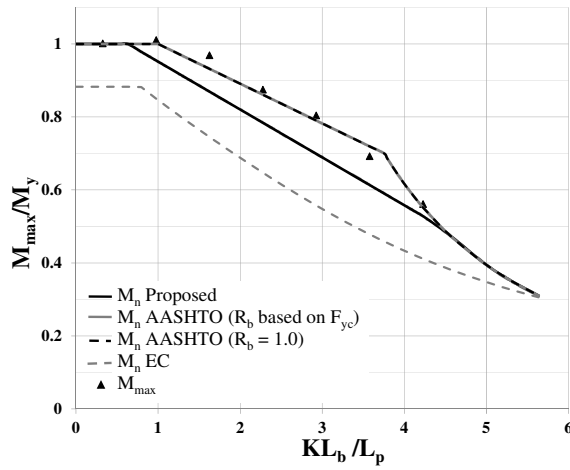
Figure C-14: Curves for LG16, $d_o/D = 1$
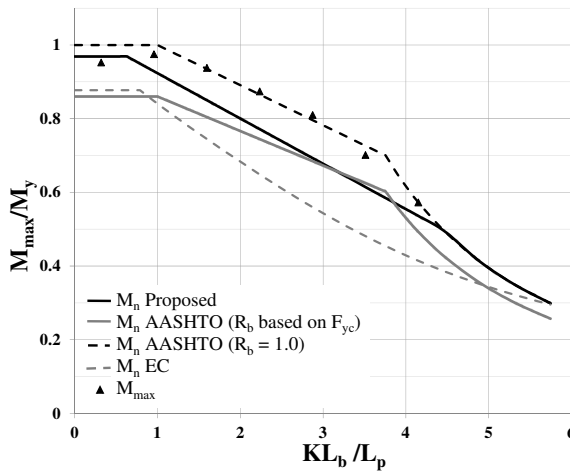
Figure C-15: Curves for LG17, $d_o/D = 1$

352
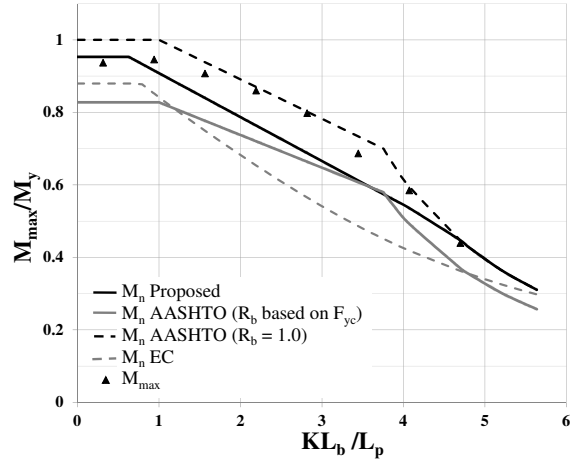
Figure C-16: Curves for LG18, $d_o/D = 1$
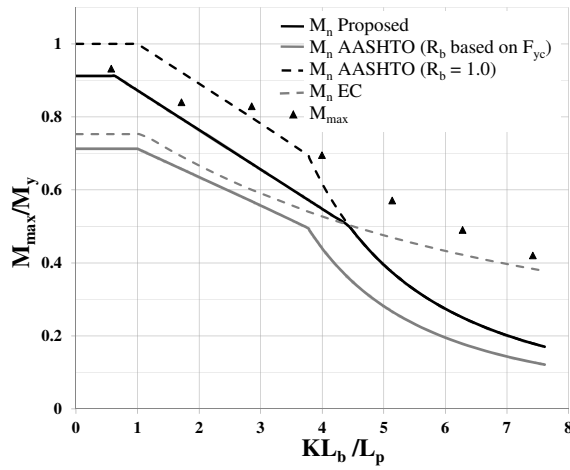
Figure C-17: Curves for LG19, $d_o/D = 1$
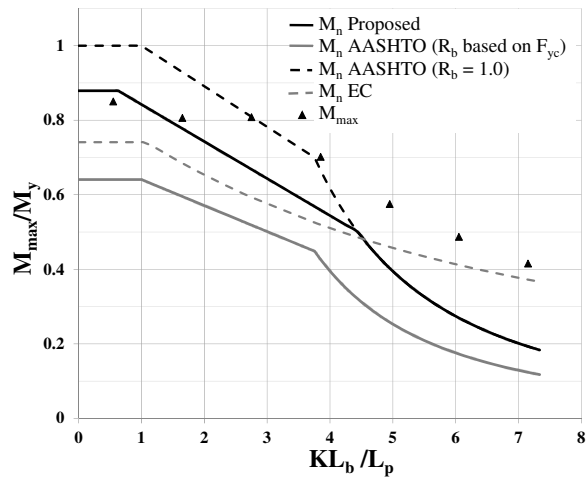
Figure C-18: Curves for LG20, $d_o/D = 1$

353
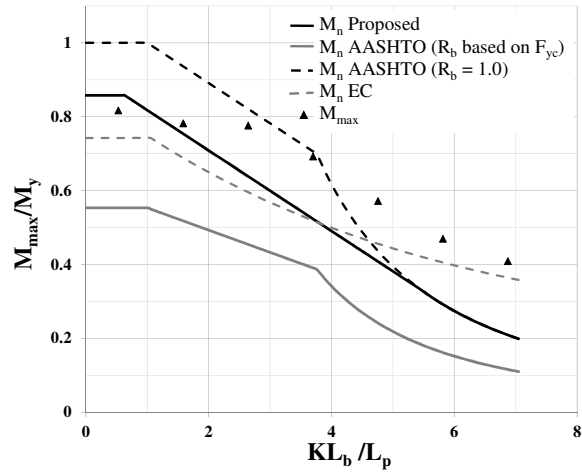
Figure C-19: Curves for LG21, $d_o/D = 1$
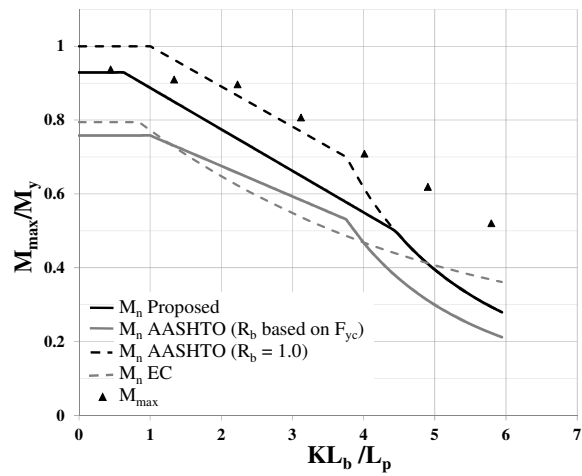
Figure C-20: Curves for LG22, $d_o/D = 1$
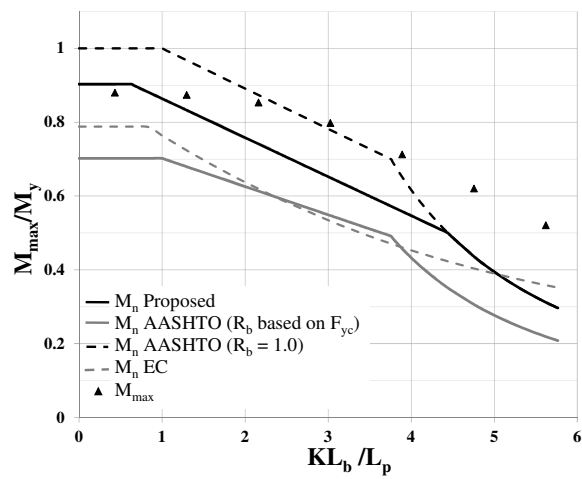
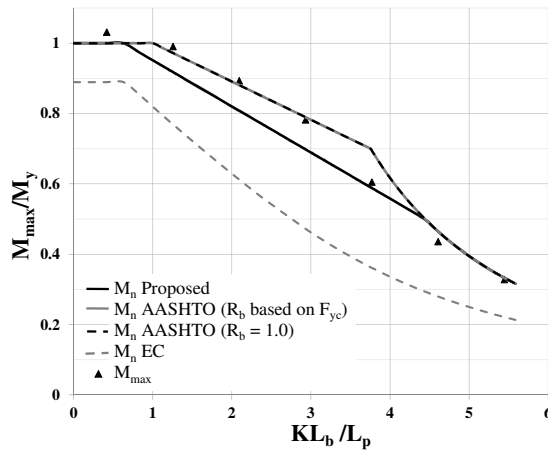**Figure C-21: Curves for LG23, $d_o/D = 1$**

354
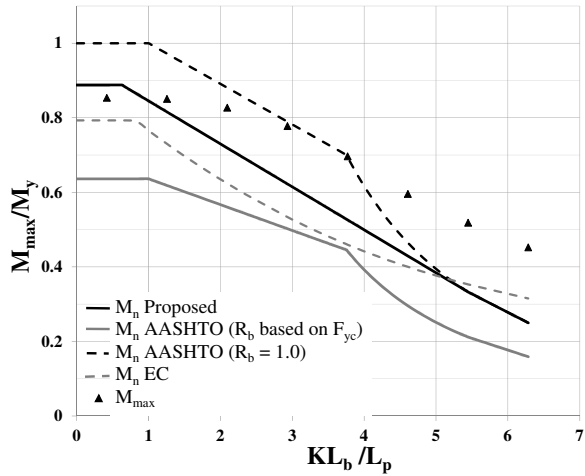
Figure C-22: Curves for LG24, $d_o/D = 1$
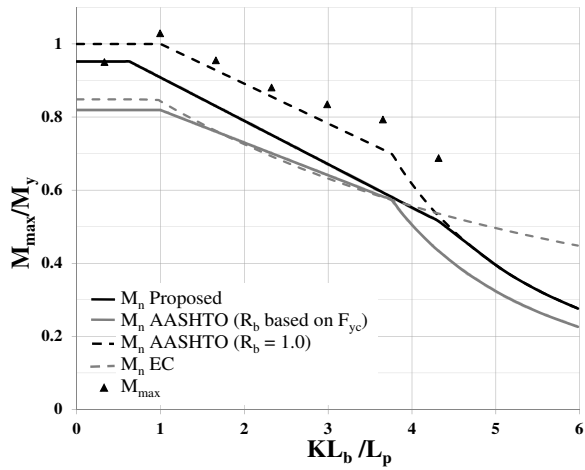
Figure C-23: Curves for LG25, $d_o/D = 1$
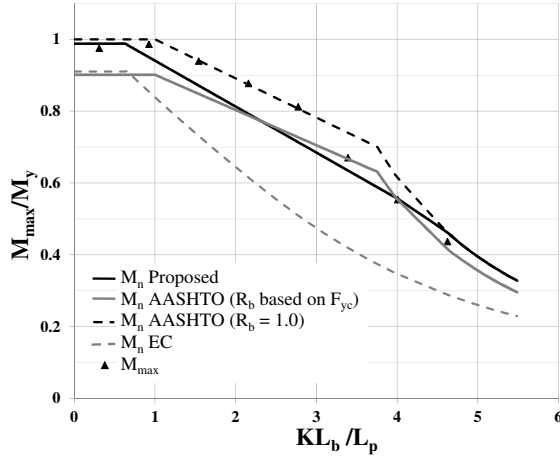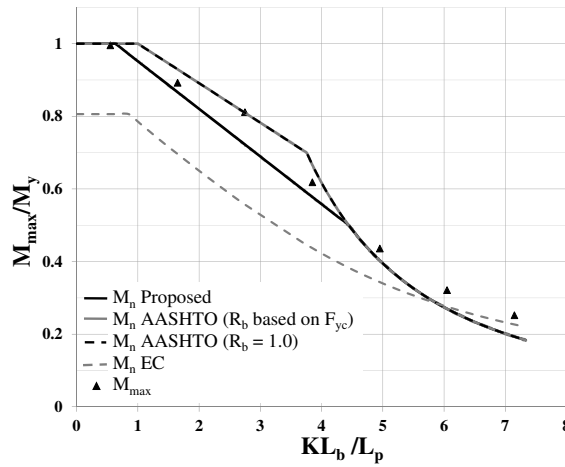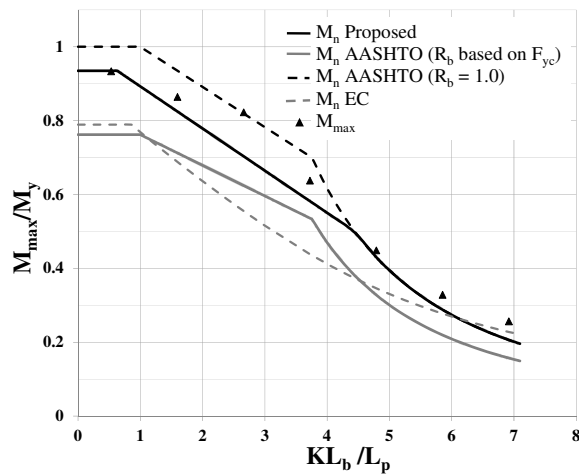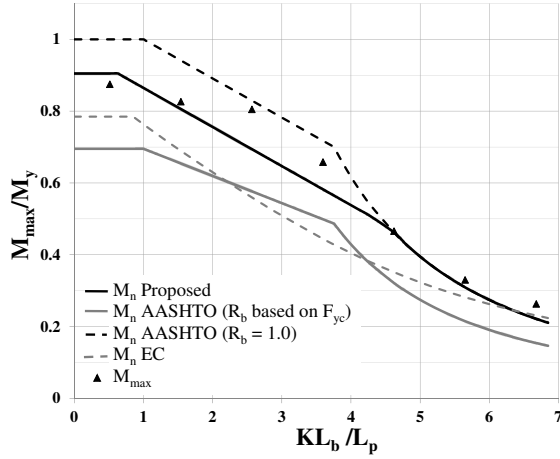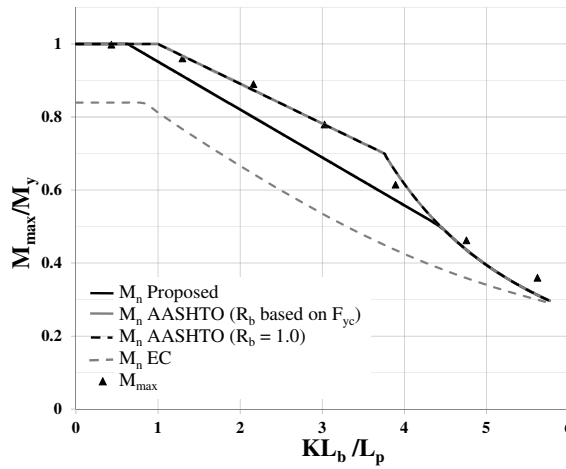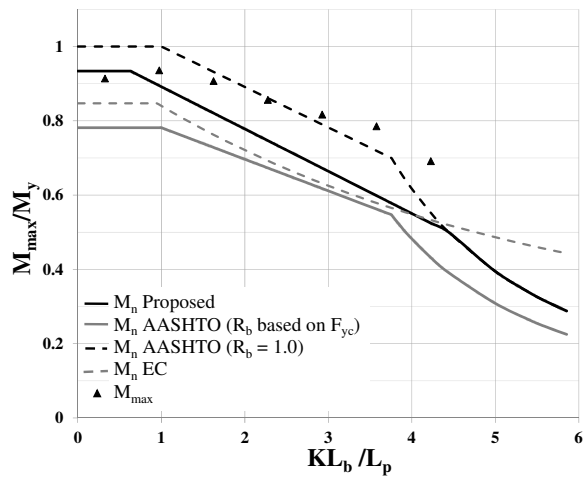

Figure C-24: Curves for LG26, $d_o/D = 1$

355

Tables C-9 through C-15 compare results from test simulations for girders with d_o/D =2.0, with strength predictions from the proposed model, AASHTO and Eurocode.

Table C-9: Results from test simulations compared with proposed, AASHTO and Eurocode strength predictions for d_o/D =2, KL_b = 300 inches

Girder	M_{max}/M_y	$M_{max}/M_{nProposed}$	$M_{max}/M_{nAASHTO}$	M_{max}/M_{nEC}
LG1	0.95	1.18	1.08	1.67
LG2	0.93	1.14	1.05	1.62
LG3	0.90	1.13	1.23	1.54
LG4	0.98	1.14	1.06	1.48
LG5	0.97	1.12	1.04	1.45
LG6	0.94	1.11	1.18	1.40
LG7	1.01	1.10	1.04	1.31
LG8	1.00	1.09	1.03	1.30
LG9	0.97	1.07	1.11	1.25
LG10	0.93	1.17	1.07	1.55
LG11	0.89	1.16	1.34	1.50
LG12	0.84	1.12	1.37	1.40
LG13	0.98	1.15	1.07	1.45
LG14	0.94	1.14	1.27	1.39
LG15	0.89	1.10	1.27	1.30
LG16	1.02	1.11	1.05	1.31
LG17	0.97	1.09	1.16	1.25
LG18	0.95	1.08	1.18	1.21
LG19	0.89	1.20	1.45	1.43
LG20	0.83	1.15	1.50	1.36
LG21	0.80	1.14	1.65	1.29
LG22	0.93	1.16	1.35	1.43
LG23	0.88	1.12	1.37	1.36
LG24	0.86	1.11	1.46	1.31
LG25	0.97	1.12	1.23	1.25
LG26	0.93	1.09	1.24	1.19
LG27	0.92	1.08	1.28	1.15

Table C-10: Results from test simulations compared with proposed, AASHTO and Eurocode strength predictions for $d_o/D = 2$, $KL_b = 450$ inches

Girder	M_{max}/M_y	$M_{max}/M_{nProposed}$	$M_{max}/M_{nAASHTO}$	M_{max}/M_{nEC}
LG1	0.75	1.13	0.99	1.84
LG2	0.76	1.11	0.98	1.80
LG3	0.76	1.12	1.18	1.75
LG4	0.84	1.11	1.00	1.61
LG5	0.84	1.10	1.00	1.59
LG6	0.84	1.11	1.16	1.56
LG7	0.92	1.10	1.02	1.42
LG8	0.91	1.09	1.01	1.40
LG9	0.90	1.08	1.10	1.37
LG10	0.73	1.13	0.98	1.55
LG11	0.74	1.14	1.27	1.55
LG12	0.74	1.15	1.37	1.52
LG13	0.83	1.11	1.00	1.46
LG14	0.83	1.14	1.23	1.46
LG15	0.81	1.13	1.27	1.41
LG16	0.91	1.10	1.02	1.35
LG17	0.90	1.11	1.16	1.32
LG18	0.87	1.08	1.16	1.26
LG19	0.74	1.21	1.41	1.37
LG20	0.74	1.19	1.53	1.37
LG21	0.71	1.22	1.69	1.33
LG22	0.82	1.17	1.33	1.47
LG23	0.81	1.16	1.40	1.45
LG24	0.79	1.17	1.48	1.40
LG25	0.90	1.14	1.23	1.27
LG26	0.87	1.11	1.24	1.22
LG27	0.85	1.10	1.28	1.18

Table C-11: Results from test simulations compared with proposed, AASHTO and Eurocode strength predictions for $d_o/D = 2$, $KL_b = 600$ inches

Girder	M_{max}/M_y	$M_{max}/M_{nProposed}$	$M_{max}/M_{nAASHTO}$	M_{max}/M_{nEC}
LG1	0.56	1.07	1.02	1.93
LG2	0.56	1.03	0.96	1.84
LG3	0.56	1.01	1.10	1.77
LG4	0.71	1.10	0.96	1.79
LG5	0.72	1.10	0.95	1.76
LG6	0.73	1.11	1.12	1.74
LG7	0.84	1.12	1.01	1.57
LG8	0.84	1.12	1.01	1.56
LG9	0.85	1.12	1.12	1.54
LG10	0.56	1.10	1.09	1.50
LG11	0.55	1.06	1.33	1.48
LG12	0.56	1.06	1.38	1.46
LG13	0.70	1.12	0.96	1.52
LG14	0.71	1.13	1.19	1.52
LG15	0.72	1.15	1.27	1.51
LG16	0.84	1.13	1.01	1.43
LG17	0.84	1.14	1.18	1.43
LG18	0.82	1.13	1.19	1.38
LG19	0.62	1.30	1.83	1.29
LG20	0.62	1.22	1.88	1.31
LG21	0.61	1.30	1.99	1.29
LG22	0.74	1.23	1.35	1.52
LG23	0.74	1.22	1.44	1.54
LG24	0.72	1.25	1.52	1.50
LG25	0.84	1.18	1.26	1.31
LG26	0.83	1.16	1.28	1.28
LG27	0.81	1.17	1.31	1.24

Table C-12: Results from test simulations compared with proposed, AASHTO and Eurocode strength predictions for d_o/D = 2, KL_b = 750 inches

Girder	M_{max}/M_y	$M_{max}/M_{nProposed}$	$M_{max}/M_{nAASHTO}$	M_{max}/M_{nEC}
LG1	0.40	1.12	1.12	1.85
LG2	0.39	1.04	1.04	1.73
LG3	0.39	0.98	1.20	1.65
LG4	0.54	1.01	0.96	1.77
LG5	0.54	0.99	0.92	1.72
LG6	0.55	0.99	1.04	1.69
LG7	0.74	1.11	0.97	1.69
LG8	0.74	1.11	0.97	1.68
LG9	0.75	1.12	1.08	1.66
LG10	0.40	1.24	1.24	1.38
LG11	0.40	1.14	1.50	1.34
LG12	0.40	1.07	1.54	1.32
LG13	0.54	1.05	1.03	1.43
LG14	0.55	1.04	1.22	1.43
LG15	0.56	1.05	1.26	1.42
LG16	0.74	1.13	0.99	1.48
LG17	0.75	1.15	1.15	1.48
LG18	0.75	1.16	1.19	1.46
LG19	0.50	1.66	2.32	1.18
LG20	0.50	1.52	2.37	1.18
LG21	0.49	1.40	2.51	1.18
LG22	0.62	1.25	1.65	1.47
LG23	0.63	1.22	1.69	1.50
LG24	0.62	1.30	1.73	1.49
LG25	0.78	1.22	1.27	1.32
LG26	0.78	1.22	1.31	1.31
LG27	0.76	1.24	1.34	1.27

Table C-13: Results from test simulations compared with proposed, AASHTO and Eurocode strength predictions for $d_o/D = 2$, $KL_b = 900$ inches

Girder	M_{max}/M_y	$M_{max}/M_{nProposed}$	$M_{max}/M_{nAASHTO}$	M_{max}/M_{nEC}
LG1	0.29	1.19	1.19	1.77
LG2	0.28	1.10	1.10	1.65
LG3	0.28	1.03	1.26	1.56
LG4	0.40	1.02	1.02	1.68
LG5	0.40	0.98	0.98	1.62
LG6	0.41	0.95	1.11	1.59
LG7	0.60	1.03	0.88	1.68
LG8	0.61	1.03	0.87	1.67
LG9	0.62	1.04	0.97	1.66
LG10	0.31	1.36	1.36	1.30
LG11	0.30	1.25	1.64	1.26
LG12	0.30	1.16	1.67	1.23
LG13	0.42	1.14	1.14	1.33
LG14	0.42	1.09	1.35	1.32
LG15	0.43	1.04	1.38	1.31
LG16	0.62	1.08	0.95	1.43
LG17	0.63	1.09	1.08	1.44
LG18	0.64	1.11	1.10	1.44
LG19	0.42	2.01	2.83	1.10
LG20	0.42	1.84	2.87	1.11
LG21	0.41	1.67	3.02	1.10
LG22	0.53	1.52	2.01	1.40
LG23	0.53	1.44	2.05	1.43
LG24	0.53	1.38	2.11	1.44
LG25	0.69	1.25	1.36	1.28
LG26	0.70	1.24	1.38	1.29
LG27	0.69	1.29	1.38	1.26

Table C-14: Results from test simulations compared with proposed, AASHTO and Eurocode strength predictions for $d_o/D =2$, $KL_b = 1050$ inches

Girder	M_{max}/M_y	$M_{max}/M_{nProposed}$	$M_{max}/M_{nAASHTO}$	M_{max}/M_{nEC}
LG1	0.22	1.24	1.24	1.73
LG2	0.22	1.14	1.14	1.61
LG3	0.22	1.07	1.31	1.51
LG4	0.31	1.07	1.07	1.61
LG5	0.31	1.02	1.02	1.55
LG6	0.31	0.99	1.16	1.51
LG7	0.47	0.95	0.95	1.61
LG8	0.48	0.94	0.93	1.59
LG9	0.49	0.95	1.02	1.58
LG10	0.25	1.49	1.49	1.25
LG11	0.24	1.36	1.78	1.21
LG12	0.24	1.25	1.80	1.17
LG13	0.33	1.23	1.23	1.26
LG14	0.33	1.17	1.45	1.24
LG15	0.34	1.12	1.48	1.23
LG16	0.50	1.06	1.06	1.35
LG17	0.51	1.03	1.20	1.35
LG18	0.52	1.04	1.22	1.36
LG19	0.37	2.39	3.36	1.05
LG20	0.36	2.17	3.39	1.06
LG21	0.36	1.97	3.57	1.06
LG22	0.45	1.78	2.35	1.34
LG23	0.45	1.68	2.39	1.37
LG24	0.45	1.57	2.47	1.39
LG25	0.61	1.33	1.63	1.21
LG26	0.61	1.29	1.65	1.22
LG27	0.61	1.35	1.67	1.22

Table C-15: Results from test simulations compared with proposed, AASHTO and Eurocode strength predictions for $d_o/D = 2$, $KL_b = 1350$ inches

Girder	M_{max}/M_y	$M_{max}/M_{nProposed}$	$M_{max}/M_{nAASHTO}$	M_{max}/M_{nEC}
LG1	0.15	1.37	1.37	1.71
LG2	0.14	1.25	1.25	1.58
LG3	0.13	1.07	1.31	1.36
LG4	0.20	1.14	1.14	1.52
LG5	0.20	1.09	1.09	1.45
LG6	0.20	1.05	1.22	1.41
LG7	0.31	1.01	1.01	1.47
LG8	0.31	1.00	1.00	1.45
LG9	0.32	0.99	1.09	1.43
LG10	0.18	1.76	1.76	1.21
LG11	0.17	1.59	2.09	1.16
LG12	0.17	1.44	2.07	1.12
LG13	0.23	1.42	1.42	1.17
LG14	0.23	1.33	1.65	1.15
LG15	0.23	1.26	1.67	1.13
LG16	0.35	1.21	1.21	1.22
LG17	0.35	1.17	1.36	1.22
LG18	0.36	1.14	1.38	1.22
LG19	0.31	3.28	4.60	1.03
LG20	0.30	2.94	4.59	1.02
LG21	0.29	2.63	4.76	1.02
LG22	0.36	2.36	3.11	1.29
LG23	0.36	2.19	3.12	1.32
LG24	0.35	2.03	3.20	1.33
LG25	0.47	1.72	2.10	1.09
LG26	0.48	1.65	2.11	1.10
LG27	0.48	1.58	2.14	1.10

Figures C-25 through C-48 show the LTB curves for all girders for $d_o/D = 2$. Plots for girders LG2, LG3 and LG27 are shown in Chapter 8.

Figure C-25: Curves for LG1, $d_o/D = 2$
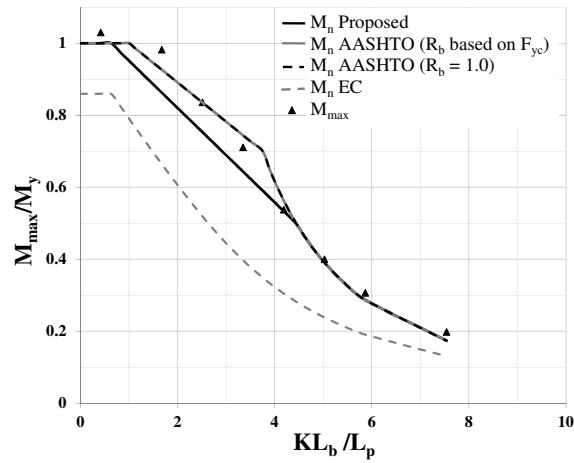
Figure C-26: Curves for LG4, $d_o/D = 2$
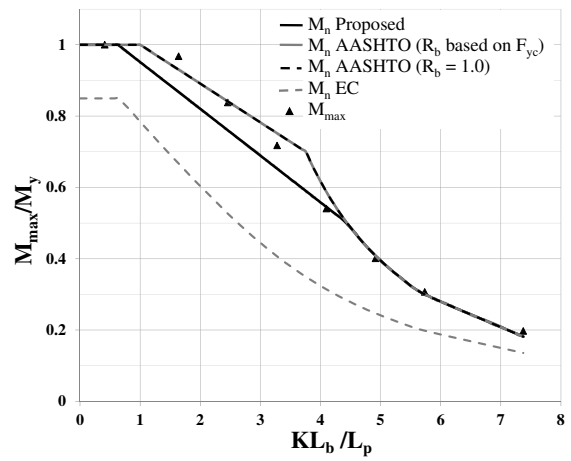
Figure C-27: Curves for LG5, $d_o/D = 2$

363
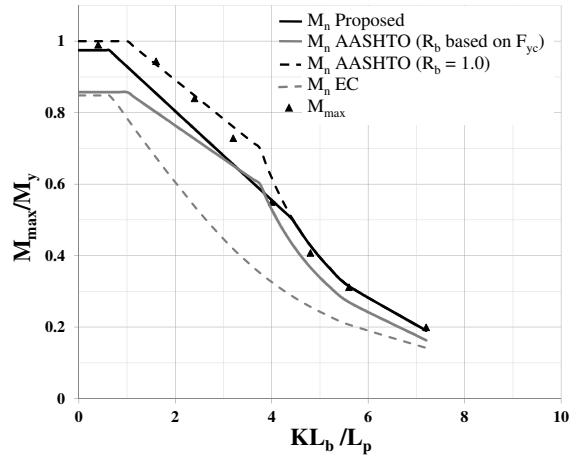
Figure C-28: Curves for LG6, *d$_o$/D* = 2
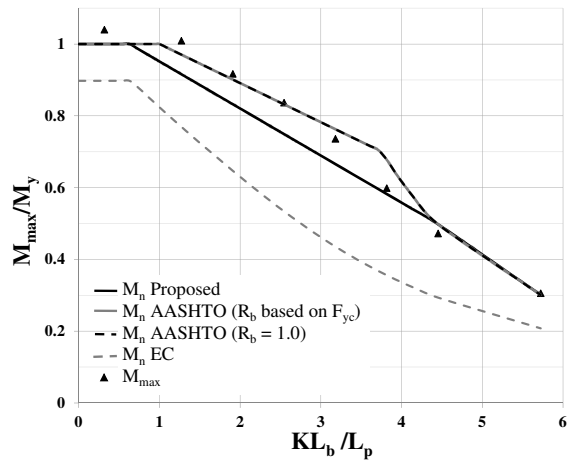
Figure C-29: Curves for LG7, *d$_o$/D* = 2
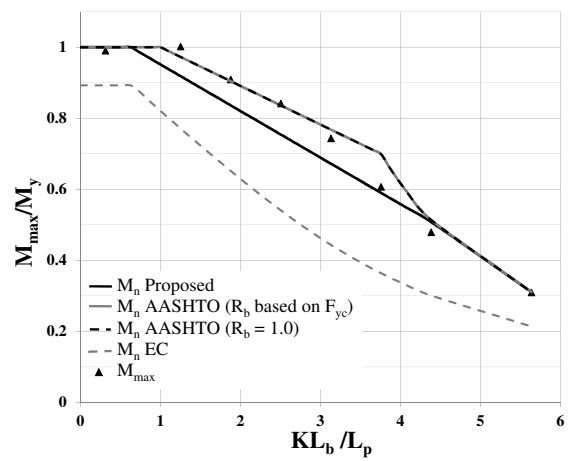
Figure C-30: Curves for LG8, *d$_o$/D* = 2

364
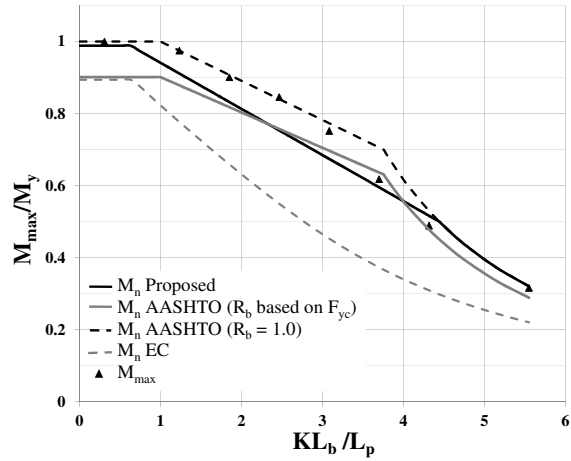
Figure C-31: Curves for LG9, $d_o/D = 2$

Figure C-32: Curves for LG10, $d_o/D = 2$

Figure C-33: Curves for LG11, $d_o/D = 2$

365

Figure C-34: Curves for LG12, $d_o/D = 2$

Figure C-35: Curves for LG13, $d_o/D = 2$

Figure C-36: Curves for LG14, $d_o/D = 2$

366

Figure C-37: Curves for LG15, *do/D* = 2

Figure C-38: Curves for LG16, *do/D* = 2

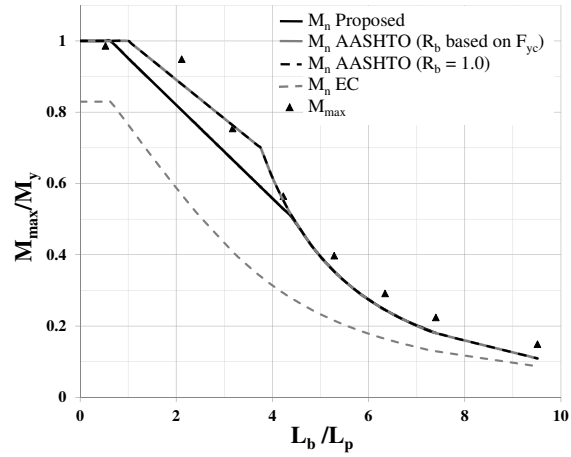**Figure C-39: Curves for LG17, *do/D* = 2**

367
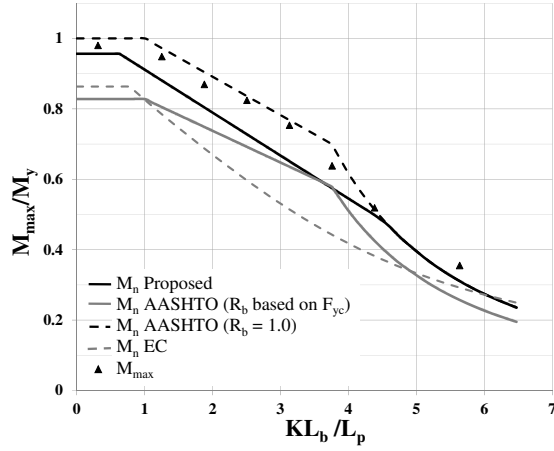
Figure C-40: Curves for LG18, $d_o/D = 2$
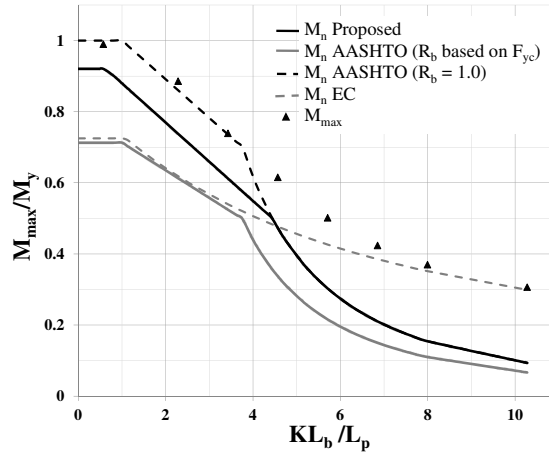
Figure C-41: Curves for LG19, $d_o/D = 2$
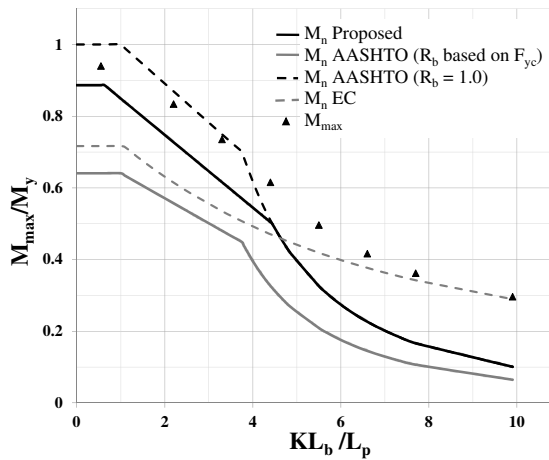
Figure C-42: Curves for LG20, $d_o/D = 2$

368
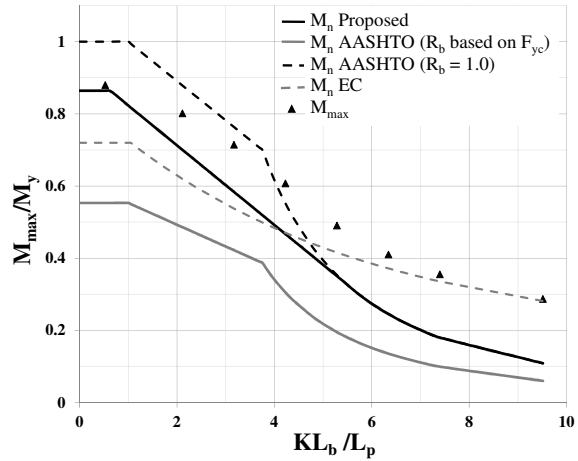
Figure C-43: Curves for LG21, $d_o/D = 2$
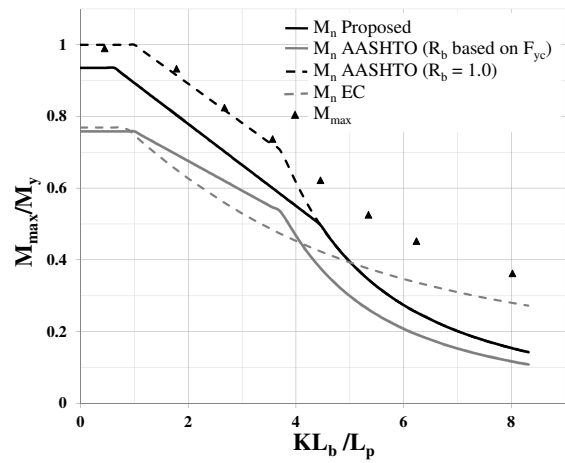
Figure C-44: Curves for LG22, $d_o/D = 2$
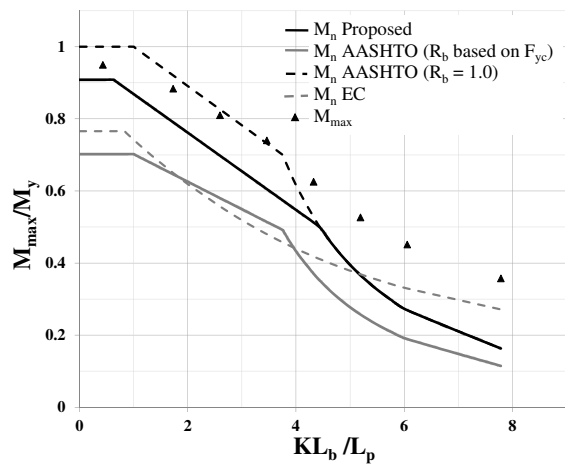
**Figure C-45: Curves for LG23, $d_o/D = 2$**

369

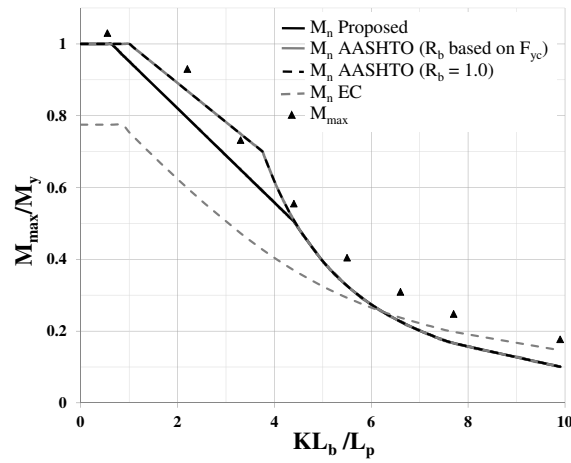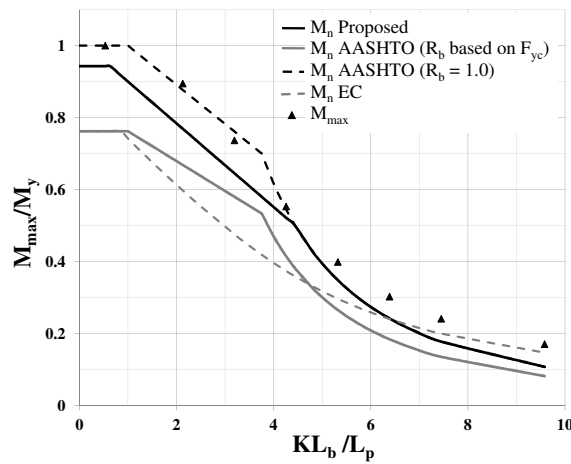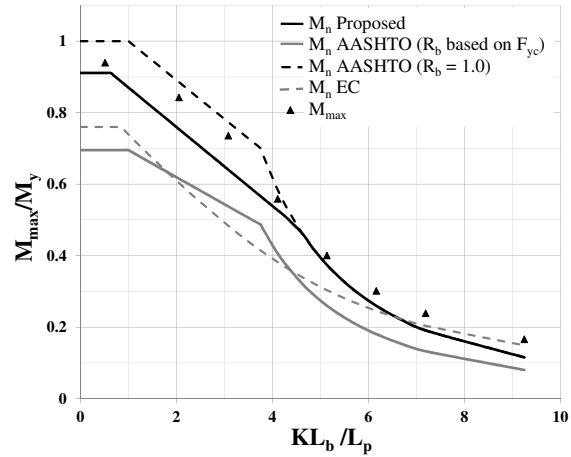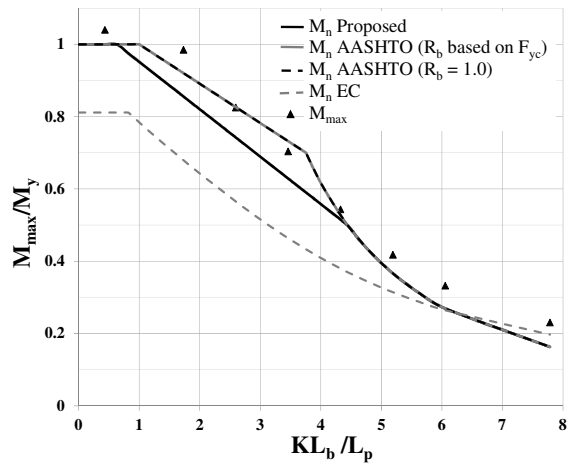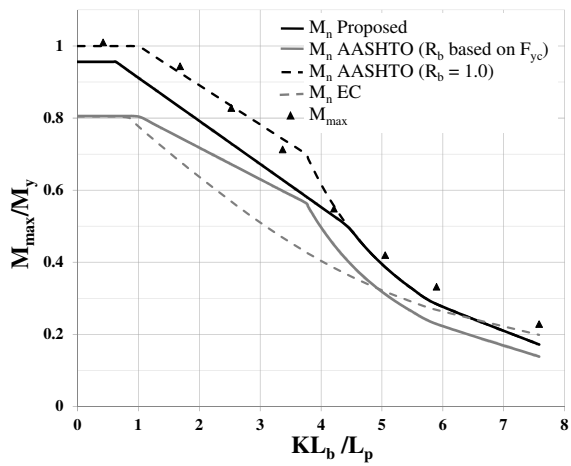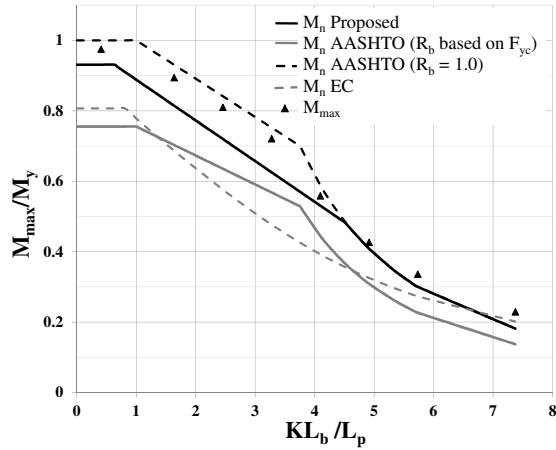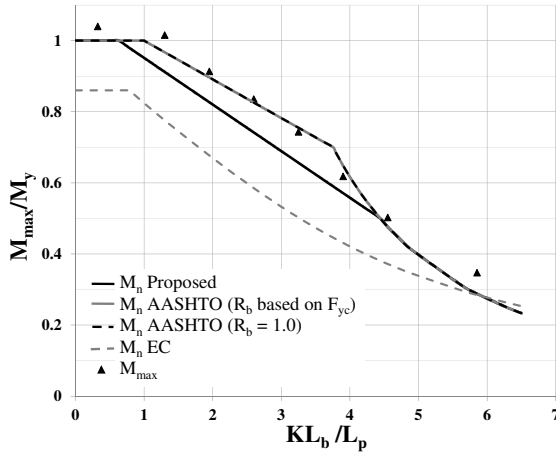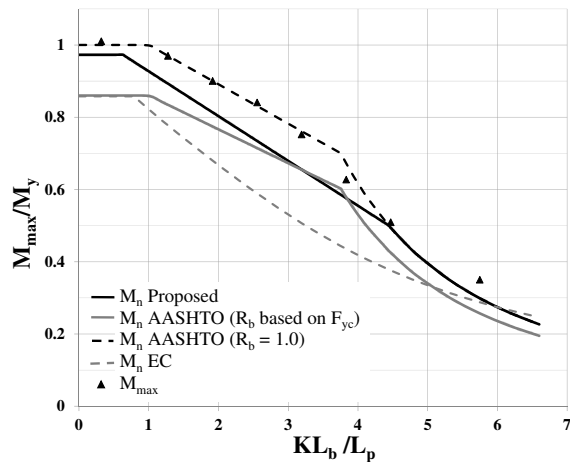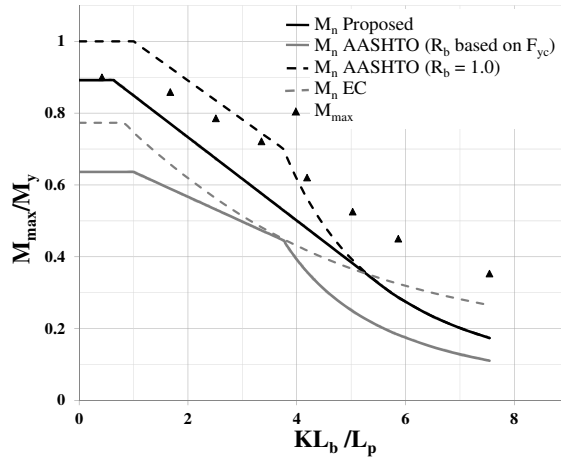**Figure C-46: Curves for LG24, $d_o/D = 2$**
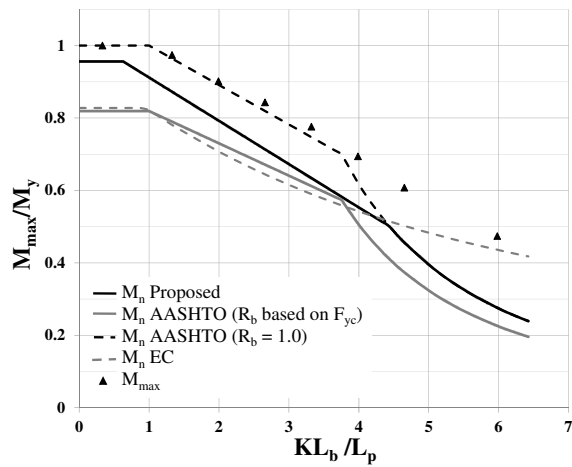
Figure C-47: Curves for LG25, $d_o/D = 2$
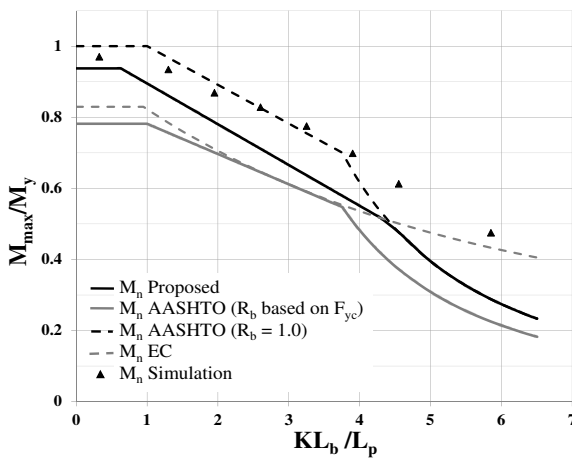
Figure C-48: Curves for LG26, $d_o/D = 2$

370

APPENDIX D

ADDITIONAL RESULTS FOR LTB OF LONGITUDINALLY

STIFFENED GIRDERS SUBJECTED TO MOMENT GRADIENT

This appendix lists the results for longitudinally stiffened girders subjected to moment gradient, with flexure controlled by the LTB limit state. Tables D-1 through D-5 list the results for the six girders considered in Section 9.2 at various unbraced lengths. All the plots are shown in Figures 9-16 through 9-21.

Table D-1: Results from test simulations compared with proposed, AASHTO and Eurocode strength predictions for d_o/D =1, KL_b = 450 inches, C_b = 1.75

Girder	M_{max}/M_y	$M_{max}/M_{nProposed}$	$M_{max}/M_{nAASHTO}$	M_{max}/M_{nEC}
LG2	0.74	0.74	0.74	1.35
LG3	0.70	0.72	0.85	1.25
LG11	0.82	0.87	1.07	1.39
LG12	0.77	0.85	1.11	1.30
LG20	0.82	0.93	1.28	1.31
LG21	0.79	0.92	1.42	1.26

Table D-2: Results from test simulations compared with proposed, AASHTO and Eurocode strength predictions for d_o/D =1, KL_b = 600 inches, C_b = 1.75

Girder	M_{max}/M_y	$M_{max}/M_{nProposed}$	$M_{max}/M_{nAASHTO}$	M_{max}/M_{nEC}
LG2	0.77	0.80	0.77	1.76
LG3	0.79	0.82	0.96	1.77
LG11	0.75	0.82	1.03	1.50
LG12	0.76	0.84	1.10	1.52
LG20	0.81	0.92	1.41	1.41
LG21	0.83	1.01	1.55	1.45

Table D-3: Results from test simulations compared with proposed, AASHTO and Eurocode strength predictions for $d_o/D = 1$, $KL_b = 750$ inches, $C_b = 1.75$

Girder	M_{max}/M_y	$M_{max}/M_{nProposed}$	$M_{max}/M_{nAASHTO}$	M_{max}/M_{nEC}
LG2	0.60	0.92	0.92	1.75
LG3	0.62	0.89	1.09	1.75
LG11	0.61	1.01	1.32	1.46
LG12	0.63	0.96	1.38	1.48
LG20	0.73	1.28	2.00	1.39
LG21	0.72	1.17	2.10	1.37

Table D-4: Results from test simulations compared with proposed, AASHTO and Eurocode strength predictions for $d_o/D = 1$, $KL_b = 900$ inches, $C_b = 1.75$

Girder	M_{max}/M_y	$M_{max}/M_{nProposed}$	$M_{max}/M_{nAASHTO}$	M_{max}/M_{nEC}
LG2	0.47	1.03	1.03	1.72
LG3	0.48	1.00	1.22	1.71
LG11	0.50	1.19	1.56	1.41
LG12	0.52	1.13	1.63	1.43
LG20	0.69	1.75	2.73	1.41
LG21	0.68	1.59	2.87	1.41

Table D-5: Results from test simulations compared with proposed, AASHTO and Eurocode strength predictions for $d_o/D = 1$, $KL_b = 1050$ inches, $C_b = 1.75$

Girder	M_{max}/M_y	$M_{max}/M_{nProposed}$	$M_{max}/M_{nAASHTO}$	M_{max}/M_{nEC}
LG2	0.37	1.12	1.12	1.69
LG3	0.39	1.09	1.33	1.68
LG11	0.41	1.33	1.75	1.35
LG12	0.42	1.27	1.82	1.37
LG20	0.63	2.17	3.38	1.38
LG21	0.62	1.96	3.54	1.37

APPENDIX E

BASIC VERIFICATION OF FINITE ELEMENT TEST

SIMULATIONS

The findings from this research are largely based on results from nonlinear finite element test simulations conducted in ABAQUS. Analytical solutions for strengths of members that are partially yielded are not available in closed form, rendering direct verification of FE solutions of such members difficult. However, it is possible to verify the FE simulations via correlation with analytical solutions in the LTB plateau region and with elastic buckling solutions. The following points illuminate some of the key characteristics of the FE simulations that establish the correctness of the solutions.

1. Non-longitudinally stiffened girders:

    a. It is observed in Section 6.5 that the test simulations with uniform moment attain the plastic moment capacity for rolled beams of very small unbraced lengths. The plastic moment capacity is the theoretical maximum achievable strength by these sections.

    b. It is also observed in Section 7.1 that the rolled beams attain the plastic moment capacity, or higher in tests with small unbraced lengths subjected to moment gradient. This corroborates with the expected and often observed phenomenon of strain-hardening within such members.

    c. It is further observed in Section 6.5 that rolled beams as well as doubly-symmetric welded plate girders attain the theoretical elastic LTB strengths (same as the Specification elastic LTB strengths) at long unbraced lengths.

It is evident that the FE simulations are accurate in the plateau and elastic LTB regions.

d. Section 7.1 introduces a computational tool SABRE2 that performs rigorous inelastic buckling solutions using stiffness reduction factors, and compares the results from SABRE2 with the FE simulation data obtained using ABAQUS. It is demonstrated that the FE test data and SABRE2 strength predictions correlate very well. This, along with the excellent correlation of the FE simulations with the experimental data in the inelastic LTB region (Section 6.2.3), provides confidence in the FE simulations conducted in this research for LTB of unstiffened girders.

2. Longitudinally stiffened girders:

a. Section 4.6 presents results for longitudinally stiffened girders governed by the yield limit state. Girders that have theoretical bend-buckling strengths greater that F_{yc} are expected to attain their full yield strengths. It is observed that test simulation results capture this behavior correctly, with no bend-buckling or stress redistribution in the webs of such girders. This is established by observing that the average compressive stresses through the mid-thickness of the web is largely linear at failure of these girders.

b. Section 8.4 presents results for the LTB strengths of longitudinally stiffened girders. As discussed above for non-longitudinally stiffened members, the test simulation strengths correlate well with the theoretical elastic LTB strengths at long unbraced lengths for doubly-symmetric girders. This indicates that the elastic buckling responses of these girders are well

captured by the FE simulations. Given these observations and the performance of the simulations in capturing the inelastic LTB response of unstiffened girders, it is reasonable to state that the inelastic LTB strengths captured by FE test simulations are reliable.

c. It is also clear from Section 10.5 that the proposed cross-section model based on FE test simulations predict experimental data available on longitudinally stiffened girders with reasonable accuracy.

REFERENCES

AASHTO (2014). *AASHTO LRFD Bridge Design Specifications. 7th Edition*, American Association of State Highway and Transportation Officials, Washington, DC.

Adams, P. F., Lay, M. G., and Galambos, T. V. (1964). "Experiments on High Strength Steel Members." Fritz Engineering Laboratory Rep. No. 297.8, Lehigh University ., Bethlehem, Pa.

AISC (2010a). *Specifications for Structural Steel Buildings, ANSI/AISC 360-10*, American Institute of Steel Construction, Chicago, IL.

AISC (2010b). *Code of Standard Practice for Steel Buildings and Bridges, AISC 303-05*, American Institute of Steel Construction, Chicago, IL.

AISI (2014). *North American Specification for the Design of Cold-Formed Structural Steel Members*, American Institute of Steel Construction, Washington, DC.

ASCE (1968). "Design of Hybrid Steel Beams, Report of the Subcommittee 1 on Hybrid Beams and Girders, Joint ASCE-AASHTO Committee on Flexural Members." *Proc; American Society of Civil Engineers*, Journal of the Structural Division, Vol. 94, No. ST6, New York, NY., p.1397-1425.

AWS (2010). *Structural Welding Code–Steel, AWS D1.1: D1.1M, 22nd ed*, AWS Committee on Structural Welding.

Basler, K., and Thurliman, B. (1961). "Strength of Plate Girders in Bending." *Journal of Structural Division - American Society of Civil Engineers*, 87(ST6), 153-181.

Beg, D., Kuhlmann, U., Davaine, L., and Braun, B. (2010). *Design of Plated Structures*, 1st Edition, ECCS - European Convention for Constructional Steelwork.

Boissonnade, N., Jaspart, J. P., Muzeau, J. P., and Villette, M. (2002). "Improvement of the interaction formulae for beam columns in Eurocode 3." *Comput Struct*, 80(27-30), 2375-2385.

CEN (2005). *Design of Steel Structures, Part 1-1: General Rules and rules for buildings, EN 1993-1-1:2005:E, Incorporating Corrigendum February 2006*, European Committee for Standardization, Brussels, Belgium.

CEN (2006a). *Eurocode 3: Design of Steel Structures, Part 1-5: General Rules - Plated Structural Elements, EN 1993-1-5:2006: E, Incorporating Corrigendum April 2009*, European Committee for Standardization, Brussels, Belgium.

CEN (2006b). *Eurocode 3: Design of Steel Structures, Part 2: Steel Bridges, EN 1993-2:2006: E, Incorporating Corrigendum July 2009*, European Committee for Standardization, Brussels, Belgium.

Chwalla, E. (1936a). "Beitrag Zur Stabiltats Theorie Des Stegbleches Vollwandiger Trager (Contribution to the Buckling Theory of Webs of Plate Girders)." *Stahlbau*, 9, p. 161.

Chwalla, E. (1936b). "Die Bemessung Der Waagerecht Ausgesteiften Stegbleche Vollwandiger Trager (The design of Longitudinally Stiffened Webs of Plate Girders)." *Preliminary Publications IABSE, and Congress*, p. 957.

Chwalla, E. (1944). "Uber Die Biegebeulung Der Langsversteiften Platte Und Das Problem Der "Mindeststeifigkeit (On the Buckling Problem of a Longitudinally Stiffened Plate Under Bending Moments and the Problem of Optimum Stiffness)." *Stahlbau*, 17, p. 84.

Cooper, P. B. (1963). "Literature Survey on Longitudinally Stiffened Plates." Fritz Engineering Laboratory Rep. No. 304.2, Lehigh University ., Bethlehem, Pa.

Cooper, P. B. (1965). "Bending and Shear Strength of Longitudinally Stiffened Plate Girders." Fritz Engineering Laboratory Rep. No. 304.6, Lehigh University ., Bethlehem, Pa.

Cooper, P. B. (1967). "Strength of Longitudinally Stiffened Plate Girders." *Journal of Structural Division - American Society of Civil Engineers*, 93(ST2), 419-451.

Dibley, J. E. (1969). "Lateral Torsional Buckling of I-Sections in Grade 55 Steel." *P I Civil Eng*, 43(Aug), 599-&.

Dubas, C. (1948). "Contribution A` L' E'tude Du Voilement Des To`les Raidies (A Contribution to the Buckling of Stiffened Plates)."

Dux, P. F., and Kitipornchai, S. (1983). "Inelastic Beam Buckling Experiments." *J Constr Steel Res*, 3(1), 3-9.

Frank, K. H., and Helwig, T. A. (1995). "Buckling of Webs in Unsymmetric Plate Girders." *Engineering Journal*, 32(2), 43-53.

Fukumoto, Y., and Kubo, M. (1977). "Ultimate Strength of Plate Girders with Longitudinal Stiffeners by Lateral Instability." *Der Stahlbau*.

Galambos, T. V. (1988). *Guide to Stability Design Criteria for Metal Structures*, 4th Edition, Wiley, N.Y.

Galambos, T. V., and Ketter, R. L. (1959). "Columns Under Combined Bending and Thrust." *Journal of the Engineering Mechanics Division, ASCE*, 85(EM2), 135-152.

Greiner, R., and Kaim, P. (2001). "Comparison of LT-Buckling Design Curves with Test Results." ECCS TC8, Report 23, 23.

Hampl, M. (1937). "Ein Beitrag Zur Stabilitate Des Horizontal Ausgesteiften Stegbleches (A contribution to the Stability of Longitudinally Stiffened Web Plates)." *Stahlbau*, 10, p. 16.

Helwig, T. A., Frank, K. H., and Yura, J. A. (1997). "Lateral-torsional Buckling of Singly Symmetric I-Beams." *Journal of Structural Engineering* 123(9), 1172-1179.

Hendy, C. R., and Murphy, C. J. (2007). *Designers' Guide to EN 1993-2 Eurocode 3: Design of steel structures. Part 2: Steel bridges*, Thomas Telford Publishing, Thomas Telford Ltd, London.

Jakab, G., Szabo, G., and Dunai, L. (2006). *Imperfection Sensitivity of Welded Beams: Experiment and Simulation*, Steel - A New and Traditional material for Building – Dubina & Ungureanu, Taylor & Francis Group, London.

Johansson, B., Maquoi, R., Sedlacek, G., Muller, C., and Beg, D. (2007). *Commentary and Worked Examples to EN 1993-1-5, Plated Structural Elements*, 1st Edition, ECCS - JRC Report No. EUR 22898 EN.

Johansson, B., and Veljkovic, M. (2009). "Review of Plate Buckling Rules in EN 1993-5." *Steel Construction*, 2(4), 228-234.

Johnston, B. G. (1976). *Guide to Stability Design Criteria for Metal Structures*, 3rd Edition, Wiley, N.Y.

Kim, Y. D. (2010). "Behavior and Design of Metal Building Frames Using General Prismatic and Web-Tapered Steel I-Section Members."Doctoral Dissertation, Georgia Institute of Technology, Atlanta, GA.

Kloppel, K., and Scheer, J. (1956). "Das Praktische Aufstellen Von Beuldeterminanten Fur Rechteckplatten Mit Randparallelen Steifen Navierschen Randbedingungen (The Derivation of Buckling Determinants of Rectangular Plate Stiffeners, The Plate Being Simply Supported and the Stiffeners Parallel to the Edges)." *Stahlbau*, 25, p. 117.

Kromm, A. (1944). "Zur Frage der Mindeststeifigkeiten Von Plattenaussteifungen (On the Problem of Optimum Rigidity of Stiffened Plates)." *Stahlbau*, 17, p. 81.

Lokhande, A. M., and White, D. W. (2014). "Evaluation of Steel I-Section Beam and Beam-column Bracing Requiremengts by Test Simulation."M.S. Thesis, Georgia institute of Technology, Atlanta, GA.

Longbottom, E., and Heyman, J. (1956). "Experimental Verification of the Strengths of Plate Girders Designed in Accordance with the Revised British Standard 153: Tests on Full Size and on Model Plate Girders." *P I Civil Eng*, 5, Part III, p.462.

Massonnet, C. (1940). "La Stabilite' De L`Ame Des Poutres Munies De Raidisseurs Horizontaux Et Sollicitees Par Flexion Pure (The Web stability of Longitudinally Stiffened Plate Girders Subjected to Pure Bending)."

Massonnet, C. (1954). "Essais de Voilement sur Poutres a` A`me Raidie." *Publications, Internatl. Assn. of Bridge and Structural Engrs.,Zurich, Switzerland*, 14, 125.

Massonnet, C. E. L. (1960). "Stability considerations in the Design of Steel Plate Girders." *Journal of Structural Division - American Society of Civil Engineers*, 86(ST1), 71-97.

Nethercot, D. A. (1976). "Buckling of Welded Hybrid Steel I-Beams." *Journal of the Structural Division - American Society of Civil Engineers*, 102(3), 461-474.

Ostapenko, A. (1964). "Local Buckling." *Structural Steel Design*, The Ronald Press, New York, N.Y.

Ostapenko, A., and Chern, C. (1971). "Ultimate Strength of Longitudinally Stiffened Plate Girders Under Combined Loads." Fritz Engineering Laboratory Rep. No. 328.10A, Lehigh University ., Bethlehem, Pa.

Owen, D. R., Rockey, K. C., and Skaloud, M. (1970). "Ultimate Load Behavior of Longitudinally Reinforced Web Plates Subjected to Pure Bending." *Kajima Inst Constr Tech / Japan*(30), 113-148.

Prawel, S. P., Morrell, M. L., and Lee, G. C. (1974). "Bending and Buckling Strength of Tapered Structural Members." *Welding Research Supplement*, 53, 75-84.

Richter, J. F. (1998). "Flexural Capacity of Slender Web Plate Girders."M.S. Thesis, The University of Texas at Austin, Austin, TX.

Righman, J. (2005). "Rotation Compatibility Approach to Moment Redistribution for Design and Rating of Steel I-Girders."Doctoral Dissertation, West Virginia University.

Roberts, T. M., and Narayanan, R. (1988). "Strength of Laterally Unrestrained Monosymmetric Beams." *Thin-Walled Structures*, 6(4), 305-319.

Rockey, K. C., and Leggett "The Buckling of a Plate Girder Web under Pure Bending when Reinforced by a Single Longitudinal Stiffener." *Proc., Inst. Civil Engrs*, January, 21, p.161.

Simulia (2013). *ABAQUS/Standard Version 6.12-1*, Simulia, Inc, Providence, RI.

Szalai, J., and Papp, F. (2005). "A New Residual Stress Distribution for Hot-Rolled I-shaped Sections." *J Constr Steel Res*, 61(6), 845-861.

Timoshenko, S. P. (1921). "Uber Die Stabilitat Versteifter Platten (On the Stability of Stiffened Plates)." *Eisenbau*, 12, 147.

Vigh, L. G., and Dunai, L. (2010). "Advanced Stability Analysis of Regular Stiffened Plates and Complex Plated Elements." *SDSS' Rio 2010 Stability and Ductility of Steel Structures,*Rio de Janeiro, Brazil.

Vincent, G. S. (1969). "Tentative Criteria for Load Factor Design of Steel Highway Bridges." *AISI Bulletin*, American Iron and Steel Institute, Washington. DC.

White, D. W. (2008). "Unified flexural resistance equations for stability design of steel I-section members: Overview." *Journal of Structural Engineering-American Society of Civil Engineers*, 134(9), 1405-1424.

White, D. W., and Barker, M. G. (2008). "Shear Resistance of transversely Stiffened I-Girders." *Journal of Structural Engineering, ASCE*, 134(9), 1425-1436.

White, D. W., Barker, M. G., and Azizinamini, A. (2008). "Shear Strength and Moment-Shear Interaction in Transversely Stiffened I-Girders." *Journal of Structural Engineering, ASCE*, 134(9), 1437-1449.

White, D. W., Jeong, W. Y., and Togay, O. (2015). "Comprehensive Stability Design of Steel Members and Systems via Inelastic Buckling Analysis." *8th International Symposium on Steel Structures*,Jeju, Korea. .

White, D. W., and Jung, S.-K. (2004). "Unified Flexural Resistance Equations for Stability Design of Steel I-Section Members – Uniform Bending Tests." *Structural Engineering, Mechanics and Materials*

Report No. 28, School of Civil and Environmental Engineering, Georgia Institute of Technology, Atlanta, GA.

White, D. W., and Jung, S.-K. (2007). "Effect of web distortion on the buckling strength of noncomposite discretely-braced steel I-section members." *Engineering Structures*, 29(8), 1872-1888.

Wongchung, A. D., and Kitipornchai, S. (1987). "Partially Braced Inelastic Beam Buckling Experiments." *J Constr Steel Res*, 7(3), 189-211.

VITA

Lakshmi Priya was born on 13 May, 1985 in Chennai, India. She spent most of her childhood in Hyderabad. She received her Bachelor of Technology in Civil Engineering in 2006 from Visvesvaraya National Institute of Technology, Nagpur. She received her Masters degree in Civil Engineering from The University of Texas at Austin in 2008. She worked as a Structural Engineer at Walter P. Moore and Associates at Houston, Texas from 2008 to 2012. She is a licensed PE in the state of Texas. She entered the PhD program at Georgia Institute of Technology in August 2012.

Email: pslakshmipriya@gmail.com